# COMPUTATIONAL OPTIMIZATION AND INVESTIGATION OF CONJUGATE HEAT AND MASS TRANSFER IN POROUS CAVITY

**AZEEM**

**THESIS SUBMITTED IN FULFILMENT OF THE REQUIREMENTS FOR THE DEGREE OF DOCTOR OF PHILOSOPHY**

**FACULTY OF COMPUTER SCIENCE AND INFORMATION TECHNOLOGY**
**UNIVERSITY OF MALAYA**
**KUALA LUMPUR**

**2017**

**UNIVERSITI MALAYA**

**ORIGINAL LITERARY WORK DECLARATION**

Name of Candidate: AZEEM (I.C/Passport No:

Registration/Matric No: WHA110059

Name of Degree: PhD COMPUTER SCIENCE

Title of Project Paper/Research Report/Dissertation/Thesis ("this Work"):

COMPUTATIONAL OPTIMIZATION AND INVESTIGATION OF CONJUGATE HEAT AND MASS TRANSFER IN POROUSCAVITY

Field of Study: SCIENTIFIC COMPUTING

I do solemnly and sincerely declare that:

(1) I am the sole author/writer of this Work;
(2) This Work is original;
(3) Any use of any work in which copyright exists was done by way of fair dealing and for permitted purposes and any excerpt or extract from, or reference to or reproduction of any copyright work has been disclosed expressly and sufficiently and the title of the Work and its authorship have been acknowledged in this Work;
(4) I do not have any actual knowledge nor do I ought reasonably to know that the making of this work constitutes an infringement of any copyright work;
(5) I hereby assign all and every rights in the copyright to this Work to the University of Malaya ("UM"), who henceforth shall be owner of the copyright in this Work and that any reproduction or use in any form or by any means whatsoever is prohibited without the written consent of UM having been first had and obtained;
(6) I am fully aware that if in the course of making this Work I have infringed any copyright whether intentionally or otherwise, I may be subject to legal action or any other action as may be determined by UM.

Candidate's Signature Date

Subscribed and solemnly declared before,

Witness's Signature Date

Name:
Designation:

## ABSTRACT

Conjugate heat transfer in porous medium is a complex phenomenon that depends on coupled partial differential equations which are difficult to solve directly. The governing equations of conjugate heat transfer are coupled to each other thus any change in one equation affects the other equations and vice-versa. The governing equations are non-dimensionalised with the help of suitable non-dimensional parameters. These equations can be solved with the help of few numerical methods but that involves generation of huge number of simpler equations. The large number of equation evolved takes enormous amount of computational resources to solve and study the phenomenon. The current research is undertaken to develop an optimized algorithm that takes lesser amount of time to solve the resulting equations from application of a popular numerical techniques known as finite element method. The governing partial differential equations are converted into a set of algebraic equations that further assembled into a matrix form of equations. The porous solid domain subjected to conjugate heat transfer is divided into smaller segments with the help of triangular elements. The stiffness matrix of each element is assembled into a global stiffness matrix. A tight convergence criterion is maintained for all the governing equations. The optimized algorithm is compared with its conventional method of solution for conjugate heat transfer as well as conjugate heat and mass transfer.

It is found that the developed algorithm works perfectly to predict the single diffusion as well as double diffusion in a square porous cavity having a small solid placed at various locations. The developed algorithm is found to take considerable lesser amount of iterations and time to arrive at the solution as compared to its counterpart i.e. conventional method of solution for conjugate heat transfer. The study revealed that the placement of solid has significant effect on the heat and mass transfer behavior in the cavity.

# ABSTRAK

Pemindahan haba konjugat dalam medium berliang adalah satu fenomena kompleks yang bergantung kepada persamaan pembezaan separa yang sukar untuk diselesaikan secara langsung. Persamaan pengelola konjugat pemindahan haba adalah berkaitan antara satu sama lain. Maka apa-apa perubahan dalam satu persamaan akan memberi kesan kepada persamaan lain dan sebaliknya. Persamaan-persamaan yang mengawal adalah tidak didimensikan dengan bantuan parameter tanpa dimensi yang sesuai. Persamaan ini boleh diselesaikan dengan bantuan beberapa kaedah berangka tetapi ia melibatkan persamaan mudah yang sangat banyak. Bilangan persamaan yang berkembang secara pesat mengambil sejumlah besar sumber pengiraan untuk menyelesaikan dan mengkaji fenomena ini.Penyelidikan semasa dijalankan untuk membina dan mengoptimumkan algoritma supaya mengambil masa yang lebih sigkat dalam menyelesaikan persamaan menggunakan teknik berangka popular dikenali sebagai kaedah unsur terhingga. Persamaan pembezaan separa ditukar kepada satu set persamaan algebra yang disusun dalam persamaan bentuk matriks. Domain pepejal berliang mengkonjugat pemindahan haba dibahagikan kepada beberapa bahagian dengan bantuan unsur segi tiga.Matriks kekukuhan setiap elemen disusun kepada bentuk matriks kekukuhan global.Satu kriteria penumpuan dikekalkan secara ketat untuk semua persamaan yang mengawal.Algoritma dioptimumkan dibandingkan dengan kaedah penyelesaian pemindahan konjugat haba konvensional begitu juga dengan pemindahan konjugat haba dan jisim.

Didapati bahawa algoritma yang dibangunkan berfungsi dengan sempurna untuk meramalkan penyebaran tunggal serta penyebaran berganda dalam rongga berliang segi empat yang mempunyai pepejal kecil yang diletakkan dipelbagai lokasi. Algoritma yang dibangunkan didapati mempunyai kurang lelaran dan masa untuk tiba pada penyelesaian

berbanding dengan kaedah lain iaitu kaedah konvensional penyelesaian untuk pemindahan konjugat haba. Kajian ini menunjukkan bahawa penempatan pepejal mempunyai kesan yang besar ke atas tingkah laku pemindahan haba dan jisim dalam rongga.

## ACKNOWLEDGEMENT

In the name of ALLAH, Most Gracious, Most Merciful, All praises belong to Him alone. I am indeed grateful to Almighty ALLAH for bestowing His mercy upon me to pursue higher education.

I would like to express my deepest gratitude from the bottom of my heart to my supervisors Associate Prof. Dr. Irfan Anjum Magami, Dr. Mohd Yamani Idna Bin Idris and Dr. Nik Nazri Bin Nik Ghazali for their persistent guidance, invaluable suggestions and relentless support throughout the research. In fact their supervision and kind cooperation made everything feasible to accomplish my research.

I would like to dedicate this work to one of my eldest sister who is my first teacher, mentor, she taught me since my childhood when I was weak in my studies, inspired me towards love for education, motivated me to learn and excel. I am greatly indebted to her for my whole life for her sacrifice, and for inculcating treasured moral values into me which elevates human being from the rest of the creation. May ALLAH reward her with the best in this world and hereafter, Aameen.

Moreover I pay my heartiest regards to all the authorities and staff for their kind support for providing all necessary facilities for their co-operation during the course. Also I thank all my friends who assisted me with their earnest prayers and support.

Last but not least, I would like to convey my heartiest gratitude to my parents, my brothers, sisters, my wife and children for their concern and encouragement. I would not have completed this thesis without their constant support.

## TABLE OF CONTENTS

## LIST OF FIGURES

## LIST OF TABLES

## LIST OF SYMBOLS AND ABBREVIATIONS

| | |
|---|---|
| $b, c$ | Element constants |
| $C, \overline{C}$ | Species concentration |
| $g$ | Acceleration due to gravity (m/s$^2$) |
| $h$ | Solid height (m) |
| $k$ | Thermal conductivity (W/m-$^o$C) |
| $k_p$ ,$k_s$ | Porous and Solid thermal conductivity respectively (W/m-$^o$C) |
| $K$ | Permeability of porous medium (m$^2$) |
| $Kr = k_s/k_p$ | Conductivity ratio |
| $L$ | Height and length of cavity (m) |
| $Le$ | Lewis number |
| $Nu$ | *N*usselt number |
| $N$ | Buoyancy ratio |
| $R_d$ | Radiation parameter |
| $Ra$ | Raleigh number |
| $Sh$ | Sherwood number |
| $T, \overline{T}$ | Temperature |
| $u, v$ | Velocity components in x and y direction respectively (m/s) |

$x, y$ Cartesian co-ordinates

$\bar{x}, \bar{y}$ Non-dimensional co-ordinates

$T_w$ surface temperature

$T_\infty$ temperature of the ambient fluid

***Greek Symbols***

$\alpha$ Thermal diffusivity ($m^2/s$)

$\beta$ Coefficient of thermal expansion ($1/^oC$)

$\rho$ Density ($kg/m^3$)

$v$ Coefficient of kinematic viscosity($m^2/s$)

$\sigma$ Stephan Boltzmann constant ($W/m^2$-$K^4$)

$\beta_r$ Absorption coefficient (1/m)

$\psi$ Stream function

$\bar{\psi}$ Non-dimensional stream function

$\theta$ dimensionless temperature function

$\theta_w$ dimensionless surface temperature ($T_w/T_\infty$)

***Subscripts***

$_h$ Hot

$_c$ Cold

$p$ Porous

$s$ Solid

$_{1,2,3}$ Positions corresponding to nodes i, j and k respectively for an element.

## ABBREVIATIONS

| | | |
|---|---|---|
| **PDE** | **:** | Partial Differential Equation |
| **FVM** | **:** | Finite Volume Method |
| **FEM** | **:** | Finite Element Method |
| **FDM** | **:** | Finite Difference Method |
| **OpenFOAM** | **:** | Open source Field Operation And Manipulation |
| **IMPES** | **:** | IMplicit Pressure Explicit Saturation |
| **CUDA** | **:** | Compute Unified Device Architecture |
| **GAs** | **:** | Genetic Algorithms |
| **AD** | **:** | Algorithmic Differentiation |
| **DAEs** | **:** | Differential Algebraic Equation systems |
| **FDEs** | **:** | fractional differential equations |
| **BEM** | **:** | boundary element method |
| **ODEs** | **:** | ordinary and partial differential equations |
| **SODEs** | **:** | systems of ordinary differential equations |
| **PSO** | **:** | particle swarm optimization |
| **GPU** | **:** | Graphical Processing Unit |
| **PRNGs** | **:** | Pseudo Random Number Generators |
| **RODE** | **:** | random ordinary differential equation |
| **LTNE** | **:** | local thermal nonequilibrium |
| **BDPM** | **:** | bi-dispersed porous medium |

# CHAPTER 1: INTRODUCTION

## 1.1. Research Background

The development of fast and efficient optimization algorithms have become inevitable in almost every single department of life, which has led to the incredible emphasis on increased awareness and creative ideas in developing the optimization techniques. This trend has profound effects, in particular, on research and innovation as well as solution techniques adopted for solving various scientific and industrial problems in the area of computer science as evident from the open literature.  Furthermore, in engineering the optimization techniques have become customary and often indispensable especially in actively pursued research area. However with the rapid advancement in computer science and information technology, it has become comparatively, easily achievable task. Therefore it comes as no surprise, as the emergence of interdisciplinary research collaborations are considered as the most effective tools in research and innovation fields, such as; bio instrumentation engineering, mechatronics engineering, bio medical engineering and so on. In a similar trend there is a need to develop optimized yet efficient and faster algorithms to investigate the various issues in heat transfer study. To accomplish this need of efficient and optimized algorithmic tools in view, which could be more helpful in obtaining the solutions to the non-linear partial differential equations with acceptable accuracy in minimum time. In particular the conjugate heat transfer phenomenon, which has more complicated equations to handle, require the best possible solution technique that can execute with high efficiency and minimal computation time to achieve a desirable accuracy.

The heat transfer in porous medium is one of the center points of research by several eminent researchers, during the last few decades, due to its vast applications in science and technology, research and innovation, industry and even in our everyday applications. Many engineering applications involve the complex conjugate heat transfer phenomenon such as heat exchangers, automotive and aerospace industries and chemical processing, as well as applications in recently emerging technologies in materials and life sciences including environmental protection, bio- and nanotechnology, pharmacology, and medicine. Unlike the other phenomena, the conjugate heat transfer analysis, do not require the external and internal heat transfer coefficients on the walls of the conduction surfaces, instead it only requires the boundary conditions at the inlet and exit of the gas and coolant passages.

Recent studies have shown promising results in analyzing this complex conjugate heat transfer analysis with the help of the advanced computing technologies and optimized computational methods. However the importance of the efficient and reliable numerical methods cannot be undermined. The solution to the governing partial differential equations involved in the conjugate heat transfer analysis could only be achieved employing suitable methodology and mathematical techniques.

## 1.2 Conjugate heat transfer analysis

The conjugate heat transfer refers to a situation where heat transfer occurs simultaneously between fluid and solid emanating a complex boundary condition between fluid and solid. Generally, the conjugate heat transfer is reported for the cases where the solid wall is attached to whole of the surface at one end of geometry under investigation. There are applications such as heat exchangers, solar cell technology, nuclear reactors and many more, where the porous medium is fixed adjacent to a solid section. This kind of situations produces different heat transfer behavior than having no solid region adjacent to the porous medium. This happens because of the fact that the boundary conditions are generally known at the one side of solid wall and the porous medium, but no information is available at the meeting point of solid and the porous region which can be termed as solid-porous interface. Thus the heat transfer in the porous medium is dictated by the solid wall characteristics. This phenomenon is generally termed as conjugate heat transfer. Literatures pertaining to the conjugate heat transfer in different geometries such as vertical wall, vertical (I Pop, Sunada, Cheng, & Minkowycz, 1985) cylindrical fin (Liu, Minkowycz, & Cheng, 1986), sphere (Kimura & Pop, 1994), vertical circular pin and vertical flat plate (Cha, Chen, & Chen, 1990), embedded in porous medium explicating various aspects have been reported. Thus there is increased interest by the eminent researchers to understand the heat transfer characteristics and fluid flow behavior inside the porous domain as evident from open literature.

### 1.3 MathematicalFormulation

Mathematics is the base of scientific and engineering developments which have led to the advancements in many fields of human life. Mathematics can be used to imitate any physical phenomenon without having to build the physical structure accomplishing the phenomenon. Mathematical modeling requires the basic laws of science to be written, arranged and operated with the help of mathematical rules to finally come up with a single or multiple equations which can predict the behavior of the physical system understudy. There are two distinct advantages of using mathematical modeling over experimental studies. Firstly, it avoids the heavy cost involved in building the prototype of physical system. Secondly, it compresses the time required to study a system by many folds as compared to that of experimental studies. The beauty of mathematical modeling lies in the fact that it can answer many questions about the behavior of system in very short period of time. Analytical and numerical studies in recent times have become very popular due to accuracy with in required range, fast, inexpensive due to the advanced computer technology.

### 1.4 Optimization in numerical study

The investigation of heat transfer through porous medium has received incredible attention from the various eminent researchers due to its, prevalence in the various engineering and industrial applications and its complexity. The difficulty in dealing with the governing equations for the heat transfer and fluid flow through porous medium has given rise to the implementation of the various numerical techniques to solve these nonlinear partial differential equations. The need for the solutions to the governing nonlinear partial differential equations has motivated to develop various verities of optimized numerical techniques. The researchers have suggested various optimization techniques to deal with these complex analyses as in the case of the study carried out by (Das & Prasad, 2015) and (Kamali, Kumaresan, & Ratnavelu, 2015).

The present study deals with the solution of the governing non linear partial differential equations to investigate the heat transfer characteristics and fluid flow pattern in a square porous domain fixed with solid at arbitrary position. The study is accomplished by using the most popular numerical technique Finite element Method FEM in which the partial differenitail equations are converted in to the simple algebariac equations by means of Galerkin’s method. Furthermore these algebraic equations are solved for various physical and geometrical parameters by using the Matlab codes, generated to understand the effects of various physical and geometrical parametrs on the heat transfer and fluid flow behaviour. Many computer codes, for instance, physical phenomnon as mentioned in above study, consumes too much time and needs advanced technology to handle the robust analysis(de Rocquigny, Devictor, & Tarantola, 2008). Thus it needs an efficient, in fact a specialized, optimized algorithm to circumvent the unnecessary huge time and resources to carry out the analyses.

### 1.5 ProblemStatement and Objectives

The magnificent work carried out by the researchers in the last few decades has addressed various unsolved problems related to the heat transfer and fluid flow analysis using mathematical models that can effectively be simulated to run on computer systems. Furthermore the plenty of new areas have been explored to take the research in to the further advanced stages. Eventually the new aspects pertaining to the heat transfer and the porous media approach have been opened as a new challenge to correlate the previous fundamental research to the newly emerged problems pertaining to the research in the heat transfer in various geometries. The important phenomena such as the conjugate heat transfer; double diffusion conjugate heat transfer has not received sufficient attention from the researchers as evident from the literature which has been discussed in the next chapter. Moreover, the simulation results for the solution of conjugate heat transfer consumes huge amount of computing resources to arrive at the solution. These results highlight a possible constraint with respect to real life applications for many industries that cannot afford high performance servers Thus addressing these important and untouched problems has motivated to carry out the in-depth research in this specific area of engineering science to understand the macro level as well as to some extent micro level details predominantly related to the heat transfer and fluid flow analysis and also in heat and mass transfer in some special case as well.

## 1.6 Objectives

Thus the objectives of the forgoing study can be listed as below.

1. To optimize the computational resources of conjugate heat and mass transfer phenomenon that reduces the required computational time.
2. To simulate and study the effect of size and location of solid placed inside the porous cavity, on heat transfer based on the optimized method.
3. To simulate and study the effect of size and location of solid on double diffusion inside the porous medium based on the optimized method.

## 1.7 Scopeof the study

The research emphasizes on convective heat transfer mechanism in a porous square cavity using mathematical models to develop efficient and faster algorithms based on computer simulation. The complexity of the convective heat transfer has been studied thoroughly. The scope is a confined simulation of a mathematical model that is to optimize the conjugate single diffusion as well as double diffusion in porous medium. The optimized model is applied to study the size and location of solid wall placed at arbitrary positions inside the porous cavity. Conjugate single as well as double diffusion with respect to various locations of solid and its size are subjected to in-depth analysis.

## 1.8 Thesis Organization

The thesis is organized into seven chapters that systematically explain the objectives of this research. The description of each chapter is as follows:

**Chapter1** gives the introduction to the basic concept of heat transfer and relevant applications of heat transfer in porous medium. Thereafter the different aspects of the convection are explained. The methodology and the scope of the study of the research is described briefly.

**Chapter 2** deals with the extensive literature survey of t h e past research work carried out by various researchers and ends with review of the work.

**Chapter3** presents the mathematical formulation of governing equations of the fluid flow and the solution methodology obtained in detail.

**Chapter 4, 5 and 6** are the important chapters that explains the micro level details of the optimized algorithm for heat transfer and heat mass transfer phenomenon in porous medium with respect to the different cases of the convective heat transfer and heat mass transfer analysis.

**Chapter 7** provides the conclusion and recommendations for the future works.

# CHAPTER 2: LITERATURE REVIEW

## 2.1 Introduction

It is evident from number of published research articles in last few decades that the porous medium plays an important role in many scientific and engineering fields. Heat transfer in porous medium which is also referred to as single diffusion and, Heat and Mass transfer in porous medium which is alternately referred as double diffusion turns into more complex phenomenon when any solid obstruction is encountered in the porous medium that substantially changes the flow behavior leading to change in heat transfer and mass transfer characteristics. Researchers identified the significance of evaluating the mutual thermal effects of solid bodies and the fluid surrounding them. Later on this problem was referred to conjugate and the phenomenon that was employed to study the transfer of heat and mass through porous media was known as *conjugate heat and mass transfer in porous media.* The current chapter is devoted to look into the research work being carried out by various researchers in the field of conjugate heat or conjugate heat and mass transfer in porous medium. Many Industrial applications such as heat exchanger design and continuous processes of convective drying are in fact some of the conjugate problems.

## 2.2 Conjugate Heat Transfer Geometries

### 2.2.1 Square/ Rectangular geometry:

Badruddin et al (Badruddin, Zainal, Narayana, & Seetharamu, 2007)investigated heat transfer by convection, conduction and radiation in a saturated porous medium enclosed in a square cavity using a thermal non-equilibrium model. The flow is assumed to follow Darcy law. The governing partial differential equations are non-dimensionalised and solved numerically using finite element method. The left vertical surface of the square cavity is maintained at an isothermal temperature $T_h$ and the right vertical surface at $T_c$ such that $T_c < T_h$. The top and bottom surfaces of the cavity are assumed to be adiabatic. Effect of various parameters on Nusselt number such as the inter-phase heat transfer coefficient, modified conductivity ratio, radiation parameter and Rayleigh number are analyzed. They concluded that the local Nusselt number for fluid and solid decreases with increase of cavity height at hot wall and vice-versa at cold wall.

Chamkha & Ismael(Chamkha & Ismael, 2013a) studied conjugate natural convection-conduction heat transfer in a square domain composed of Nano fluids filled porous cavity heated by a triangular solid wall under steady-state conditions. The triangular solid is kept at the left corner of the cavity. The vertical and horizontal walls of the triangular solid wall are kept isothermal and at the same hot temperature $T_h$. The other boundaries surrounding the porous cavity are kept adiabatic except the right vertical wall where it is kept isothermally at the lower temperature $T_c$. Governing equations are based on Darcy model and were solved using the over-successive relaxation finite-difference method. Their results concluded that the heat transfer within Nano fluids-saturated porous media may be enhanced or deteriorated with increasing the Nano particles volume fraction and the Nusselt number is an increasing function of the Rayleigh number.

Later they extended their investigation with the same geometry to Rayleigh number Ra (100-1000), solid to fluid saturated porous medium thermal conductivity ratio Kr (0.1–10), and the triangular wall thickness D (0.05-1). They observed an uncommon effect of the solid wall thickness D, when D was increasing it had two contrary effects. These are: increasing the thermal resistance (reduction of heat transfer), and increasing the contact interface (enhancement of heat transfer). It was evident that the effect of Ra and D became noticeable when Kr>0.1. (Chamkha & Ismael, 2013b)

Alhashash, Saleh, & Hashim(Alhashash, Saleh, & Hashim, 2013) carried numerical study on conjugate natural convection in a square porous enclosure sandwiched by finite walls under the influence of non-uniform heat generation and radiation. They considered left vertical wall heated isothermally to hot temperature $T_h$ and the right vertical wall is kept isothermally at the lower temperature $T_c$ and top and bottom horizontal walls are kept adiabatic. Darcy model is employed in mathematical formulation and the governing equations are solved using finite difference method. The governing parameters considered are the ratio of wall thickness to its width, the wall to porous thermal conductivity ratio, the internal heating and the local heating exponent parameters. They concluded that the flow strength circulation increases with increasing the radiation intensity and the average Nusselt number on the hot and cold interfaces also increases with an increase in radiation intensity.

Badruddin et al (Badruddin, Al-Rashed, Ahmed, & Kamangar, 2012) analyzed the heat transfer characteristics in a porous duct. They solved the mathematical model of heat transfer in a porous duct by converting the governing partial differential equations into a set of algebraic equations with the help of finite element method. A simple three noded triangular element is used to mesh the duct domain. The current problem consists of a square duct with outer walls being exposed to hot temperature $T_h$, and inner walls subjected to cool temperature $T_c$. The Emphasis is given to investigate the effect of width ratio of cavity on heat and fluid flow characteristics inside the porous medium. They reported the results for various duct width ratios, Rayleigh number etc. They found that the Nusselt number increases with increase in height of cavity along the vertical walls of duct; however the Nusselt number for certain values of duct ratio oscillates along the width of the porous medium at bottom wall of the cavity.

Baytas, Liaqat, Grosan, & Pop (A. C. Baytas, Liaqat, Grosan, & Pop, 2001) studied a two-dimensional square cavity under the influence of a gravitational field filled with a fluid-saturated porous medium. The left and right vertical walls of the cavity are maintained at constant and different levels of temperatures $T_h$ and $T_c$ respectively where $T_h > T_c$.The upper and lower horizontal walls of equal thickness *b* are assumed to be of the same material with a non-zero thermal conductivity, while the outside of horizontal solid walls are kept adiabatic. They concluded that the flow characteristics are significantly influenced by the coupling effect between solid walls and the fluid-saturated porous medium, for large values of the conductivity ratio parameter k., and small changes were observed when the conductivity of the solid walls is small when compared to fluid-saturated porous medium.

Saeid (Nawaf H. Saeid, 2007) studied numerically steady conjugate natural convection in a two-dimensional vertical porous layer sandwiched between two equal-thickness walls. The horizontal heating is considered, where the outer surfaces of the vertical walls are isothermal at different temperatures with adiabatic horizontal boundaries. The Darcy model is used in mathematical formulation for the porous layer and finite volume method is used to solve the dimensionless governing equations. The governing parameters considered are the ratio of the wall thickness to its height, the wall to porous thermal conductivity ratio and the Rayleigh number. The author concluded that as Rayleigh number increases the average Nusselt number is increasing with higher slope for the thin walls than that for thick walls.

Saleh & Hashim (Saleh & Hashim, 2012) carried numerical study on effects of a conductive wall on natural convection in a square porous enclosure having internal heating at a rate proportional to a power of temperature difference. The horizontal heating is considered and the left and right vertical walls are heated isothermally at $T_h$ and $T_c$ where $T_h > T_c$. while the horizontal walls are kept adiabatic. The equations are solved using Darcy model and finite difference method. They concluded that the heat transfer remains stable for any values of the thermal conductivity ratio at very low Rayleigh number and increasing thermal conductivity ratio value and/or decreasing the thickness of solid wall can increase the maximum fluid temperature.

### 2.2.2 Annular/ Cylindrical geometry:

Mikhail A. Sheremet & Trifonova(Mikhail A. Sheremet & Trifonova, 2013b)studied numerical simulation of transient conjugate natural convection in a vertical cylinder partially filled with a porous medium in conditions of convective cooling from an environment. They found that an increase in the porous layer height ratio leads to a decrease in several parameters like the average Nusselt number, the cooling rate of the analyzed domain, and an intensity of the toroidal vortex.

Tao, Wu, Chen, & Deng(Z. Tao, Wu, Chen, & Deng, 2005) presented numerical model for the process of microwave freeze-drying within a cylindrical porous media with cylindrical dielectric cores. The set of transient governing equations developed were solved numerically with variable time-step finite volume method. Their study was mainly concentrated on the influences of control parameters, such as loss factor, initial saturation and electric field strength, on microwave freeze-drying. They concluded that: proper usage of cylindrical dielectric cores could dramatically reduce the drying time, The loss factor of the cylindrical dielectric core is an important parameter influencing the drying behavior, two sublimation fronts can exist within the porous media due to the existence of inner dielectric cores and the impact of cylindrical dielectric cores on drying could not be ignored even though the initial saturation is low.

Badruddin et al(Badruddin et al., 2015) studied heat transfer in a porous medium sandwiched between two solid walls of an annular vertical cylinder applying finite element method on governing equations with a focus on the effect of solid wall thickness, variable wall thickness, variable wall thickness at inner and the outer radius, the conductivity ratio and the solid wall conductivity ratio. Their results concluded that there is no much temperature variation inside the inner solid when the wall thickness is small, the increase in the conductivity ratio Kr increases the heat transfer rate and that the average Nusselt number decreases with increase in the wall.

Salman et al(Salman et al., 2014) investigated heat transfer behavior in a porous annular vertical cylinder having a solid wall at the inner surface. The inner and outer surfaces of the annulus are maintained isothermally. It was noticed that the increase in conductivity ratio lead to an increase in temperature at the solid-porous interface. Lastly they concluded that temperature along the interface layer increases with the decrease in solid wall thickness due to decrease in thermal resistance of the wall.

Pop & Na(I. Pop & Na, 2000) investigated the steady conjugate free convection over a vertical slender, hollow circular cylinder with the inner surface at a constant temperature embedded in a porous medium. The governing equations are solved using the Keller box method. The results are presented in terms of temperature profiles, the interface temperature profiles and the local Nusselt numbers.

Kaya(Kaya, 2011) studied mixed convection heat transfer about a vertical slender hollow cylinder due to buoyancy and conjugate heat transfer effects in the porous medium with high porosity. They considered the wall conduction parameter, the porous medium parameter, the Forchheimer parameter and the Richardson number as main parameters for their investigation and the author found that local skin friction and the local heat transfer coefficients increase with an increase in buoyancy, porous medium, Forchheimer parameters and decrease with conjugate heat transfer parameter.

Abd Kadir, Rees, & Pop(Abd Kadir, Rees, & Pop, 2008) aimed to determine the effect of different conductivity ratios on forced convection past a circular cylinder embedded in a porous medium, where the solid cylinder forms a uniform heat source. They employed finite difference method to obtain the resulting steady-state solutions. They found that the thermal field within the cylinder and in the external porous region depends strongly on the ratio of the respective conductivities.

Berletta & Storesletten(Berletta & Storesletten, 2011) investigated the onset of convective rolls in a circular porous duct for various values of Biot number. The determination of the neutral stability along with the critical values of the wave number and the Rayleigh number were studied for different Biot numbers. The Galerkin finite-element method was used to solve the elliptic governing equations.

A numerical investigation of heat transfer in porous medium in cylindrical geometries/ cavity was carried out by Badruddin et.al.((I. A Badruddin, N. J. S Ahmed, et al., 2012; Badruddin, Zainal, Aswatha Narayana, & Seetharamu, 2006; Badruddin, Zainal, Aswatha Narayana, Seetharamu, & Siew, 2006; Badruddin, Zainal, Khan, & Mallick, 2007; Badruddin, Zainal, Narayana, & Seetharamu, 2006a, 2006b, 2006c) They employed the finite element method to convert non-linear partial differential equations into algebraic equations. They studied the effects of Rayleigh number, radiation parameter, aspect ratio, radius ratio etc. on the heat transfer and fluid flow behavior. Similar kind of study was carried out by Ahmed et.al. (N. J. S. Ahmed, I. A. Badruddin, Z. A. Zainal, H. M. T. Khaleed, & J. Kanesan, 2009; N. J. Salman Ahmed, Badruddin, Kanesan, Zainal, & Nazim Ahamed, 2011)

Chen & Sutton(Chen & Sutton, 2005) studied a circular geometry with inner layer occupied by the porous medium and outer layer by the fluid. They concluded that the increase of the Darcy number of porous medium will increase the heat transfer.

Shivakumara et al (Shivakumara, Prasanna, Rudraiah, & Venkatachalappa, 2002) carried a numerical investigation of transient free convection in a vertical cylindrical annulus filled with a fluid saturated porous medium with the inner wall heated to a uniform temperature, the outer wall cooled to a uniform temperature while the top and bottom surfaces were maintained adiabatically. A finite difference implicit method which incorporates upwind differencing for nonlinear convective terms and the successive line over relaxation (SLOR) method for convergence was used to solve the coupled nonlinear governing equations. The effects of Darcy number, radii ratio, viscosity ratio and Rayleigh number on the temperature and velocity fields were studied.

Rashad et al (Rashad & EL-Hakiem, 2007) studied the effects of both free convection and radiation with nonlinear Forchheimer terms from a vertical cylinder embedded in a fluid-saturated porous medium on fluid. They considered fluid viscosity to vary as an inverse linear function of temperature. The boundary-layer equations governing flow were solved numerically by using the second-level local non-similarity method, which was used to convert the non-similar equations into a system of ordinary differential equations.

Numerical results for dimensionless velocity, temperature profiles and the local Nusselt number were presented.

Minkowycz & Ping(Minkowycz & Ping, 1976) studied the natural convection in a vertical cylinder embedded in a saturated porous medium. They considered temperature of the wall varying along the height of the cylinder in a power law fashion.

Prasad & Kulacki(Prasad & Kulacki, 1984) studied the steady free convection in a vertical annulus filled with saturated porous medium. The vertical walls were maintained at varying temperature, whereas the horizontal surfaces were insulated. They concluded that the velocity of the fluid in the upper half of the annulus is higher than that of the velocity in the lower half of the annulus.

Rajamani et al(Rajamani, Srinivas, Nithiarasu, & Seetharamu, 1995)applied finite element method by employing Galerkin's approach to analyze free convection heat transfer in axisymmetric fluid saturated porous bodies. They studied the effect of aspect ratio and radius ratio on Nusselt number in the case of a porous cylindrical annulus. Two cases of isothermal and convective boundary conditions are considered. They concluded that the Nusselt number is always found to increase with radius ratio and Rayleigh number.

Hossain & Alim(Hossain & Alim, 1997) studied the interaction of natural convection and radiation on boundary layer flow along a thin vertical cylinder to predict the heat transfer rate by means of temperature profile, velocity profile and Nusselt Number for various parameters. The effects of the parameters such as the radiation parameter, $R_d$, the surface temperature parameter, $\theta w$, taking Prandtl number, Pr, equals 0.7, on temperature and velocity profile have been evaluated in the study and eventually graphically presented.

They concluded that the increment in the radiation parameter, $R_d$, or temperature parameter, $\theta_w$ resulted in the increase of the local heat transfer rate.

Reda(Reda, 1986) conducted an experiment on finite vertical cylinder. The study was based on the nuclear waste isolation in which the inner heat source along the length of the cylinder was maintained whereas the outer cylinder was maintained at constant temperature. He found that the radial temperature drops across the annulus systematically from the finite length cylinder conduction solution as heater power was increased.

**2.2.3 Vertical Plate/ Miscellaneous geometry:**

Kuznetsov & Nield(Kuznetsov & Nield, 2001) made an analytical investigation on the effects of variation of permeability and thermal conductivity on a fully developed forced convection in a parallel plate channel or circular duct filled with a saturated porous medium based on Darcy model for the cases of isoflux and isothermal boundaries. They found that the results for the circular duct are generally similar to those for the parallel plate channel and the most prominent difference being that the Nusselt numbers for the circular duct are generally higher than those for the parallel plate channel.

Mahmud & Fraser(Mahmud & Fraser, 2005) performed analytical and numerical analysis for fully developed forced convection in a fluid-saturated porous medium channel bounded by two parallel plates. The channel walls were assumed to be of finite thickness. The flow of heat transfer in porous material is described by the Darcy-Brinkman momentum equation. Analytical expressions for velocity, temperature, and Nusselt number were obtained after simplifying and solving the governing differential equations with reasonable approximations. They concluded that the velocity profiles are high near wall and flat near the center of the channel. Temperature profile inside the fluid region showed parabolic distribution while inside the solid wall linear. Lastly they observed that higher heat transfer rate occurs at lower clearance ratio and lower Darcy number.

Vaszi et al (Vaszi, Elliott, Ingham, & Pop, 2004) investigated two-dimensional conjugate free convection in a porous medium from a vertical plate fin. The governing equations of the convective flow in the porous medium were coupled to the governing equation for the heat flow in the fin by the conditions of continuity of the temperature and the heat flux at the solid/porous media interface. The governing non-dimensional parameters were the convection-conduction parameter and the aspect ratio of the fin. They solved the equations by using finite differences and iterative solution method. They concluded that for most values of the conduction-convection parameter, the total heat transfer from the fin increases with increasing values of the aspect ratio.

Char & Lin(Char & Lin, 2001) studied theoretically the conjugate film condensation and natural convection along the vertical plate between a saturated vapor porous medium and a fluid-saturated porous medium. The governing equations are solved using cubic spline collocation method and they concluded that as the Jakob number increases, the film thickness increases, while the plate temperature variation and the local heat transfer rate decreases.

Al-Amiri et al (Al-Amiri, Khanafer, & Pop, 2008) made a numerical investigation using finite element method for steady conjugate natural convection in a fluid-saturated porous cavity boarded to a conducting vertical wall. They predicted the fluid motion using the general formulation of the porous medium, which accounts for the inertial and solid viscous effect. The momentum and energy transport processes are explored and results of streamlines, isotherms, wall inter-face temperature and average Nusselt numbers are presented for a wide range of dimensionless parameters. Their results showed that as the wall thick-ness increases, the temperature difference between the inter-face temperature and the cold boundary reduces, which accordingly brings about a reduction in the overall Nusselt number.

Vaszi et al (Vaszi, Elliott, Ingham, & Pop, 2002) investigated the phenomenon of conjugate free convection in a semi-infinite porous medium above a heated finite plate using numerical solution and concluded that representation of fluid region in elliptical coordinates provides a very effective survey method which naturally magnifies the region close to the plate. In addition the use of inflow and outflow boundary conditions employed at the outer boundary allows a considerable reduction in the fluid region investigated for high Rayleigh numbers, which is extremely important because in this case a very refined mesh is required close to the plate.

Higuera & Pop(Higuera & Pop, 1997) studied the problem of coupled heat transfer by natural convection between two fluid-saturated porous media at different temperatures separated by a vertical conductive wall by investigating them analytically and numerically taking account of two-dimensional thermal conduction in the separating wall by considering the main parameters of the problem as the ratio of thickness to height of the wall and the ratio of the thermal resistance of one of the boundary layers to the thermal resistance of the wall. They observed asymptotic solutions for large and small values of heat conduction and aspect ratio.

Vaszi et al (Vaszi, Elliott, Ingham, & Pop, 2003) studied the problem of conjugate free convection in a porous medium from a vertical plate and a vertical cylindrical fin . The governing equations are coupled for the heat flow in the fin by the conditions of continuity for the temperature and the heat flux at the interface. They concluded that the thin fin approximation provides decreasing conjugate boundary temperature profiles with increasing values of the fin aspect ratio, when the model for a non-insulated fin tip is employed. For the larger aspect ratios more heat is conducted to the fluid by the tip of the fin, and also it was noticed apparently for the cylindrical fin as well but only for relatively small values of the conduction convection parameter.

Varol et al (Varol, Oztop, & Pop, 2009) studied the conjugate heat transfer via natural convection and conduction in a triangular enclosure filled with porous mediums; Darcy flow model is used to write governing equations with Boussinesq approximation. The transformed governing equations are solved numerically using finite difference technique. Numerical study is performed to examine the steady laminar natural convection conduction in triangular enclosure filled with fluid-saturated porous media with a conducting bottom solid wall for different Rayleigh number, thickness of the bottom wall and thermal conductivity ratio. They concluded that flow strength becomes lower for thin wall or low values of thermal conductivity ratio. It is also found that increasing of the thick wall, reduces the mean Nusselt number due to decreasing of temperature difference. For the constant wall thickness and thermal conductivity ratio, Nusselt number increases with increasing of Rayleigh number.

Shu & Pop(Shu & Pop, 1998) presented a theoretical study using Karman-Pohlhausen method for describing the transient heat exchange between the boundary-layer free convection and a vertical plate embedded in a porous medium. They observed the development of unsteady behavior after generation of an impulsive heat flux step at the right hand side of the plate while the left hand side of the plate is thermally insulated. They considered two cases of the plate with finite and no thickness. They addressed the problem by considering analytical and numerical solutions for all possible values of time and space evolution of the interface temperature.

Paik(Paik, Nguyen, & Pop, 1998) carried out numerical investigation of the transient conjugate mixed convection flow about a sphere embedded in a porous medium saturated with pure or saline water and they found that the heat capacity ratio between the sphere and the surrounding media has more significant effect on the calculated heat transfer rate than the thermal conductivity ratio.

DeGroot & Straatman(DeGroot & Straatman, 2011) proposed a numerical model for computing fluid flow and heat transfer in conjugate fluid-porous domains using unstructured, nonorthogonal grids. It is noticed that the major contribution of this model is its ability to use nonorthogonal grids to discretize complex geometries without affecting the robustness of the model.

Char, Lin, & Chen(Char, Lin, & Chen, 2001) investigated numerically the coupling of the wall conduction with laminar mixed-convection film condensation along a vertical plate within a saturated vapor porous medium. They employed Darcy-Brinkman-Forchheimer model to treat the flow field and the effect of heat conduction across the wall. The governing system of equations is solved using cubic spline collocation method. Their results has shown that the effect of wall conduction has great influences on the film wise condensation heat transfer, and reduces the local heat transfer rate and dimensionless interfacial temperature in comparison with the isothermal plate case. They also found that the local heat transfer rate increases with a decrease in the Jakob number, the Peclet number, and the inertial parameter or an increase in the conjugate heat transfer parameter.

Belleghem et al (Belleghem, Backer, Janssens, & Paepe, 2012) considered dried medium as a porous material and drying medium as moist air. The emphasis is laid on the modelling of convective drying of porous building materials by implementing a boundary condition. They developed a model to simulate the convective drying of a sample of a ceramic brick.

These simulations were then compared with measurements from literature and a good agreement was found. They employed validated finite volume HAM (Heat, Air and Moisture transport) model and their results were in agreement with the experiments found in literature.

Nield & Kuznetsov(D. A. Nield & Kuznetsov, 2004) investigated analytically forced convection in a plane channel filled with a saturated bi-disperse porous medium, coupled with conduction in plane slabs bounding the channel on the basis of two-velocity and two-temperature model. They concluded that decrease in Nusselt number (Nu) also decreases Biots number (Bi).

Mendez et al (Mendez, Trevino, Pop, & Linan, 2002) studied the steady state heat transfer characteristics of a thin vertical strip with internal heat generation placed in a porous medium. They considered non-dimensional temperature distribution in the strip. They concluded that the mass flow rate of fluid induced by heating the strip decreases as the longitudinal heat conduction effects along the strip decreases.

Al-Farhany & Turan(Al-Farhany & Turan, 2011b) carried the numerical investigation on unsteady conjugate natural convective heat transfer in a two-dimensional porous cavity sandwiched between two finite thickness walls comprising an isotropic porous medium. The outer surfaces of the vertical walls are maintained at fixed different temperatures, while the horizontal boundaries of the cavity are adiabatic. Boussinesq approximation model is used to solve the governing equations in the saturated porous region. A finite volume approach is used to solve the non-dimensional governing equations. Their results has shown that as the Darcy number increases, the average Nusselt number decreases and the time required to reach steady state is longer, while the time required to reach steady state is shorter for high Rayleigh number and longer for the low Rayleigh number.

Betchen et al (Betchen, Straatman, & Thompson, 2006) proposed a mathematical and numerical model for the treatment of conjugate fluid flow and heat transfer problems in domains containing pure fluid, porous, and pure solid regions. The model is developed for implementation on a simple collocated finite-volume grid and allows for local thermal non-equilibrium in the porous region. Rigorous validations have demonstrated the ability of the model to provide accurate solutions to a variety of problems.

C. S. Lee et al (C. S. Lee, Haghighat, & Ghaly, 2006) developed an analytical and numerical method using conventional convection approach. The simulation results indicated that the effect on the volatile organic compounds source/sink behavior is quantified by the total transfer time, this model results in less than 5% error in the predicted value.

Nield & Kuznetsov(D. A. Nield & Kuznetsov, 1999) carried analytical investigation on forced convection in a plane channel filled with a saturated porous medium, coupled with conduction in plane slabs bounding the channel on the basis of a two-temperature model allowing for local thermal nonequilibrium and it is found that the effect of the finite thermal resistance due to the slabs is to reduce both the heat transfer to the porous medium and the degree of local thermal nonequilibrium.

El-Shaarawi et al (El-Shaarawi, Al-Nimr, & Al Yah, 1999) conducted a parametric study to explore the effects of the Darcy number, the inertia term, the Peclet number and the porous medium heat capacity ratio on the transient thermal behavior in a given annulus. They concluded that the axial conduction can be neglected for Peclet number greater than 120 and increasing the porous medium thermal capacity ratio increases the heat transfer by reducing the thermal entrance length.

Wong & Saeid(Wong & Saeid, 2009) carried numerical investigation on the mixed convection-conduction problem of impingement cooling of a finite thickness solid wall conjugated with a porous medium. The heat transfer is examined over wide ranges of governing parameters such as Rayleigh number, Peclet number, solid wall thickness, heat transfer coefficient parameter and solid wall thermal conductivity . They found that the average Nusselt number increases with the increase in solid wall thermal conductivity and the increase in thickness of the solid wall decreases the average Nusselt numbers.

Zhang et al (Zhang, Zou, Li, & Ye, 2011) employed Darcy-Brinkman-Forchheimer model and finite volume method to simulate coupled fluid flow and heat transfer problems in hybrid porous/fluid/solid domains. They found that when the flow direction is parallel to the porous/fluid interface, the interfacial stress-continuity and stress-jump conditions have obvious effects on velocity profiles but when the flow direction is almost normal to the interface, the effects of the interfacial stress-continuity and stress-jump conditions are weak.

**2.3 Conjugate heat and mass transfer on MHD:**

Pathak et al (Pathak, Mulcahey, & Ghiaasiaan, 2013) studied numerically hydrodynamics and conjugate heat transfer in porous media subjected to unidirectional-steady state as well as steady-periodic flow. They simulated two-dimensional flows in porous media composed of periodically configured arrays of square cylinders using computational fluid dynamics tool. Simulations were conducted for flow oscillation frequencies of 0-60 Hz, and low and high velocity amplitudes for a 75% porous domain. They concluded that the proposed method can be used as a computational aid to study the effects of pore-scale energy transport on its macroscopic behavior for cases where geometrically complex flow domains and interphase thermal coupling are important.

Ali et al (Ali, Khan, Samiulhaq, & Shafie, 2013) studied the combined effects of radiation and chemical reaction on magneto hydrodynamic (MHD) free convection flow of an electrically conducting incompressible viscous fluid over an inclined plate embedded in a porous medium. The dimensionless momentum equation coupled with the energy and mass diffusion equations are analytically solved using the Laplace transform method. They concluded that: the effects of the permeability and magnetic parameters on velocity are opposite, velocity increases with increasing permeability, Grashof number, radiation parameter and time.

Kaya(Kaya, 2012) investigated the flow and heat transfer characteristic for the non-Darcy Magneto hydro dynamics(MHD) mixed convection flow over a thin vertical plate with wall conduction effect in the porous medium of high porosity. The fluid is assumed to be incompressible and dense. The nonlinear coupled parabolic partial differential equations governing the flow are transformed into the non-similar boundary layer equations, which are then solved numerically using the Keller box method. The author concluded firstly that an increase in the conjugate heat transfer parameter decreases the velocity and the temperature gradient and therefore decreases the dimensionless interfacial temperature distribution, the local skin friction, and the local heat transfer parameters and secondly an increase in the porous medium parameter and Forchheimer parameter increases the local skin friction and local heat transfer parameters and decreases the dimensionless interfacial temperature distributions.

### 2.4 Conjugate heat and mass transfer:

Belleghem (Belleghem et al., 2012) gave a short overview of the state of the art in conjugate heat and mass transport modelling for convective drying. The review highlighted shortcomings of currently applied modelling approaches and they developed a new model to simulate the convective drying of a sample of ceramic brick. They concluded that the discrepancies between the experiments and the model were because of three causes: uncertainty of the material properties, deviations between measurements and simulations and the correct implementation of the boundary conditions.

Lopez Penha et al(Lopez Penha et al., 2012) developed a computational method using numerical method for performing pore-scale (microscopic) simulations of fluid flow and conjugate heat transfer. It is noticed that the proposed method can be used as a computational aid to study the effects of pore-scale energy transport on its macroscopic behavior for cases where geometrically complex flow domains and interphase thermal coupling are significant. They observed that the computed Nusselt number predictions were accurate for very modest grid resolutions, with a maximum relative error of approximately 3% for flow in a square tube with 16 x 16 grid points in cross section. Accurate results were obtained for flow domains that were aligned with the grid showing second-order convergence of the field variables.

Khan et al (Khan, Fischer, & Straatman, 2015) presented a numerical formulation capable of simulating fluid flow and non-equilibrium heat and mass transfer in three-dimensional conjugate fluid/solid/porous domains. The governing transport equations are presented for the fluid, solid and porous regions, with special consideration given towards the manner in which moisture is accounted for in the air-water vapour mixture. The results show that model predictions follow the expected trends with respect to flow Reynolds number and inlet relative humidity.

Wu et al(Wu et al., 2004) developed a model for the conjugate heat and mass transfer for microwave freeze drying within porous media with dielectric cores. The set of governing equations were developed using finite volume method with variable time-steps and concluded that the size and loss factor of the dielectric core are the two important parameters influencing the drying process and careful choosing of loss factor and size of the dielectric cores could dramatically reduce the drying time.

Aleshkova & Sheremet(Aleshkova & Sheremet, 2010) carried out mathematical simulation of unsteady natural convection modes in a square cavity filled with a porous medium having finite thickness heat-conducting walls with local heat source in conditions of heterogeneous heat exchange with an environment at one of the external boundaries. Numerical analysis was based on Darcy-Forchheimer model in dimensionless variables such as a stream function, a vorticity vector and a temperature. It is noticed that the increase in the dimension less time leads to warming up of the gas cavity and the prevention of cooling of the object of research owing to the influence of an environment. Lastly they concluded that the conduction starts to dominate at the reduction of the permeability of medium that leads to decrease in the average Nusselt number at an internal surface of the left solid wall.

Oliveira & Haghighi(Oliveira & Haghighi, 1998) proposed a methodology for the analysis of conjugate problems in the convective drying of porous media. In this study the interface between porous medium and external convective flow is treated as an internal boundary within a two-phase system rather than a geometric limit. The performance of the proposed methodology is evaluated by applying it to wood-drying problems. A finite-element code was developed to solve the set of equations for the heat and mass transport in both the porous medium and the boundary layer. Their results agreed with the expected physical behavior and were indicative for the good performance of the proposed solution methodology.

Mikhail A. Sheremet & Trifonova(Mikhail A. Sheremet & Trifonova, 2013a) studied numerically the transient natural convection in a vertical cylinder partially filled with a porous media with heat-conducting solid walls of finite thickness in conditions of convective heat exchange with an environment and they employed Darcy and Brinkman extended Darcy models with Boussinesq approximation to solve the flow and heat transfer in the porous region. The Oberbeck-Boussinesq equations have been used to describe the flow and heat transfer in the pure fluid region. The Beavers-Joseph empirical boundary condition is considered at the fluid-porous layer interface with the Darcy model. The governing equations were formulated in terms of the dimensionless stream function, vorticity, and temperature has been solved using the finite difference method. They considered the influence of Darcy number, porous layer height ratio, thermal conductivity ratio and dimensionless time on the fluid flow and heat transfer on the basis of the Darcy and non-Darcy models. They have done comprehensive analysis of an effect of these key parameters on the Nusselt number at the bottom wall, average temperature in the cylindrical cavity, and maximum absolute value of the stream function. They concluded that an increase in conductivity ratio leads to more essential quantitative differences between the results obtained on the basis of the Darcy model and the Brinkman-extended Darcy model.

M. A. Sheremet & Pop(M. A. Sheremet & Pop, 2014) investigated steady-state natural convection heat transfer in a square porous enclosure having solid walls of finite thickness and a conductivity filled by a nanofluid model proposed by Buongiorno. The nanofluid model took into account the Brownian diffusion and thermophoresis effects. The governing equations were solved by finite difference method. They concluded that high thermophoresis parameter, low Brownian motion parameter, low Lewis and Rayleigh numbers and high thermal conductivity ratio reflected essential non-homogeneous distribution of the nanoparticles inside the porous cavity.

Al-Farhany & Turan(Al-Farhany & Turan, 2011a) carried a numerical study on steady conjugate double-diffusive natural convective heat and mass transfer in a two-dimensional variable porosity layer sandwiched between two walls. They employed Forchheimer-Brinkman-extended Darcy model to solve the governing equations in the saturated porous region. The governing equations are solved using finite volume method. They concluded that the Nusselt number increases when the Rayleigh number increases, while it decreases when the thermal conductivity ratio, Lewis number and the wall thickness increase.

Lamnatou et al (Lamnatou, Papanicolaou, Belessiotis, & Kyriakis, 2010) employed the numerical procedure for modelling the heat/mass transfer based on Luikov's model and finite-volume method. The results exhibited a realistic physical behavior for a range of materials compared to results available in literature. They concluded that the aspect ratio of the drying plate and flow separation phenomena can influence the flow field as well as heat/mass transfer coefficients and they found that reduction of plate thickness combined with the blockage effect as well as with the increase of the contact surfaces between solid and fluid can lead to higher heat/mass transfer coefficients and thus better drying behavior.

Defraeye et al (Defraeye, Blocken, & Carmeliet, 2011) analyzed convective drying of an unsaturated porous flat plate at low Reynolds numbers by means of conjugate modelling of heat and mass transport in the air flow and porous material. Comparisons are made with porous-material modelling using spatially and/or temporally constant convective transfer coefficients. Both spatial and temporal variations of the convective boundary conditions are found to have a distinct impact on the drying behavior.

Juncu(Juncu, 2014) carried out numerical investigation to study the influence of the porous media permeability on the unsteady conjugate heat transfer from a permeable sphere embedded in another porous medium. The flow inside and outside of the sphere is considered to be two dimensional. It is found that their results show the local Nusselt number profiles are similar to those of the surface radial velocity, regardless of the values of the conductivity ratio.

**Table: 2.1:**Conjugate heat transfer in various porous geometries

| Phenomenon | Geometry | Solid wall position | Author |
|---|---|---|---|
| Conjugateheat transfer | Porous Annular vertical cylinder | Inner surface | (Salman et al., 2014) |
| | Triangular | Bottom left | (Chamkha & Ismael, 2013b) |
| | Porous channel | Bounded by parallel plates | (Mahmud & Fraser, 2005) |
| | Porous channel(LTNE) | Slabs bounding the channel | (D. A. Nield & Kuznetsov, 1999) |
| | Porous channel(BDPM) | Slabs bounding the channel | (D. A. Nield & Kuznetsov, 2004) |
| | Rectangular | Top and bottom | (A. C. Baytas et al., 2001) |
| | | Left and right side | (Nawaf H. Saeid, 2007) |
| | | Left side | (Al-Amiri et al., 2008) |
| | | Left and right side | (Alhashash et al., 2013) |
| | | Left side | (Saleh & Hashim, 2012) |
| | | Centre | (Kaya, 2012) |
| | Arbitrary | Vertical slender, hollow circular cylinder | (Kaya, 2011) |
| | | Vertical plate fin | (Vaszi et al., 2002) |
| | | Vertical wall | (Higuera & Pop, 1997) |
| | | Vertical rounded fin Rounded tip | (Vaszi et al., 2004) |
| | | bottom | (Varol et al., 2009) |
| | | Vertical plate | (Shu & Pop, 1998) |
| | | Circular cylinder | (Abd Kadir et al., 2008) |
| | | Sphere | (Paik et al., 1998) |
| | | Unstructured grids | (DeGroot & Straatman, 2011) |

| Phenomenon | Geometry | Solid wall position | Author |
|---|---|---|---|
| Conjugate heat and mass transfer on MHD | Inclined plate | | (Ali et al., 2013) |
| Conjugate heat and mass transfer | Square | Bottom center | (Aleshkova & Sheremet, 2010) |
| | | Bottom | (Oliveira & Haghighi, 1998) |
| | | Top, Bottom | (Mikhail A. Sheremet & Trifonova, 2013a) |
| | | Left side and right side corner | (M. A. Sheremet & Pop, 2014) |
| Conjugate heat and mass transfer | Rectangular | Left and Right | (Al-Farhany & Turan, 2011a) |
| | Drying-chamber scale | Centre | (Lamnatou et al., 2010) |
| | Arbitrary | Flat plate | (Defraeye et al., 2011) |
| | | Spherical | (Juncu, 2014) |

**Table: 2.1:** continued…

## 2.5 Numerical Methodology

Partial differential equations (PDE) are fundamental to the modeling of natural phenomena. The typical problem in partial differential equations consists of finding the solution of a PDE or a system of PDEs subjected to certain boundary conditions. The nature of boundary and initial conditions which lead to well-posed problems depends in a very essential way on the specific PDE under consideration.

The methods such as FEM, FDM, and FVM are so important in engineering practice they consume an enormous number of CPU cycles. Finite element solvers are not easy to write; most people use dedicated packages. In addition to the core routines for solving large sparse matrix problems and systems of ordinary differential equations, it is necessary to specify the input geometry and then visualize the output results.

In mathematics, computer science and operations research, mathematical optimization alternatively, optimization or mathematical programming is the selection of a best element with regard to some criteria from some set of available alternatives.

The principle of all methods for the numerical solution of PDEs is to obtain discrete numerical values that is, a finite number which ‘approximate’ (in a suitable sense, to be made precise) the exact solution. In this process two fundamental points are to be noted: first, we do not calculate exact solutions but approximate ones; second, we discretize the problem by representing functions by a finite number of values, that is, we move from the ‘continuous’ to the ‘discrete’. There are numerous methods for the numerical approximation of PDEs. The oldest and simplest, called the finite difference method and another method, called the finite element method.

The advent of computers and the development of advanced numerical techniques and powerful computers in the late 1970s, the solution of complex heat transfer problems in porous medium became humanly possible and economically viable. Since then heat transfer problems have been investigated extensively, The Numerical Techniques such as Finite Element Method, Finite difference method and Finite volume methods etc. were employed to solve the system of coupled equations for heat and mass transfer inside the porous medium. The heat and mass transfer coefficients were evaluated iteratively. The finite volume method was used to discretize and solve the highly nonlinear system of coupled differential equations.(Oliveira & Haghighi, 1998). Table 2.2 shows some of the literature work in porous medium with various kinds of numerical methods being adopted.

**Table 2.2:** Porous medium with various numerical methods

| **Method** | **Author** |
|---|---|
| Finite Element Method | (Oliveira & Haghighi, 1998)<br>(Salman et al., 2014)<br>(Badruddin et al., 2015)<br>(Badruddin, Al-Rashed, Salman Ahmed, & Kamangar, 2012)<br>( N. J Salman Ahmed, Badruddin, Zainal, Khaleed, & Kanesan, 2009)<br>(I. A Badruddin, Z. A. Zainal, A. P. A. Narayana, & K. N. Seetharamu, 2006b)<br>(I.  A Badruddin, Abdullah A. A. A. Al-Rashed, et al., 2012)<br>(Badruddin, Zainal, Narayana, et al., 2007)<br>(I. A Badruddin, Z. A. Zainal, A. P. A. Narayana, & K. N. Seetharamu, 2006a)<br>(I. A. Badruddin, Z. A. Zainal, A. P. A. Narayana, K. N. Seetharamu, & L. W. Siew, 2006)<br>(I. A Badruddin, Z. A. Zainal, A. P. A. Narayana, & K. N. Seetharamu, 2006c) |
| Finite Volume Method | (Belleghem et al., 2012)<br>(Lamnatou et al., 2010)<br>(Z. Tao et al., 2005) |
| Finite Difference Method | (Mikhail A. Sheremet & Trifonova, 2013a)<br>(M. A. Sheremet & Pop, 2014)<br>(Chamkha & Ismael, 2013b)<br>(Vaszi et al., 2004)<br>(Varol et al., 2009)<br>(Abd Kadir et al., 2008)<br>(El-Shaarawi et al., 1999)<br>(Mikhail A. Sheremet & Trifonova, 2013b), (Juncu, 2014) |
| Laplace Transform Method | (Ali et al., 2013) |
| Keller Box Method | (Kaya, 2012)<br>(I. Pop & Na, 2000) |
| Cubic Spline Collocation Method | (Char & Lin, 2001) |
| Finite Volume Method | (Zhang et al., 2011)<br>(Wong & Saeid, 2009)<br>(Nawaf H. Saeid, 2007)<br>(Wu et al., 2004) |
| Finite Volume HAM(Heat Air and Moisture Transport) Model | (Belleghem et al., 2012) |

## 2.6 Introduction to Optimization

Optimization is a very old subject which has shown resurgence since the appearance of computers and whose methods are applied in numerous domains: economics, management, planning, logistics, robotics, optimal design, engineering, signal processing, etc. Optimization is also a vast subject which touches on calculus of variations, operations research (optimization of management or decision processes), and optimal control.

Henderson et al (Henderson, Brêttas, & Sacco, 2015) discussed the applicability of the three-parameter Kozeny–Carman generalized equation to trigger immiscible viscous fingers and described it in a fractal heterogeneous porous media, with numerical simulations of water flooded operations in oil reservoirs. Numerical results were generated from intensive simulations and viscous fingers were visualized graphically for three different well patterns: Line-Drive, Five-Spot and Inverted Five-Spot. Their results concluded that the TPKCG (three-parameter Kozeny–Carman generalized) equation is a theoretical tool to be used in numerical simulations of oil recovery processes, including those susceptible to hydrodynamic instability phenomena.

Das & Prasad(Das & Prasad, 2015) considered the inverse problem through a porous fin, aiming to retrieve the fluid's diffusivity and the fin's porosity using temperature at three points using DE(Differential Evolution) optimization technique. Their results have concluded that DE can retrieve the value of porosity quite well, but the diffusivity of the fluid is rather difficult to retrieve.

Feng(Feng, 1997) studied porous medium equation on a d-dimensional torus obtained as a hydrodynamic scaling limit, with the usual diffusion scaling, of the empirical measures of a sequence of reversible Markov jump processes on approximating periodic lattices. Each process is viewed as a randomly interacting configuration of sticks (or energies, etc.) The configuration evolves through exchanges of stick portions that occur between nearest neighbours through a zero-range pressure mechanism, with conservation of total sticklength.

Horgue et al (Horgue, Soulaine, Franc, Guibert, & Debenest, 2015) developed a toolbox OpenFOAM(Open source Field Operation And Manipulation) which includes libraries for porous models (relative permeability, capillary pressure and phase model) and a specific porous boundary condition. A classical IMPES (IMplicit Pressure Explicit Saturation) solver has been developed to validate the provided models by comparison with analytical solutions. A study on the parallel efficiency (up to 1024 cores) has also been performed on a complex multiphase flow. The underlying idea of this approach is to provide an easily adaptable tool that can be used in further studies to test new mathematical models or numerical methods.Lastly they concluded that the easily modifiable nature of the OpenFOAM platform can be useful to test new numerical schemes or solution methods.

Di Pietro et al (Di Pietro, Flauraud, Vohralík, & Yousef, 2014) derived a posteriori error estimates for the compositional model of multiphase darcy flow in porous media, consisting of a system of strongly coupled nonlinear unsteady partial differential and algebraic equations. They demonstrated how to control the dual norm of the residual augmented by a nonconformity evaluation term by fully computable estimators. Later they decomposed the estimators into the space, time, linearization, and algebraic error components;this allowed them to formulate criteria for stopping the iterative algebraic solver and the iterative linearization solver when the corresponding error components do not affect significantly the overall error. However, the spatial and temporal error components were balanced by time step and space mesh adaptation. Their analysis is applied to a broad class of standard numerical methods, and is independent of the linearization and of the iterative algebraic solvers employed. Numerical results on two real-life reservoir engineering examples confirm that significant computational gains can be achieved on fixed meshes, without any noticeable loss of precision.

Rohan & Lukeš(Rohan & Lukeš, 2015) proposed a nonlinear extension of the standard Biot continuum which was derived by upscaling the fluid–structure interaction problem at the microscopic level. This model allows for respecting a kind of the physical nonlinearity, in particular, the influence of deformation on the effective permeability and other poroelastic material coefficients; for each of these coefficients linear expansions were obtained using the material derivative approach applied to differentiate the associated Integral formulae involving the characteristic microstructure responses. To solve numerically the nonlinear problem arising after the time discretization, they proposed an algorithm based on the Newton–Raphson iterations. They concluded that the numerical examples reported only 3 to 4 iterations to resolve the problem of one time increment step with a given tolerance, whereby the rate of convergence was better than $10^2$.

Cimolin & Discacciati(Cimolin & Discacciati, 2013) considered the modeling and numerical simulation of incompressible fluid flows in regions partially occupied by porous media. The motivation for this work came from a specific industrial problem of internal ventilation for motorcycle helmets. They concluded that the NSF (Navier–Stokes/Forchheimer) model allows representing carefully the physics of the problem since it permits to precisely locate the interface and it features ad-hoc models for each sub region. Moreover, its implementation was rather complex and its solution required ad-hoc algorithms whose convergence properties were varying depending on the considered problem.

Sadegh Zadeh & Montas(Sadegh Zadeh & Montas, 2014) developed multi-objective optimization algorithm and applied to parameterize bio-fluid flow processes in partially saturated porous media. They formulated the forward problem as a nonlinear partial differential equation and solved it by an efficient Galerkin finite element method. They validated numerical simulator with reference and analytical solutions. The inverse problem was formulated in a nonlinear optimization framework in which model parameters were estimated by minimizing a complex penalty function, representing the discrepancies between the observed and predicted attributes of the physical system. They investigated several optimization scenarios and concluded that the proposed multi-objective optimization shows excellent agreements with the experimental datasets for all state variables.

Gunzburger et al (Gunzburger, Peterson, & Kwon, 1999) presented optimization-based domain decomposition method for the solution of partial differential equations. The existence of optimal solutions for the optimization problem is shown as the convergence to the exact solution of the given problem. They derived an optimality system of partial differential equations from which solutions of the domain decomposition problem was determined. Finite element approximations to solutions of the optimality system were defined and analyzed as well as an eminently parallelizable gradient method is developed for solving the optimality system. Lastly they concluded the results of some numerical experiments and extended the method to nonlinear problems such as the Navier-Stokes equations.

Khader et al (Khader, Sweilam, & Mahdy, 2015) considered two efficient numerical methods for solving system of fractional differential equations (SFDEs) . They described fractional derivative in the Caputo sense. The first method is based upon Chebyshev approximations, where the properties of Chebyshev polynomials are utilized to reduce SFDEs to system of algebraic equations; the second method is the fractional finite difference method (FDM), where they implemented the Grunwald–Letnikov's approach. They studied the stability of the obtained numerical scheme. They laid special attention to study the convergence and estimate the error of the presented methods. They presented Numerical examples to illustrate the validity and the great potential of both proposed techniques. Lastly they concluded that these solutions are in excellent agreement with the exact solution.

Kamali et al (Kamali et al., 2015) presented an implementation of a nontraditional modified ant colony programming (ACP). The modified ACP algorithm was unique as it does not use the criteria of distance. It utilized the probability function which related to the quantity of the pheromone level in the ACP. The Comparison between the ACP and the Genetic Programming (GP) method showed that the present ACP gives faster solutions within reasonable range of average number of generations. Lastly they concluded that ACP can be used to solve complicated differential equations with reasonable computational time and the average number of generations for finding the solutions increases as the differential equations becomes more difficult.

D. Lee et al(D. Lee et al., 2012) presented optimization strategies for compute- and memory-bound algorithms for the Compute Unified Device Architecture (CUDA). For compute-bound algorithms, the registers are reduced through variable reuse via shared memory and the data throughput is increased through heavier thread workloads and maximizing the thread configuration for a single thread block per multiprocessor. For memory-bound algorithms, fitting the data into the fast but limited GPU resources is achieved through reorganizing the data into self-contained structures and employing a multi-pass approach. Lastly they concluded by considering their two applications, by demonstrating the optimized GPU implementations performing 1.2× to 6× faster than unoptimized ones. Overall, a peak speedup of 129× over CPU implementations for the 3D unbiased image registration and 93× for the level set based non-local means surface shape denoising are achieved by reducing the registration computational time from 7.2 h to 2.5 min and the denoising time from 7.3 h to 4.6 min.

Schittkowski (Schittkowski, 2004) presented a couple of practical applications from industry and academia, to give an impression on the complexity of real-life systems of partial differential equations. The domains of application are pharmaceutics, geology, mechanical engineering, chemical engineering, food engineering, and electrical engineering.

McCall(McCall, 2005) presented an introduction to Genetic Algorithms(GAs) aimed at immunologists and mathematicians interested in immunology. They described how to construct a GA and the main strands of GA theory before speculatively identifying possible applications of GAs to the study of immunology. Lastly an illustrative example of using a GA for a medical optimal control problem is provided. They concluded by including a brief account of the related area of artificial immune systems.

Elsheikh (Elsheikh, 2015) presented Algorithmic Differentiation (AD) approach for sensitivity analysis of Differential Algebraic Equation systems (DAEs). The Algorithmic specification of a computationally memory-efficient equation-based AD technique is elaborated. This approach is mainly targeted towards equation-based modeling and simulation tools capable of constructing high-level models using state of the art object-oriented modeling principles. The author's approach is based on fundamental tree algorithms that are applicable on implicit equation systems of long formulas, the main building blocks of model components. The author concluded that the runtime performance using modern variable-step integration methods tends to achieve the expected theoretical complexity of the forward differentiation scheme under few realistic assumptions.

Katsikadelis(Katsikadelis, 2011) presented a numerical method for the solution of partial fractional differential equations (FDEs) arising in engineering applications and in general in mathematical physics. The author provided a solution procedure that can be applied to both linear and nonlinear problems described by evolution type equations involving fractional time derivatives in bounded domains of arbitrary shape. Their method is based on the concept of the analog equation, which in conjunction with the boundary element method (BEM) enables the spatial discretization and converts a partial FDE into a system of coupled ordinary multi-term FDEs. Lastly the method is illustrated by solving second order partial FDEs and its efficiency and accuracy are validated.

Chaquet & Carmona(Chaquet & Carmona, 2012) presented a mesh-free approach for solving differential equations based on Evolution Strategies (ESs) . Any structure is assumed in the equations making the process general and suitable for linear and nonlinear ordinary and partial differential equations (ODEs and PDEs), as well as systems of ordinary differential equations (SODEs). Candidate solutions are expressed as partial sums of Fourier series. Harmonic coefficients are taken into account one by one starting with the lower order ones. Experimental results are reported on several problems extracted from the literature to illustrate the potential of the proposed approach. Two cases (an initial value problem and a boundary condition problem) have been solved using numerical methods and a quantitative comparative is performed. Lastly they concluded that in terms of accuracy and storing requirements the proposed approach outperforms the numerical algorithm.

A general algorithm is presented to approximately solve a great variety of linear and nonlinear ordinary differential equations (ODEs) independent of their form, order, and given conditions. The ODEs are formulated as optimization problem. Some basic fundamentals from different areas of mathematics are coupled with each other to effectively cope with the propounded problem. The Fourier series expansion, calculus of variation, and particle swarm optimization (PSO) are employed in the formulation of the problem. Both boundary value problems (BVPs) and initial value problems (IVPs) are treated in the same way. Boundary and initial conditions are both modeled as constraints of the optimization problem. The robust metaheuristic optimization technique of the PSO is employed to find the solution of the extended variation problem. Finally, illustrative examples demonstrate practicality and efficiency of the presented algorithm as well as its wide operational domain. (Babaei, 2013)

Riesinger et al (Riesinger, Neckel, Rupp, Hinojosa, & Bungartz, 2014) presented an optimized Graphical Processing Unit ( GPU) implementation for a random ordinary differential equation (RODE) approach to simulations of multi-storey wireframe buildings under earthquake excitations using the Kanai-Tajimi model. As pseudo random number generation is the most time-consuming part of the application, a representative set of different Pseudo Random Number Generators (PRNGs) has been benchmarked. The resulting optimized variants outperform standard library implementations. The techniques and improvements shown in this contribution can be generalized to other RODE or stochastic models. Current work is on higher-order RODE schemes to complement the Averaged Euler method and allow time integration with arbitrary order.

Zelinka(Zelinka, 2015) presented history of swarm and evolutionary algorithms and discussed in general their dynamics, structure and behavior. The core of this paper is an overview of an alternative way on how dynamics of arbitrary swarm and evolutionary algorithms can be visualized, analyzed and controlled. Swarm and evolutionary based algorithms representing a class of search methods that can be used for solving optimization problems mimic natural principles of evolution and swarm based societies like ants, bees, by employing a population-based approach in mutual communication and information sharing and processing, including randomness. Lastly selected representative applications are discussed at the end.

Save et al (Save, Narayanan, & Patkar, 2011)presented a general scheme for converting the linear equations arising from FEM to the constraints of an electrical network. The conversion is element by element and therefore linear in time on the size of the problem. For convenience, they have used the linear shape function. However, the approach is also valid for Higher order shape functions as, even in that case, the resultant matrix arising from FEM is linear. They have validated their approach by solving some typical Partial Differential Equations with known solution: Poisson equation, another elliptical PDE, a time dependent parabolic PDE, and a nonlinear PDE. All of these were over a rectangular domain. Lastly they concluded Limitations of the approach are identical to those of standard FEM.

Based on the idea of equidistributing meshes Deng et al (Deng, Zhao, & Wu, 2015) designed efficient numerical schemes, which have linearly increasing computation cost with time t but not losing the accuracy at the same time. Error estimates for the proposed schemes are performed; and the numerical examples demonstrated the efficacy of algorithms.

## 2.7 Summary

From the above literature survey it is evident that there is not much of effort dedicated to study the effectiveness of currently available technique to solve the conjugate heat or conjugate heat and mass transfer in porous medium. Since the solution is dependent on numerical techniques that in turn generate huge number of equations leading to consumption of large amount of computational time to solve them. Thus, there seems to be a need to develop an alternate way to reduce the time required to solve those equations. Apart from this, it is very clear that the conjugate heat transfer or conjugate heat and mass transfer has been studied by considering the large size of solid either embedded to left, right top and bottom of cavity. There is no study that has investigated the effect of small solid being placed at various locations inside the porous region. This scenario arises in drying processes or electronic devices where a small solid could be placed in the porous domain. Thus, it necessitates the investigation of effect of size and location of solid being placed in the porous domain. The current study is undertaken to address this particular problem.

# CHAPTER 3 : MATHEMATICAL MODELING

## 3.1 Introduction

Mathematics is the fundamental tool for any simulation. The present chapter is dedicated to describe the mathematical modeling of the problem under investigation. It is worth mentioning that the present work is based on Darcy flow model. As pointed out previously, the present work revolves around porous media enclosed in a square cavity. The following section deals with mathematical modeling of heat as well as heat and mass transfer in a porous cavity.

## 3.2 Governing equations for heat transfer in cavity

Consider a porous cavity having the dimension LxL saturated with fluid. The x and y coordinates are taken along the horizontal and vertical directions respectively. The following assumptions are applied.

- The convective fluid and the porous medium are in local thermodynamic equilibrium in the domain.
- There is no phase change of the fluid in the medium.
- The properties of the fluid and those of the porous medium are homogeneous and isotropic.
- Fluid properties are constant except the variation of density with temperature.
- The radiative heat flux in the y-direction is negligible in comparison to that in the x-direction.

With above mentioned assumptions the governing equations in Cartesian coordinates can be written as

The continuity equation:

$$\frac{\partial \mathrm{u}}{\partial x}+\frac{\partial \mathrm{v}}{\partial y}=0 \tag{3.2.1}$$

The fluid velocity in *x* and *y* directions can be described by Darcy law as:

Velocity in horizontal direction

$$\mathrm{u}=\frac{-K}{\mu}\frac{\partial p}{\partial x} \tag{3.2.2}$$

Velocity in vertical direction

$$\mathrm{v}=\frac{-K}{\mu}\left(\frac{\partial p}{\partial y}+\rho g\right) \tag{3.2.3}$$

The permeability $K$ of porous medium can be expressed as (Donald A Nield & Bejan, 2006) $K=\dfrac{D_p{}^2\varphi^3}{180(1-\varphi)^2}$ (3.2.4)

The variation of density with respect to temperature can be described by Boussinesq approximation as:

$$\rho=\rho_\infty\left[1-\beta_T(T-T_\infty)\right] \tag{3.2.5}$$

The equations (3.2.2) and (3.2.3) have pressure terms in respective direction. In order to facilitate the solution, these terms can be eliminated by mathematical operations.

Differentiating equation (3.2.2) with respect to *y* yields:

$$\frac{\partial u}{\partial y}=\frac{-K}{\mu}\frac{\partial^2 p}{\partial x\partial y} \tag{3.2.6}$$

Similarly differentiating equation (3.2.3) with respect to *x* after incorporating Boussinesq approximation results:

$$\frac{\partial \mathrm{v}}{\partial x} = \frac{-K}{\mu}\left(\frac{\partial^2 p}{\partial y \partial x} - \rho_\infty \beta_T g \frac{\partial T}{\partial x}\right) \tag{3.2.7}$$

Eliminating pressure term from equation (3.2.6) and (3.2.7) gives:

$$\frac{\partial \mathrm{v}}{\partial x} - \frac{\partial \mathrm{u}}{\partial y} = \frac{gK\beta}{\nu}\frac{\partial T}{\partial x} \tag{3.2.8}$$

The energy equation is given as:

$$\mathrm{u}\frac{\partial T}{\partial x} + \mathrm{v}\frac{\partial T}{\partial y} = \alpha\left(\frac{\partial^2 T}{\partial x^2} + \frac{\partial^2 T}{\partial y^2}\right) - \frac{1}{\rho C_p}\frac{\partial q_r}{\partial x} \tag{3.2.9}$$

The last term on right hand side of equation (3.2.9) describes the radiation and can be approximated by Rosseland hypothesis (Modest, 1993) as:

$$q_r = -\frac{4n^2\sigma}{3\beta_R}\frac{\partial T^4}{\partial x} \tag{3.2.10}$$

Thus equation (3.2.9) takes the form:

$$\mathrm{u}\frac{\partial T}{\partial x} + \mathrm{v}\frac{\partial T}{\partial y} = \alpha\left(\frac{\partial^2 T}{\partial x^2} + \frac{\partial^2 T}{\partial y^2}\right) + \frac{1}{\rho C_p}\frac{4n^2\sigma}{3\beta_R}\frac{\partial^2 T^4}{\partial x^2} \tag{3.2.11}$$

The continuity equation (3.2.1) can be satisfied automatically by introducing the stream function ψ as:

$$\mathrm{u} = \frac{\partial \psi}{\partial y} \tag{3.2.12a}$$

$$\mathrm{v} = -\frac{\partial \psi}{\partial x} \tag{3.2.12b}$$

The domain is subjected to following boundary conditions:

at $x = 0$ $\quad u = 0,\ v = 0 \quad T = T_h$

at $x = L$, $\quad u = 0,\ v = 0 \quad T = T_c$

at $y = 0$ *and* $y = L$, $\quad u = 0,\ v = 0 \quad \frac{\partial T}{\partial y} = 0$ (3.2.12c)

Since there is no heat storage in the medium, the following condition at solid-porous interface has to be satisfied.

at $x = x_{sp}$ $\quad u = 0,\ v = 0 \quad T_s = T_p \quad k_s \frac{\partial T_s}{\partial x} = k_p \frac{\partial T_p}{\partial x}$

at $y = y_{sp}$ $\quad u = 0,\ v = 0 \quad T_s = T_p \quad k_s \frac{\partial T_s}{\partial y} = k_p \frac{\partial T_p}{\partial y}$ (3.2.12d)

Equation (3.2.8) and (3.2.11) are the two governing partial differential equations in dimensional form with many variables. These equations can be converted to dimensionless form to reduce the number of variables and thus facilitate the solution. The following non-dimensional parameters are used to convert above said equations into dimensionless form:

Dimensionless Width $\quad \bar{x} = \frac{x}{L}$ (3.2.13a)

Dimensionless Height $\quad \bar{y} = \frac{y}{L}$ (3.2.13b)

Dimensionless Stream function $\quad \bar{\psi} = \frac{\psi}{\alpha}$ (3.2.13c)

Dimensionless Temperature $\quad \bar{T} = \frac{(T - T_\infty)}{(T_w - T_\infty)}$ (3.2.13d)

Radiation parameter $\quad R_d = \frac{4\sigma n^2 T_\infty^{\ 3}}{\beta_R k_s}$ (3.2.13e)

Rayleigh Number $$Ra = \frac{g\beta_T \Delta TKL}{\nu\alpha} \tag{3.2.13f}$$

The non-linear term $T^4$ in the equation (3.2.10) can be expanded in Taylor series. Expanding $T^4$ about $T_c$ and neglecting higher order terms (Raptis, 1998) results:

$$T^4 \approx 4TT_\infty^{\ 3} - 3T_c^{\ 4} \tag{3.2.14}$$

Substitution of equations (3.2.12 –3.2.14) into equations (3.2.8) and (3.2.11) gives rise to following non-dimensional equations:

Momentum equation

$$\frac{\partial^2 \overline{\psi}}{\partial \overline{x}^2} + \frac{\partial^2 \overline{\psi}}{\partial \overline{y}^2} = -Ra \frac{\partial \overline{T}}{\partial \overline{x}} \tag{3.2.15}$$

Energy equation for porous region

$$\left[\frac{\partial \overline{\psi}}{\partial \overline{y}} \frac{\partial \overline{T}}{\partial \overline{x}} - \frac{\partial \overline{\psi}}{\partial \overline{x}} \frac{\partial \overline{T}}{\partial \overline{y}}\right] = \left(\left(1 + \frac{4R_d}{3}\right)\frac{\partial^2 \overline{T}}{\partial \overline{x}^2} + \frac{\partial^2 \overline{T}}{\partial \overline{y}^2}\right) \tag{3.2.16}$$

Energy equation for solid region

$$\frac{\partial^2 T_s}{\partial x^2} + \frac{\partial^2 T_s}{\partial y^2} - \frac{1}{\alpha\rho C_p}\frac{\partial q_r}{\partial x} = 0 \tag{3.2.17}$$

By substituting the non-dimensional parameters, into 3.2.17 becomes

$$\left(1 + \frac{4R_d}{3}\right)\frac{\partial^2 \overline{T}}{\partial \overline{x}^2} + \frac{\partial^2 \overline{T}}{\partial \overline{y}^2} = 0 \tag{3.2.18}$$

The non-dimensionalisation of boundary conditions leads to

The corresponding boundary conditions are

at $\overline{x} = 0$ $\quad \overline{\psi} = 0 \quad \overline{T} = 1$

at $\overline{x} = 1$ $\quad \overline{\psi} = 0 \quad \overline{T} = 0$

at $\overline{y} = 0$ *and* $\overline{y} = 1,$ $\quad \overline{\psi} = 0 \quad \dfrac{\partial \overline{T}}{\partial \overline{y}} = 0$

at $\bar{x} = x_{sp}$ $\bar{\psi} = 0$, $Kr\dfrac{\partial \bar{T}_s}{\partial \bar{x}} = \dfrac{\partial \bar{T}_p}{\partial \bar{x}}$

at $\bar{y} = \bar{y}_{sp}$ $\bar{\psi} = 0$ $Kr\dfrac{\partial \bar{T}_s}{\partial \bar{y}} = \dfrac{\partial \bar{T}_p}{\partial \bar{y}}$ (3.2.19)

The Nusselt number is given by:

$$Nu = -\left(\left(1 + \frac{4}{3}R_d\right)\frac{\partial \bar{T}}{\partial \bar{x}}\right)_{\bar{x}=0} \qquad (3.2.20)$$

## 3.3 Governing equations for heat and mass transfer in cavity

Equations (3.2.1) to (3.2.3) are applicable here as well but in order to accommodate the mass transfer inside the porous medium, equation (3.2.5) gets transformed in more complex form

The variation of density is given by:

$$\rho = \rho_\infty\left[1 - \beta_T\left(T - T_\infty\right) - \beta_C\left(C - C_\infty\right)\right] \qquad (3.3.1)$$

The equation for species concentration can be written as:

$$\mathrm{u}\frac{\partial C}{\partial x} + \mathrm{v}\frac{\partial C}{\partial y} = D\left(\frac{\partial^2 C}{\partial x^2} + \frac{\partial^2 C}{\partial y^2}\right) \qquad (3.3.2)$$

Due to mass transfer, equation (3.1.7) changes the form to:

$$\frac{\partial \mathrm{v}}{\partial x} = \frac{-K}{\mu}\left(\frac{\partial^2 p}{\partial y \partial x} - \rho_\infty g\left(\beta_T\frac{\partial T}{\partial x} + \beta_c\frac{\partial C}{\partial x}\right)\right) \qquad (3.3.3)$$

Subjected to boundary conditions:

at $x=0$ $\quad u=0,\ v=0 \quad T=T_h \quad C=C_h$

at $x=L$, $\quad u=0,\ v=0 \quad T=T_c \quad C=C_c$

at $y=0$ *and* $y=L$, $\quad u=0,\ v=0 \quad \dfrac{\partial T}{\partial y}=0$ (3.3.4)

Following additional dimensionless parameters are used

Dimensionless Concentration $\quad \overline{C}=\dfrac{(C-C_c)}{(C_w-C_c)}$ (3.3.4a)

Lewis number $\quad Le=\dfrac{\alpha}{D}$ (3.3.4b)

Buoyancy ratio $\quad N=\left(\dfrac{\beta_c \Delta C}{\beta_T \Delta T}\right)$ (3.3.4c)

Thus the momentum equation for coupled heat and mass transfer in dimensionless form is:

$$\frac{\partial^2\overline{\psi}}{\partial\overline{x}^2}+\frac{\partial^2\overline{\psi}}{\partial\overline{y}^2}=-Ra\left[\frac{\partial\overline{T}}{\partial\overline{x}}+N\frac{\partial\overline{C}}{\partial\overline{x}}\right] \tag{3.3.5}$$

Energy equation in porous region is:

$$\frac{\partial\overline{\psi}}{\partial\overline{y}}\frac{\partial\overline{T}}{\partial\overline{x}}-\frac{\partial\overline{\psi}}{\partial\overline{x}}\frac{\partial\overline{T}}{\partial\overline{y}}=\left(\left(1+\frac{4R_d}{3}\right)\frac{\partial^2\overline{T}}{\partial\overline{x}^2}+\frac{\partial^2\overline{T}}{\partial\overline{y}^2}\right) \tag{3.3.6}$$

Energy equation in solid region

$$\left(1+\frac{4R_d}{3}\right)\frac{\partial^2\overline{T}}{\partial\overline{x}^2}+\frac{\partial^2\overline{T}}{\partial\overline{y}^2}=0 \tag{3.3.7}$$

Equation for species concentration is:

$$\frac{\partial\overline{\psi}}{\partial\overline{y}}\frac{\partial\overline{C}}{\partial\overline{x}}-\frac{\partial\overline{\psi}}{\partial\overline{x}}\frac{\partial\overline{C}}{\partial\overline{y}}=\frac{1}{Le}\left(\frac{\partial^2\overline{C}}{\partial\overline{x}^2}+\frac{\partial^2\overline{C}}{\partial\overline{y}^2}\right) \tag{3.3.8}$$

The corresponding boundary conditions are

at $\bar{x}=0 \quad \bar{\psi}=0 \quad \bar{T}=1 \ \ \bar{C}=1$

at $\bar{x}=1 \quad \bar{\psi}=0 \quad \bar{T}=0 \quad \bar{C}=0$

at $\bar{y}=0 \quad and \quad \bar{y}=1, \quad \bar{\psi}=0 \quad \dfrac{\partial \bar{T}}{\partial \bar{y}}=0$

at $\bar{x}=x_{sp} \quad \bar{\psi}=0, \quad Kr\dfrac{\partial \bar{T}_s}{\partial \bar{x}} = \dfrac{\partial \bar{T}_p}{\partial \bar{x}}$

at $\bar{y}=\bar{y}_{sp} \quad \bar{\psi}=0 \quad Kr\dfrac{\partial \bar{T}_s}{\partial \bar{y}} = \dfrac{\partial \bar{T}_p}{\partial \bar{y}}$ (3.3.8a)

The heat and mass transfer rate at the hot surface can be calculated using following relations:

Nusselt number:

$$Nu=-\left(\left(1+\frac{4}{3}R_d\right)\frac{\partial \bar{T}}{\partial \bar{x}}\right)_{\bar{x}=0} \tag{3.3.8b}$$

The Sherwood number is expressed as:

$$Sh=\left(-\frac{\partial \bar{C}}{\partial \bar{x}}\right)_{\bar{x}=0} \tag{3.3.8c}$$

## 3.4 Solution of governing equations

Thus far we have derived the partial differential equations, which describe the heat and fluid flow behavior in the vicinity of porous medium. The development of governing equations is one part but the second and important part is to solve these equations in order to predict the various parameters of interest in the porous medium. There are various numerical methods available to achieve the solution of these equations, but the most popular numerical methods are: finite difference method, finite volume method and the finite element method. The selection of these numerical methods is an important decision, which is influenced by variety of factors amongst which the geometry of domain plays a vital role. Other factors include the ease with which these partial differential equations can be transformed into simpler forms, the computational time required and the flexibility in development of computer code. In the present study, we have used finite element method (FEM) due to its ability to handle the complex geometry and ease of coding. The following sections enlighten the finite element method and present its application to solve the above mentioned equations.

The finite element method is a deservingly popular method amongst scientific community. This method was originally developed to study the mechanical stresses in a complex air frame structure (Clough, 1960) and lately popularized by Zienkiewicz and Cheung (Zienkiewicz & Cheung, 1965) by applying it to continuum mechanics. Since then the application of finite element method has been exploited to solve the numerous problems in various engineering disciplines.

The great thing about finite element method is its ease with which it can be generalized to myriad engineering problems comprised of different materials. Another admirable feature of the finite element method (FEM) is that it can be applied to a wide range of geometries having irregular boundaries, which is highly difficult to achieve with other contemporary methods.

FEM can be said to have comprised of roughly 5 steps to solve any particular problem. The steps can be summarized as:

1. **Discretizing the domain:** This step involves the division of whole physical domain into smaller segments known as elements, and then identifying the nodes, coordinates of each node and ensuring proper connectivity between the nodes.
2. **Specifying the equation:** In this step, the governing equation is specified and an equation is written in terms of nodal values
3. **Development of Global matrix:** the equations are arranged in a global matrix, which takes into account the whole domain
4. **Solution:** The equations are solved to get the desired variables at each node in the domain
5. **Evaluate the quantities of interest:** After solving the equations a set of values are obtained for each node, which can be further processed to get the quantities of interest.

There are varieties of elements available in FEM, which are distinguished by the presence of number of nodes. The present study is carried out by using a simple 3-noded triangular element as shown in figure 3.1

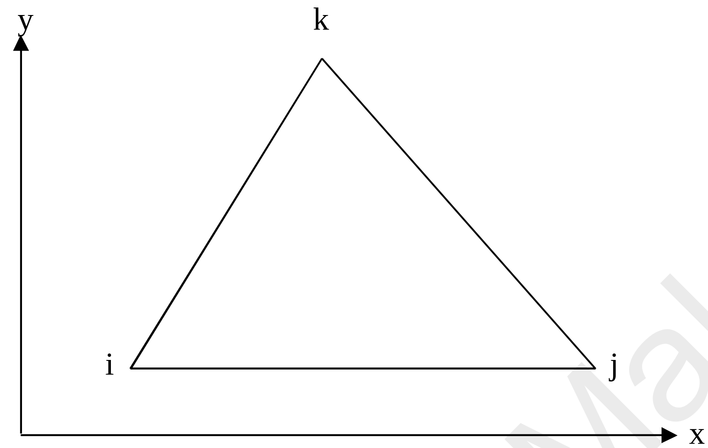


**Figure 3.1:** Typical triangular element

Let us consider that the variable to be determined in the triangular area is $\psi$ *or* $T$ polynomial function for $\psi$ *or* $T$ can be expressed as:

$$\psi = \alpha_1 + \alpha_2 x + \alpha_3 y \tag{3.4.1}$$

$$T = \alpha_1 + \alpha_2 x + \alpha_3 y \tag{3.4.2}$$

Let us consider equation (3.4.1) and try to find out the constants $\alpha_1, \alpha_2$ *and* $\alpha_3$. The variable $T$ has the values $\psi_i, \psi_j \,\&\, \psi_k$ at the nodal position *i, j and k* of a triangular element. The *x* and *y* coordinates at these points are $x_i, x_j, x_k$ and $y_i, y_j, y_k$ respectively. Substitution of these nodal values in the equation (3.4.1) helps in determining the constants $\alpha_1, \alpha_2, \alpha_3$, which are:

$$\alpha_1 = \frac{1}{2A}\left[(x_j y_k - x_k y_j)\psi_i + (x_k y_i - x_i y_k)\psi_j + (x_i y_k - x_j y_i)\psi_k\right] \tag{3.4.3}$$

$$\alpha_2 = \frac{1}{2A}\left[(y_j - y_k)\psi_i + (y_k - y_i)\psi_j + (y_i - y_j)\psi_k\right] \tag{3.4.4}$$

$$\alpha_3 = \frac{1}{2A}\left[(x_k - x_j)\psi_i + (x_i - x_k)\psi_j + (x_j - x_i)\psi_k\right] \quad (3.4.5)$$

Where $A$ is area of the triangle given as:

$$2A = \begin{vmatrix} 1 & x_i & y_i \\ 1 & x_j & y_j \\ 1 & x_k & y_k \end{vmatrix} \quad (3.4.6)$$

Substitution of $\alpha_1, \alpha_2, \alpha_3$ in the equation (3.4.1) and mathematical arrangement of the terms results into:

$$\psi = N_i\psi_i + N_j\psi_j + N_k\psi_k \quad (3.4.7)$$

In equation (3.4.7), $N_i, N_j \;\&\; N_k$ are the shape functions given by

$$N_m = \frac{a_m + b_m x + c_m y}{2A}, \qquad m = i, j, k \quad (3.4.8)$$

The constants can be expressed in terms of coordinates as:

$$\begin{aligned} a_i &= x_j y_k - x_k y_j \\ b_i &= y_j - y_k \\ c_i &= x_k - x_j \end{aligned} \quad (3.4.8a)$$

$$\begin{aligned} a_j &= x_k y_i - x_i y_k \\ b_j &= y_k - y_i \\ c_j &= x_i - x_k \end{aligned} \quad (3.4.8b)$$

$$\begin{aligned} a_k &= x_i y_j - x_j y_i \\ b_k &= y_i - y_j \\ c_k &= x_j - x_i \end{aligned} \quad (3.4.8c)$$

Good insight into the FEM is given in Segerlind (Segerlind, 1982); (ElShayeb & Beng, 2000); (Bullo & Lewis, 2004). Galerkin method is employed to convert the partial differential equations into matrix form of equation for an element.

The steps involved are as given below. Please note that the nodal terms $i, j \,\&\, k$ are replaced by *1,2& 3* respectively in subsequent discussions for simplicity.

Application of Galerkin method to equation (3.2.15) yields:

$$\left\{R^e\right\} = -\int_A N^T \left( \frac{\partial^2 \overline{\psi}}{\partial \overline{x}^2} + \frac{\partial^2 \overline{\psi}}{\partial \overline{y}^2} + Ra \frac{\partial \overline{T}}{\partial \overline{x}} \right) dA \qquad (3.4.9)$$

Where $R^e$ is the residue. Consider the individual terms of equation (3.4.9)

The differentiation of following term results into:

$$\frac{\partial}{\partial \overline{x}} \left( [N]^T \frac{\partial \overline{\psi}}{\partial \overline{x}} \right) = [N]^T \frac{\partial^2 \overline{\psi}}{\partial \overline{x}^2} + \frac{\partial [N]^T}{\partial \overline{x}} \frac{\partial \overline{\psi}}{\partial \overline{x}} \qquad (3.4.10)$$

Thus

$$\int_A N^T \frac{\partial^2 \overline{\psi}}{\partial \overline{x}^2} dA = \int_A \frac{\partial}{\partial \overline{x}} \left( [N]^T \frac{\partial^2 \overline{\psi}}{\partial \overline{x}^2} \right) dA - \int_A \frac{\partial [N]^T}{\partial \overline{x}} \frac{\partial \overline{\psi}}{\partial \overline{x}} \qquad (3.4.11)$$

The first term on right hand side of equation (3.4.11) can be transformed into surface integral by the application of Greens theorem and leads to inter-element requirement at boundaries of an element. The boundary conditions are incorporated in the force vector.

Making use of (3.4.7) produces:

$$\int_A N^T \frac{\partial^2 \overline{\psi}}{\partial \overline{x}^2} dA \; = -\int_A \frac{\partial N^T}{\partial \overline{x}} \frac{\partial N}{\partial \overline{x}} \begin{Bmatrix} \overline{\psi}_1 \\ \overline{\psi}_2 \\ \overline{\psi}_3 \end{Bmatrix} dA \qquad (3.4.12)$$

Substitution of (3.4.8) into (3.4.12) gives:

$$= -\frac{1}{(2A)^2} \int_A \begin{bmatrix} b_1 \\ b_2 \\ b_3 \end{bmatrix} \begin{bmatrix} b_1 & b_2 & b_3 \end{bmatrix} \begin{Bmatrix} \overline{\psi}_1 \\ \overline{\psi}_2 \\ \overline{\psi}_3 \end{Bmatrix} dA$$

$$= -\frac{1}{4A} \begin{bmatrix} b_1{}^2 & b_1 b_2 & b_1 b_3 \\ b_1 b_2 & b_2{}^2 & b_2 b_3 \\ b_1 b_2 & b_2 b_3 & b_3{}^2 \end{bmatrix} \begin{Bmatrix} \overline{\psi}_1 \\ \overline{\psi}_2 \\ \overline{\psi}_3 \end{Bmatrix} \qquad (3.4.13)$$

Similarly

$$\int_A N^T \frac{\partial^2 \overline{\psi}}{\partial \overline{y}^2} dA = -\frac{1}{4A}\begin{bmatrix} c_1{}^2 & c_1c_2 & c_1c_3 \\ c_1c_2 & c_2{}^2 & c_2c_3 \\ c_1c_2 & c_2c_3 & c_3{}^2 \end{bmatrix}\begin{Bmatrix} \overline{\psi}_1 \\ \overline{\psi}_2 \\ \overline{\psi}_3 \end{Bmatrix} \tag{3.4.14}$$

The third term of equation (3.4.9) is:

$$\int_A N^T Ra \frac{\partial \overline{T}}{\partial \overline{x}} dA = Ra \int_A N^T \frac{\partial \overline{T}}{\partial \overline{x}} dA \tag{3.4.15}$$

In order to get the matrix equation of (3.4.15), the following method can be applied:

The triangular element can be subdivided into three triangles with a point in the center of original triangle as shown in figure 3.2

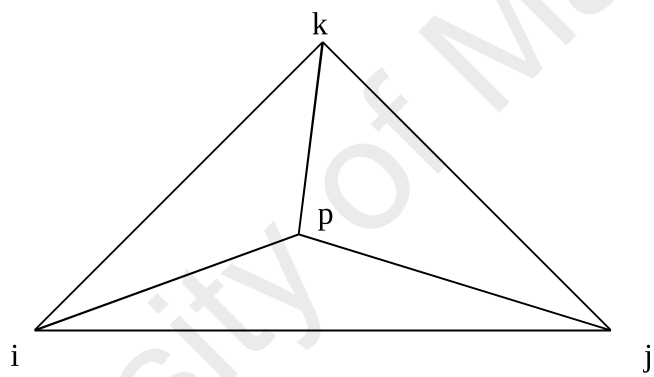


**Figure 3.2:** Sub triangular areas

Defining the new area ratios as:

$$L_1 = \frac{area\ pij}{area\ ijk} \tag{3.4.16a}$$

$$L_2 = \frac{area\ pjk}{area\ ijk} \tag{3.4.16b}$$

$$L_3 = \frac{area\ pki}{area\ ijk} \tag{3.4.16c}$$

It can be shown (ElShayeb & Beng, 2000) that

$$L_1 = N_1 \tag{3.4.17a}$$

$$L_2 = N_2 \tag{3.4.17b}$$

$$L_2 = N_3 \tag{3.4.17c}$$

Replacing shape functions in equation (3.4.15) by (3.4.17) yields:

$$\int_A N^T Ra \frac{\partial \overline{T}}{\partial \overline{x}} dA = Ra \int_A \begin{bmatrix} L_1 \\ L_2 \\ L_3 \end{bmatrix} \frac{\partial [N]}{\partial \overline{x}} \begin{bmatrix} \overline{T}_i \\ \overline{T}_j \\ \overline{T}_k \end{bmatrix} dA \tag{3.4.18}$$

The area integration can be evaluated by a simple relation (Segerlind, 1982)

$$\int_A L1^d\, L2^e\, L3^f = \frac{d!e!f!}{(d+e+f+2)!} 2A \tag{3.4.19}$$

Application of equation (3.4.19) into equation (3.4.18) gives rise to:

$$= Ra \frac{A}{3} \begin{bmatrix} 1 \\ 1 \\ 1 \end{bmatrix} \frac{1}{2A} \begin{bmatrix} b_1 & b_2 & b_3 \end{bmatrix} \begin{bmatrix} \overline{T}_1 \\ \overline{T}_2 \\ \overline{T}_3 \end{bmatrix} \tag{3.4.20}$$

$$= \frac{Ra}{6} \begin{Bmatrix} b_1\overline{T}_1 + b_2\overline{T}_2 + b_3\overline{T}_3 \\ b_1\overline{T}_1 + b_2\overline{T}_2 + b_3\overline{T}_3 \\ b_1\overline{T}_1 + b_2\overline{T}_2 + b_3\overline{T}_3 \end{Bmatrix} \tag{3.4.21}$$

Now equation (3.3.15) can be written in the matrix form as:

$$\frac{1}{4A} \left\{ \begin{bmatrix} b_1^2 & b_1 b_2 & b_1 b_3 \\ b_1 b_2 & b_2^2 & b_2 b_3 \\ b_1 b_2 & b_2 b_3 & b_3^2 \end{bmatrix} + \begin{bmatrix} c_1^2 & c_1 c_2 & c_1 c_3 \\ c_1 c_2 & c_2^2 & c_2 c_3 \\ c_1 c_2 & c_2 c_3 & c_3^2 \end{bmatrix} \right\} \begin{Bmatrix} \overline{\psi}_1 \\ \overline{\psi} 2 \\ \overline{\psi} 3 \end{Bmatrix} = \frac{Ra}{6} \begin{Bmatrix} b_1\overline{T}_1 + b_2\overline{T}_2 + b_3\overline{T}_3 \\ b_1\overline{T}_1 + b_2\overline{T}_2 + b_3\overline{T}_3 \\ b_1\overline{T}_1 + b_2\overline{T}_2 + b_3\overline{T}_3 \end{Bmatrix} \tag{3.4.22}$$

In simple form equation (3.4.22) can be represented as:

$$[K_s]\{\overline{\psi}\} = \{f\} \tag{3.4.23}$$

Where, $K_s$ is stiffness matrix and $f$ is the force vector. For equation (3.3.15) they are:

$$[K_s] \;=\; \frac{1}{4A}\left\{\begin{bmatrix} b_1^{\,2} & b_1b_2 & b_1b_3 \\ b_1b_2 & b_2^{\,2} & b_2b_3 \\ b_1b_2 & b_2b_3 & b_3^{\,2} \end{bmatrix} + \begin{bmatrix} c_1^{\,2} & c_1c_2 & c_1c_3 \\ c_1c_2 & c_2^{\,2} & c_2c_3 \\ c_1c_2 & c_2c_3 & c_3^{\,2} \end{bmatrix}\right\} \tag{3.4.23a}$$

$$\{\overline{\psi}\} = \begin{Bmatrix} \overline{\psi}_1 \\ \overline{\psi}2 \\ \overline{\psi}3 \end{Bmatrix} \tag{3.4.23b}$$

$$\text{and}\,\{f\} = \frac{Ra}{6}\begin{Bmatrix} b_1\overline{T}_1 + b_2\overline{T}_2 + b_3\overline{T}_3 \\ b_1\overline{T}_1 + b_2\overline{T}_2 + b_3\overline{T}_3 \\ b_1\overline{T}_1 + b_2\overline{T}_2 + b_3\overline{T}_3 \end{Bmatrix} \tag{3.4.23c}$$

FEM formulation of energy equation (3.3.16)

$$\{R^e\} = -\int_A [N]^T \left[\left[\frac{\partial\overline{\psi}}{\partial\overline{y}}\frac{\partial\overline{T}}{\partial\overline{x}} - \frac{\partial\overline{\psi}}{\partial\overline{x}}\frac{\partial\overline{T}}{\partial\overline{y}}\right] - \left(\left(1+\frac{4R_d}{3}\right)\frac{\partial^2\overline{T}}{\partial\overline{x}^2} + \frac{\partial^2\overline{T}}{\partial\overline{y}^2}\right)\right] dA \tag{3.4.24}$$

Considering the terms individually

$$\int_A [N]^T \frac{\partial\overline{\psi}}{\partial\overline{y}}\frac{\partial\overline{T}}{\partial\overline{x}}\, dA = \int_A \begin{bmatrix} L_1 \\ L_2 \\ L_3 \end{bmatrix} \frac{\partial[N]}{\partial\overline{y}}\{\overline{\psi}\}\frac{\partial[N]}{\partial\overline{x}}\{\overline{T}\}\, dA \tag{3.4.25}$$

$$= \int_A \begin{bmatrix} L_1 \\ L_2 \\ L_3 \end{bmatrix} dA \times \frac{1}{4A^2}\left[c_1\overline{\psi}_1 + c_2\overline{\psi}_2 + c_3\overline{\psi}_3\right]\left[b_1\; b_2\; b_3\right]\begin{Bmatrix} \overline{T}_1 \\ \overline{T}_2 \\ \overline{T}_3 \end{Bmatrix} \tag{3.4.26}$$

$$= \frac{1}{12A}\begin{Bmatrix} c_1\overline{\psi}_1 + c_2\overline{\psi}_2 + c_3\overline{\psi}_3 \\ c_1\overline{\psi}_1 + c_2\overline{\psi}_2 + c_3\overline{\psi}_3 \\ c_1\overline{\psi}_1 + c_2\overline{\psi}_2 + c_3\overline{\psi}_3 \end{Bmatrix}\left[b_1\; b_2\; b_3\right]\begin{Bmatrix} \overline{T}_1 \\ \overline{T}_2 \\ \overline{T}_3 \end{Bmatrix} \tag{3.4.27}$$

Following the steps as discussed earlier results:

$$\int_A N^T \frac{\partial \overline{\psi}}{\partial \overline{x}} \frac{\partial T}{\partial \overline{y}} dA = \frac{1}{12A} \begin{Bmatrix} b_1\overline{\psi}_1 + b_2\overline{\psi}_2 + b_3\overline{\psi}_3 \\ b_1\overline{\psi}_1 + b_2\overline{\psi}_2 + b_3\overline{\psi}_3 \\ b_1\overline{\psi}_1 + b_2\overline{\psi}_2 + b_3\overline{\psi}_3 \end{Bmatrix} \begin{bmatrix} c_1 & c_2 & c_3 \end{bmatrix} \begin{Bmatrix} \overline{T}_1 \\ \overline{T}_2 \\ \overline{T}_3 \end{Bmatrix} \qquad (3.4.28)$$

The remaining two terms of energy equation are evaluated in similar manner as that of equation (3.4.12)

$$\int_A N^T \left(1 + \frac{4}{3} R_d\right) \frac{\partial^2 \overline{T}}{\partial \overline{x}^2} dA = -\frac{1}{4A} \left(1 + \frac{4}{3} R_d\right) \begin{bmatrix} b_1^{\,2} & b_1 b_2 & b_1 b_2 \\ b_1 b_2 & b_2^{\,2} & b_2 b_3 \\ b_1 b_3 & b_2 b_3 & b_3^{\,2} \end{bmatrix} \begin{Bmatrix} \overline{T}_1 \\ \overline{T}_2 \\ \overline{T}_3 \end{Bmatrix} \qquad (3.4.29)$$

$$\int_A N^T \frac{\partial^2 \overline{T}}{\partial \overline{y}^2} dA = -\frac{1}{4A} \begin{bmatrix} c_1^{\,2} & c_1 c_2 & c_1 c_3 \\ c_1 c_2 & c_2^{\,2} & c_2 c_3 \\ c_1 c_2 & c_2 c_3 & c_3^{\,2} \end{bmatrix} \begin{Bmatrix} \overline{T}_1 \\ \overline{T}_2 \\ \overline{T}_3 \end{Bmatrix} \qquad (3.4.30)$$

Thus the element equation is:

$$\frac{1}{12A} \begin{Bmatrix} c_1\overline{\psi}_1 + c_2\overline{\psi}_2 + c_3\overline{\psi}_3 \\ c_1\overline{\psi}_1 + c_2\overline{\psi}_2 + c_3\overline{\psi}_3 \\ c_1\overline{\psi}_1 + c_2\overline{\psi}_2 + c_3\overline{\psi}_3 \end{Bmatrix} \begin{bmatrix} b_1 & b_2 & b_3 \end{bmatrix} - \frac{1}{12A} \begin{Bmatrix} b_1\overline{\psi}_1 + b_2\overline{\psi}_2 + b_3\overline{\psi}_3 \\ b_1\overline{\psi}_1 + b_2\overline{\psi}_2 + b_3\overline{\psi}_3 \\ b_1\overline{\psi}_1 + b_2\overline{\psi}_2 + b_3\overline{\psi}_3 \end{Bmatrix} \begin{bmatrix} c_1 & c_2 & c_3 \end{bmatrix}$$

$$+ \frac{1}{4A} \left[ \left(1 + \frac{4}{3} R_d\right) \begin{bmatrix} b_1^{\,2} & b_1 b_2 & b_1 b_2 \\ b_1 b_2 & b_2^{\,2} & b_2 b_3 \\ b_1 b_3 & b_2 b_3 & b_3^{\,2} \end{bmatrix} + \begin{bmatrix} c_1^{\,2} & c_1 c_2 & c_1 c_3 \\ c_1 c_2 & c_2^{\,2} & c_2 c_3 \\ c_1 c_2 & c_2 c_3 & c_3^{\,2} \end{bmatrix} \right] \begin{Bmatrix} \overline{T}_1 \\ \overline{T}_2 \\ \overline{T}_3 \end{Bmatrix} = 0 \qquad (3.4.31)$$

FEM formulation of energy equation of solid

Application of Galerkin method to energy equation of solid results:

$$\{R^e\} = \int_A \left( \left(1 + \frac{4R_d}{3}\right) \frac{\partial^2 \overline{T}}{\partial \overline{x}^2} + \frac{\partial^2 \overline{T}}{\partial \overline{y}^2} \right) \qquad (3.4.32)$$

The above equation is similar to the energy equation of porous region except that it has $\overline{\psi} = 0$.

Thus element equation is

$$\frac{1}{4A}\left[\left(1+\frac{4}{3}R_d\right)\begin{bmatrix} b_1{}^2 & b_1b_2 & b_1b_2 \\ b_1b_2 & b_2{}^2 & b_2b_3 \\ b_1b_3 & b_2b_3 & b_3{}^2 \end{bmatrix} + \begin{bmatrix} c_1{}^2 & c_1c_2 & c_1c_3 \\ c_1c_2 & c_2{}^2 & c_2c_3 \\ c_1c_2 & c_2c_3 & c_3{}^2 \end{bmatrix}\right]\begin{Bmatrix} \overline{T}_1 \\ \overline{T}_2 \\ \overline{T}_3 \end{Bmatrix} = 0$$

FEM formulation of the heat and mass transfer equations i.e. (3.4.5), (3.4.6) and (3.4.8)

$$\left\{R^e\right\} = -\int_A N^T \left[\frac{\partial^2 \overline{\psi}}{\partial \overline{x}^2} + \frac{\partial^2 \overline{\psi}}{\partial \overline{y}^2} + Ra\left[\frac{\partial \overline{T}}{\partial \overline{x}} + N\frac{\partial \overline{C}}{\partial \overline{x}}\right]\right] dA \tag{3.4.33}$$

The matrix form of equation (3.4.5) can be shown to be:

$$\frac{1}{4A}\left\{\begin{bmatrix} b_1{}^2 & b_1b_2 & b_1b_3 \\ b_1b_2 & b_2{}^2 & b_2b_3 \\ b_1b_2 & b_2b_3 & b_3{}^2 \end{bmatrix} + \begin{bmatrix} c_1{}^2 & c_1c_2 & c_1c_3 \\ c_1c_2 & c_2{}^2 & c_2c_3 \\ c_1c_2 & c_2c_3 & c_3{}^2 \end{bmatrix}\right\}\begin{Bmatrix} \overline{\psi}_1 \\ \overline{\psi}2 \\ \overline{\psi}3 \end{Bmatrix}$$

$$= \frac{Ra}{6}\left[\begin{Bmatrix} b_1\overline{T}_1 + b_2\overline{T}_2 + b_3\overline{T}_3 \\ b_1\overline{T}_1 + b_2\overline{T}_2 + b_3\overline{T}_3 \\ b_1\overline{T}_1 + b_2\overline{T}_2 + b_3\overline{T}_3 \end{Bmatrix} + N\begin{Bmatrix} b_1\overline{C}_1 + b_2\overline{C}_2 + b_3\overline{C}_3 \\ b_1\overline{C}_1 + b_2\overline{C}_2 + b_3\overline{C}_3 \\ b_1\overline{C}_1 + b_2\overline{C}_2 + b_3\overline{C}_3 \end{Bmatrix}\right] \tag{3.4.34}$$

Similarly the application of Galerkin method to (3.4.8) yields:

$$\left\{R^e\right\} = -\int_A N^T \left[\frac{\partial \overline{\psi}}{\partial \overline{y}}\frac{\partial \overline{C}}{\partial \overline{x}} - \frac{\partial \overline{\psi}}{\partial \overline{x}}\frac{\partial \overline{C}}{\partial \overline{y}} - \frac{1}{Le}\left(\frac{\partial^2 \overline{C}}{\partial \overline{x}^2} + \frac{\partial^2 \overline{C}}{\partial \overline{y}^2}\right)\right] dA \tag{3.4.35}$$

$$\frac{1}{12A}\begin{Bmatrix} c_1\overline{\psi}_1 + c_2\overline{\psi}_2 + c_3\overline{\psi}_3 \\ c_1\overline{\psi}_1 + c_2\overline{\psi}_2 + c_3\overline{\psi}_3 \\ c_1\overline{\psi}_1 + c_2\overline{\psi}_2 + c_3\overline{\psi}_3 \end{Bmatrix}\left[b_1\ b_2\ b_3\right] - \frac{1}{12A}\begin{Bmatrix} b_1\overline{\psi}_1 + b_2\overline{\psi}_2 + b_3\overline{\psi}_3 \\ b_1\overline{\psi}_1 + b_2\overline{\psi}_2 + b_3\overline{\psi}_3 \\ b_1\overline{\psi}_1 + b_2\overline{\psi}_2 + b_3\overline{\psi}_3 \end{Bmatrix}\left[c_1\ c_2\ c_3\right]$$

$$+\frac{1}{4A\,Le}\left[\begin{bmatrix} b_1{}^2 & b_1b_2 & b_1b_2 \\ b_1b_2 & b_2{}^2 & b_2b_3 \\ b_1b_3 & b_2b_3 & b_3{}^2 \end{bmatrix} + \begin{bmatrix} c_1{}^2 & c_1c_2 & c_1c_3 \\ c_1c_2 & c_2{}^2 & c_2c_3 \\ c_1c_2 & c_2c_3 & c_3{}^2 \end{bmatrix}\right]\begin{Bmatrix} \overline{C}_1 \\ \overline{C}2 \\ \overline{C}3 \end{Bmatrix} = 0 \tag{3.4.36}$$

Application of Galerkin method to energy equation of solid results:

$$\{R^e\} = \int_A \left( \left(1 + \frac{4R_d}{3}\right) \frac{\partial^2 \overline{T}}{\partial \overline{x}^2} + \frac{\partial^2 \overline{T}}{\partial \overline{y}^2} \right) \tag{3.4.37}$$

The above equation is similar to the energy equation of porous region except that it has $\overline{\psi} = 0$. Thus element equation is

$$\frac{1}{4A}\left[\left(1 + \frac{4}{3}R_d\right)\begin{bmatrix} b_1^{\ 2} & b_1 b_2 & b_1 b_2 \\ b_1 b_2 & b_2^{\ 2} & b_2 b_3 \\ b_1 b_3 & b_2 b_3 & b_3^{\ 2} \end{bmatrix} + \begin{bmatrix} c_1^{\ 2} & c_1 c_2 & c_1 c_3 \\ c_1 c_2 & c_2^{\ 2} & c_2 c_3 \\ c_1 c_2 & c_2 c_3 & c_3^{\ 2} \end{bmatrix}\right]\begin{Bmatrix} \overline{T}_1 \\ \overline{T}_2 \\ \overline{T}_3 \end{Bmatrix} = 0 \tag{3.4.38}$$

## 3.5 Solution procedure

Any simulation work related with the mathematical modeling is basically comprised of 2 distinct stages. The first step involves the development of the mathematical equations, which describes the phenomenon under investigation, and the second important step is to solve those mathematical equations.

In the present case, the governing mathematical equations describing various phenomenon have either two or three equations, which are coupled with each other. The coupling of equations arises due to the reason that the change of variables in one equation affects the other equation and vice versa. One of the fundamental requirements of the FEM is that it demands the physical domain to be modeled geometrically and then meshed with chosen elements. The meshing process involves defining of the nodes at each corner of an element and also defining the connectivity of all elements in the domain. Meshing also requires the coordinates of each node to be identified. These nodal coordinates and connectivity are building blocks of the FEM matrix equations.

In the present study, the geometry is modeled and meshed with triangular elements as shown in figure 3.3. The number of elements, size of elements and the pattern of meshing the domain influences the solution strategy. The general principle followed is that, more number of elements are placed in a region where large variations in the temperature, fluid and concentration parameters are expected thus allowing to capture these variables accurately. Figure 3.3 shows the mesh patterns being used in current study for porous medium embedded or enclosed in square geometry.

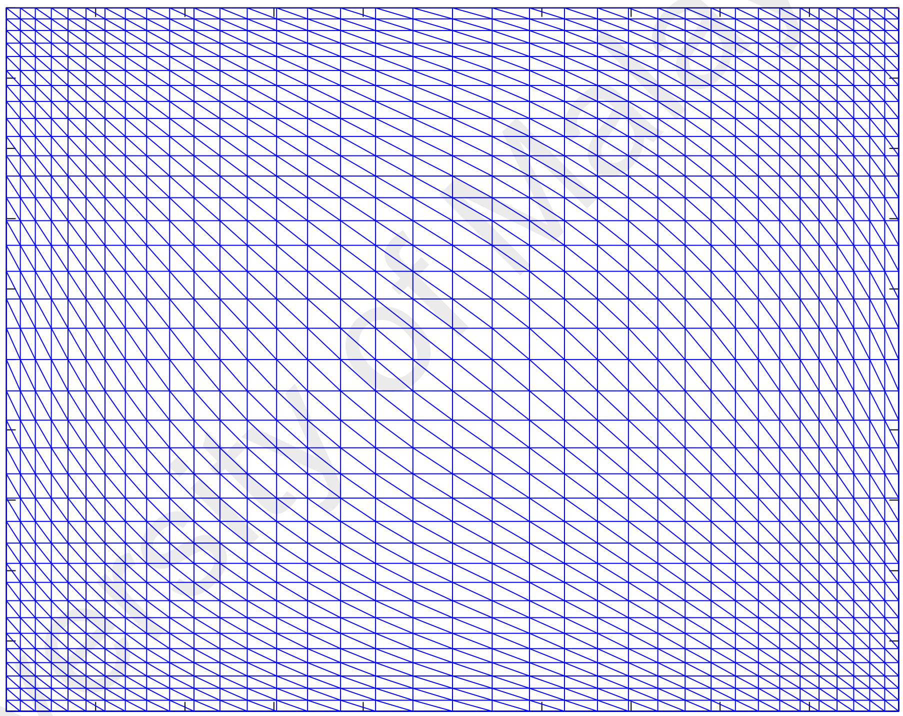

**Figure 3.3:** Mesh pattern for porous medium enclosed in a cavity

The elemental matrix forms of the equations are assembled in a global matrix with respect to the nodal position of the elements in the domain. A code is developed to solve this matrix form of equations. Since the equations are coupled with each other, an iterative process is adopted to solve them. The iterative process continues until a satisfactorily lower level of error is reached. The tolerance or error level for solution of the variables such as stream function, temperature and concentration are kept at $10^{-7}$, $10^{-5}$ and $10^{-5}$ respectively. This implies that when the difference between two successive iterations produces the above said tolerance level at all nodes then the iterative process is terminated. It may be noted that sufficiently dense mesh of 2592 well-organized elements is chosen in current study. It is evident from table 3.1 that the chosen numbers of elements have mesh independency since the variation in Nusselt and Sherwood numbers are marginal but time consumed is substantial for higher number of elements.

**Table 3.1:** $\overline{Nu}$ variation with mesh size

| No of Elements | $\overline{Nu}$ | $\overline{Sh}$ | Time (s) |
|---|---|---|---|
| 1800 | 4.5043 | 6.2911 | 23.0156 |
| 2592 | 4.4992 | 6.2677 | 58.6666 |
| 4232 | 4.4909 | 6.2430 | 228.8154 |

Wherever possible, the current solution is compared with open available literature so as to validate our methodology. The comparative results are discussed while presenting the results and discussion.

# CHAPTER 4 : DEVELOPMENT OF A SIMPLE AND OPTIMIZED SOLUTION ALGORITHM FOR CONJUGATE HEAT AND MASS TRANSFER

The conjugate heat and mass transfer or just conjugate heat transfer is quite involved phenomenon due to interconnectivity of porous and solid region where heat can cross both the region because of temperature difference. The phenomenon is governed by complex set of partial differential equations. The aim of current chapter is to develop a simple and optimized algorithm/method to solve the governing equations of conjugate heat and mass or conjugate heat transfer in porous medium.

## 4.1 Optimized Solution of Conjugate Heat and Mass Transfer in Porous Medium

The present chapter is dedicated to describe the simple and optimized algorithm being developed to solve the governing equations of a conjugate heat and mass transfer in porous medium. It has been discussed in chapter 3 that the conjugate heat transfer in porous medium is governed by 3 partial differential equations namely, momentum equation, energy equation of porous medium and energy equation of solid. There will be an additional equation namely concentration equation when mass transfer is considered along with heat transfer, thus effectively turning into 4 equation model. The current discussion is based on heat and mass transfer due to its higher complexity than just heat transfer problem.

The coupling of equations makes them inter dependent and any change in one equation affects all other equations. Thus it is a very complex and tricky set of equations which need to be solved simultaneously. The 4 governing equations of problem under investigation that dictates the heat and fluid flow behavior are:

$$\frac{\partial^2 \overline{\psi}}{\partial \overline{x}^2} + \frac{\partial^2 \overline{\psi}}{\partial \overline{y}^2} = -Ra\left[\frac{\partial \overline{T}}{\partial \overline{x}} + N\,\frac{\partial \overline{C}}{\partial \overline{x}}\right] \tag{4.1}$$

$$\frac{\partial \overline{\psi}}{\partial \overline{y}}\frac{\partial \overline{T}}{\partial \overline{x}} - \frac{\partial \overline{\psi}}{\partial \overline{x}}\frac{\partial \overline{T}}{\partial \overline{y}} = \left(\left(1+\frac{4R_d}{3}\right)\frac{\partial^2 \overline{T}}{\partial \overline{x}^2} + \frac{\partial^2 \overline{T}}{\partial \overline{y}^2}\right) \tag{4.2}$$

$$\left(1+\frac{4R_d}{3}\right)\frac{\partial^2 \overline{T}_s}{\partial \overline{x}^2} + \frac{\partial^2 \overline{T}_s}{\partial \overline{y}^2} = 0 \tag{4.3}$$

$$\frac{\partial \overline{\psi}}{\partial \overline{y}}\frac{\partial \overline{C}}{\partial \overline{x}} - \frac{\partial \overline{\psi}}{\partial \overline{x}}\frac{\partial \overline{C}}{\partial \overline{y}} = \frac{1}{Le}\left(\frac{\partial^2 \overline{C}}{\partial \overline{x}^2} + \frac{\partial^2 \overline{C}}{\partial \overline{y}^2}\right) \tag{4.4}$$

These equations are difficult to solve directly, thus they are converted into matrix form of equations by employing Galerkin method. The resulting matrix forms of equations are given as:

$$\frac{1}{4A}\left\{\begin{bmatrix} b_1^2 & b_1b_2 & b_1b_3 \\ b_1b_2 & b_2^2 & b_2b_3 \\ b_1b_2 & b_2b_3 & b_3^2 \end{bmatrix} + \begin{bmatrix} c_1^2 & c_1c_2 & c_1c_3 \\ c_1c_2 & c_2^2 & c_2c_3 \\ c_1c_2 & c_2c_3 & c_3^2 \end{bmatrix}\right\}\begin{Bmatrix} \overline{\psi}_1 \\ \overline{\psi}2 \\ \overline{\psi}3 \end{Bmatrix} = \frac{Ra}{6}\left[\begin{Bmatrix} b_1\overline{T}_1 + b_2\overline{T}_2 + b_3\overline{T}_3 \\ b_1\overline{T}_1 + b_2\overline{T}_2 + b_3\overline{T}_3 \\ b_1\overline{T}_1 + b_2\overline{T}_2 + b_3\overline{T}_3 \end{Bmatrix} + N\begin{Bmatrix} b_1\overline{C}_1 + b_2\overline{C}_2 + b_3\overline{C}_3 \\ b_1\overline{C}_1 + b_2\overline{C}_2 + b_3\overline{C}_3 \\ b_1\overline{C}_1 + b_2\overline{C}_2 + b_3\overline{C}_3 \end{Bmatrix}\right] \tag{4.5}$$

$$\frac{1}{12A}\begin{Bmatrix} c_1\overline{\psi}_1 + c_2\overline{\psi}_2 + c_3\overline{\psi}_3 \\ c_1\overline{\psi}_1 + c_2\overline{\psi}_2 + c_3\overline{\psi}_3 \\ c_1\overline{\psi}_1 + c_2\overline{\psi}_2 + c_3\overline{\psi}_3 \end{Bmatrix}\begin{bmatrix} b_1 & b_2 & b_3 \end{bmatrix} - \frac{1}{12A}\begin{Bmatrix} b_1\overline{\psi}_1 + b_2\overline{\psi}_2 + b_3\overline{\psi}_3 \\ b_1\overline{\psi}_1 + b_2\overline{\psi}_2 + b_3\overline{\psi}_3 \\ b_1\overline{\psi}_1 + b_2\overline{\psi}_2 + b_3\overline{\psi}_3 \end{Bmatrix}\begin{bmatrix} c_1 & c_2 & c_3 \end{bmatrix}$$

$$+\ \frac{1}{4A}\left[\left(1+\frac{4}{3}R_d\right)\begin{bmatrix} b_1^2 & b_1b_2 & b_1b_2 \\ b_1b_2 & b_2^2 & b_2b_3 \\ b_1b_3 & b_2b_3 & b_3^2 \end{bmatrix} + \begin{bmatrix} c_1^2 & c_1c_2 & c_1c_3 \\ c_1c_2 & c_2^2 & c_2c_3 \\ c_1c_2 & c_2c_3 & c_3^2 \end{bmatrix}\right]\begin{Bmatrix} \overline{T}_1 \\ \overline{T}_2 \\ \overline{T}_3 \end{Bmatrix} = 0 \tag{4.6}$$

$$\frac{1}{4A}\left[\left(1+\frac{4}{3}R_d\right)\begin{bmatrix} b_1^2 & b_1b_2 & b_1b_2 \\ b_1b_2 & b_2^2 & b_2b_3 \\ b_1b_3 & b_2b_3 & b_3^2 \end{bmatrix} + \begin{bmatrix} c_1^2 & c_1c_2 & c_1c_3 \\ c_1c_2 & c_2^2 & c_2c_3 \\ c_1c_2 & c_2c_3 & c_3^2 \end{bmatrix}\right]\begin{Bmatrix} \overline{T}_{1s} \\ \overline{T}_{2s} \\ \overline{T}_{3s} \end{Bmatrix} = 0 \tag{4.7}$$

$$\frac{1}{12A}\begin{Bmatrix} c_1\overline{\psi}_1 + c_2\overline{\psi}_2 + c_3\overline{\psi}_3 \\ c_1\overline{\psi}_1 + c_2\overline{\psi}_2 + c_3\overline{\psi}_3 \\ c_1\overline{\psi}_1 + c_2\overline{\psi}_2 + c_3\overline{\psi}_3 \end{Bmatrix}\begin{bmatrix} b_1 & b_2 & b_3 \end{bmatrix} - \frac{1}{12A}\begin{Bmatrix} b_1\overline{\psi}_1 + b_2\overline{\psi}_2 + b_3\overline{\psi}_3 \\ b_1\overline{\psi}_1 + b_2\overline{\psi}_2 + b_3\overline{\psi}_3 \\ b_1\overline{\psi}_1 + b_2\overline{\psi}_2 + b_3\overline{\psi}_3 \end{Bmatrix}\begin{bmatrix} c_1 & c_2 & c_3 \end{bmatrix}$$

$$+\frac{1}{4ALe}\left[\begin{bmatrix} b_1^{\,2} & b_1b_2 & b_1b_2 \\ b_1b_2 & b_2^{\,2} & b_2b_3 \\ b_1b_3 & b_2b_3 & b_3^{\,2} \end{bmatrix} + \begin{bmatrix} c_1^{\,2} & c_1c_2 & c_1c_3 \\ c_1c_2 & c_2^{\,2} & c_2c_3 \\ c_1c_2 & c_2c_3 & c_3^{\,2} \end{bmatrix}\right]\begin{Bmatrix} \overline{C}_1 \\ \overline{C}2 \\ \overline{C}3 \end{Bmatrix} = 0 \tag{4.8}$$

The equations (4.5 to 4.8) can be represented in condensed form as:

$$[k]_m\{\overline{\psi}\} = \{f\}_m \tag{4.9}$$

$$[k]_{ep}\{\overline{T}\} = 0 \tag{4.10}$$

$$[k]_{es}\{\overline{T}_s\} = 0 \tag{4.11}$$

$$[k]_c\{\overline{C}\} = \{f\}_c \tag{4.12}$$

Where, $\{k\}$ indicates the element stiffness matrix with subscripts m, ep, es and c denoting the momentum, energy porous, energy solid and concentration respectively. Similarly $\{\overline{\psi}\}$, $\{\overline{T}\}, \{\overline{T}_s\}, \{\overline{C}\}$ and $\{f\}$ indicates the solution variables and element force vector. The size of element stiffness matrix is 3x3 representing 3 nodes of triangular element whereas the solution and force vector have dimension of 3x1. The individual element matrix is transferred to a global stiffness matrix to bring connectivity among elements. The size of global stiffness matrix is equal to nxn, where n is total number of nodes in the domain. The solution and force vector get the dimension of nx1. The connectivity plays very important role in transferring the element stiffness into global stiffness matrix.

The contribution of individual element is transferred according to its nodal position in the physical domain. Let us assume that the domain is divided into 8 elements as shown in fig 4.1 which results into 8 elements and 9 nodes.

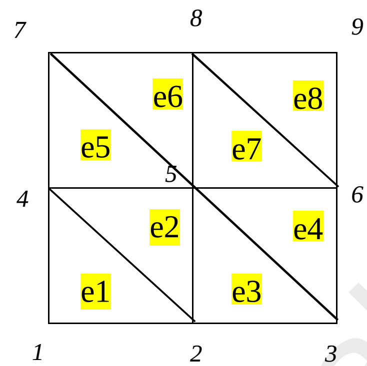


**Figure 4.1**: 8-element mesh

The connectivity matrix of 8 elements is shown in table 4.1

**Table 4.1:** Element connectivity

| Element No | Node i | Node j | Node k |
|---|---|---|---|
| **1** | 1 | 2 | 4 |
| **2** | 2 | 5 | 4 |
| **3** | 2 | 3 | 5 |
| **4** | 3 | 6 | 5 |
| **5** | 4 | 5 | 7 |
| **6** | 5 | 8 | 7 |
| **7** | 5 | 6 | 8 |
| **8** | 6 | 9 | 8 |

The global connectivity matrix for momentum equation can be built as

$$
\begin{array}{c|c}
\textit{Node} & \begin{array}{ccccccccc} 1 & 2 & 3 & 4 & 5 & 6 & 7 & 8 & 9 \end{array} \\
\begin{array}{c} 1 \\ 2 \\ 3 \\ 4 \\ 5 \\ 6 \\ 7 \\ 8 \\ 9 \end{array} &
\begin{bmatrix}
{}^{1}k_{11} & {}^{1}k_{12} & & {}^{1}k_{13} & & & & & \\
{}^{1}k_{21} & {}^{1}k_{22}+{}^{2}k_{11}+{}^{3}k_{11} & {}^{3}k_{12} & {}^{1}k_{23}+{}^{2}k_{13} & {}^{2}k_{12}+{}^{3}k_{13} & & & & \\
{}^{1}k_{31} & {}^{1}k_{32}+{}^{3}k_{21} & {}^{3}k_{22} & {}^{1}k_{33} & {}^{3}k_{23} & & & & \\
 & {}^{2}k_{31} & & {}^{2}k_{33}+{}^{4}k_{11}+{}^{5}k_{11} & {}^{2}k_{32}+{}^{4}k_{12}+{}^{5}k_{12} & & {}^{4}k_{13}+{}^{5}k_{13} & & \\
 & {}^{2}k_{21}+{}^{3}k_{31} & {}^{3}k_{32} & {}^{2}k_{13}+{}^{4}k_{21}+{}^{5}k_{21} & {}^{2}k_{12}+{}^{3}k_{33}+{}^{4}k_{22}+{}^{5}k_{22}+{}^{6}k_{11}+{}^{7}k_{11} & {}^{7}k_{12} & {}^{4}k_{33}+{}^{5}k_{13}+{}^{6}k_{23} & {}^{6}k_{12}+{}^{7}k_{13} & \\
 & & & & {}^{7}k_{21} & {}^{7}k_{22}+{}^{8}k_{11} & & {}^{7}k_{23}+{}^{8}k_{13} & {}^{8}k_{12} \\
 & & & {}^{4}k_{31}+{}^{5}k_{31} & {}^{4}k_{32}+{}^{5}k_{31}+{}^{6}k_{31} & & {}^{4}k_{33}+{}^{5}k_{33}+{}^{6}k_{33} & {}^{6}k_{32} & \\
 & & & & {}^{6}k_{21}+{}^{7}k_{33} & {}^{7}k_{32}+{}^{8}k_{31} & {}^{5}k_{23}+{}^{6}k_{33} & {}^{5}k_{22}+{}^{6}k_{32}+{}^{7}k_{33}+{}^{8}k_{33} & {}^{8}k_{32} \\
 & & & & & {}^{8}k_{21} & & {}^{8}k_{23} & {}^{8}k_{22}
\end{bmatrix}
\end{array}
$$

The above matrix is global stiffness matrix for 8 elements where subscript indicates the row and column from element stiffness matrix and superscripts shows the element number. Similarly, the solution and force vector for elements arranged as per figure 4.1 are:

$$
\begin{array}{cc}
\textit{Node} & \textit{Solution variable} \\
\begin{array}{c} 1 \\ 2 \\ 3 \\ 4 \\ 5 \\ 6 \\ 7 \\ 8 \\ 9 \end{array} &
\begin{Bmatrix} \bar{\psi}_1 \\ \bar{\psi}_2 \\ \bar{\psi}_3 \\ \bar{\psi}_4 \\ \bar{\psi}_5 \\ \bar{\psi}_6 \\ \bar{\psi}_7 \\ \bar{\psi}_8 \\ \bar{\psi}_9 \end{Bmatrix}
\end{array}
$$

$$
\begin{array}{c c}
\textit{Node} & \textit{Force Vector} \\
\begin{array}{c} 1 \\ 2 \\ 3 \\ 4 \\ 5 \\ 6 \\ 7 \\ 8 \\ 9 \end{array} &
\left\{ \begin{array}{c}
{}^{1}f_{11} \\
{}^{1}f_{21}+{}^{2}f_{21}+{}^{3}f_{11} \\
{}^{3}f_{21}+{}^{4}f_{11} \\
{}^{1}f_{31}+{}^{2}f_{31}+{}^{5}f_{11} \\
{}^{2}f_{21}+{}^{3}f_{31}+{}^{4}f_{31}+{}^{5}f_{21}+{}^{6}f_{11}+{}^{7}f_{11} \\
{}^{4}f_{21}+{}^{7}f_{21}+{}^{8}f_{11} \\
+{}^{5}f_{31}+{}^{6}f_{31} \\
+{}^{6}f_{21}+{}^{7}f_{31}+{}^{8}f_{31} \\
+{}^{8}f_{21}
\end{array} \right\}
\end{array}
$$

The global stiffness matrix along with force vector is solved for solution variable as

$$\{\overline{\psi}\} = [k]^{-1}{}_{m}\{f\}_{m} \tag{4.13}$$

There are 9 nodes which results into 9 algebraic equations when equation 4.13 expanded. They are simultaneous equations which need to be solved simultaneously. The above mentioned solution is simple if there are few elements involved, but unfortunately most of the physical problems require huge number of elements thus large number of equations are generated which necessitates the problem to be solved with the help of suitable computer program. For instance, a mesh size of 36X36 dimensions (instead of 2x2 of figure 4.1) results into 2592 elements and 1369 nodes which essentially make the global stiffness matrix of dimension 1369x1369. On top of that, there are 4 set of partial differential equations each requiring same number of nodes. It means the system has to handle 4 set of Global stiffness matrix in one particular iteration. Since the equations are coupled, they are solved in an iterative manner by setting suitable convergence criteria.

For instance, a guess value of $\bar{\psi}$ and $\bar{T}$ (most of the time these guess values are taken as zero) at all the nodes is fed into program which results into a new value of $\bar{\psi}$. This new value is fed into second equation i.e. energy equation of porous medium which generates new values of $\bar{T}$.

These new values are fed into energy equation of solid and concentration equation to get their respective new values. Once all the new values for $\bar{\psi}$, $\bar{T}$, $\bar{T}_s$ and $\bar{C}$ are available, they are compared with their corresponding values in the previous iteration. If the difference between new and previous values meets the preset criteria of convergence tolerance, then the program stops else it continues to next iteration feeding the new values into equations to get another set of fresh values and so on. The convergence criteria for all the variables are generally set as

$$\left(\bar{\psi}^i{}_n - \bar{\psi}^i{}_p\right) \le 10^{-7} \qquad \text{for node } i = 1....N \tag{4.14}$$

$$\left(\bar{T}^i{}_n - \bar{T}^i{}_p\right) \le 10^{-5} \qquad \text{for node } i = 1....N \tag{4.15}$$

$$\left(\left(\bar{T}_s\right)^i{}_n - \left(\bar{T}_s\right)^i{}_p\right) \le 10^{-5} \qquad \text{for node } i = 1....N \tag{4.16}$$

$$\left(\bar{C}^i{}_n - \bar{C}^i{}_p\right) \le 10^{-5} \qquad \text{for node } i = 1....N \tag{4.17}$$

The subscripts *n* and *p* indicates new and previous whereas *i* and *N* shows the specific node number and total number of nodes in the domain.

The usual procedure to solve the problem of conjugate heat and mass transfer in porous medium requires that the computer solves 4 set of finite element equations corresponding to 4 partials differential equations 4.1 to 4.4 as demonstrated in figure 4.2. Thus the number of equations involved is very large that consumes huge amount of computer resources.

An attempt is made to simplify and optimize the solution algorithm by reducing the number of partial differential equations from 4 to 3 for the case of heat and mass transfer in porous medium. This is possible since equation 4.2 is similar to the right hand side of equation 4.3. The similar terms of equations 4.2 and 4.3 made it possible to combine them together by controlling the boundary conditions of other variable involved i.e. $\overline{\psi}$ *in equations 4.1-4.2 and 4.4. It is noticed that the* $\overline{\psi}$ represents the velocity field in the porous medium thus by forcing its value to be zero in the region occupied by solid wall (since there cannot be any fluid movement inside the solid), it is possible to reduce equation 4.2 to that of 4.3. By doing such alterations while solving equation 4.2, the energy equation 4.3 for solid can be eliminated completely. It became viable to reduce the total number of finite element equations corresponding to equation 4.3. Thus the heat and mass transfer problem effectively reduced from 4 to 3 partial differential equations.

Apart from reducing the number of equations, the algorithm becomes simpler to code since it nullified the whole of separate subroutine required to solve the finite element equations corresponding to equation 4.3. Thus the implementation of the code was much simpler with developed algorithm. The solution procedure for developed algorithm is shown in figure 4.3.

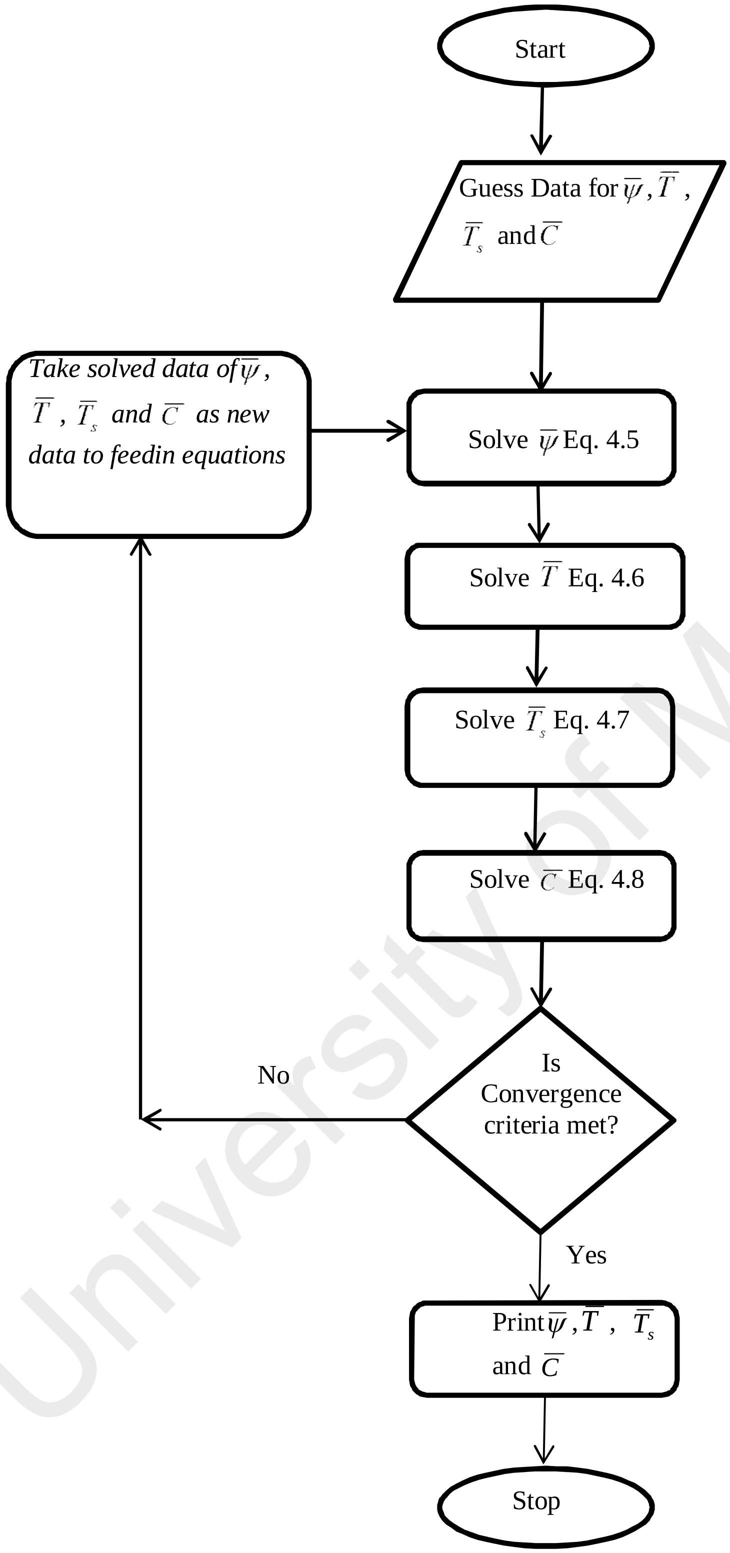


**Figure 4.2:** Flow chart of conventional solution procedure

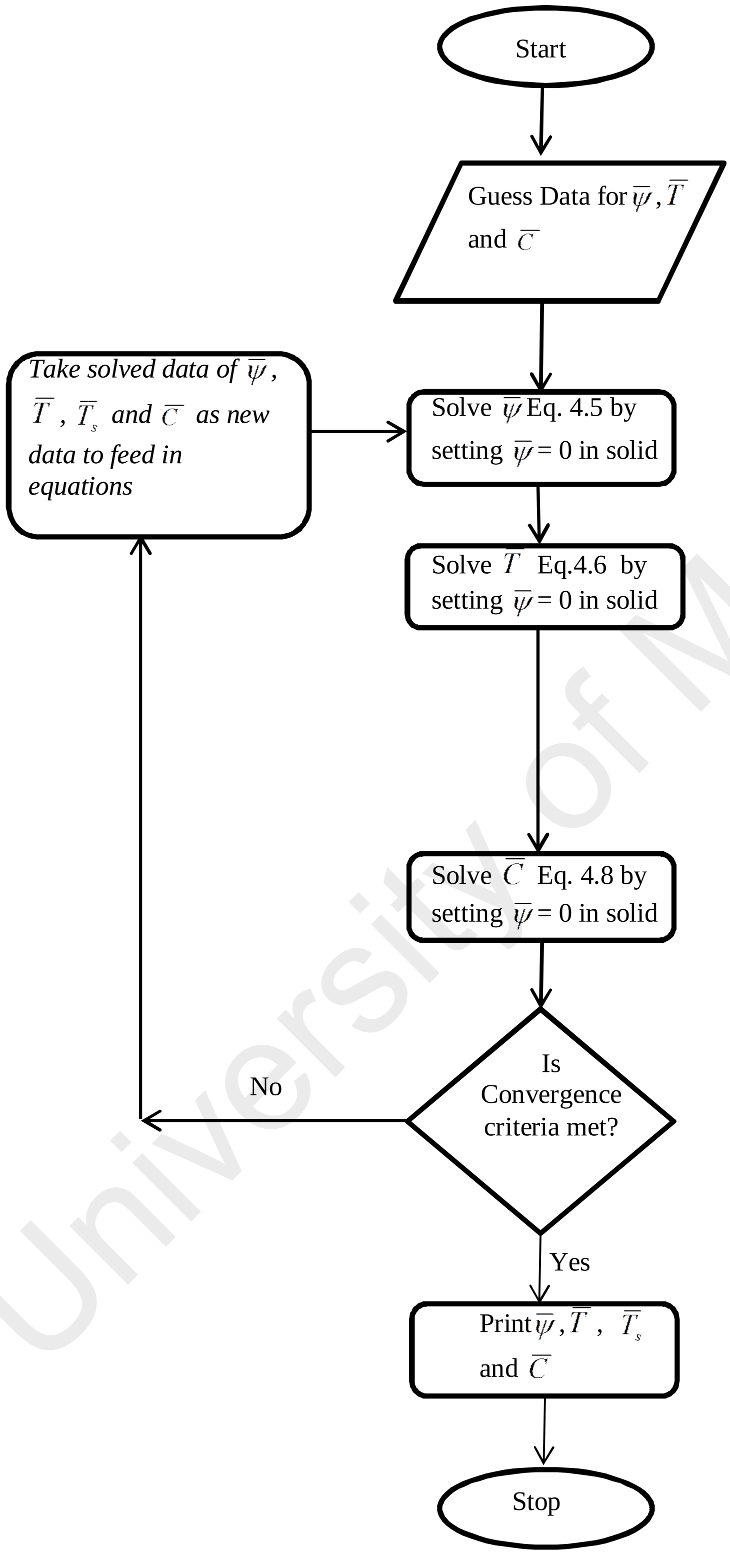


**Figure 4.3:** Flow chart of developed solution procedure

In order to establish the feasibility and thus demonstrate the advantages of developed algorithm, a simple case of conjugate heat and mass transfer in a square cavity with solid wall placed at bottom surface is solved with both i.e. conventional and developed algorithms. The whole physical domain is divided into 36x36 rows and columns that resulted into 2592 triangular elements having 1369 nodes. The mesh is generated in such a way that the smaller sized elements are placed near the surfaces where large variations in the solution variable are expected. Figure 4.4 shows the mesh of physical domain.

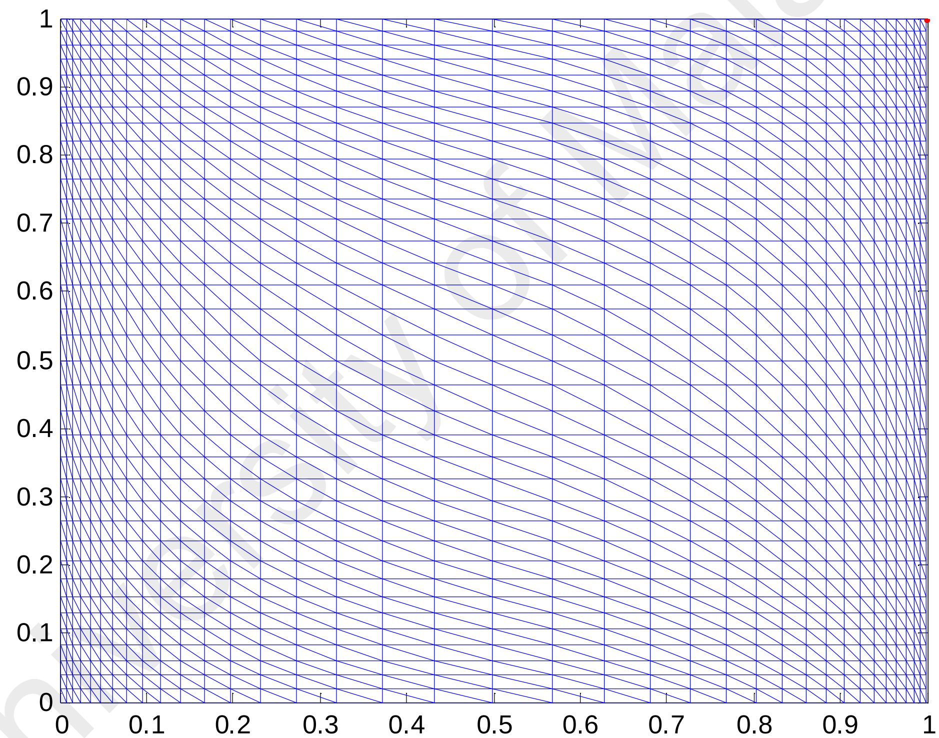


**Figure 4.4:** Mesh of physical domain

The implementation of conventional algorithm ran into 1101 lines when translated into matlab code. However, the developed algorithm with reduced number of equation took 925 lines of matlab code. This reduction of lines was result of eliminating the separate solution subroutine of solid temperature. Thus the developed method was simpler and easier to implement.

Apart from simplicity, one needs to check the performance of two algorithms for establishing its suitability for problem under investigation. Thus, the two algorithms are run for following parameters $R_d=0.5$, $N=0.2$, $Ra=100$, $Le=2$, $Kr=5$ and its performance in terms of convergence behavior, number of iterations, solution values of $\overline{\Psi}$, $\overline{T}$, $\overline{T}_s$, $\overline{C}$ and the time taken to arrive at the solution are recorded. It is worth mentioning that the maximum number of iterations were set at 500 since most of the solutions are arrived at iterations<500. According to general observation, the solution does not converge if it goes beyond 500 iterations. Thus 500 iterations were selected as upper limit to stop the program.

The current methodology for both the algorithm/method is verified by comparing the results with available literature. The comparison is carried out for two extreme cases i.e. when the solid is absent and also when whole domain is occupied with solid without any porous medium. The results are shown in table 4.2 vindicating that both algorithm/method were able to predict the heat transfer behavior accurately.

**Table 4.2:** Validation of results for case I (No Solid)

| **Author** | $Ra = 10$ | $Ra = 100$ |
|---|---|---|
| Present | 1.0821 | 3.2126 |
| (Walker & Homsy, 1978) | | 3.097 |
| (Bejan, 1979) | | 4.2 |
| (Gross, Bear, & Hickox, 1986) | | 3.141 |
| (Manole & Lage, 1993) | | 3.118 |
| (Beckermann, Viskanta, & Ramadhyani, 1986) | | 3.113 |
| (Moya, Ramos, & Sen, 1987) | 1.065 | 2.801 |
| (A. Baytas & Pop, 1999) | 1.079 | 3.16 |
| (Misirlioglu, Baytas, & Pop, 2005) | 1.119 | 3.05 |
| (I. A Badruddin, Abdullah A. A. A Al-Rashed, et al., 2012) | 1.0798 | 3.2005 |

It should be noted that the limiting case II i.e. zero porous medium reduces the problem to simple one dimensional heat conduction phenomenon given as:

$$\frac{d^2\bar{T}}{d\bar{x}^2} = 0 \tag{4.18}$$

The analytical solution of equation (4.18) is

$$T = \frac{T_2 - T_1}{L}x + T_1 \tag{4.19}$$

In terms of non-dimensional parameters, the equation(4.19) can be expressed as:

$$\bar{T} = 1 - \bar{x} \tag{4.20}$$

Table 4.3 shows the verification of two algorithms/methods with analytical solution. It is clear from this table that the two algorithms/methods have accurately predicted the heat transfer of case II.

**Table 4.3:** Validation of results for case II (No Porous)

| $\bar{x}$-Coordinate | Analytical Solution | Developed Algorithm | Conventional Algorithm |
|---|---|---|---|
| 0.1 | 0.9 | 0.9 | 0.9 |
| 0.2 | 0.8 | 0.8 | 0.8 |
| 0.3 | 0.7 | 0.7 | 0.7 |
| 0.4 | 0.6 | 0.6 | 0.6 |
| 0.5 | 0.5 | 0.5 | 0.5 |
| 0.6 | 0.4 | 0.4 | 0.4 |
| 0.7 | 0.3 | 0.3 | 0.3 |
| 0.8 | 0.2 | 0.2 | 0.2 |
| 0.9 | 0.1 | 0.1 | 0.1 |
| 1.0 | 0 | 0 | 0 |

Table 4.4 shows the number of iterations and time taken by two methods corresponding to two algorithms. It is very clear from table 4.4 that the developed algorithm outperforms the conventional algorithm when number of elements for solid is around 10%. It is important to see that the developed algorithm converged within 400 iterations for all the tested set of solid elements that in turn determine the size of solid tested. However, the conventional method/algorithm failed to converge when the size of solid is small having fewer numbers of elements. The algorithms are tested for extreme cases i.e. when no solid is present and no porous medium exists. For the case of no solid, the solid elements are zero whereas porous elements are zero when only solid exists. It is found that both algorithms perform similarly for these two extreme cases of no solid and no porous medium. The numbers of iterations are minimum for the case of only solid.

**Table 4.4:** Performance of two algorithms

| Porous Region Elements | Solid Region Elements | Developed Algorithm | | | Conventional Algorithm | | |
|---|---|---|---|---|---|---|---|
| | | Iterations | Time sec | Remark | Iterations | Time sec | Remark |
| 2520 | 72 | 396 | 2081.7 | Converged | >500 | 2449 | Unconverged |
| 2448 | 144 | 268 | 1399.1 | Converged | >500 | 2127.1 | Unconverged |
| 2376 | 216 | 203 | 1001.9 | Converged | 274 | 1194.9 | Converged |
| 2304 | 288 | 171 | 881.7 | Converged | 170 | 873.0 | Converged |
| 2592 | 0 | 48 | 169.40 | Converged | 48 | 172.16 | Converged |
| 0 | 2592 | 3 | 32.5286 | Converged | 3 | 33.3166 | Converged |

The convergence behavior of various numbers of solid elements corresponding to different solid height is shown in figures 4.5 to 4.10 for developed algorithm as well as the conventional algorithm. The convergence behavior of figures 4.5 to 4.10 is that of a representative monitored node number 1129 which falls near the top surface of meshed domain. The convergence criteria for $\bar{\psi}$, $\bar{T}$ and $\bar{C}$ are set as $10^{-7}$, $10^{-5}$ and $10^{-5}$ respectively. The solution is said to be converged when all the nodes of domain meet the above said criteria. It is found that the developed algorithm/method converged in all the cases of solid heights in the porous medium considered. However, the conventional algorithm/method found difficulty in convergence for smaller solid height with little number of solid elements. The minimum number of solid elements at which the conventional algorithm could converge is that of 216 nodes that corresponds to 3 rows of elements at bottom section. It is obvious from figure 4.5 to 4.10 that the energy and concentration equations faced difficulty in satisfying the convergence limit but the momentum equation represented by solution variable $\bar{\psi}$, marched smoothly as compared to $\bar{T}$ and $\bar{C}$.

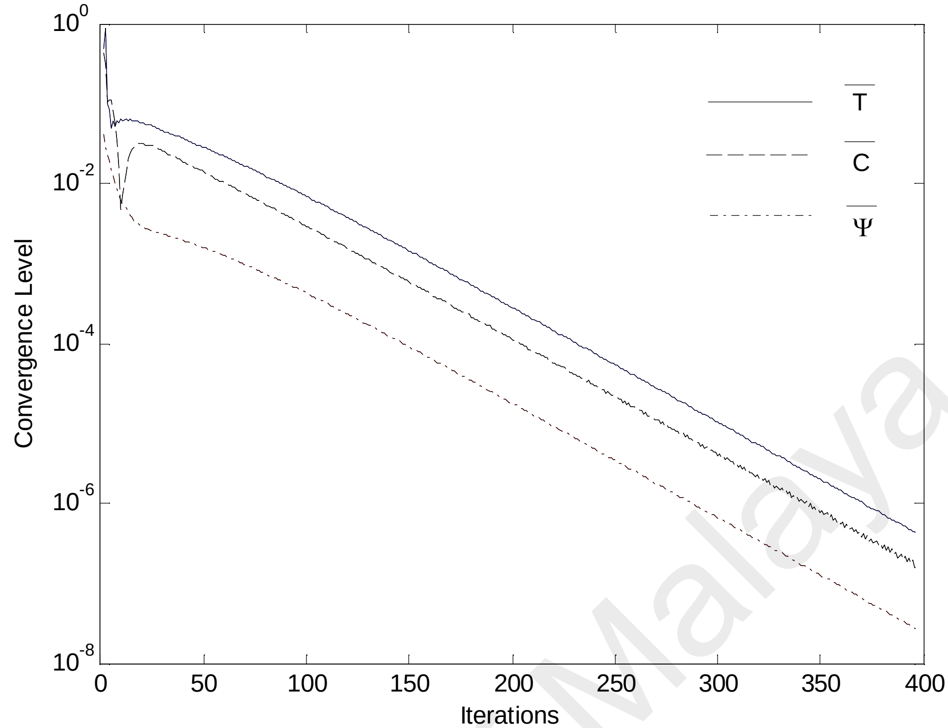


**Figure 4.5:** Convergence graph of Developed algorithm for 72 solid elements

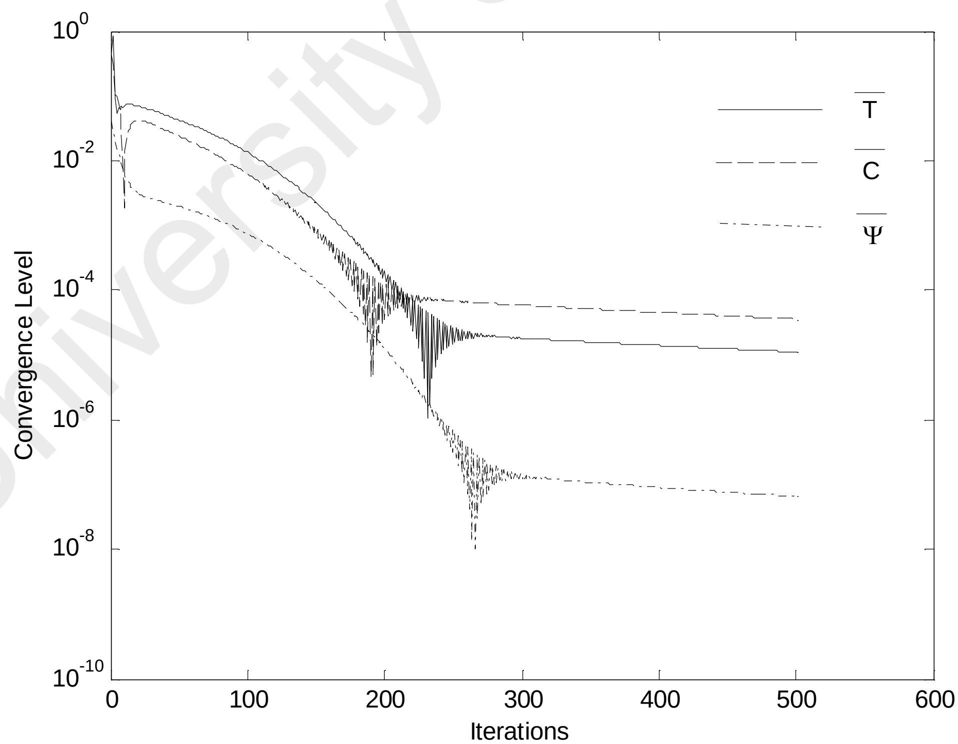


**Figure 4.6:** Convergence graph of Conventional algorithm for 72 solid elements

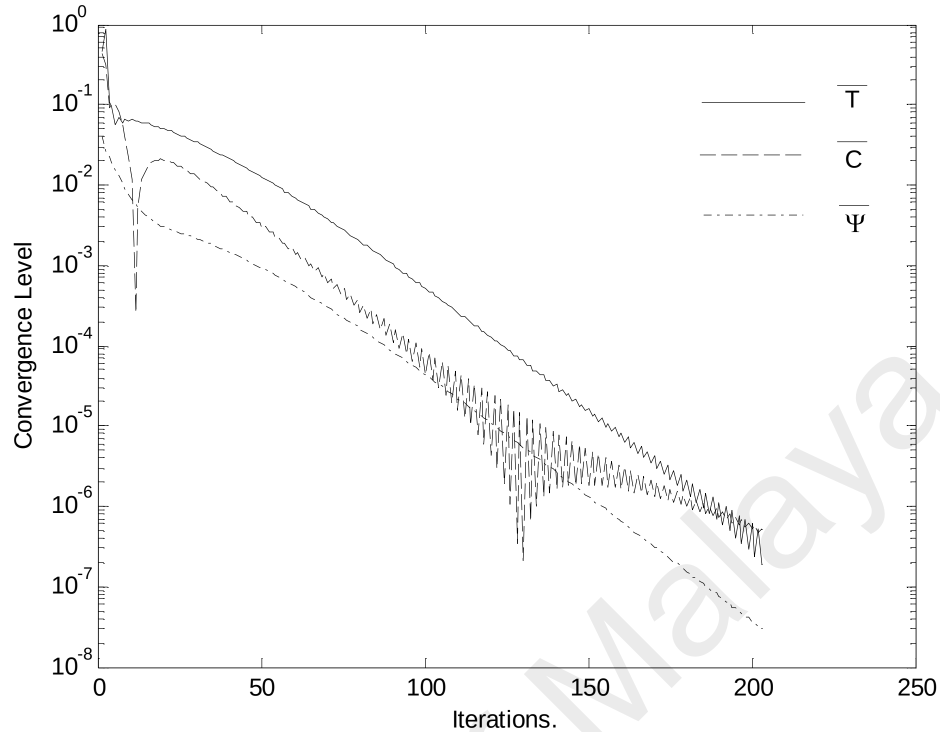


**Figure 4.7:** Convergence graph of Developed algorithm for 216 solid elements

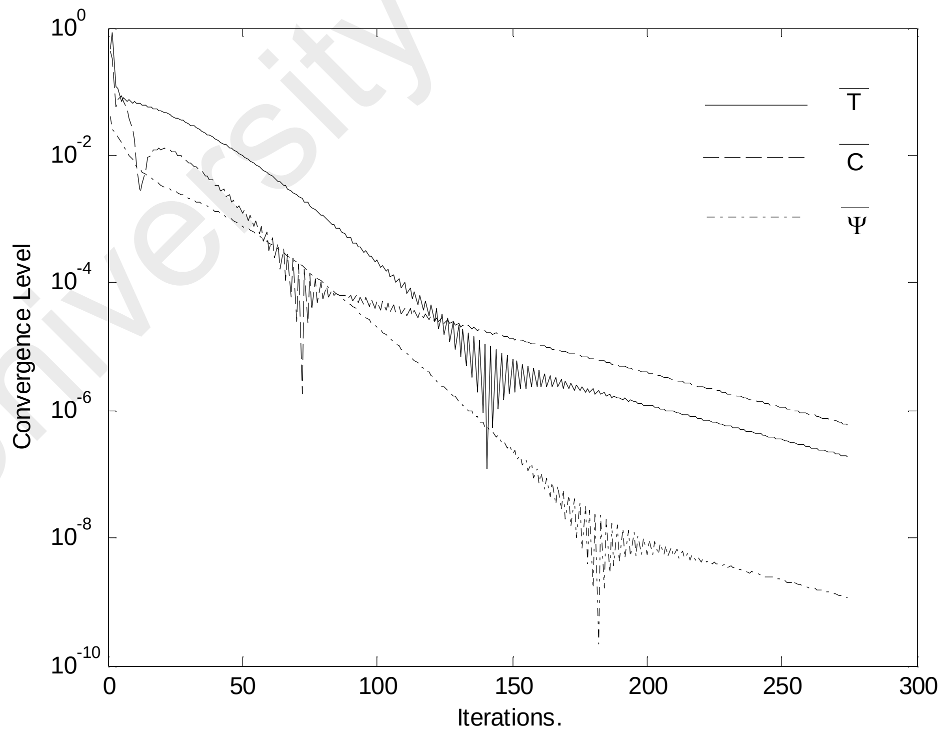


**Figure 4.8:** Convergence graph of Conventional algorithm for 216 solid elements

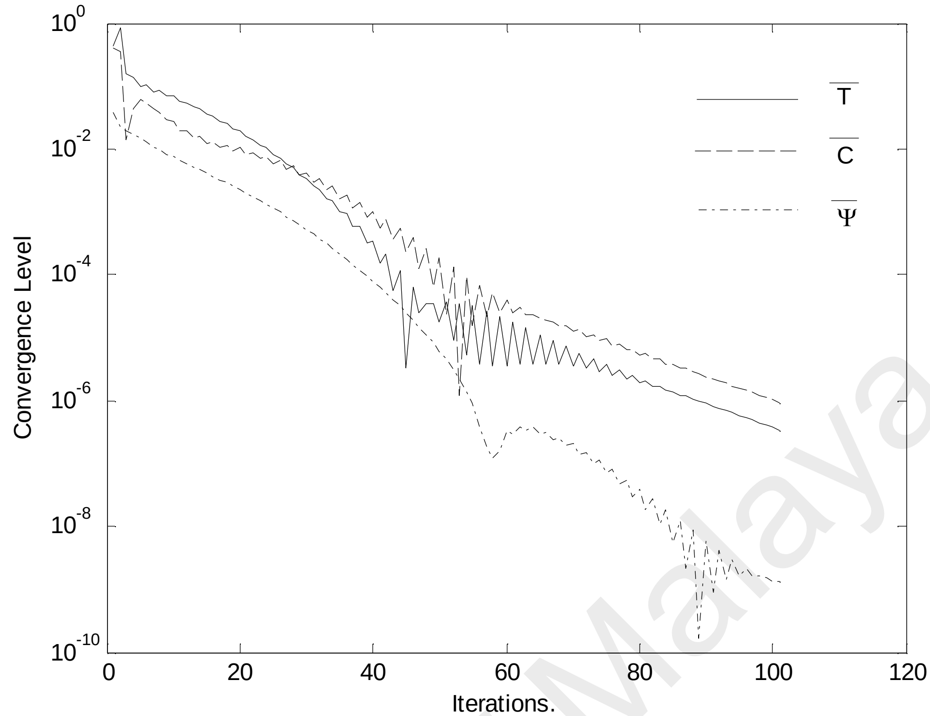


**Figure 4.9:** Convergence graph of Developed algorithm for 720 solid elements

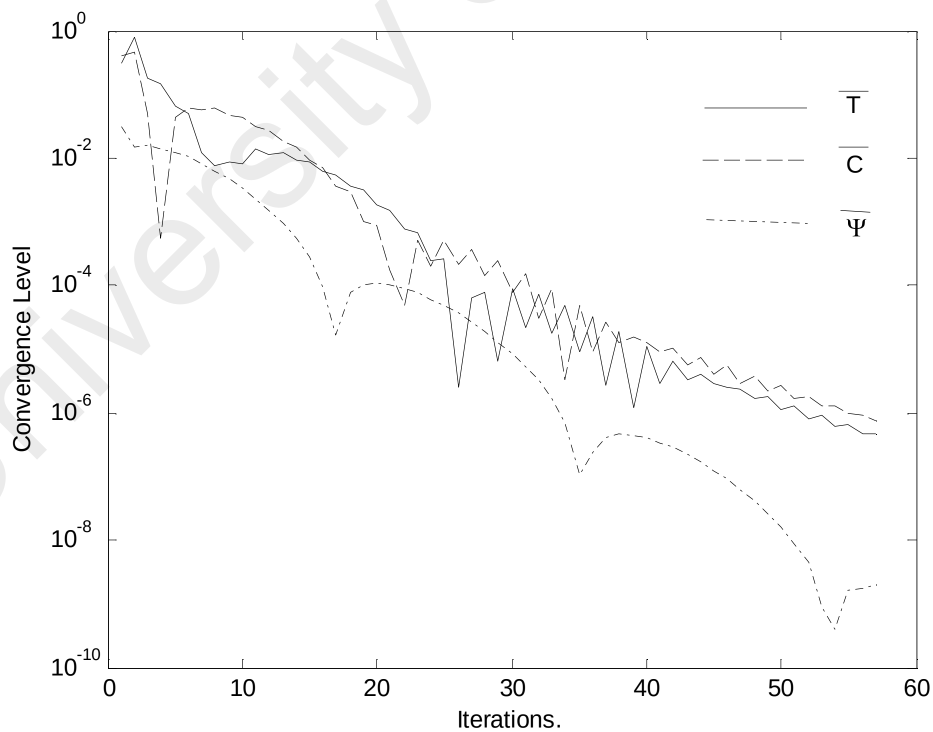


**Figure 4.10:** Convergence graph of Conventional algorithm for 720 solid elements

The results are further investigated in terms of temperature distribution obtained by two methods. The temperature distribution gives a better idea about physics of the problem considered reflecting the feasibility of method in predicting the thermal behavior in porous medium. Figure 4.11 shows the isothermal lines indicating the same temperature region in porous-solid domain when number of solid elements are 72. It should be noted that the size of solid for these many elements corresponds to first row of elements at bottom of square domain being considered. It is found that the developed algorithm predicts the expected temperature behavior of porous solid domain. The isotherms at bottom section follows different gradient due to presence of solid in that region. The developed algorithm is able to predict the variation of temperature in two dimensions in porous as well as solid region which is real behavior of thermal energy distribution. However, the conventional method could not predict the 2-dimensional temperature variation in the solid region as illustrated by figure 4.12. It is noted that the conventional algorithm/method did not satisfy the present convergence criteria even after 500 iterations are carried out for the case of 72 solid elements.

Figure 4.13 and 4.14 demonstrates the prediction of temperature distribution in porous solid region when number of solid elements are set at 216 corresponding to bottom three rows of elements of mesh (figure 4.4). It is found that the developed algorithm is able to predict the heat transfer behavior in 2-dimesional pattern for both porous as well as solid region. The isothermal behavior is very much in line with physical phenomenon of conjugate heat transfer. The conventional algorithm/method was able to predict the 2-dimensional variation of temperature in porous and solid region but failed to capture the adequate temperature variation just above the solid region where the isotherms show unrealistic pattern (figure 4.14). The temperature gradient at porous solid interface is expected to change depending upon the thermal conductivity of two mediums but it should not have sharply pointed characteristics as shown by figure 4.14.

Similarly, the developed method predicted realistically expected behavior of isotherms for the case of 720 elements, corresponding to 10 bottom rows of elements as shown in figure 4.15. However, the conventional method/algorithm shows highly unrealistic pattern of isothermal lines for same problem as shown in figure 4.16.

The reason for unrealistic prediction of conventional method/algorithm could be attributed to fewer numbers of elements of mesh domain. Generally it requires the domain to be divided into much larger number of elements to predict the heat and mass transfer behavior. However, larger the number of elements, larger is the elemental equations involved resulting into a requirement of higher amount of computational resources. Thus it can be said that the developed method is able to predict the heat and mass transfer behavior realistically with simple algorithm that consumes lesser resources as compared to that of conventional method.

Figure 4.17-4.20 shows the performance of developed and conventional algorithms for two limiting cases i.e. no solid and no porous medium. It is found that the two algorithms are very much compatible in predicting the temperature distribution in the physical domain for these limiting cases.

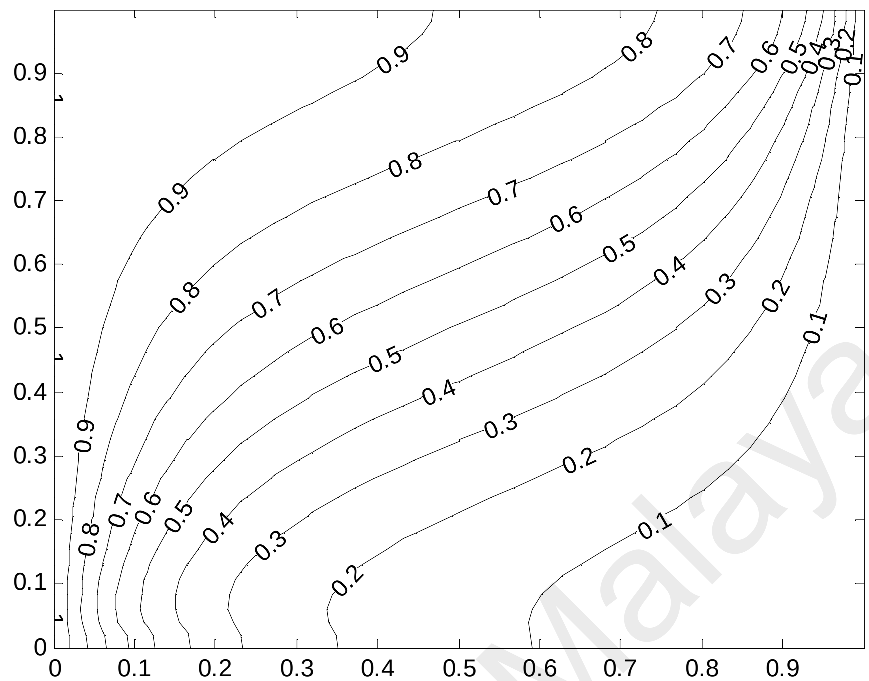


**Figure 4.11:** Isotherms of Developed algorithm for 72 solid elements

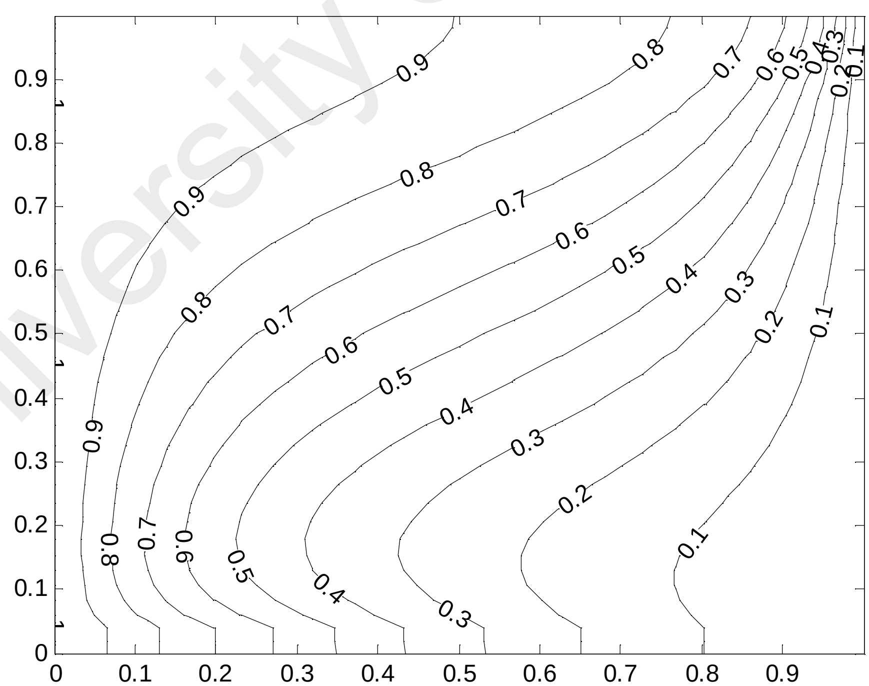


**Figure 4.12:** Isotherms of Conventional algorithm for 72 solid elements

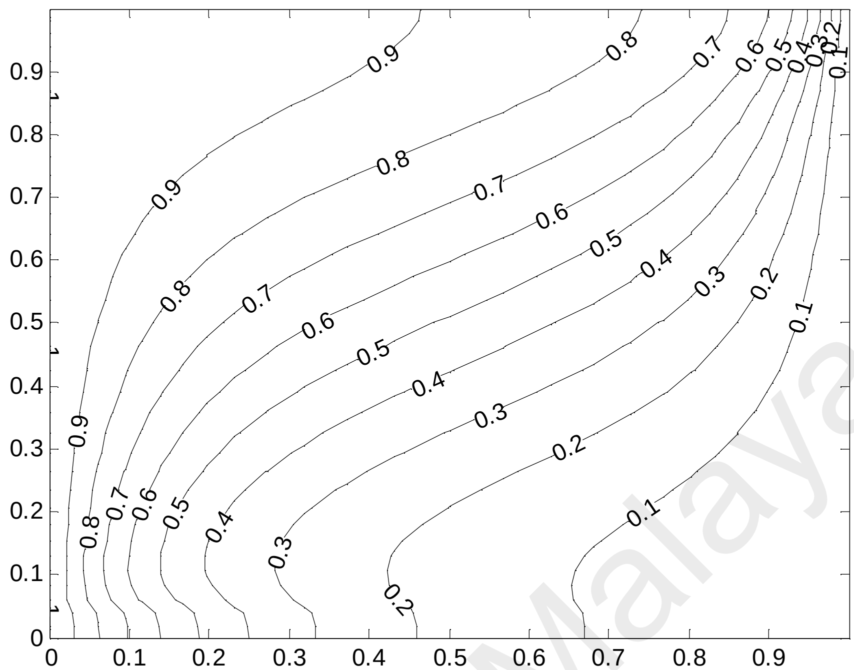


**Figure 4.13:** Isotherms of Developed algorithm for 216 solid elements

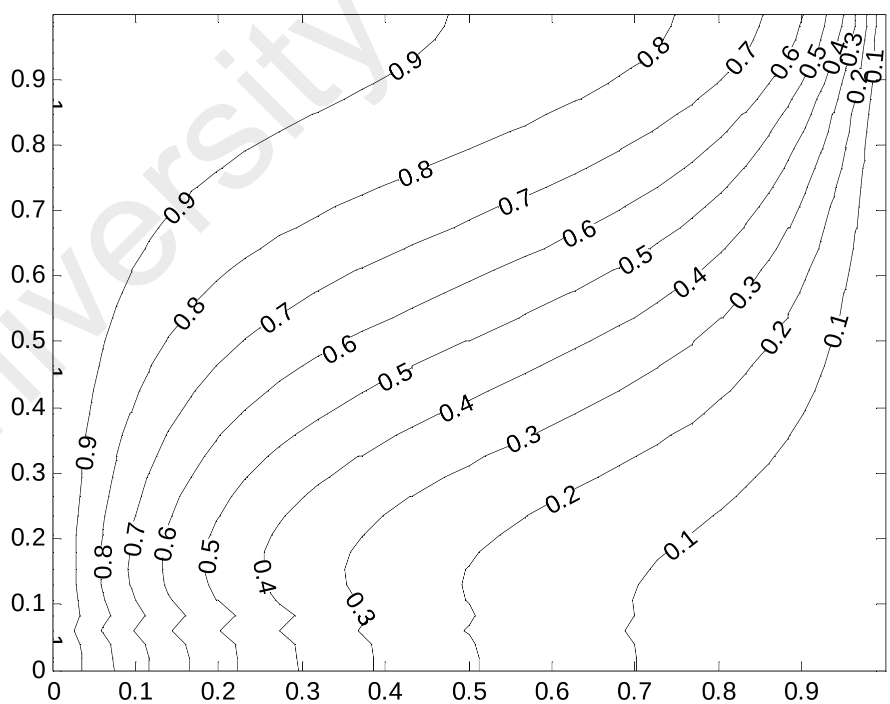


**Figure 4.14:** Isotherms of Conventional algorithm for 216 solid elements

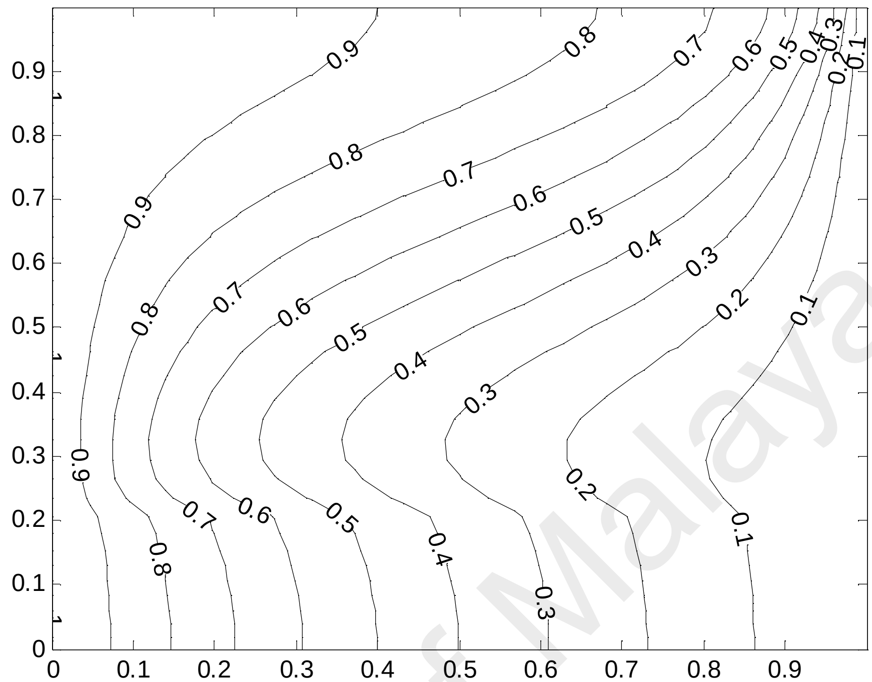


**Figure 4.15:** Isotherms of Developed algorithm for 720 solid elements

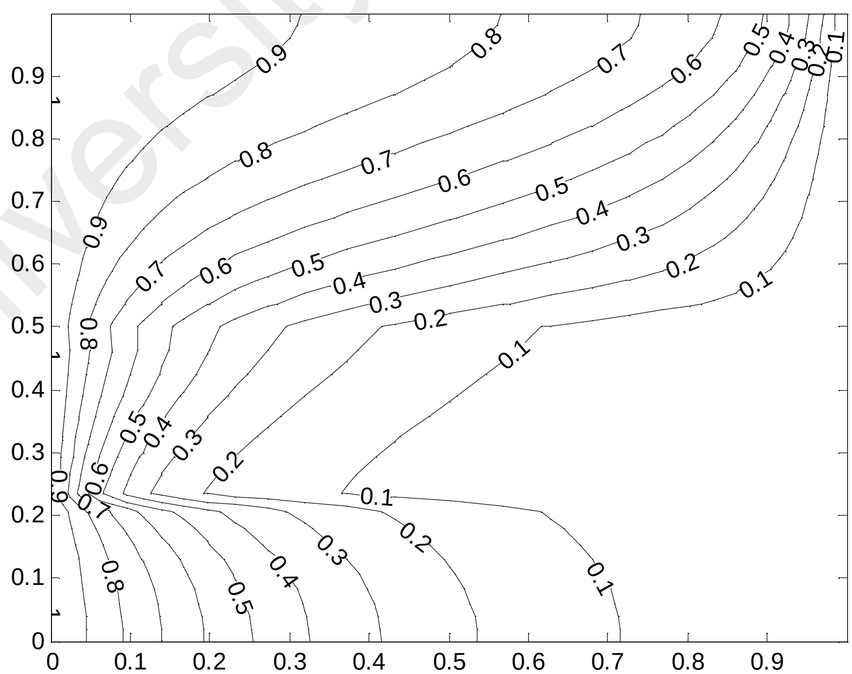


**Figure 4.16:** Isotherms of Conventional algorithm for 720 solid elements

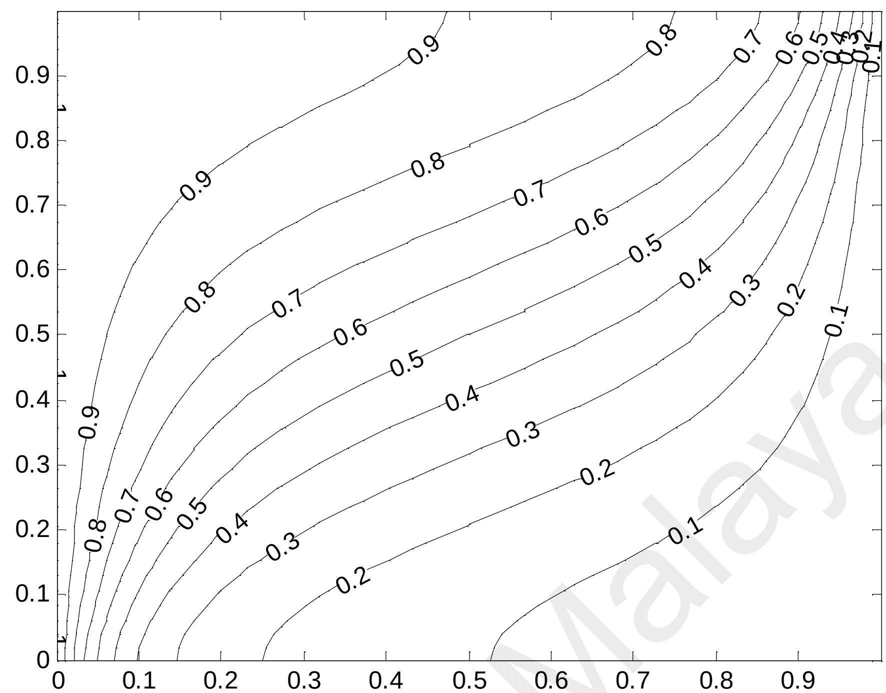


**Figure 4.17:** Isotherms of Developed algorithm for zero solid elements

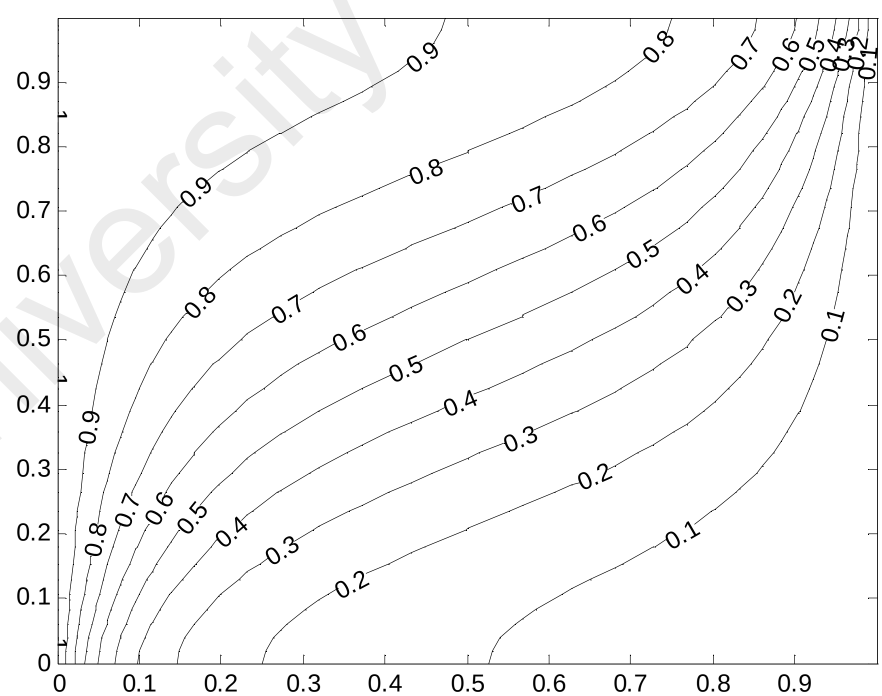


**Figure 4.18:** Isotherms of Conventional algorithm for zero solid elements

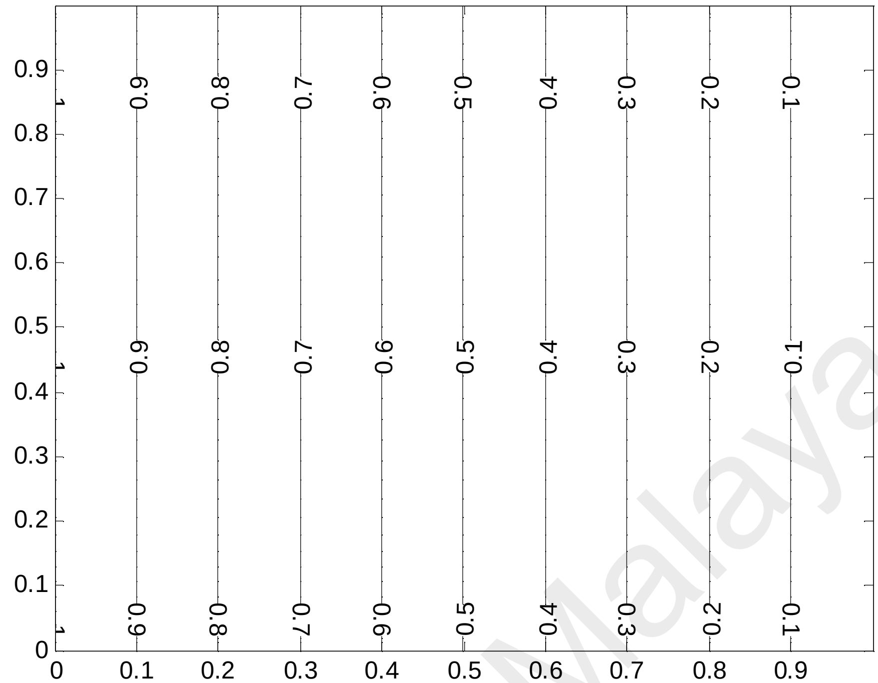


**Figure 4.19:** Isotherms of Developed algorithm for zero porous medium elements

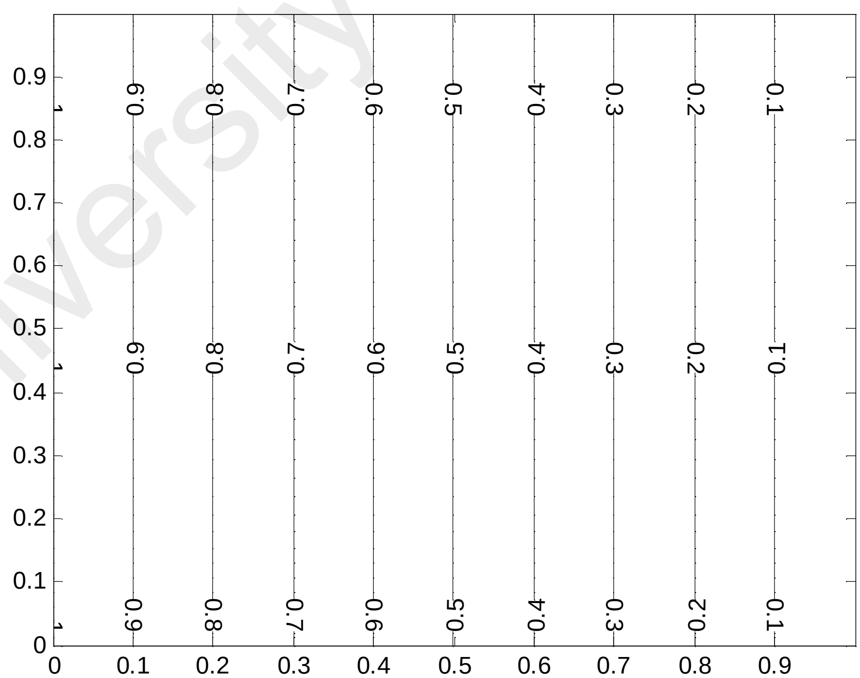


**Figure 4.20:** Isotherms of Conventional algorithm for zero porous medium elements

## 4.2 Solution of Conjugate Heat Transfer in Porous Medium

The previous section described the optimized solution of conjugate heat and mass transfer in porous medium. Similarly, the conjugate heat transfer in porous medium is optimized too. As described in chapter 3, the equations that govern conjugate heat transfer in porous medium can be written as:

$$\frac{\partial^2 \overline{\psi}}{\partial \overline{x}^2} + \frac{\partial^2 \overline{\psi}}{\partial \overline{y}^2} = -Ra \frac{\partial \overline{T}}{\partial \overline{x}} \tag{4.21}$$

$$\frac{\partial \overline{\psi}}{\partial \overline{y}} \frac{\partial \overline{T}}{\partial \overline{x}} - \frac{\partial \overline{\psi}}{\partial \overline{x}} \frac{\partial \overline{T}}{\partial \overline{y}} = \left( \left( 1 + \frac{4R_d}{3} \right) \frac{\partial^2 \overline{T}}{\partial \overline{x}^2} + \frac{\partial^2 \overline{T}}{\partial \overline{y}^2} \right) \tag{4.22}$$

$$\left( 1 + \frac{4R_d}{3} \right) \frac{\partial^2 \overline{T}_s}{\partial \overline{x}^2} + \frac{\partial^2 \overline{T}_s}{\partial \overline{y}^2} = 0 \tag{4.23}$$

The application of finite element method to 4.21 -4.23 yields:

$$\frac{1}{4A} \left\{ \begin{bmatrix} b_1^2 & b_1 b_2 & b_1 b_3 \\ b_1 b_2 & b_2^2 & b_2 b_3 \\ b_1 b_2 & b_2 b_3 & b_3^2 \end{bmatrix} + \begin{bmatrix} c_1^2 & c_1 c_2 & c_1 c_3 \\ c_1 c_2 & c_2^2 & c_2 c_3 \\ c_1 c_2 & c_2 c_3 & c_3^2 \end{bmatrix} \right\} \begin{Bmatrix} \overline{\psi}_1 \\ \overline{\psi} 2 \\ \overline{\psi} 3 \end{Bmatrix} = \frac{Ra}{6} \begin{Bmatrix} b_1 \overline{T}_1 + b_2 \overline{T}_2 + b_3 \overline{T}_3 \\ b_1 \overline{T}_1 + b_2 \overline{T}_2 + b_3 \overline{T}_3 \\ b_1 \overline{T}_1 + b_2 \overline{T}_2 + b_3 \overline{T}_3 \end{Bmatrix} \tag{4.24}$$

$$\frac{1}{12A} \begin{Bmatrix} c_1 \overline{\psi}_1 + c_2 \overline{\psi}_2 + c_3 \overline{\psi}_3 \\ c_1 \overline{\psi}_1 + c_2 \overline{\psi}_2 + c_3 \overline{\psi}_3 \\ c_1 \overline{\psi}_1 + c_2 \overline{\psi}_2 + c_3 \overline{\psi}_3 \end{Bmatrix} \begin{bmatrix} b_1 & b_2 & b_3 \end{bmatrix} - \frac{1}{12A} \begin{Bmatrix} b_1 \overline{\psi}_1 + b_2 \overline{\psi}_2 + b_3 \overline{\psi}_3 \\ b_1 \overline{\psi}_1 + b_2 \overline{\psi}_2 + b_3 \overline{\psi}_3 \\ b_1 \overline{\psi}_1 + b_2 \overline{\psi}_2 + b_3 \overline{\psi}_3 \end{Bmatrix} \begin{bmatrix} c_1 & c_2 & c_3 \end{bmatrix}$$

$$+ \frac{1}{4A} \left[ \left( 1 + \frac{4}{3} R_d \right) \begin{bmatrix} b_1^2 & b_1 b_2 & b_1 b_2 \\ b_1 b_2 & b_2^2 & b_2 b_3 \\ b_1 b_3 & b_2 b_3 & b_3^2 \end{bmatrix} + \begin{bmatrix} c_1^2 & c_1 c_2 & c_1 c_3 \\ c_1 c_2 & c_2^2 & c_2 c_3 \\ c_1 c_2 & c_2 c_3 & c_3^2 \end{bmatrix} \right] \begin{Bmatrix} \overline{T}_1 \\ \overline{T}_2 \\ \overline{T}_3 \end{Bmatrix} = 0 \tag{4.25}$$

$$\frac{1}{4A} \left[ \left( 1 + \frac{4}{3} R_d \right) \begin{bmatrix} b_1^2 & b_1 b_2 & b_1 b_2 \\ b_1 b_2 & b_2^2 & b_2 b_3 \\ b_1 b_3 & b_2 b_3 & b_3^2 \end{bmatrix} + \begin{bmatrix} c_1^2 & c_1 c_2 & c_1 c_3 \\ c_1 c_2 & c_2^2 & c_2 c_3 \\ c_1 c_2 & c_2 c_3 & c_3^2 \end{bmatrix} \right] \begin{Bmatrix} \overline{T}_{1s} \\ \overline{T}_{2s} \\ \overline{T}_{3s} \end{Bmatrix} = 0 \tag{4.26}$$

Following the similar procedure as described in section 4.1, the above equations of conjugate heat transfer in porous medium can be solved by following the process flow as shown in figure 4.21 and 4.22.

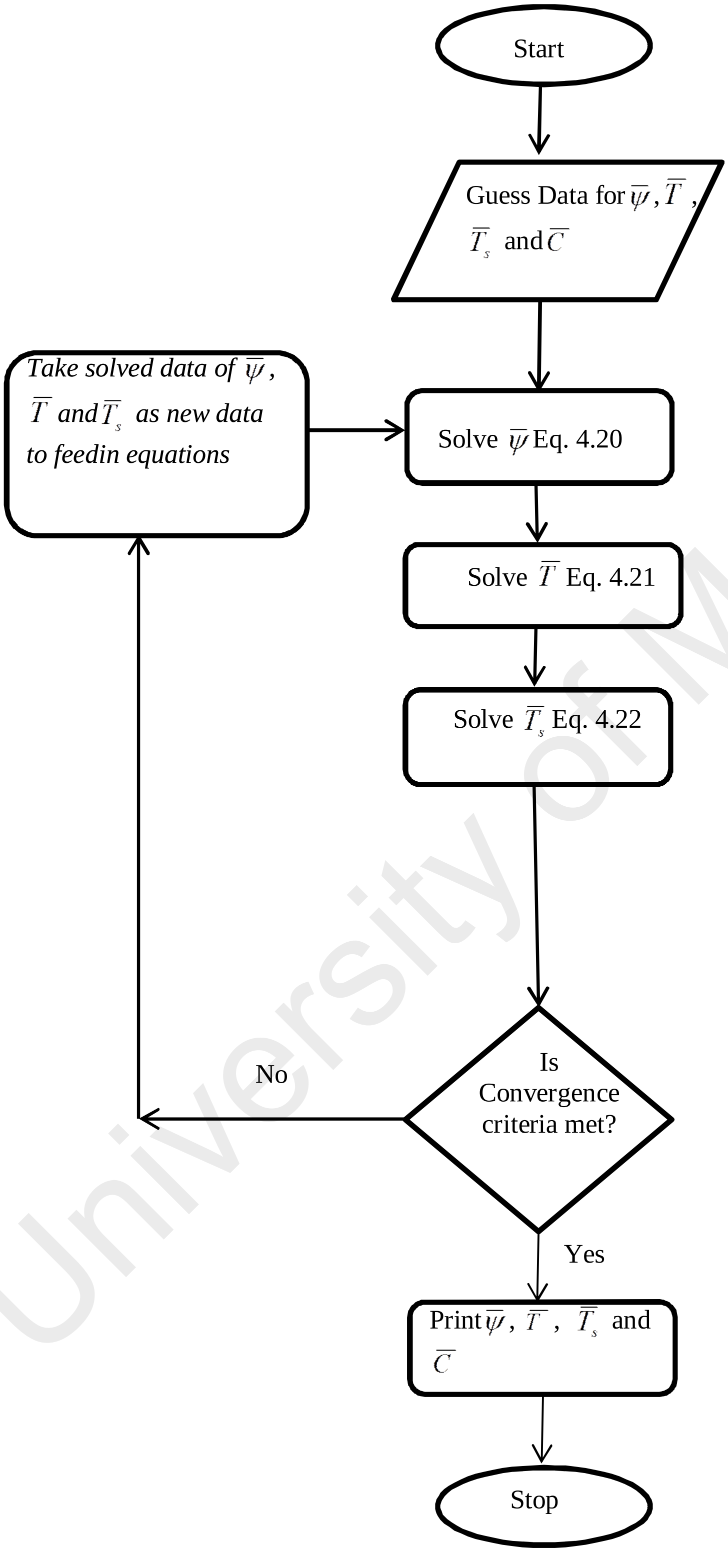


**Figure 4.21:** Flow chart of conventional solution procedure for conjugate heat transfer in porous medium

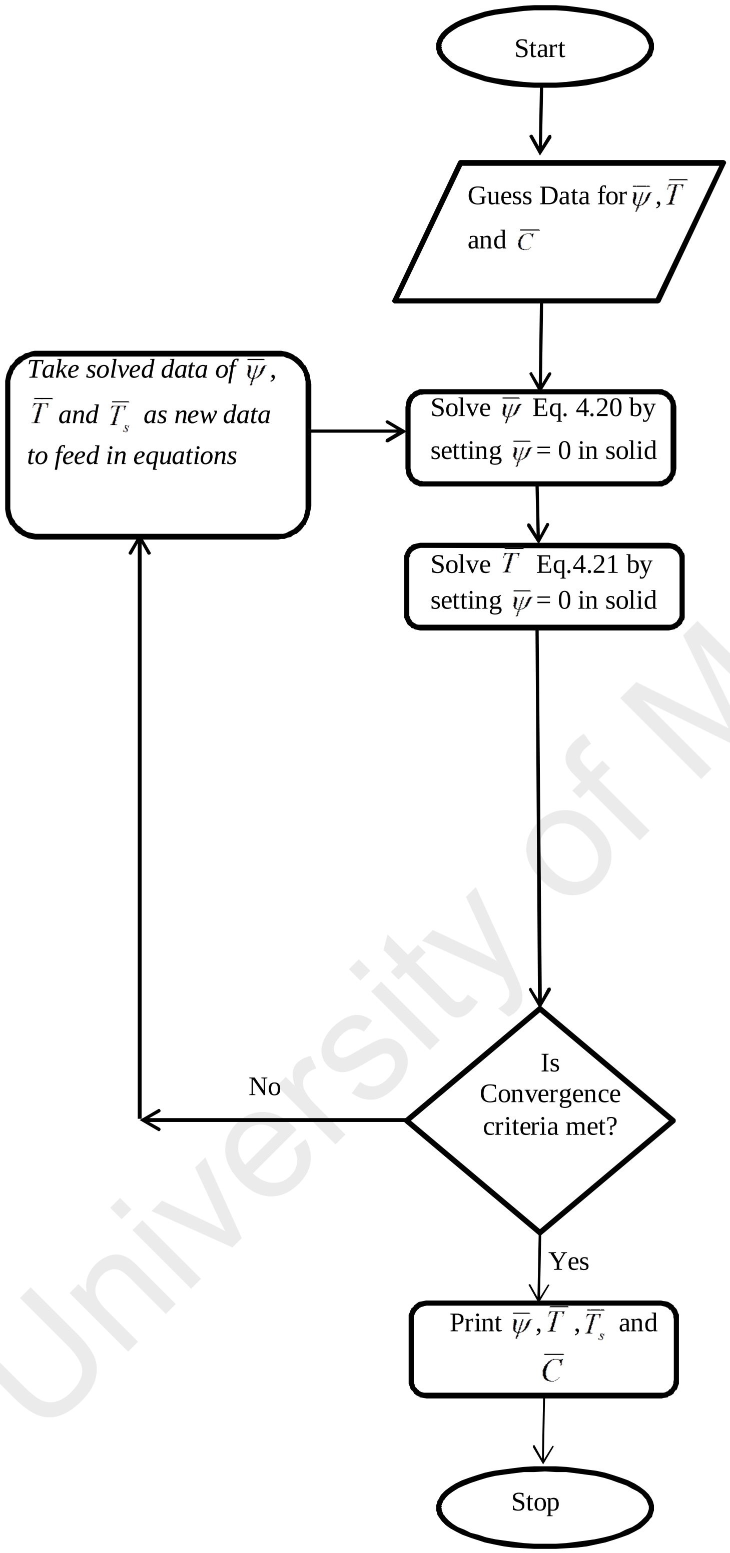


**Figure 4.22:** Flow chart of developed solution procedure for conjugate heat and mass transfer in porous medium

Comparison of Developed and Conventional Algorithm/method for conjugate heat, mass transfer and conjugate heat transfer in porous medium is listed in table 4.5

**Table 4.5:** Comparison of two solution algorithms/methods

| **Contributing Factor** | **Developed Algorithm** | **Conventional Algorithm** |
|---|---|---|
| Number of effective equations to be solved for conjugate heat and mass transfer | 3 | 4 |
| Number of effective equations to be solved for conjugate heat transfer | 2 | 3 |
| Mesh generation | It requires a regular mesh such as square domain without any discontinuity | It requires two separate mesh i.e. one each for porous region as well as solid region that should be stitched together while solution proceeds from one region to another region |
| Mesh complexity | Relatively easy | Very complex for small solid placed at any arbitrary region in cavity |
| Solution feasibility | Works well for any complex solid geometry | Works well for only simple solid geometry |
| Computer code generation | Relatively easy since it eliminates one complete subroutine for energy equation of solid | Quite involved |
| Length of code | Shorter | Longer |
| Application of boundary conditions in code | Bit difficult | Relatively easy |
| Computer resources required | Generally low | Generally high |

# CHAPTER 5 : EFFECT OF SIZE AND LOCATION OF SOLID ON CONJUGATE HEAT TRANSFER IN POROUS CAVITY

The current chapter highlights the heat transfer and fluid flow behavior of square porous cavity due to presence of a solid wall. The solid wall is small portion of the whole domain whose size is varied at 5 different locations of the cavity such as left ($\bar{x} = 0$), center ($\bar{x} = 0.5L$), right ($\bar{x} = L$), mid of left and center ($\bar{x} = 0.25L$), mid of center and right ($\bar{x} = 0.75L$) wall of cavity. The governing partial differential equations are solved using finite element method with the whole domain being divided into triangular elements. The left wall ($\bar{x} = 0$) of cavity is heated isothermally to temperature $T_h$ whereas the right wall ($\bar{x} = L$) is maintained at $T_c$ such that $T_h > T_c$.

## 5.1 Introduction

The advent of computational technology has played a vital role in solving many of the unsolved mathematical problems thus facilitating to understand the complex physical phenomenon which otherwise could have been left unanswered. Conjugate heat transfer in porous medium is one such phenomenon whose understanding was improved after the arrival of computer and advancement of computational methods. The conjugate heat transfer refers to a situation where heat transfer occurs simultaneously between fluid and solid emanating a complex boundary condition between fluid and solid. The natural convection in porous medium has been studied to a great detail addressing various issues such as geometries (Ahmed, Badruddin, Kanesan, Zainal, & Ahamed, 2011; N. S. Ahmed, I. A. Badruddin, Z. Zainal, H. Khaleed, & J. Kanesan, 2009; I.  A Badruddin, N. J. S Ahmed, et al., 2012; I.  A Badruddin, Abdullah A. A. A Al-Rashed, et al., 2012; Badruddin, Al-Rashed, Ahmed, Kamangar, & Jeevan, 2012; Kumaran & Pop, 2006; Ogulu & Amos, 2005; Raptis, 1998) but conjugate heat transfer received relatively lesser attention.

Generally, the conjugate heat transfer is reported for the cases where the solid wall is attached to whole of the surface at one end of geometry under investigation.

For instance, the solid wall attached to left wall of cavity is investigated by (Al-Amiri et al., 2008; Nawaf H Saeid, 2007; Nawaf H. Saeid, 2007). It is reported that the phenomenon of attaining maximum Nusselt number at aspect ratio around 1 vanishes when solid wall is present at the inside radius of vertical annulus (Salman et al., 2014). The attachment of two solid walls at parallel surfaces of a porous geometry affects the heat transfer behavior as compared that of single wall. It was noticed that for small values of Rayleigh number, the average Nusselt number is approximately constant and heat is transferred by conduction in both wall and porous layer in case of a porous medium sandwiched between two vertical solid wall (Nawaf H. Saeid, 2007).

A similar geometry was considered by (Alhashash et al., 2013) to investigate the effect of non-uniform heat generation along with radiation and found that there exists a critical value of wall thickness below which the thickness and heat transfer rate is directly proportional and vice versa. It was further reported that the radiation and internal heat generation do not play a crucial role on the critical thickness. Two solid walls at top and bottom surface of cavity are analyzed by (A. C. Baytas et al., 2001). The presence of two solid walls is studied for other geometries as well. For instance, the effect of varying thermal conductivity of two solids attached at internal and external radii of an annular porous cylinder was investigated to reveal that the effect of solid conductivity ratio diminishes as the solid wall thickness at inner radius increases and heat transfer rate decreases with increase in the solid conductivity ratio (Badruddin et al., 2015). The heat transfer behavior of triangular porous geometry with solid wall at bottom is reported by (Varol et al., 2009) whereas the triangular solid at the lower left corner of square cavity was investigated by (Chamkha & Ismael, 2013b). Some of other work in the area of conjugate heat transfer in porous media can be found as inclined vertical plate (Ali et al., 2013), bi-disperse porous channel (D. A. Nield & Kuznetsov, 2004),porous channel(Mahmud & Fraser, 2005), conjugate mixed convection due to a vertical surface in porous medium (I. Pop & Merkin, 1995). square cavity embedded with a small solid heat source at the bottom surface of the cavity (A. C. Baytas et al., 2001), finite horizontal flat plate in the porous medium (Aleshkova & Sheremet, 2010), vertical slender hollow cylinder (Kaya, 2011; I. Pop & Na, 2000), vertical thin strip with heat generation (I. Pop & Merkin, 1995), vertical surface in separating two porous media (Vaszi et al., 2002) and vertical rounded fin inserted in porous medium (Vaszi et al., 2004). The current work is aimed to understand the heat and fluid flow behavior due to presence of a solid wall inside the porous medium when its location is varied from left to right surface of cavity.

## 5.2 Mathematical Model

Consider a square porous cavity with a small solid wall embedded within the porous medium. The schematic of the problem under consideration and coordinate system is depicted in figure 5.1. The presence of small solid wall in the porous medium makes it a conjugate heat transfer problem. The height of solid wall is varied in two steps along with its location in 5 different positions. In first step, the left surface of solid wall coincides with the left surface of cavity i.e. $\bar{x} = 0$. In the 2nd, 3rd and 4th step, the center of solid wall is placed at 0.25L, 0.5L and 0.75L (25%, 50% and 75% of cavity width). In the last step, the right surface of solid coincides with right surface of cavity. The left and right surface of cavity is isothermally maintained at hot $T_h$ and cool temperature $T_c$ respectively, such that $T_h > T_c$. Following assumptions are applied:

a) The Darcy law is applicable in the porous medium.

b) The properties of the fluid and those of the porous medium are homogeneous.

c) Fluid properties are constant except the variation of density with temperature.

d) There is no phase change of fluid

e) The thermal equilibrium exists between fluid and solid phase of porous medium

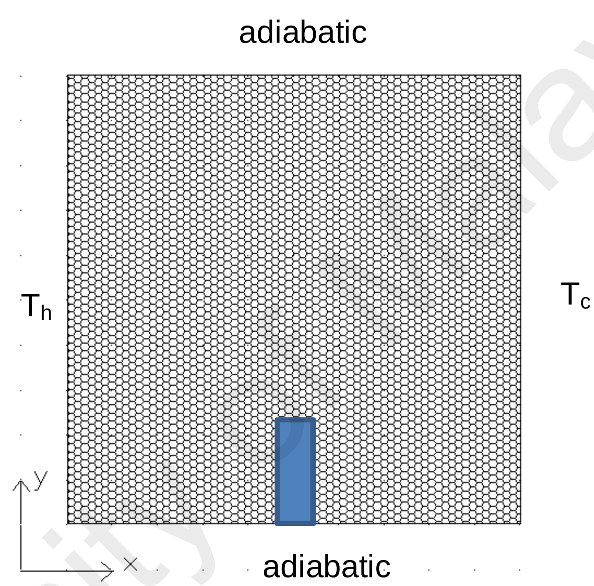


**Figure 5.1:** Porous cavity with solid at center (3rd position i.e. 50% of cavity width)

The governing equations resulting due to above mentioned problems are

Continuity equation

$$\frac{\partial u}{\partial x}+\frac{\partial \mathrm{v}}{\partial y}=0 \qquad (5.1)$$

Momentum equation

$$\frac{\partial u}{\partial y}-\frac{\partial \mathrm{v}}{\partial x}=-\frac{g\beta K}{\nu}\frac{\partial T}{\partial x} \qquad (5.2)$$

Energy equation for porous medium

$$u\frac{\partial T_p}{\partial x}+\mathrm{v}\frac{\partial T_p}{\partial y}=\alpha\left(\frac{\partial^2 T_p}{\partial x^2}+\frac{\partial^2 T_p}{\partial y^2}\right)-\frac{1}{\rho C_p}\frac{\partial q_r}{\partial x} \tag{5.3}$$

Energy equation for solid

$$\frac{\partial^2 T_s}{\partial x^2}+\frac{\partial^2 T_s}{\partial y^2}-\frac{1}{\alpha\rho C_p}\frac{\partial q_r}{\partial x}=0 \tag{5.4}$$

Subjected to boundary conditions:

at $x=0 \quad u=0 \quad T=T_h$ (5.5a)

at $x=L, \quad u=0 \quad T=T_c$ (5.5b)

Since there is no heat storage in the medium, the following condition at solid-porous interface has to be satisfied.

at $x=x_{sp} \quad u=0 \quad T_s=T_p \quad k_s\frac{\partial T_s}{\partial x}=k_p\frac{\partial T_p}{\partial x}$ (5.5c)

at $y=y_{sp} \quad v=0 \quad T_s=T_p \quad k_s\frac{\partial T_s}{\partial y}=k_p\frac{\partial T_p}{\partial y}$ (5.5d)

Equation (1) can be satisfied automatically by introducing the stream function ψ as:

$$u=\frac{\partial\psi}{\partial y} \quad \mathrm{v}=-\frac{\partial\psi}{\partial x} \tag{5.6}$$

Following non-dimensional parameters are used.

$$\bar{x}=\frac{x}{L}, \quad \bar{y}=\frac{y}{L}, \quad \bar{\psi}=\frac{\psi}{\alpha}, \quad \bar{T}=\frac{(T-T_c)}{(T_h-T_c)}, \quad Rd=\frac{4\sigma T_c^{\,3}}{\beta_r k}, \quad Ra=\frac{g\beta\ \Delta TKL}{\nu\alpha}$$

Invoking Rosseland approximation for radiation.

$$q_r=-\frac{4\sigma}{3\beta_r}\frac{\partial T^4}{\partial x} \tag{5.7}$$

Expanding $T^4$ in Taylor series about $T_c$ and neglecting higher order terms (I. A. Badruddin, Z. Zainal, A. Narayana, K. Seetharamu, & L. W. Siew, 2006; I. A Badruddin, Z. A. Zainal, P. A. Aswatha Narayana, & K. N. Seetharamu, 2006; I. A Badruddin, Z. A. Zainal, P. A. Aswatha Narayana, K. N. Seetharamu, et al., 2006; Nik-Ghazali, Badruddin, Badarudin, & Tabatabaeikia, 2014; Raptis, 1998)

$$T^4 \approx 4TT_\infty^3 - 3T_\infty^4 \tag{5.8}$$

Substituting equations (5.6-5.8) into equation (5.2-5.4) yields:

$$\frac{\partial^2\overline{\psi}}{\partial\overline{x}^2} + \frac{\partial^2\overline{\psi}}{\partial\overline{y}^2} = -Ra\frac{\partial\overline{T_p}}{\partial\overline{x}} \tag{5.9}$$

$$\left[\frac{\partial\overline{\psi}}{\partial\overline{y}}\frac{\partial\overline{T}}{\partial\overline{x}} - \frac{\partial\overline{\psi}}{\partial\overline{x}}\frac{\partial\overline{T}}{\partial\overline{y}}\right] = \left(\left(1+\frac{4R_d}{3}\right)\frac{\partial^2\overline{T}}{\partial\overline{x}^2} + \frac{\partial^2\overline{T}}{\partial\overline{y}^2}\right) \tag{5.10}$$

$$\left(1+\frac{4R_d}{3}\right)\frac{\partial^2\overline{T}}{\partial\overline{x}^2} + \frac{\partial^2\overline{T}}{\partial\overline{y}^2} = 0 \tag{5.11}$$

The corresponding boundary conditions are

at $\overline{x}=0$ $\quad \overline{\psi}=0 \quad \overline{T}=1$ (5.12a)

at $\overline{x}=1$ $\quad \overline{\psi}=0 \quad \overline{T}=0$ (5.12b)

at $\overline{x}=x_{sp}$ $\quad \overline{\psi}=0, \quad Kr\frac{\partial\overline{T_s}}{\partial\overline{x}} = \frac{\partial\overline{T_p}}{\partial\overline{x}}$ (5.12c)

at $\overline{y}=\overline{y}_{sp}$ $\quad \overline{\psi}=0 \quad Kr\frac{\partial\overline{T_s}}{\partial\overline{y}} = \frac{\partial\overline{T_p}}{\partial\overline{y}}$ (5.12d)

## 5.3 Numerical Scheme

The above mentioned equations (5.9-5.11) are complex partial differential equations subjected to intricate boundary conditions (5.12) that are difficult to solve directly. In the present case, they are solved by making use of finite element method. The whole domain is divided into smaller segments known as elements of triangular shape. The geometry is meshed with sufficient number of elements to make sure that the results are not affected due to mesh size Equations (5.9-5.11) are converted into algebraic form of equations with the help of finite element method and then solved in a iterative manner for solution variables $\bar{T}$ *and* $\bar{\psi}$ by setting the convergence criteria as $10^{-9}$ and $10^{-6}$ for $\bar{\psi}$ *and* $\bar{T}$ respectively . The tolerance level indicates the difference in the value of solution variable ( $\bar{\psi}$ *and* $\bar{T}$ ) from its previous iteration for each of the nodes in the domain. The present methodology is validated with the previously published data by setting the solid wall thickness to zero that corresponds to square porous cavity. The comparison is shown in table 1 to illustrate that the current method is accurate enough to simulate the heat transfer behavior of problem under consideration.

**Table 5.1:** Validation of results

| Author | $Ra$=10 | $Ra$ = 100 |
|---|---|---|
| Present | 1.0845 | 3.3983 |
| (Walker & Homsy, 1978) | | 3.097 |
| (Bejan, 1979) | | 4.2 |
| (Gross et al., 1986) | | 3.141 |
| (Manole & Lage, 1993) | | 3.118 |
| (Beckermann et al., 1986) | | 3.113 |
| (Moya et al., 1987) | 1.065 | 2.801 |
| (A. Baytas & Pop, 1999) | 1.079 | 3.16 |
| (Misirlioglu et al., 2005) | 1.119 | 3.05 |
| (I. A Badruddin, Abdullah A. A. A Al-Rashed, et al., 2012) | 1.0798 | 3.2005 |

### 5.4 Results and Discussion

The following section describes the results obtained by solving equations (5.9-5.11) for various values of thermal conductivity ratio, location and height of solid wall in the porous medium. The height of solid wall "$S_h$" is varied in 2 steps i.e 20% and 50% of total height of cavity. Figure 5.2 shows the isotherms and streamlines for the case when solid wall coincides with the left surface of cavity for $Ra=100$, $R_d=0.5$, $S_h=0.20$ and different values of thermal conductivity ratio i.e. $Kr=0.1$, *1 and 10*. It should be noted that $Kr$ is the ratio of thermal conductivity of solid wall and porous medium. $Kr>1$ indicates that the solid wall thermal conductivity is higher than that of porous medium and vice versa for $Kr<1$. It is seen that the increase in the thermal conductivity ratio increases the heat transfer from solid to porous region. The isotherms are clustered near the solid wall for low value of thermal conductivity ratio ($Kr=0.1$) but it spreads out of solid wall owing to increased thermal conductivity ratio. The fluid flow direction also tilts to about 35 degree to vertical as compared to being nearly horizontal at $Kr=0.1$. Figure 5.3 shows the effect of increasing the height of the solid wall from 20% to 50% of cavity height. The increased solid wall height results into more fluid to be concentrated at upper section of cavity at low Kr. This happens because of the reason that the thermal resistance is low at upper section of cavity compared to lower section occupied by solid wall, thus the fluid gets more heat in that region leading to higher activity.

Figure 5.4 depicts the isotherms and streamlines when the solid is placed at 25% of cavity width with other parameters being same as that of above mentioned case. It is seen that the fluid gets obstructed due to presence of solid wall inside the porous medium and that region is occupied with crowded streamlines. The strength of streamlines decreases due to solid wall as compared to the case when wall is attached with the left surface of cavity. Figure 5.5 shows the effect of increased solid height i.e. $S_h=0.5$ for solid being placed at 25% cavity width. It is observed that the isotherms have distorted pattern above the solid height indicating higher convective heat transfer in that area. The magnitude of streamline is considerably reduced when height of solid wall increases. This can be attributed to greater flow resistance caused by large solid wall in the path of fluid movement. The flow pattern also changed to concentrate on upper side of cavity.

Figure 5.6 shows the isotherms and streamlines when solid wall is placed exactly at the center of cavity. It is interesting to note that the solid wall attains more uniformity in temperature as compared to the earlier cases which is evident from figure 5.6 that shows only 5 isotherms (fig 5.6a) inside the solid as compared to 10 isotherms of previously discussed cases (fig 5.2-5.5). The strength of streamlines is stronger when solid is placed at the center. This could be due to the reason that the fluid does have sufficient space to gain momentum before it encounters the obstruction of solid compared to other cases. The solid temperature varies considerably when the $S_h$ is increased to 50% at center of cavity, as illustrated in figure 5.7. In this case the maximum and minimum non-dimensional temperature is found to be 0.6 and 0.15 respectively whereas this variation was only 0.3 and 0.1 when solid height was 20% (fig 5.6a). The flow is concentrated more on left side of cavity at smaller value of *Kr* but it tries to attain uniformity across cavity when *Kr* increases. The fluid cell breaks into two separate flow regions when conductivity of solid increases.

The variation of temperature in solid wall further decreases when its location is moved towards right wall of cavity as obvious from figure 5.8 that the maximum and minimum temperature is just 0.15 and 0.05 respectively. The fluid flow strength further increases when solid is moved farther away from left wall. It is notable that the fluid strength is not dependent on conductivity ratio *Kr* for this particular case since the maximum value of $\overline{\psi}$ is 0.44 for all three values of *Kr*. However, there is slight increase in fluid strength (absolute value of $\overline{\psi}$ increases from 0.034 to 0.036) when solid height is increased to 50% at same location and *Kr* is increased from 0.1 to 10, as shown in figure 5.9.

Figure 5.10 illustrates the effect of moving the solid wall to cold wall. It is seen that the solid wall attains minimum temperature compared to all other corresponding positions (fig 5.2, 5.4, 5.6, 5.8) when placed at right wall of cavity for $S_h=0.20$. The solid wall temperature is similar to that of cold wall when conductivity ratio *Kr* is increased to 10. The flow strength is similar to that of previous case (fig 5.9). The increase in solid wall height at cold wall of cavity makes the solid to have different temperatures along the x-direction similar to previously discussed cases (fig 5.11). However, the increased *Kr* forces the solid temperature to be similar to that of cold wall.

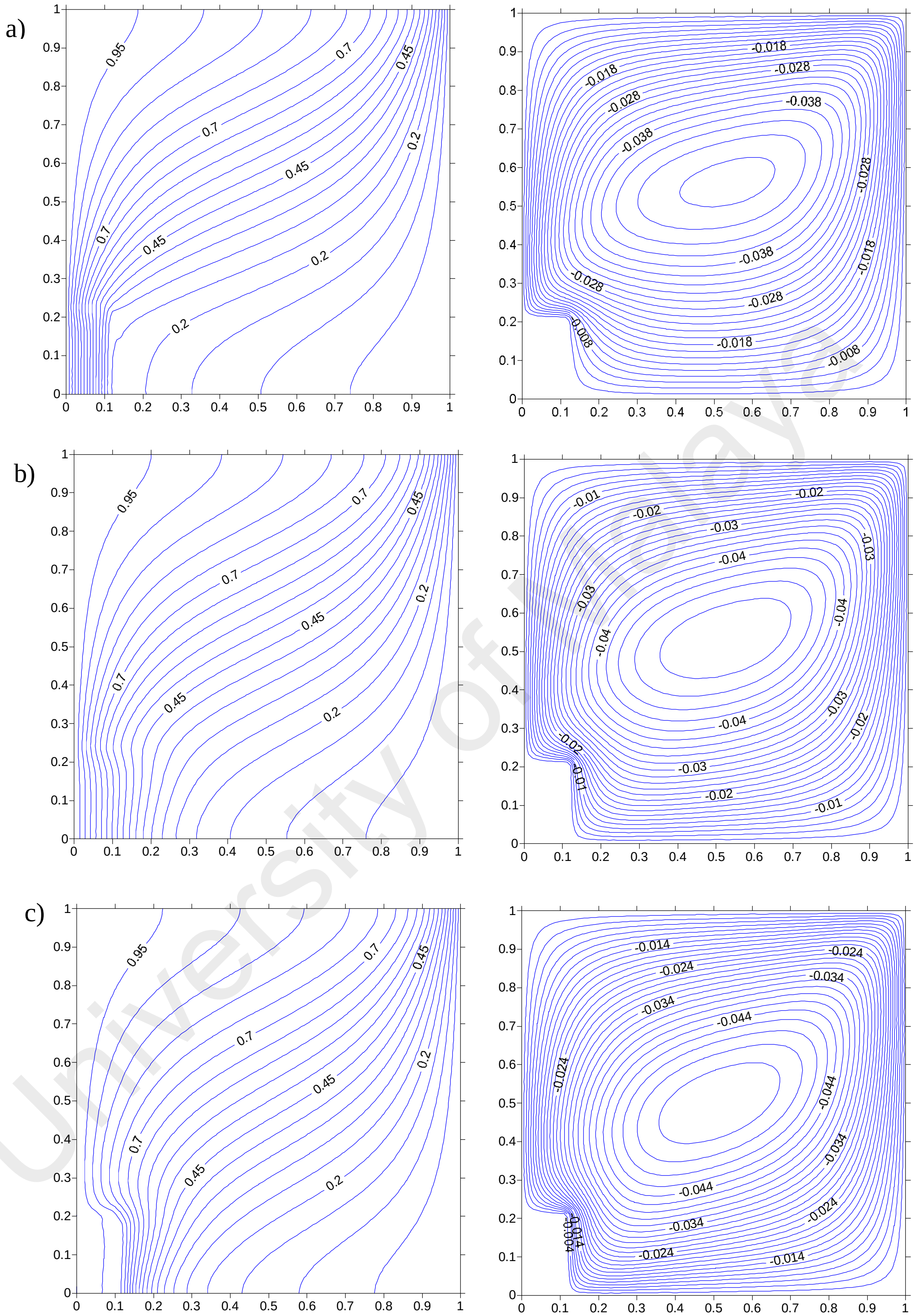


**Figure 5.2:** Isotherms (left) and Streamline (right) when solid wall placed at *L=0* for $S_h$*=0.20 a) Kr=0.1 b) Kr=1 c) Kr=10*

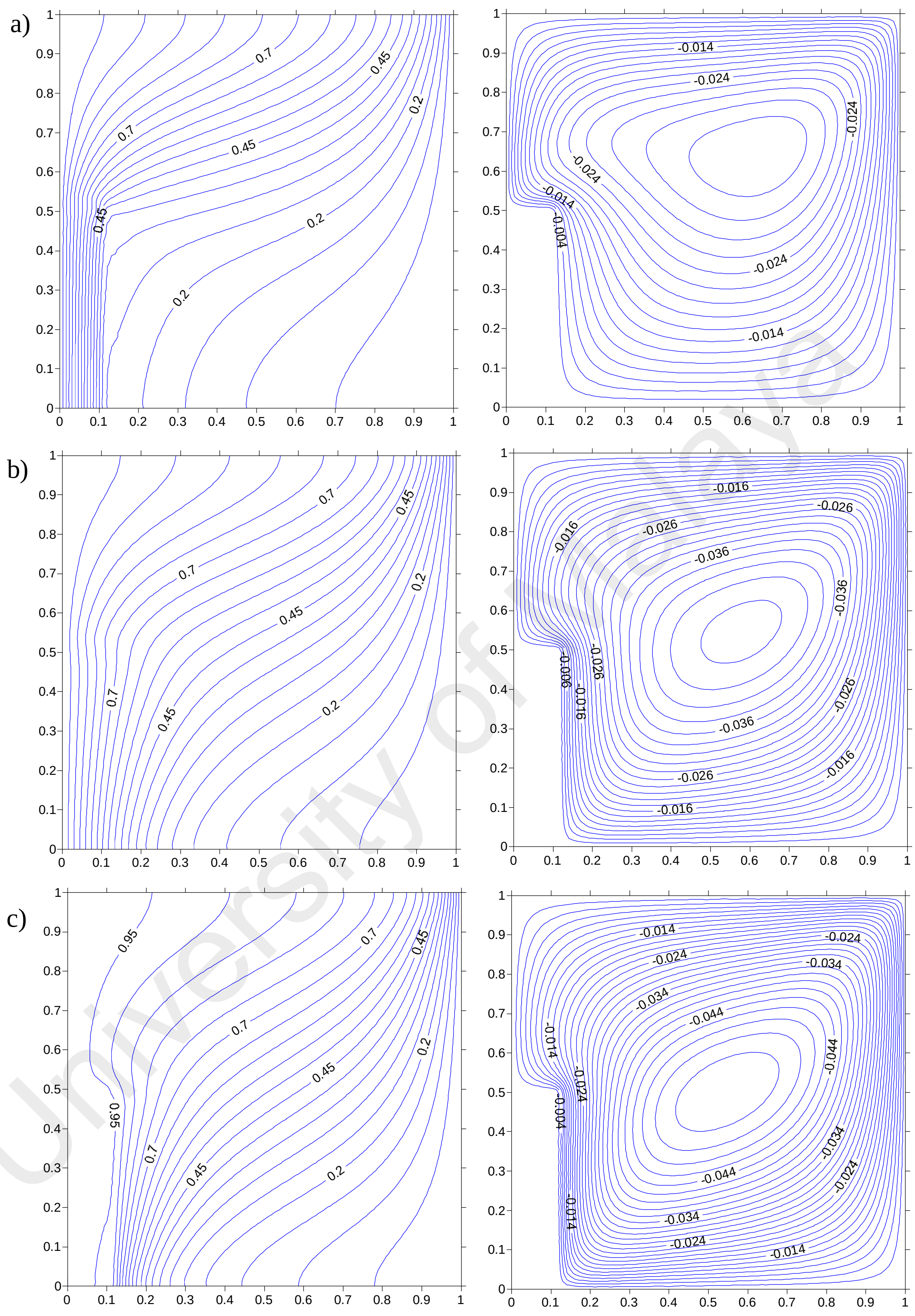


**Figure 5.3:** Isotherms (left) and Streamline (right) when solid wall placed at *L=0* for *$S_h$=0.5 a) Kr=0.1 b) Kr=1 c) Kr=10*

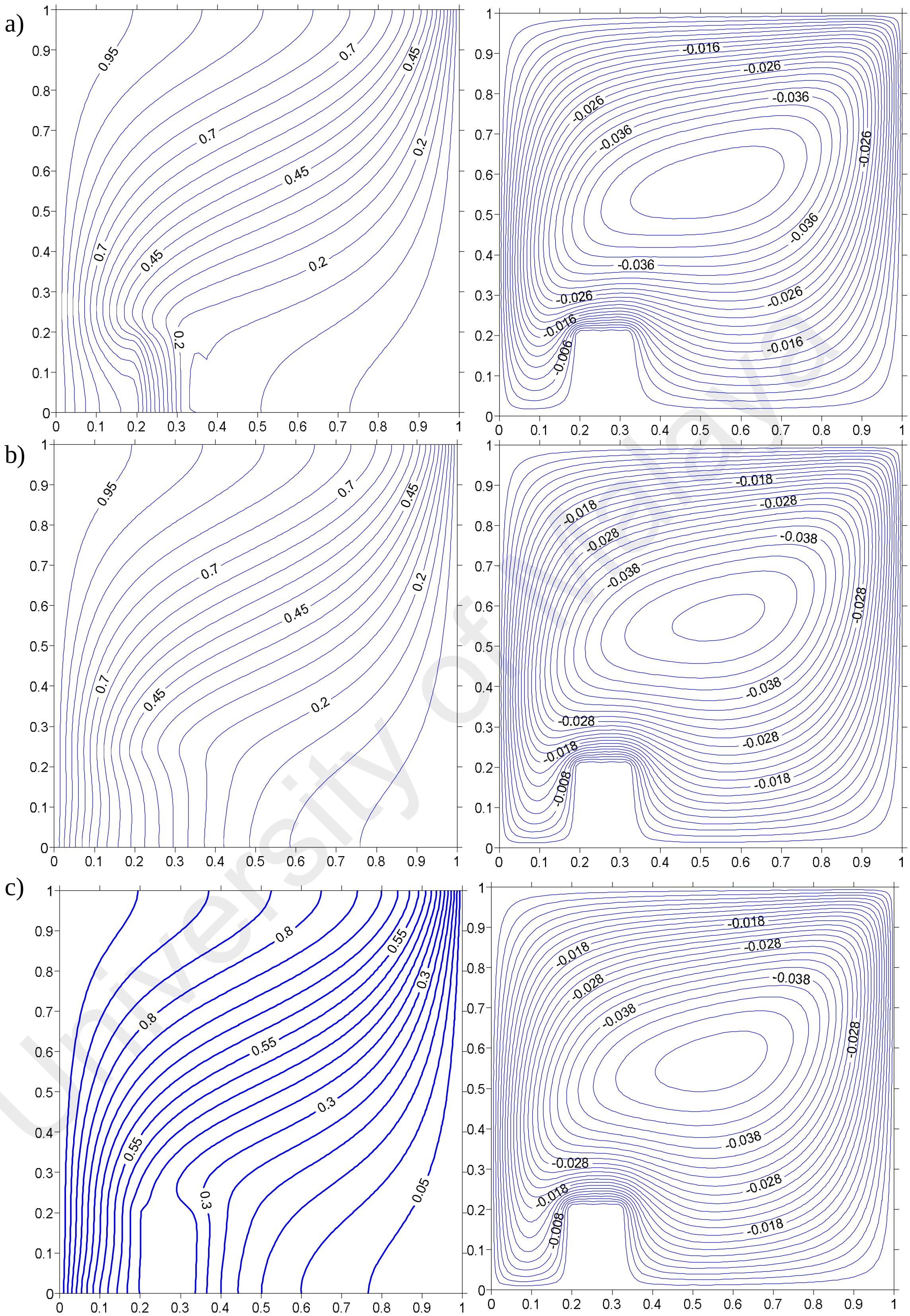




**Figure 5.4:** Isotherms (left) and Streamline (right) when solid wall placed at *L=0.25* for *$S_h$=0.20 a) Kr=0.1 b) Kr=1 c) Kr=10*

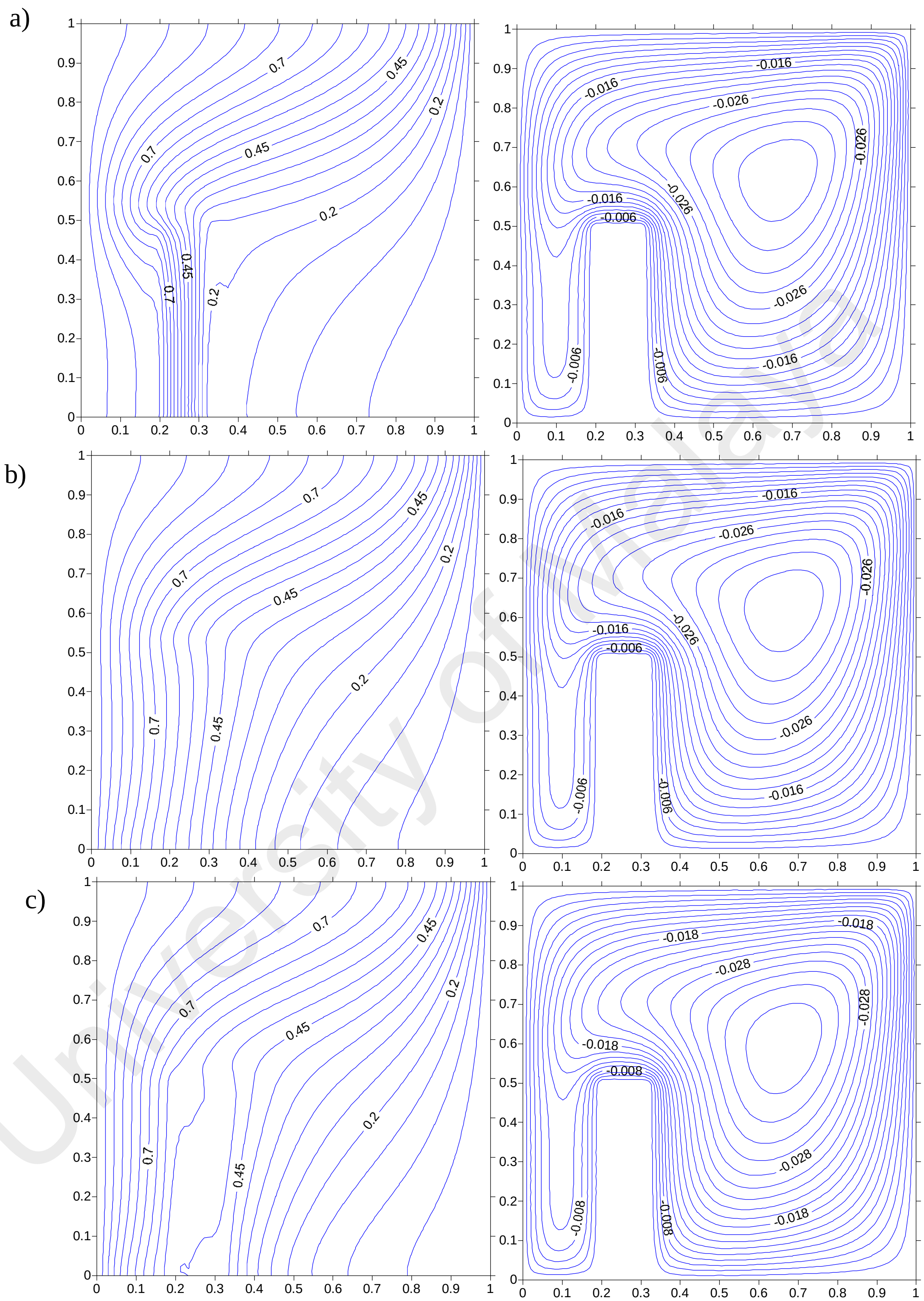


**Figure 5.5:** Isotherms (left) and Streamline (right) when solid wall placed at *L=0.25* for $S_h$*=0.5 a) Kr=0.1 b) Kr=1 c) Kr=10*

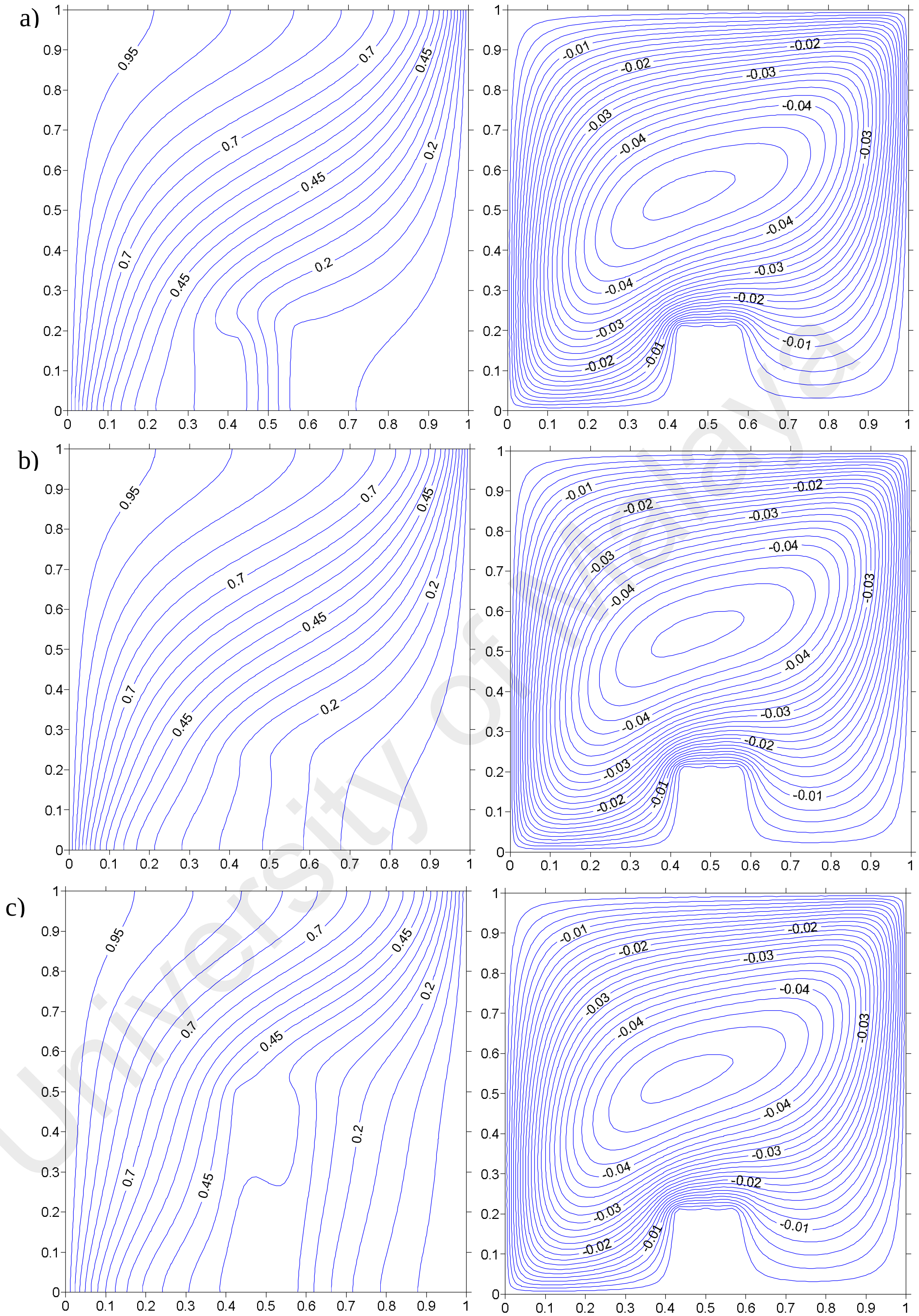


**Figure 5.6:** Isotherms (left) and Streamline (right) when solid wall placed at *L=0.5* for $S_h$*=0.20 a) Kr=0.1 b) Kr=1 c) Kr=10*

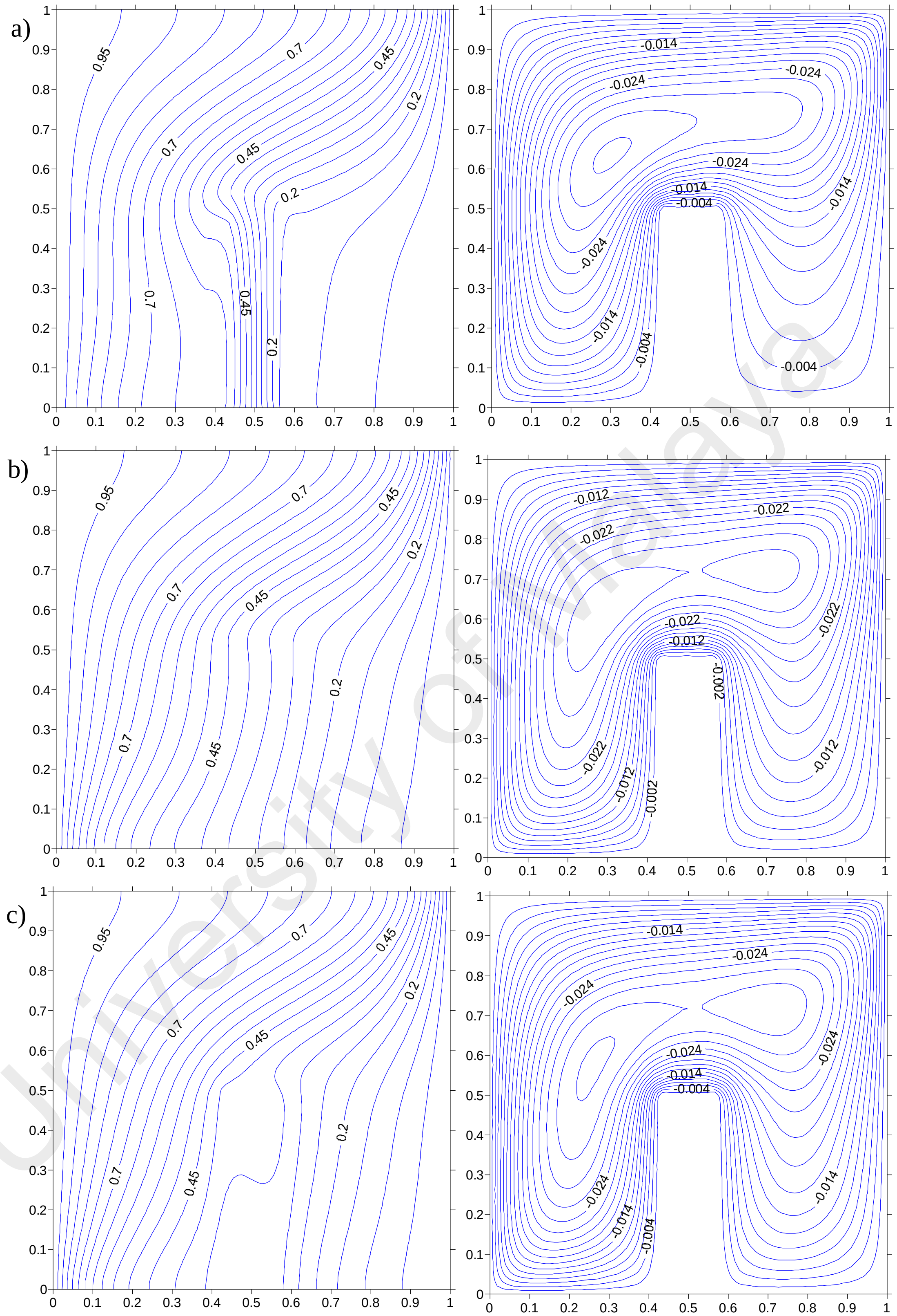


**Figure 5.7:** Isotherms (left) and Streamline (right) when solid wall placed at *L=0.5* for *$S_h$=0. 5 a) Kr=0.1 b) Kr=1 c) Kr=10*

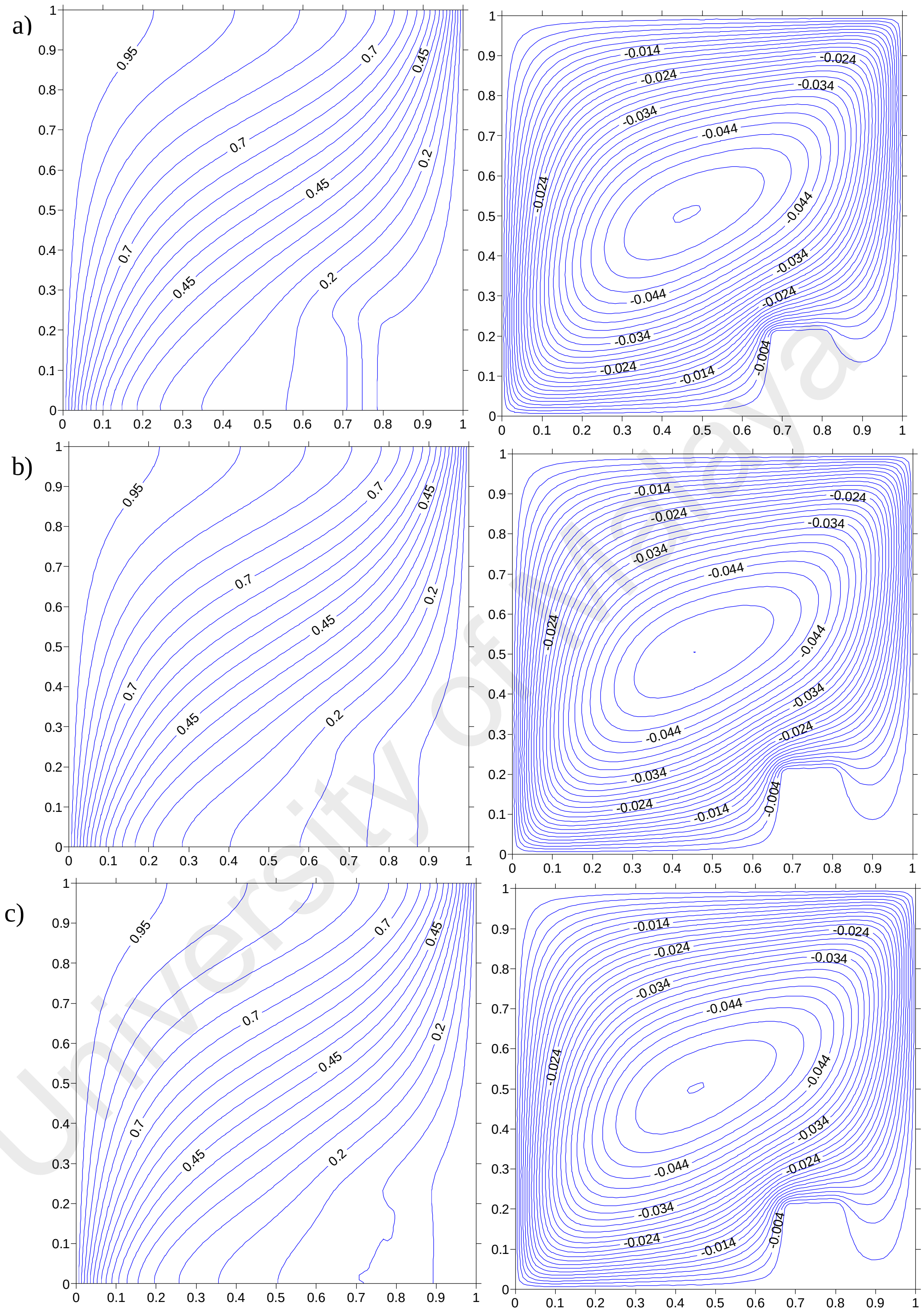


**Figure 5.8:** Isotherms (left) and Streamline (right) when solid wall placed at *L=0.75*for $S_h$*=0.20 a) Kr=0.1  b) Kr=1 c) Kr=10*

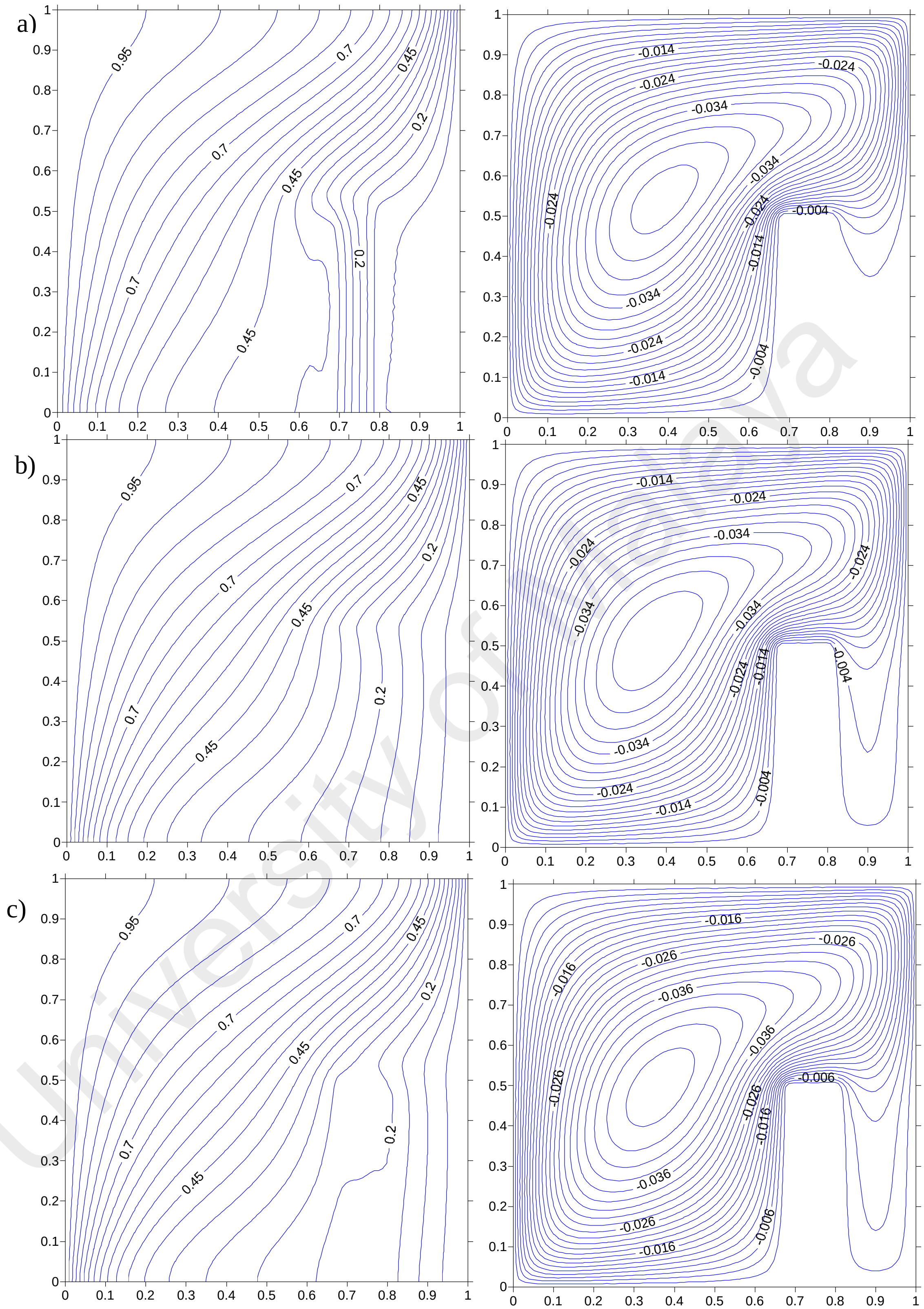


**Figure 5.9:** Isotherms (left) and Streamline (right) when solid wall placed at *L=0.75* for *$S_h$=0.5 a) Kr=0.1 b) Kr=1 c) Kr=10*

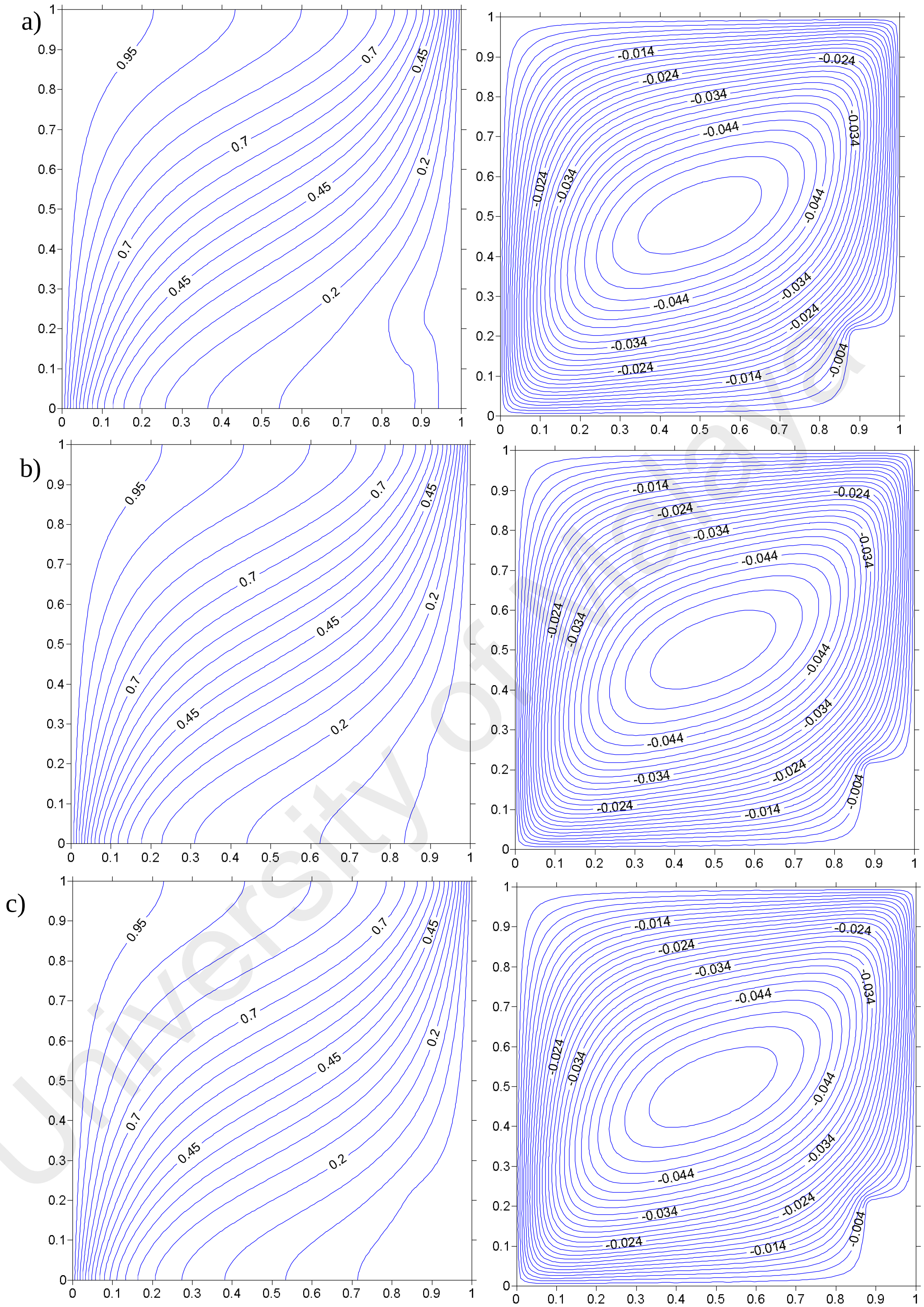


**Figure 5.10:** Isotherms (left) and Streamline (right) when solid wall placed at *L=1* for $S_h$*=0.20 a) Kr=0.1 b) Kr=1 c) Kr=10*

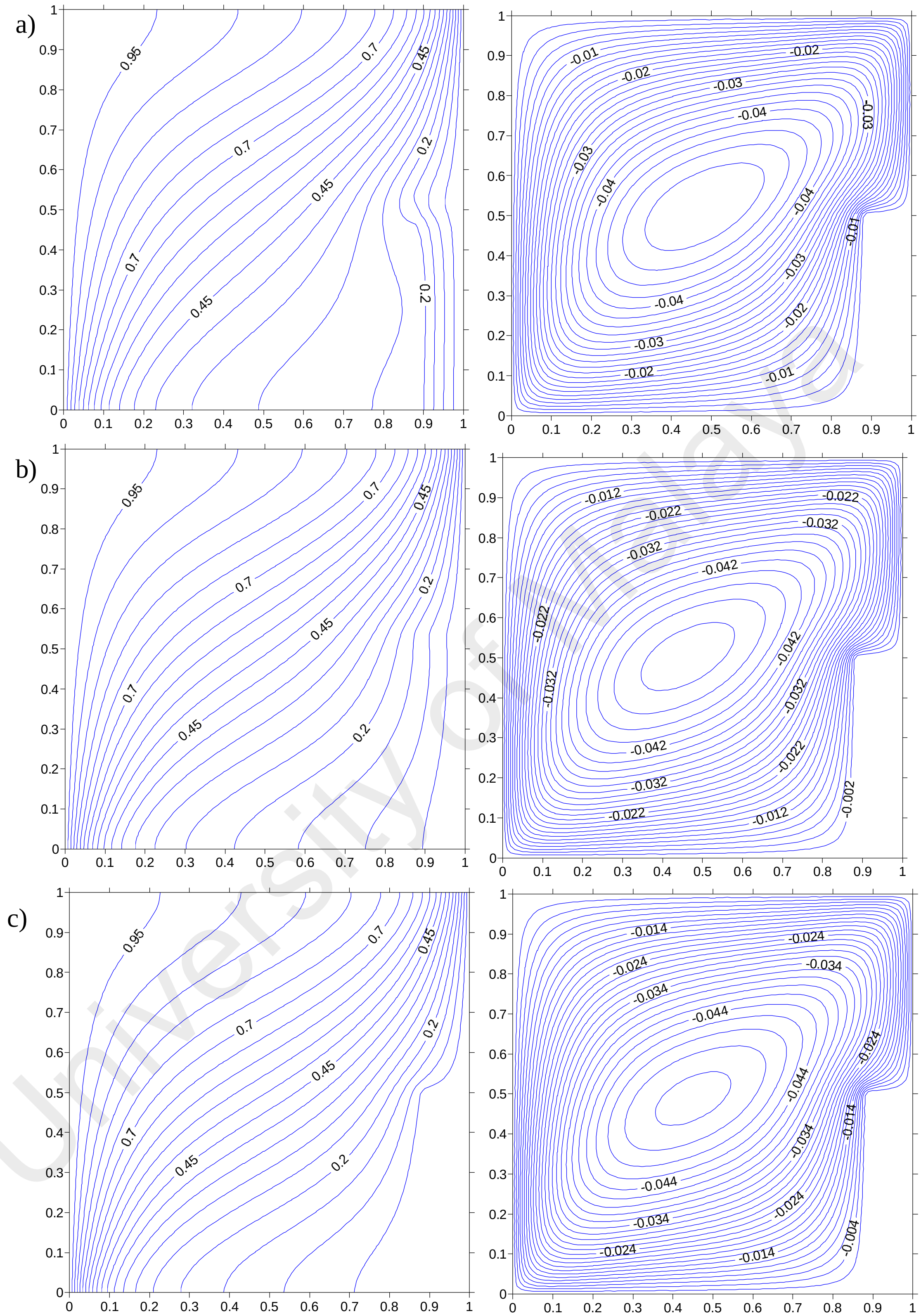


**Figure 5.11:** Isotherms (left) and Streamline (right) when solid wall placed at $L=1$ for $S_h=0.5$ *a)* $Kr=0.1$ *b)* $Kr=1$ *c)* $Kr=10$

### 5.5 Nusselt number variation

The following section describes the variation of Nusselt number at hot surface of cavity with respect to the thermal conductivity ratio and location of solid wall inside the porous medium. The results are presented for 4 different values of height (10%, 20%, 30% and 50% of cavity height) and 2 values of solid width (13% and 25% of cavity width). 10% height indicates that the height of solid is 0.1 times the height or width of cavity. Similarly, 13% width indicates that the width of solid is 0.13 times the height or width of cavity. Figure 5.12 shows the Nusselt number when solid wall is placed at 25% of the cavity width for $Ra=100$ *and* $R_d=0.5$. It is worth mentioning that the Nusselt number is a reflection of heat transfer rate from hot surface to the porous region. Higher the Nusselt number, higher is the heat transfer rate. It is obvious from figure 5.12 that the Nusselt number for $S_w=0.13$ (13%) increases with increases in $Kr$ until a point and then the variations are seized. However, the Nusselt number keeps increasing with increase in $Kr$ for wider solid $(S_w=0.25)$. The increased conductivity ratio moves the isotherm towards the hot surface as depicted in figure 5.4-5.5 which in turn increases the temperature gradient at hot surface leading to increased heat transfer rate. In general, the Nusselt number for shorter solid height is higher than that of longer solid at smaller $Kr$ with exception of $S_h=0.1$. This is due to the reason that the longer solid obstructs the fluid movement to greater extent thus rendering the overall heat transfer capacity of fluid.

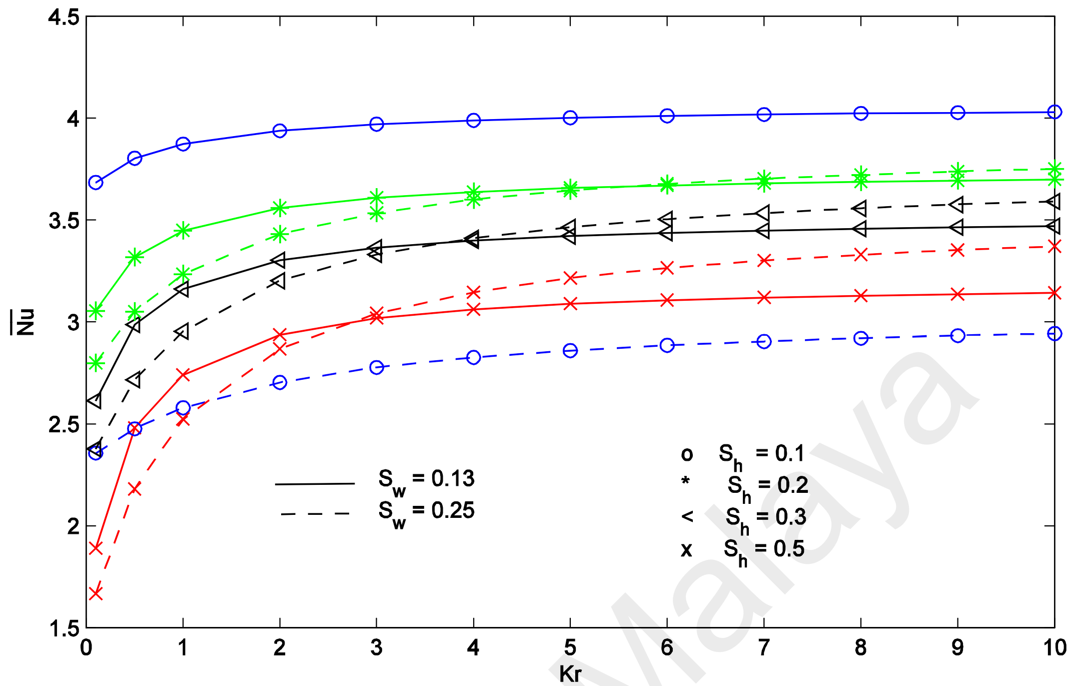


**Figure 5.12:** Average Nusselt number variation with *Kr* for solid at 0.25L

Figure 5.13 shows the Average Nusselt number when solid is placed at the center of cavity with other parameters being same as that of figure 5.12. It is seen that the shifting of solid from 0.25L to 0.5L which is the center of cavity, results into higher Nusselt number for shorter solid width as compared to larger width for all values of *Kr* being investigated. This could be attributed to increased fluid velocity due to lesser resistance in the vicinity of hot surface which is further corroborated by streamlines of figure 5.6. The attainment of maximum $\overline{Nu}$ shifts towards smaller *Kr* when location of solid is moved from 0.25L to 0.5L.

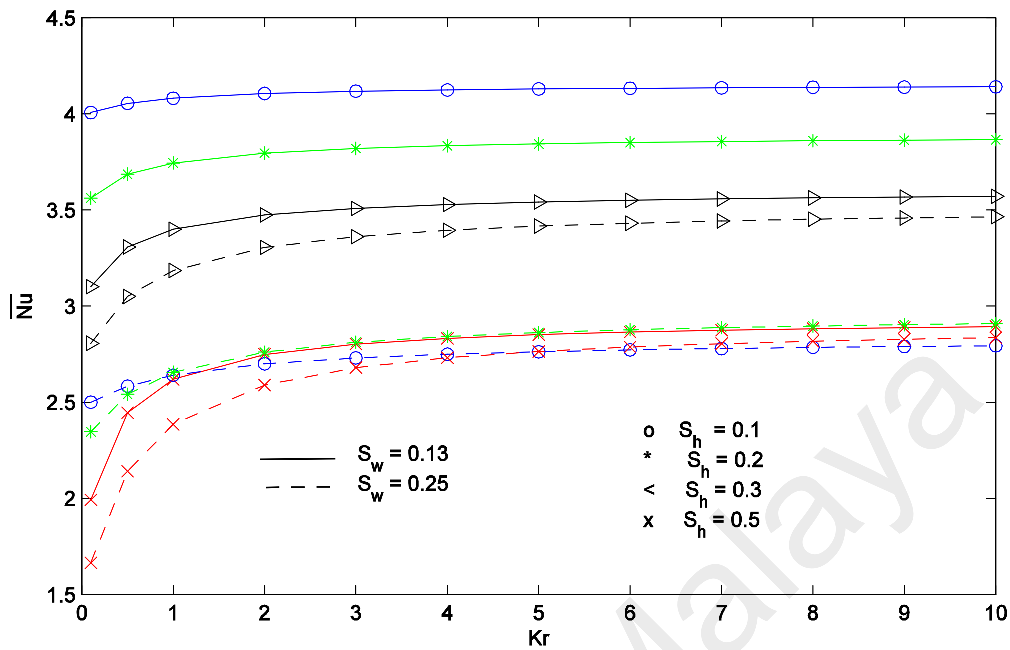


**Figure 5.13:** Average Nusselt number variation with *Kr* for solid at 0.5L

Figure 5.14 shows the effect of solid being placed at 0.75L keeping all other parameters same as previous case i.e. figure 5.12. The heat transfer rate increases by pushing the solid towards right surface. The average Nusselt number for wider solid is higher at larger value of *Kr*. The heat transfer rate further increases when the solid wall is placed at the right surface i.e. cold surface of cavity as shown in figure 5.15. The effect of *Kr* on heat transfer rate is substantial for $S_h=0.5$ as compared to other values of $S_h$.

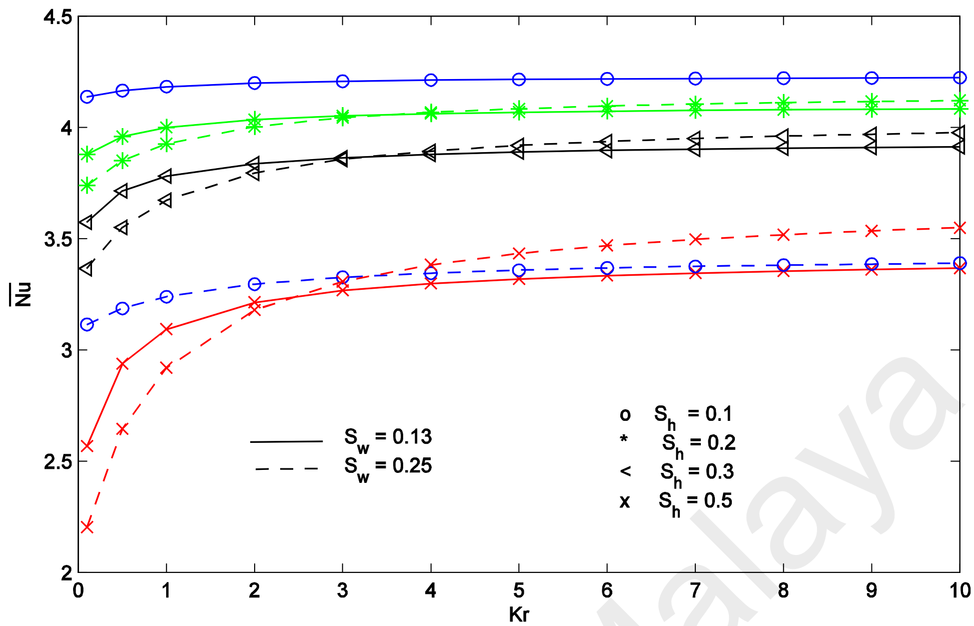


**Figure 5.14:** Average Nusselt number variation with *Kr* for solid at 0.75L

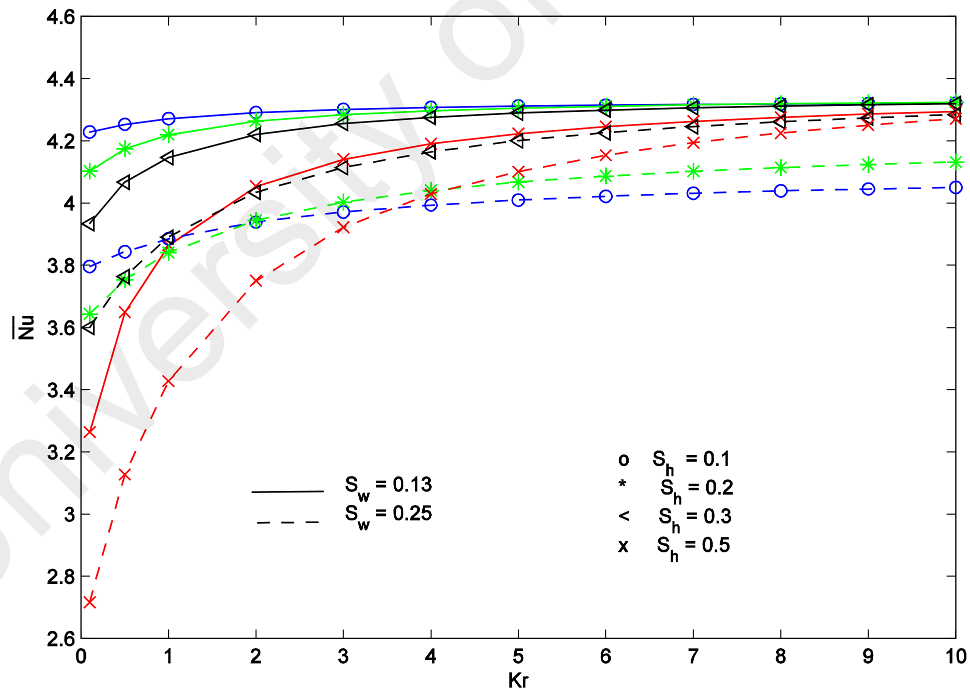


**Figure 5.15:** Average Nusselt number variation with *Kr* for solid at L (cold surface)

# CHAPTER 6 : CONJUGATE HEAT AND MASS TRANSFER IN SQUARE POROUS CAVITY

This Chapter deals with the issue of heat and mass transfer which is also known as double diffusion, in a square porous cavity having a small solid wall or block inserted at various places at bottom surface. The main objective is to investigate the effect of size of solid wall and its location inside the porous cavity on double diffusive convention. The heat and mass transfer behavior is governed by momentum, energy and concentration equations which are converted into a set of finite element equation with the help of Galerkin method. The left surface of cavity is maintained at higher temperature and concentration, $T_h$ and $C_h$ as compared to that of right surface at $T_c$ and $C_c$. The results are presented in terms of thermal, concentration and fluid flow profiles across the porous cavity.

## 6.1 Introduction

The thorough understanding of the convective heat transfer and the fluid flow through porous medium have gained considerable attraction by the eminent researchers during the last few decades, as evident from the number of articles published in this area. The deep insight to the fundamental concept of the heat transfer and fluid flow has been dealt meticulously by many authors, such as; (Donald A Nield & Bejan, 2006),(Ingham & Pop, 1998) Ingham and Pop(1998), (Vafai, 2000), (Bejan & Kraus, 2003; Ioan Pop & Ingham, 2001).The conjugate heat transfer refers to a situation where heat transfer occurs simultaneously between fluid and solid emanating a complex boundary condition between fluid and solid, whereby it analyzes simultaneously heat transfer both in solid as well as fluid(Joshi & Nakayama 2003) . The different aspects of the convective heat transfer have been reported in the available literature (N. J. S. Ahmed et al., 2009; Ahmed et al., 2011; I. A Badruddin, N. J. S Ahmed, et al., 2012; I. A Badruddin et al., 2012; I. A Badruddin, Abdullah A. A. A. Al-Rashed, et al., 2012; Kumaran & Pop, 2006; Ogulu & Amos, 2005; Raptis, 1998) but conjugate heat transfer received relatively lesser attention.

In conjugate heat transfer the solid fluid interface is governed by the conduction and convection phenomenon thus making it more peculiar to analyze. Thus it becomes inevitable to solve the energy equations both in solid as well as fluid media simultaneously (Iqbal, Syed, & Ishaq, 2015). The ratio of the conductivity of the wall and the fluid and the wall thickness has profound effect on the heat transfer characteristics(Mori, Sakakibara, & Tanimoto, 1974).The effect of the wall heat conduction in an annulus region is also found to be significantly high as reported by the (Sakakibara, Mori, & Tanimoto, 1987). In a similar study, (W.-Q. Tao, 1987) analyzed and reported that the ratio of the heat capacities of the fluids has significant effect on the finned tube heat transfer in a conjugate heat transfer analyses.

Even though the conjugate heat transfer has received lesser attention in recent studies, however it is fairly understood that there has been considerable efforts made by many researchers to shed light on various aspects of the conjugate heat transfer as evident from the above literature. Apart from the conjugate heat transfer there has been growing interest on the effect of combined heat and mass transfer in in porous medium as it addresses many issues in the practical applications sought in the food processing industries. The heat and mass transfer which is also referred as double diffusion is a complex diffusion where the diffusion of heat affects the mass as well. The mass transfer is countered by additional equation (mass diffusion equation) coupled with energy and momentum equation. For instance Oliveira and (Oliveira & Haghighi, 1998) have addressed the flow peculiarities to generate the temperature and the moisture contours during wood drying process. In another study similar attempt was made by (Lamnatou, Papanicolaou, Belessiotis, & Kyriakis,

2009) for a square cylinder of a model food substrate where in emphasis was given on the flow blockage and its influence over heat and mass transfer.

Thus few others also attempted to address the different aspects of the combined conjugate heat and mass transfer process in the literature (Kaya (De Bonis & Ruocco, 2008; Kaya, Aydın, & Dincer, 2006; Mohan & Talukdar, 2010; Suresh, Narayana, & Seetharamu, 2001).The current work is aimed to understand the heat and fluid flow behavior due to presence of a solid wall/block inside the porous medium when its location is varied from left to right surface of cavity.

### 6.2 Mathematical Model

The mathematical model of problem under investigation is based on momentum, energy and species concentration equations that are coupled together with suitable parameters. A square cavity filled with porous medium is considered with a small solid placed at various positions along the bottom surface as depicted in figure 6.1. The x and y coordinates are taken along horizontal and vertical directions respectively. The left surface of cavity is maintained at temperature $T_h$ and concentration $C_h$ which are higher than its corresponding temperature and concentration at cold surface with notation $T_c$ and $C_c$ respectively.

The following assumptions are applied while investigating the heat and mass transfer behavior in porous cavity.

a) The Darcy law is applicable in the porous medium.

b) The properties of the fluid and those of the porous medium are homogeneous.

c) Fluid properties are constant except the variation of density with temperature.

d) There is no phase change of fluid

e) The thermal equilibrium exists between fluid and solid phase of porous medium

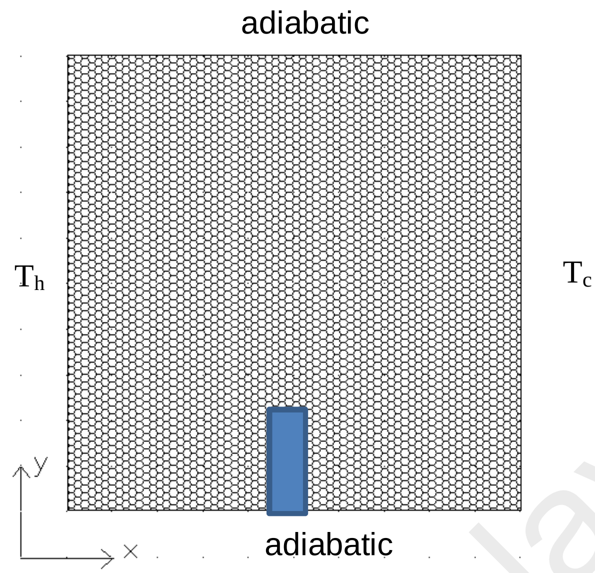


**Figure 6.1:** Porous cavity with solid

The governing equations resulting due to above mentioned problems are

Continuity equation

$$\frac{\partial u}{\partial x}+\frac{\partial \mathrm{v}}{\partial y}=0 \tag{6.1}$$

Momentum equation

$$\frac{\partial u}{\partial y}-\frac{\partial \mathrm{v}}{\partial x}=-\frac{g\beta K}{\nu}\frac{\partial T}{\partial x} \tag{6.2}$$

Energy equation for porous medium

$$u\frac{\partial T_p}{\partial x}+\mathrm{v}\frac{\partial T_p}{\partial y}=\alpha\left(\frac{\partial^2 T_p}{\partial x^2}+\frac{\partial^2 T_p}{\partial y^2}\right)-\frac{1}{\rho C_p}\frac{\partial q_r}{\partial x} \tag{6.3}$$

Energy equation for solid

$$\frac{\partial^2 T_s}{\partial x^2}+\frac{\partial^2 T_s}{\partial y^2}-\frac{1}{\alpha\rho C_p}\frac{\partial q_r}{\partial x}=0 \tag{6.4}$$

Concentration equation

$$u\frac{\partial C}{\partial x}+\mathrm{v}\frac{\partial C}{\partial y}=D\left(\frac{\partial^2 C}{\partial x^2}+\frac{\partial^2 C}{\partial y^2}\right) \tag{6.5}$$

Subjected to boundary conditions:

at $x=0 \quad u=0,\ v=0 \quad T=T_h \quad C=C_h$ (6.6a)

at $x=L, \quad u=0,\ v=0 \quad T=T_c \quad C=C_c$ (6.6b)

at $y=0 \quad and \quad y=L, \quad u=0,\ v=0 \quad \frac{\partial T}{\partial y}=0$ (6.6c)

The application of principal of no heat storage in the solid, results into following additional boundary conditions at solid porous interphase.

at $x = x_{sp} \quad u=0,\ v=0 \quad T_s = T_p \quad k_s \frac{\partial T_s}{\partial x} = k_p \frac{\partial T_p}{\partial x}$ (6.6d)

at $y = y_{sp} \quad u=0,\ v=0 \quad T_s = T_p \quad k_s \frac{\partial T_s}{\partial y} = k_p \frac{\partial T_p}{\partial y}$ (6.6e)

Equation (6.1) can be satisfied automatically by introducing the stream function ψ as:

$$u = \frac{\partial \psi}{\partial y} \quad \mathrm{v} = -\frac{\partial \psi}{\partial x} \tag{6.7}$$

Following non-dimensional parameters are used.

$$\bar{x} = \frac{x}{L} \quad , \quad \bar{y} = \frac{y}{L} \quad , \quad \bar{\psi} = \frac{\psi}{\alpha} \quad , \quad \bar{T} = \frac{(T-T_c)}{(T_w-T_c)} \quad , \quad \bar{C} = \frac{(C-C_c)}{(C_w-C_c)}$$

$$R_d = \frac{4\sigma T_c^{\ 3}}{\beta_R k} \quad , Ra = \frac{g\beta_T \Delta T K L_c}{\nu\alpha} \quad , \quad Le = \frac{\alpha}{D} \quad , \quad N = \left(\frac{\beta_c \Delta C}{\beta_T \Delta T}\right)$$

Invoking Rosseland approximation for radiation.

$$q_r = -\frac{4\sigma}{3\beta_r}\frac{\partial T^4}{\partial x} \tag{6.8}$$

Expanding $T^4$ in Taylor series about $T_c$ and neglecting higher order terms (Irfan Anjum Badruddin et al., 2006; I. A Badruddin, Z. A. Zainal, P. A. Aswatha Narayana, & K. N. Seetharamu, 2006; I. A Badruddin, Z. A. Zainal, P. A. Aswatha Narayana, K. N. Seetharamu, et al., 2006; Nik-Ghazali et al., 2014; Raptis, 1998)

$$T^4 \approx 4TT_c^{\,3} - 3T_c^{\,4} \tag{6.9}$$

Substituting equations (6.6-6.9) into equation (6.2-6.5) yields:

Momentum equation

$$\frac{\partial^2 \overline{\psi}}{\partial \overline{x}^2} + \frac{\partial^2 \overline{\psi}}{\partial \overline{y}^2} = -Ra\left[\frac{\partial \overline{T}}{\partial \overline{x}} + N\frac{\partial \overline{C}}{\partial \overline{x}}\right] \tag{6.10}$$

Energy equation of porous region

$$\frac{\partial \overline{\psi}}{\partial \overline{y}}\frac{\partial \overline{T}}{\partial \overline{x}} - \frac{\partial \overline{\psi}}{\partial \overline{x}}\frac{\partial \overline{T}}{\partial \overline{y}} = \left(\left(1 + \frac{4R_d}{3}\right)\frac{\partial^2 \overline{T}}{\partial \overline{x}^2} + \frac{\partial^2 \overline{T}}{\partial \overline{y}^2}\right) \tag{6.11}$$

Energy equation in solid region

$$\left(1 + \frac{4R_d}{3}\right)\frac{\partial^2 \overline{T}}{\partial \overline{x}^2} + \frac{\partial^2 \overline{T}}{\partial \overline{y}^2} = 0 \tag{6.12}$$

Concentration equation

$$\frac{\partial \overline{\psi}}{\partial \overline{y}}\frac{\partial \overline{C}}{\partial \overline{x}} - \frac{\partial \overline{\psi}}{\partial \overline{x}}\frac{\partial \overline{C}}{\partial \overline{y}} = \frac{1}{Le}\left(\frac{\partial^2 \overline{C}}{\partial \overline{x}^2} + \frac{\partial^2 \overline{C}}{\partial \overline{y}^2}\right) \tag{6.13}$$

The corresponding boundary conditions are

at $\overline{x} = 0 \qquad \overline{\psi} = 0 \qquad \overline{T} = 1 \quad \overline{C} = 1$ (6.14a)

at $\overline{x} = 1 \qquad \overline{\psi} = 0 \qquad \overline{T} = 0 \quad \overline{C} = 0$ (6.14b) at $\bar{y}=0 \quad and \quad \bar{y}=1, \qquad \bar{\psi}=0 \qquad \frac{\partial \bar{T}}{\partial \bar{y}}=0$ (6.14c)

at $\bar{x}=x_{sp} \quad \bar{\psi}=0, \qquad Kr\frac{\partial \bar{T}_s}{\partial \bar{x}}=\frac{\partial \bar{T}_p}{\partial \bar{x}}$ (6.14d)

at $\bar{y}=\bar{y}_{sp} \qquad \bar{\psi}=0 \qquad Kr\frac{\partial \bar{T}_s}{\partial \bar{y}}=\frac{\partial \bar{T}_p}{\partial \bar{y}}$ (6.14e)

The heat and mass transfer rate at the hot surface can be calculated using following relations:

$$Nu=-\left(\left(1+\frac{4}{3}R_d\right)\frac{\partial \bar{T}}{\partial \bar{x}}\right)_{\bar{x}=0} \tag{6.15}$$

The Sherwood number is expressed as:

$$Sh=\left(-\frac{\partial \bar{C}}{\partial \bar{x}}\right)_{\bar{x}=0} \tag{6.16}$$

### 6.3 Numerical Scheme

It is worth mentioning that the present problem is governed by 4 partial differential equations (6.10-6.13) subjected to complex boundary conditions as given in equation 6.14. These set of equations are difficult to solve directly. Therefore as an alternate solution technique, finite element method is used to arrive at solution. The above mentioned equations are converted into matrix form of equations with the help of Galerkin method. Total of 2592 triangular elements are used to divide the physical domain into smaller segments. An iterative algorithm is adopted to solve the resulting finite element equations. The convergence criteria for $\bar{\psi}$, $\bar{T}$ *and* $\bar{C}$ are set at$10^{-7}$, $10^{-5}$and $10^{-5}$ respectively.

### 6.4 Results and Discussion

#### 6.4.1 Temperature, concentration and fluid flow profile.

The following section describes the results obtained for various geometrical as well as physical parameters that affect the conjugate heat and mass transfer in a square porous cavity. Figure 6.2 represents the heat and mass transfer behavior in terms of isotherms, iso-concentration lines and streamlines reflecting the temperature, concentration and velocity distribution in the square cavity. This figure is obtained by setting the parameters as $Ra = 100, R_d = 0.5, N = 0.2, L = 10$, for solid wall placed at the left surface of cavity with $S_h=0.2$.The geometric parameter $S_h$ is ratio of height of solid wall to the height of porous cavity thus $S_h=0.2$ indicates that the height of solid wall is 20% of total cavity height. The left column of figure 2 corresponds to $Kr=0.1$ whereas the right column belongs to $Kr=25$.Based on the results presented in figure 2, it is obvious that the isotherms penetrates deeper into the porous medium due to increased conductivity ratio, $Kr$. It should be noted that the conductivity ratio $Kr$ represents the thermal conductivity ratio of solid wall to the porous medium. A value of $Kr>1$ indicates that the solid wall conductivity is higher than that of porous medium and vice versa for $Kr<1$.It can be conveniently said that the larger area of cavity is occupied with high concentration lines for $Kr=0.1$ than that of $Kr=25$ as reflected by figure 6.2.

This can be inferred from iso-concentration lines where more than 50% of porous region is occupied by $\bar{C} \geq 0.45$ at $Kr=0.1$ than that of $Kr=25$. This could be the result of higher fluid velocity at smaller value of $Kr$ as illustrated by streamlines of figure 6.2 where magnitude of stream-function is higher at $Kr=0.1$ than that of $Kr=25$. The effect of solid placed at left wall of cavity is further investigated (figure 6.3) when height of solid wall is increased from 20% ($S_h=0.2$) to 50% ($S_h=0.5$) keeping all other parameters same as corresponding to that of figure 6.2. The convective heat transfer rate at top of cavity increases due to increased thermal gradient in that area for $S_h=0.5$ as compared to $S_h=0.2$. The high concentration area reduces owing to increase in solid height. The effect of solid wall is much more pronounced at $Kr=0.1$ than that of $Kr=25$. This is a result of fluid cell which changes flow pattern from being oval to near circular. Furthermore, the fluid movement shifts the whole of the cell in upward section of cavity at $Kr=0.1$. This combined effect of fluid cell affects the concentration distribution to a greater extent.

The aim of present work is to study the size as well as location of solid wall in the porous medium. In this regard, the location of solid is varied at 5 places such as at $\bar{x} = 0$, $\bar{x} = 0.25$ , $\bar{x} = 0.5$ , $\bar{x} = 0.75$ and $\bar{x} = 1$ . Figure 6.2-6.3 corresponded to $\bar{x} = 0$whereas figure 6.4 shows the heat and mass transfer behavior when solid is placed at $\bar{x} = 0.25$. Other parameters for figure 3 are set at $a = 100, Rd = 0.5, N = 0.2, L = 10$. It is observed that the heat transfer rate from hot wall to porous medium does not change much at $Kr=0.1$ from its counterpart of solid being placed at left wall ($\bar{x} = 0$, figure 6.2 ). However, there is an important observation that needs to be elaborated that the temperature variation inside the solid wall decreases owing change of solid wall location. The temperature variation in solid wall further decreases at higher $Kr$ as shown by isotherms of figure 6.2-6.4, corresponding to $Kr=25$. This behavior can be attributed to the fact that the thermal conductivity and temperature difference in a solid are inversely related to each other, thus the increased $Kr$ is an indication of higher thermal conductivity of solid wall which in turn helps in reducing the temperature difference across the solid. The concentration diffusion seems to re-arrange itself due to presence of an obstruction in the form of solid wall. The increased solid height reduces the heat content of porous medium to the right of solid wall as shown in figure 6.5. It is noticeable that the temperature variation across solid wall increases at *Kr=0.1* when the height of solid is increased to 50%. The concentration distribution shifts towards upward section of cavity due to increased obstruction. However, this obstruction is overcome by some extent, due to increased fluid velocity for the case of *Kr=25*, thus filling the lower section of cavity with low concentration lines.

The placement of solid wall at center of cavity i.e. $\bar{x} = 0.5$, further reduces the temperature difference across the solid as follows from figure 6.6. This is because of the reason that the availability of thermal energy decreases as one moves from hot to cold surface of porous cavity which is vindicated by figures 6.2 and 6.4, thus leading to decrease in temperature variation inside the solid wall placed far away from hot surface. The concentration profiles moves little bit upward direction as compared to figure 6.2 and 6.4 with similar solid height.

The fluid flow has distinct pattern as compared to other cases (figure 6.2-6.6) when solid with $S_h=0.5$ is placed at center of cavity. The flow pattern is very close to splitting the fluid into two cells at *Kr=25* as outlined in figure 6.7.

The temperature in the solid further declines as shown in figure 6.8 when the solid is moved to $\bar{x} = 0.75$, as compared to the cases discussed earlier in this chapter. This is clear indication of inability of heat to reach far away region of porous cavity towards the cold surface. However, it is noted that the effect of thermal conductivity ratio on concentration profile as well as fluid profile diminishes for solid ($S_h=0.2$) placed at $\bar{x} = 0.75$.

However, the increased solid height ($S_h=0.5$) at this location brings in little bit variation of concentration and fluid profile with respect to variation in *Kr* as demonstrated by figure 6.9. It is noted that the heat content of solid wall is minimum when it is placed at right surface of cavity as shown in figure 6.10 as compared to all other cases. Only two isotherms are affected by presence of solid wall at $Kr=0.1$. However, the increase in solid height to 50% improves the heat content of solid as depicted in figure 6.11. The concentration and streamlines are not much affected with respect to *Kr* when solid wall is placed at right surface. The magnitude of stream function is found to be maximum when the solid wall is placed at right surface (figure 6.10-6.11).

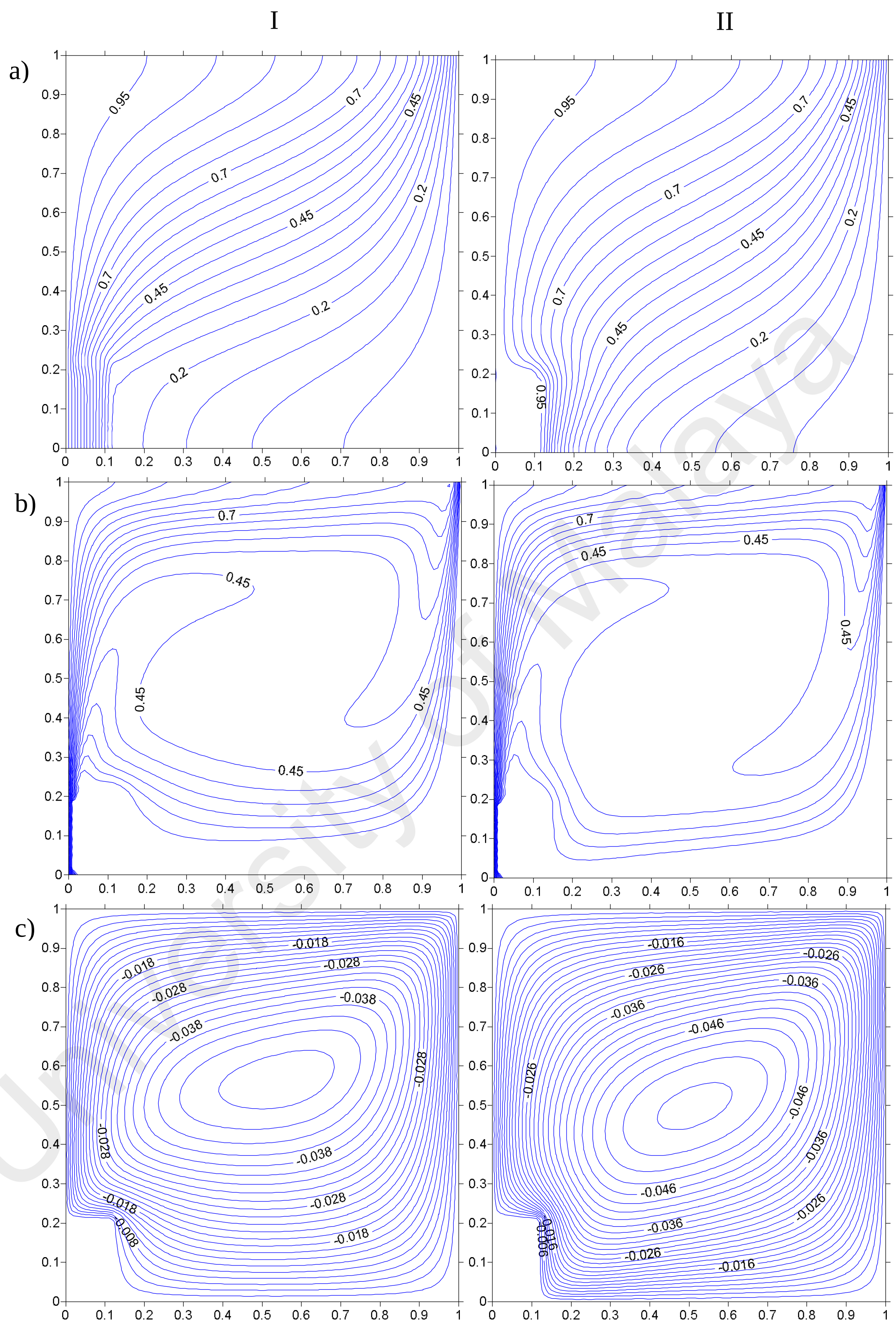


**Figure 6.2:** Effect of *Kr* and solid ($S_h$*=0.2*) at $\bar{x} = 0$, I) *Kr* = 0.1 II) *Kr=25*
a) Isotherms b) Iso-concentration c) Streamlines

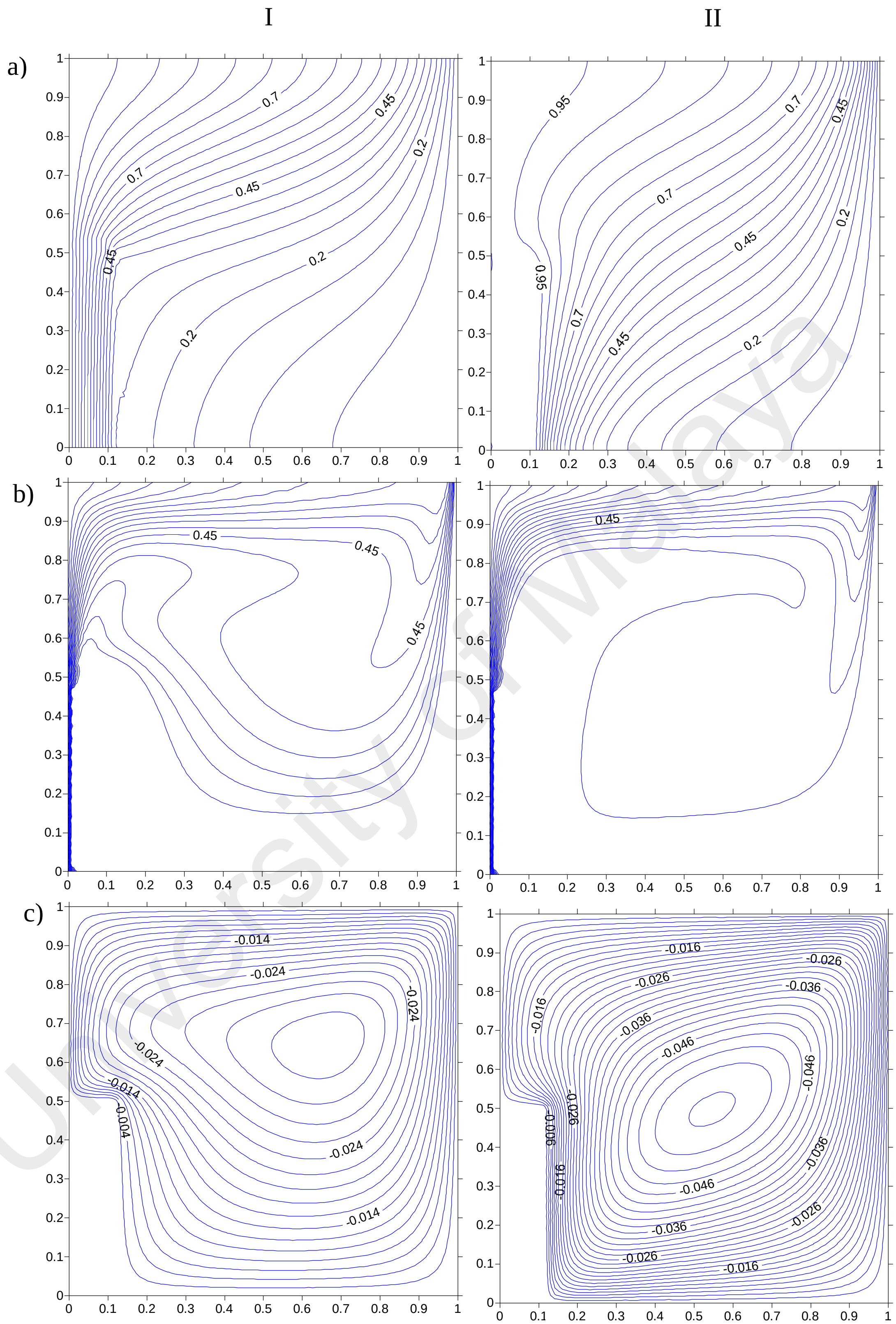


**Figure 6.3:** Effect of *Kr* and solid ($S_h$=*0.5*) at $\bar{x} = 0$, I) *Kr* = 0.1 II) *Kr=25*
a) Isotherms b) Iso-concentration c) Streamlines

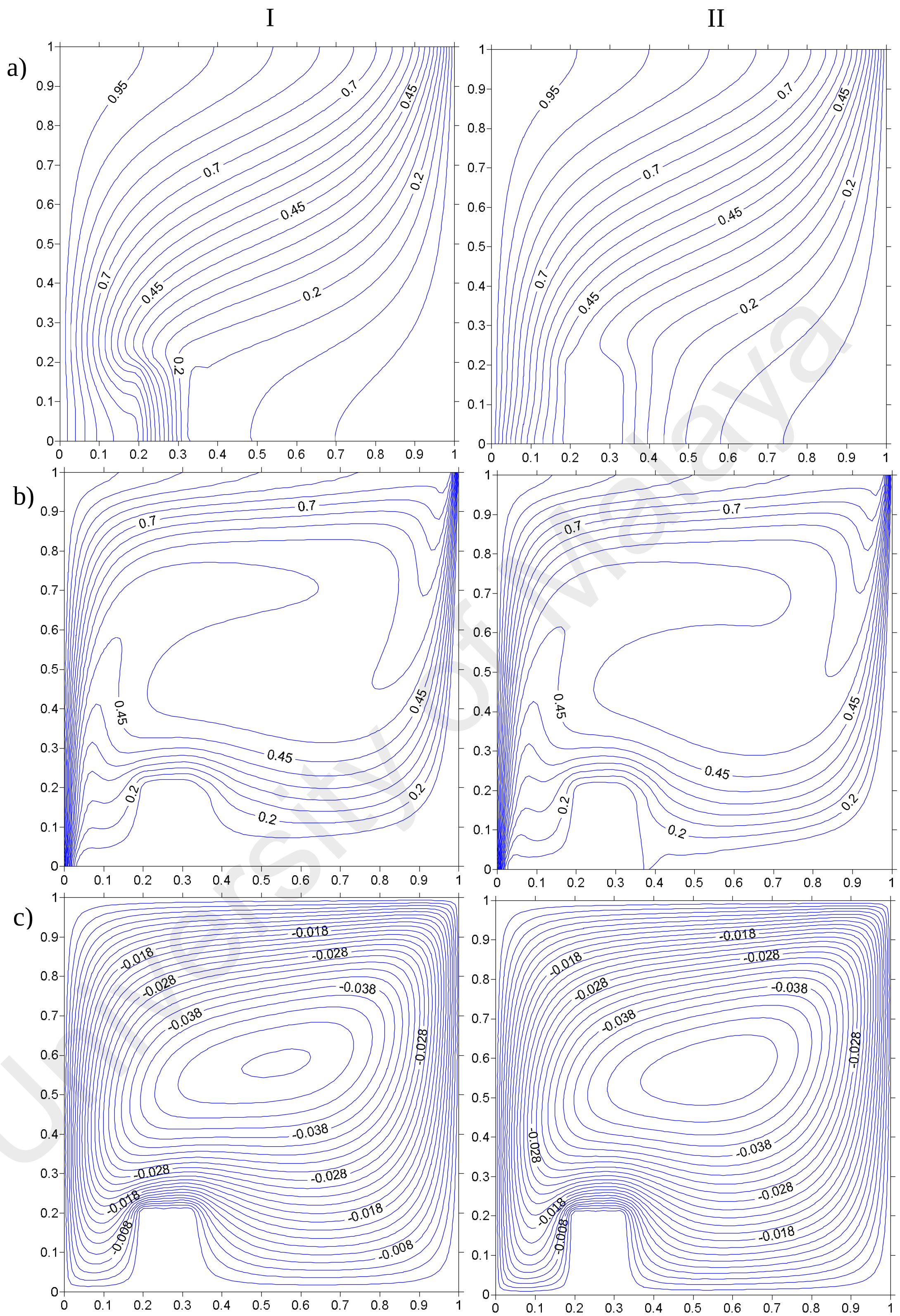


**Figure 6.4:** Effect of *Kr* and solid ($S_h$=*0.2*) at $\bar{x}$ = 0.25 , I) *Kr* = 0.1 II) *Kr=25*
a) Isotherms b) Iso-concentration c) Streamlines

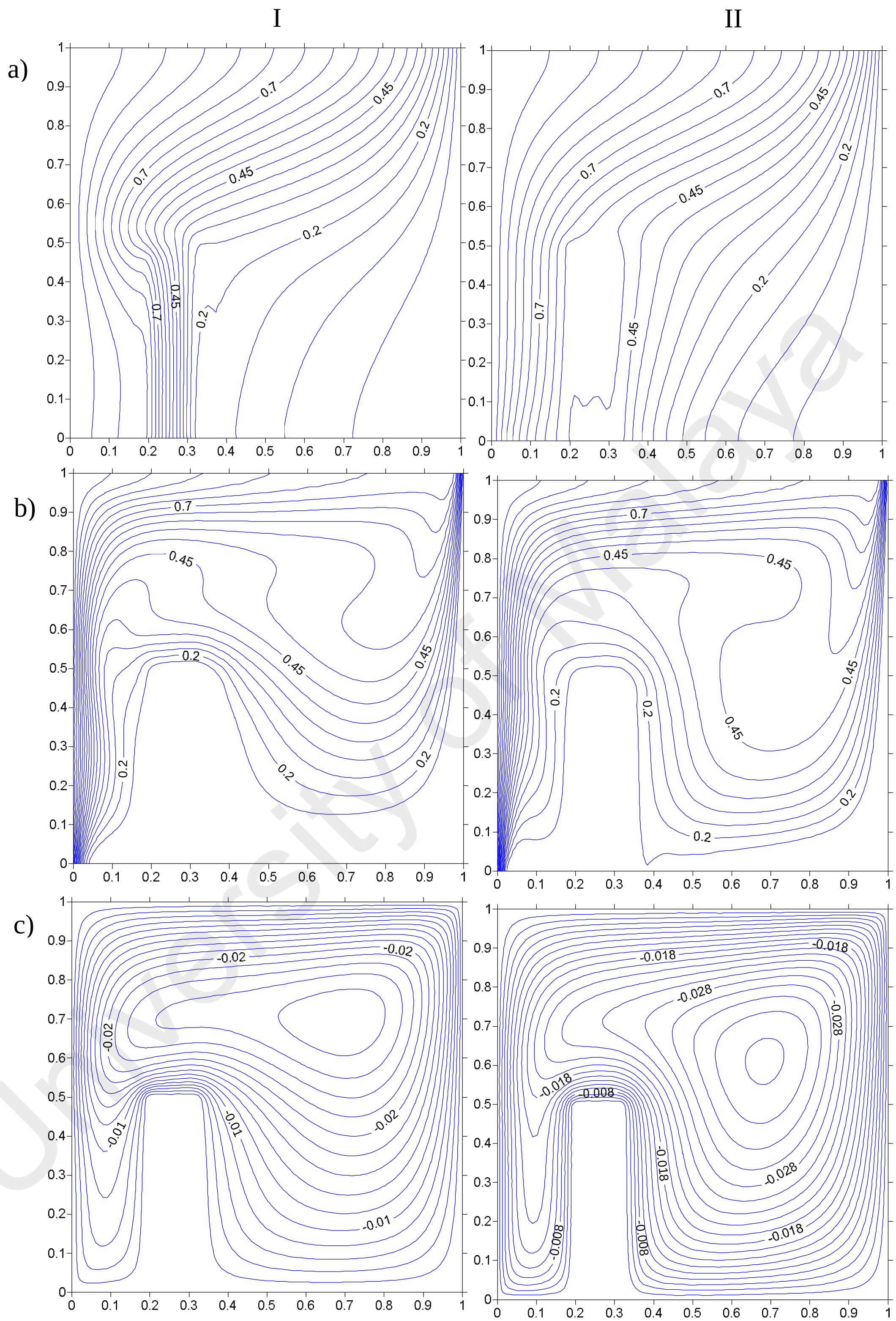


**Figure 6.5:** Effect of *Kr* and solid ($S_h$=*0.5*) at $\bar{x}$ = 0.25 , I) *Kr* = 0.1 II) *Kr=25*
a) Isotherms b) Iso-concentration c) Streamlines

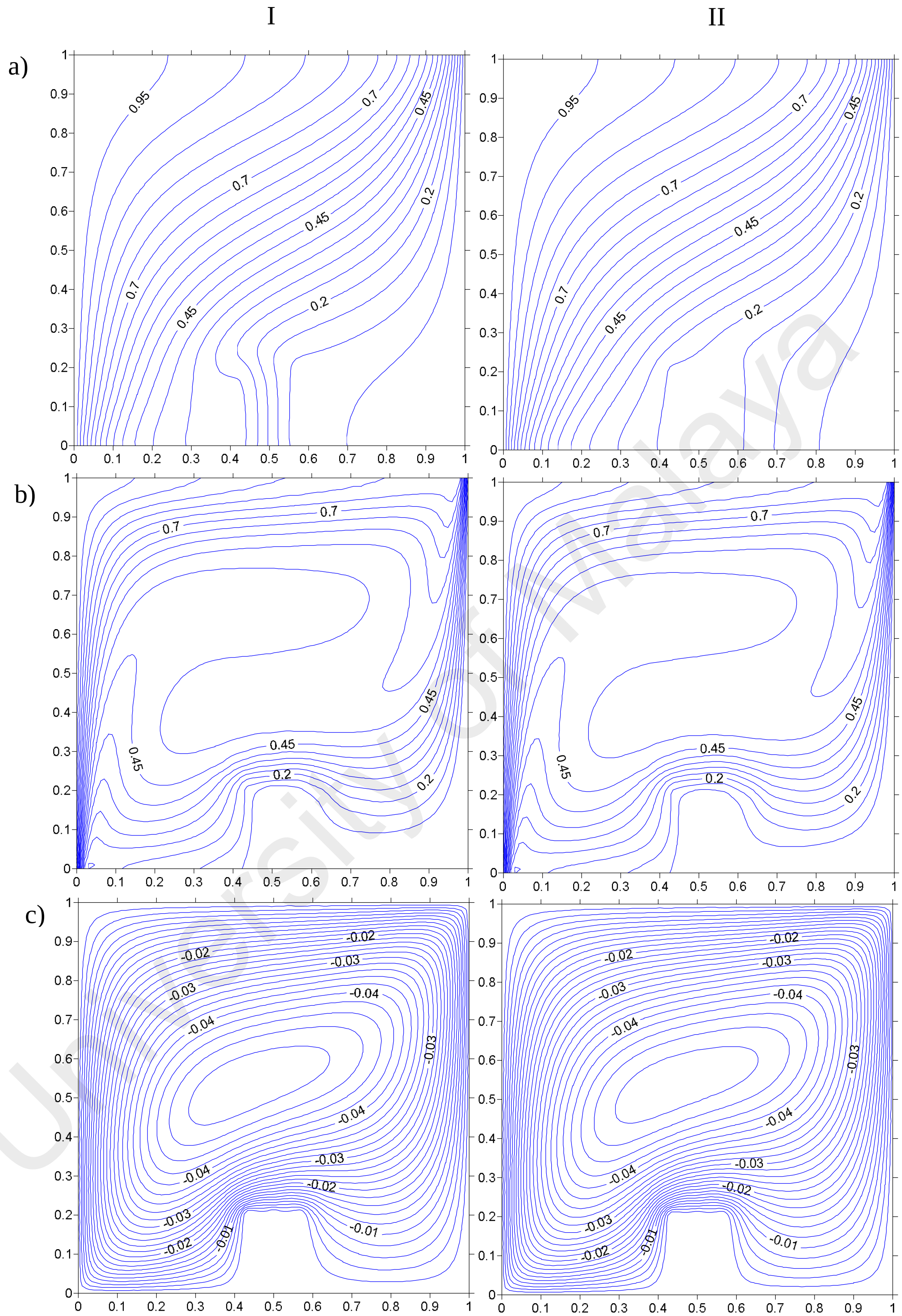


**Figure 6.6:** Effect of *Kr* and solid ($S_h=0.2$) at $\bar{x} = 0.5$, I) $Kr$ = 0.1 II) $Kr=25$
a) Isotherms b) Iso-concentration c) Streamlines

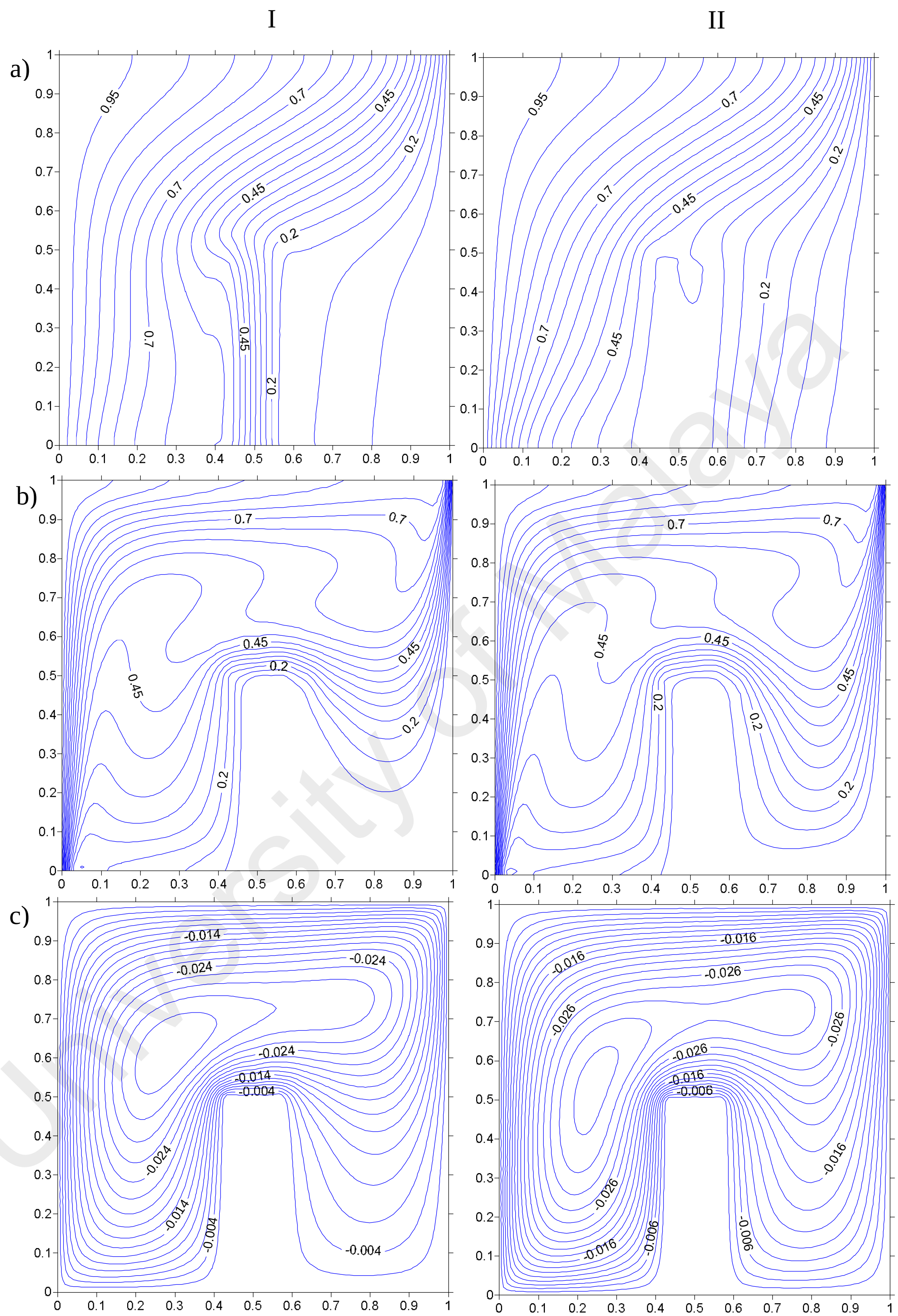


**Figure 6.7:** Effect of *Kr* and solid ($S_h$=0.5) at $\bar{x}$ = 0.5 , I) *Kr* = 0.1 II) *Kr*=25
a) Isotherms b) Iso-concentration c) Streamlines

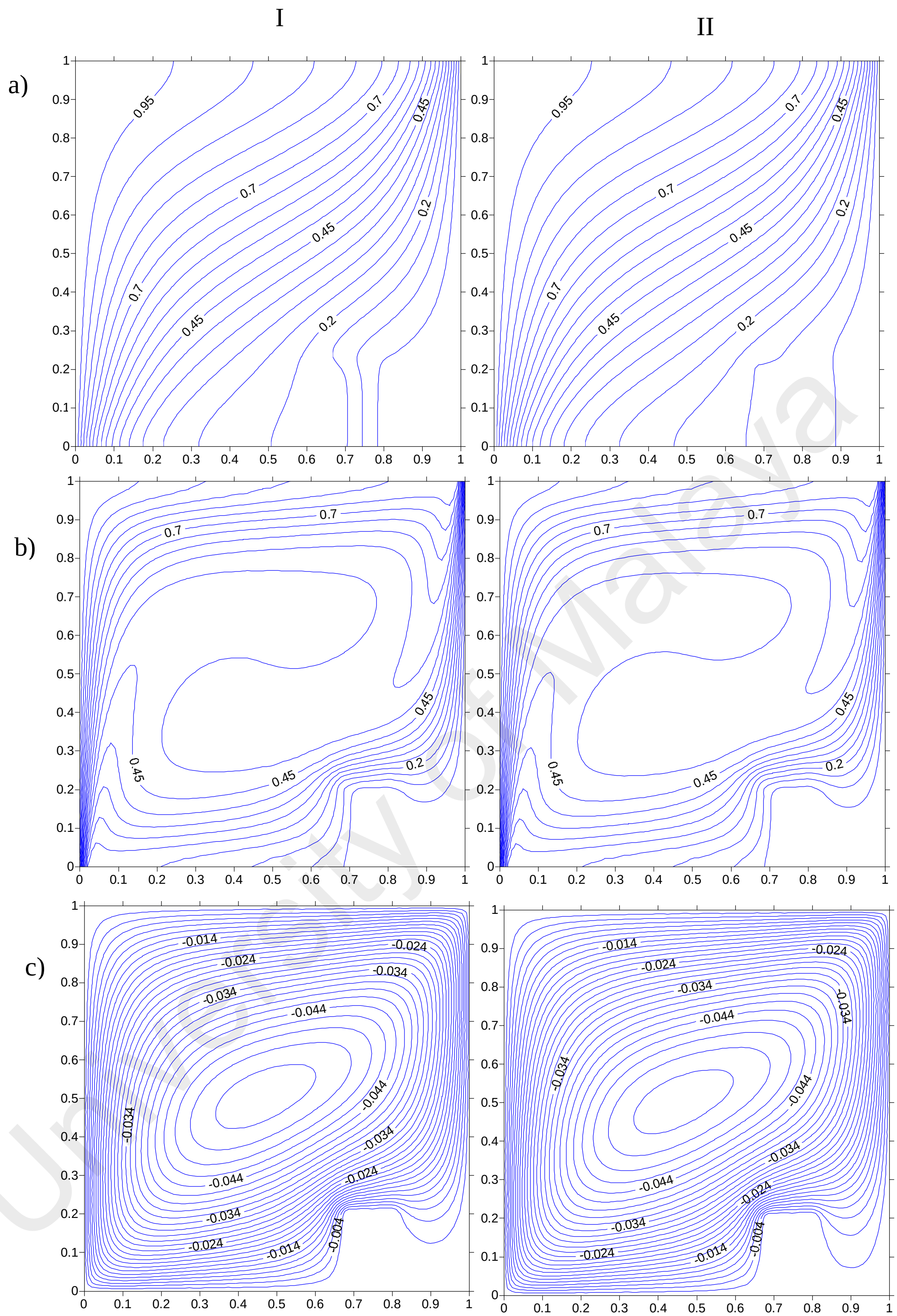


**Figure 6.8:** Effect of *Kr* and solid ($S_h=0.2$) at $\bar{x} = 0.75$ , I) *Kr* = 0.1 II) *Kr=25*
a) Isotherms b) Iso-concentration c) Streamlines

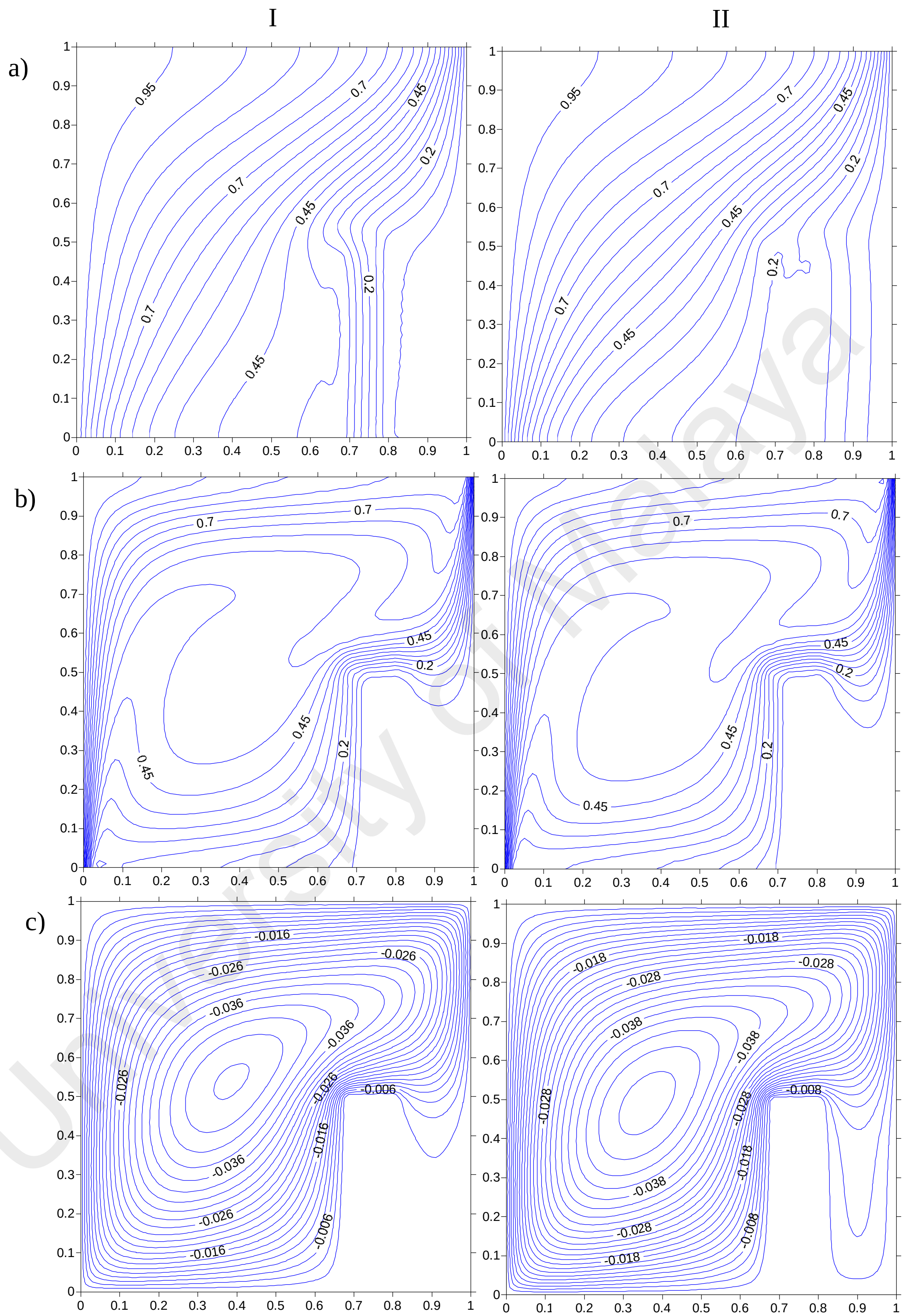


**Figure 6.9:** Effect of *Kr* and solid ($S_h=0.5$) at $\bar{x}$ = 0.75 , I) *Kr* = 0.1 II) *Kr=25* a) Isotherms b) Iso-concentration c) Streamlines

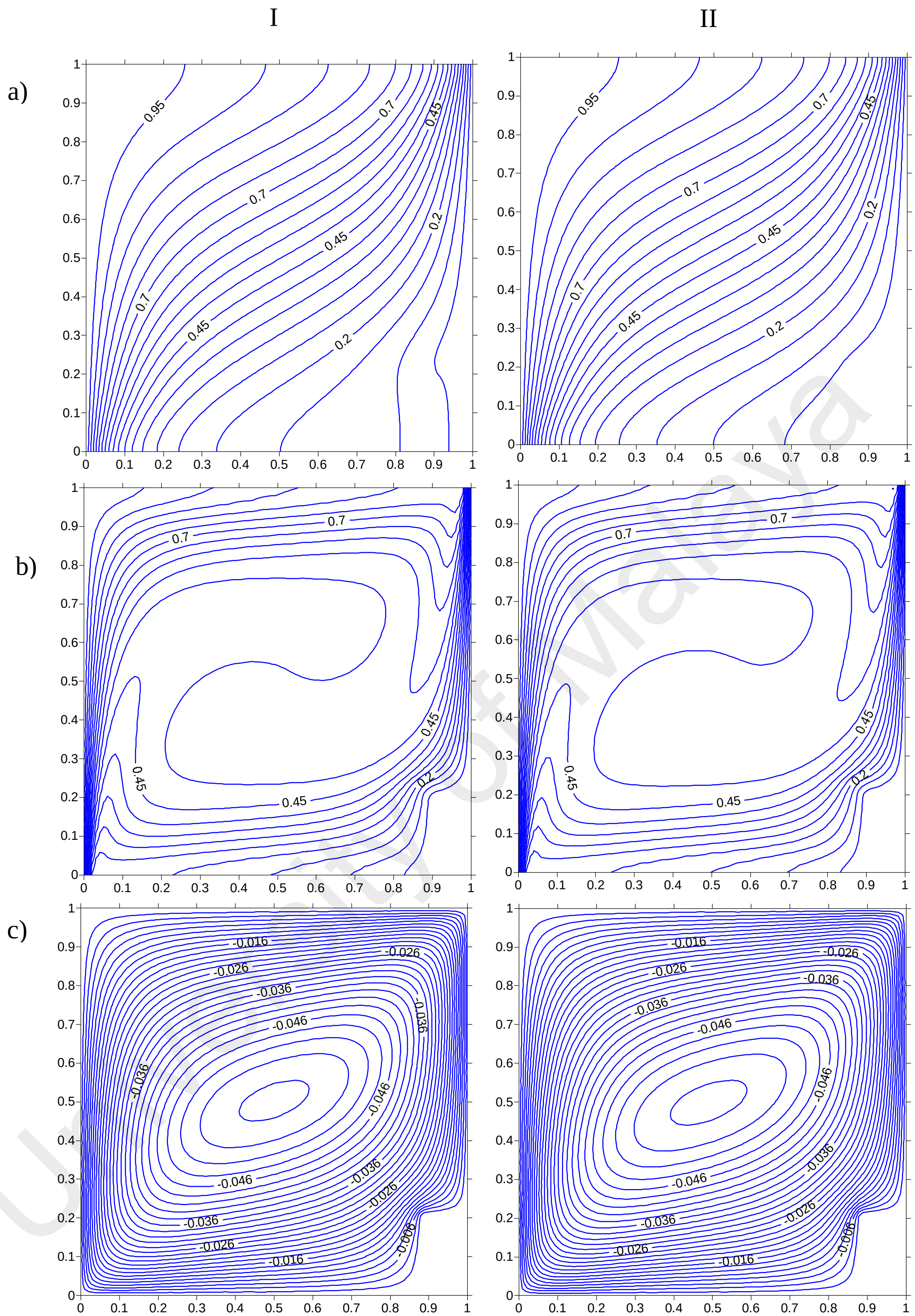


**Figure 6.10:** Effect of *Kr* and solid ($S_h$*=0.2*) at $\bar{x} = 1$ , I) *Kr* = 0.1 II) *Kr=25*
a) Isotherms b) Iso-concentration c) Streamlines

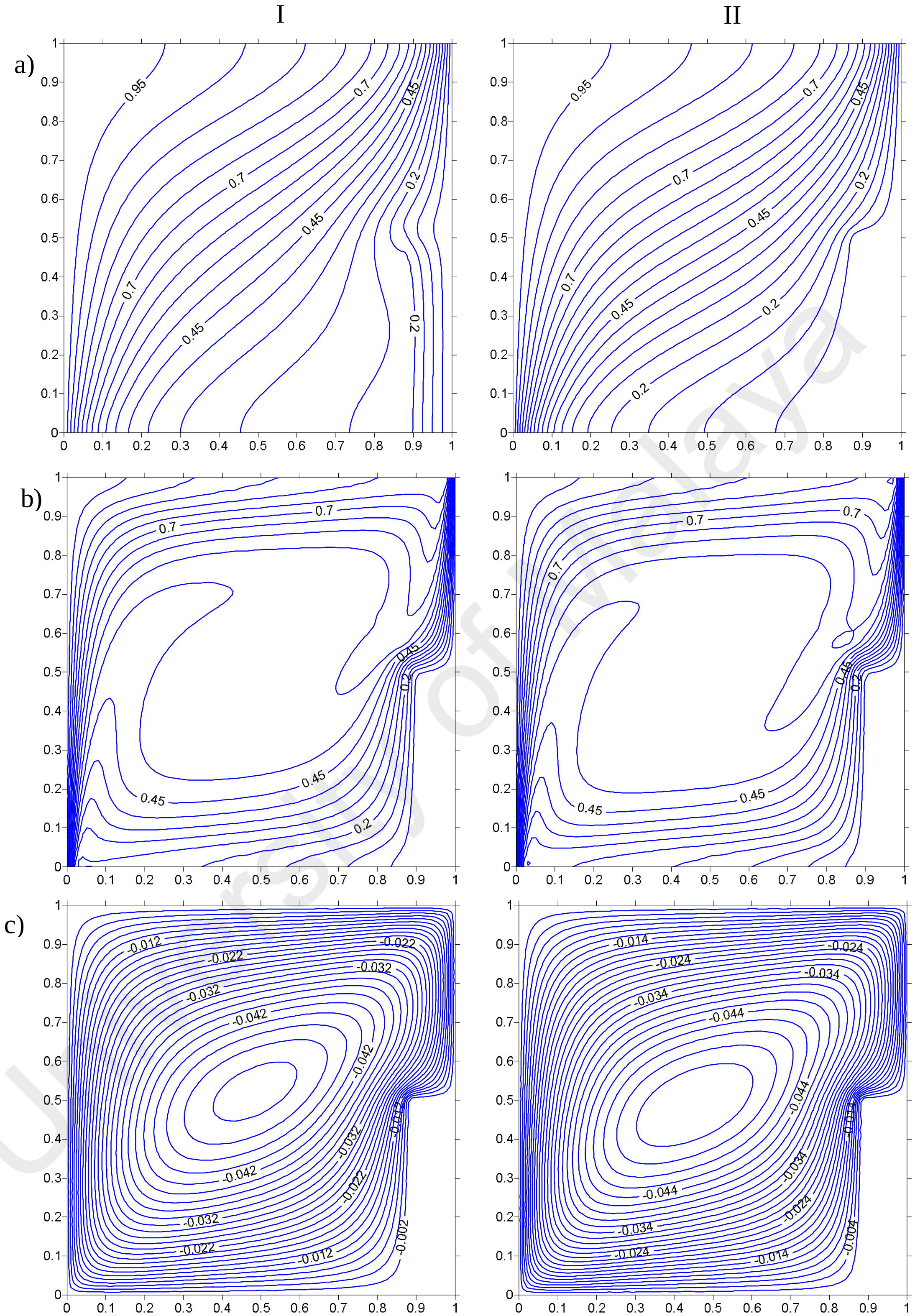


**Figure 6.11:** Effect of *Kr* and solid ($S_h$=*0.5*) at $\bar{x} = 1$, I) *Kr* = 0.1 II) *Kr=25*
a) Isotherms b) Iso-concentration c) Streamlines

The previous figures highlighted the effect of conductivity ratio along with size and location of solid inside the porous region. The study is further explored to investigate the two important mass flow parameters i.e. buoyancy ratio and Lewis number. These parameters are investigated for location of solid at $\bar{x} = 0.25, \bar{x} = 0.5 \; and \; \bar{x} = 0.75$.

figure 6.12 shows the isothermal lines, iso-concentration lines and streamlines for the case *N=-0.5 and N=0.5*. The buoyancy ratio indicates the relative strength of the two buoyant forces i.e. thermal and concentration buoyancy. The buoyancy ratio can vary from negative to positive value also including zero. The sign of buoyancy ratio indicates the relative direction in which thermal and concentration buoyant forces act in the medium. The concentration buoyant force may act vertically upward or downward based on the weight of the concentration molecules. However, the thermal buoyancy force always acts in vertically upward direction due to temperature gradient. Thus the direction of concentration buoyancy decides the sign of buoyancy ratio. The negative sign indicates that the two buoyant forces are opposing each other and positive sign shows that they are acting in the same direction leading to each other's assistance. When buoyancy ratio is zero then the flow becomes purely thermal driven.

Figure 6.12 is obtained at $Ra = 100, Rd = 0.5, Le = 10 \; and \; Kr = 10$, $S_h=0.2$ *and* $\bar{x} = 0.25$. It is seen from isotherms of figure 6.12 that opposing flow which corresponds to negative value of $N$, has higher conduction effect as compared to that of assisting flow arising due to positive value of buoyancy ratio, which is reflected by the fact that the isotherms are more straightened in case of *N=-0.5* as opposed to that of *N=0.5*. This should lead to increased heat transfer rate in case of assisting flow as compared to opposing flow. Similarly the concentration lines gets more crowded near hot surface when N is increased from -0.5 to 0.5 thus increasing the concentration gradient near hot surface that in turn leads to increased mass transfer rate from hot surface to porous medium. This behavior is consistent with all other studies reported for heat and mass transfer in porous medium. (Angirasa, Peterson, & Pop, 1997; I. A Badruddin, N. J. S Ahmed, et al., 2012)

The increase in the solid size to 0.5 ($S_h$=$0.5$) from 0.2 further pushes the isotherms away from the hot surface as evident from figure 6.13 which illustrates the effect of increased solid height. It is seen that the heat transfer rate along the hot surface is almost constant as a result of nearly constant thermal gradient for N=-0.5. However, the thermal gradient varies along the hot surface with higher gradient at lower part and lower gradient at upper section when N is increased to 0.5. This happens because of the reason that the assisting flow helps the transfer of heat, as well as mass transfer by acting in same direction. Mass transfer is substantially affected due to increased solid height. It is noted that most of the porous medium is occupied by very low concentration at opposing flow but the concentration level significantly improves for the case of assisting flow. The fluid flows in three different cells at opposing flow and concentrates in the region after the solid block. However, the fluid flow turns into one continuous cell covering almost all area of porous medium illustrated by the streamlines of figure 6.13.

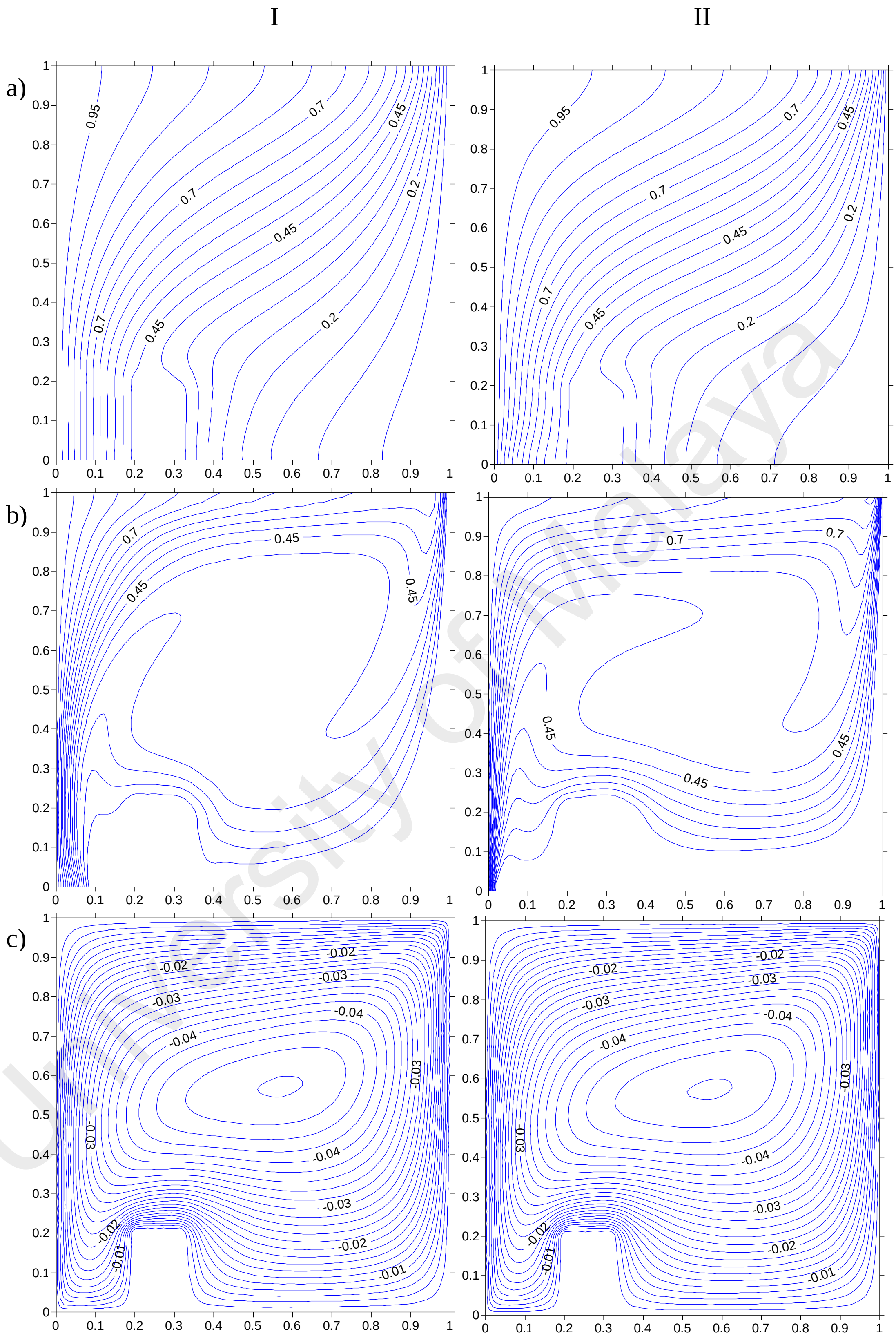


**Figure 6.12:** Effect of $N$ and solid ($S_h$=*0.2*) at $\bar{x} = 0.25$ , I) $N$ = -0.5 II) $N$=*-0.5*
a) Isotherms b) Iso-concentration c) Streamlines

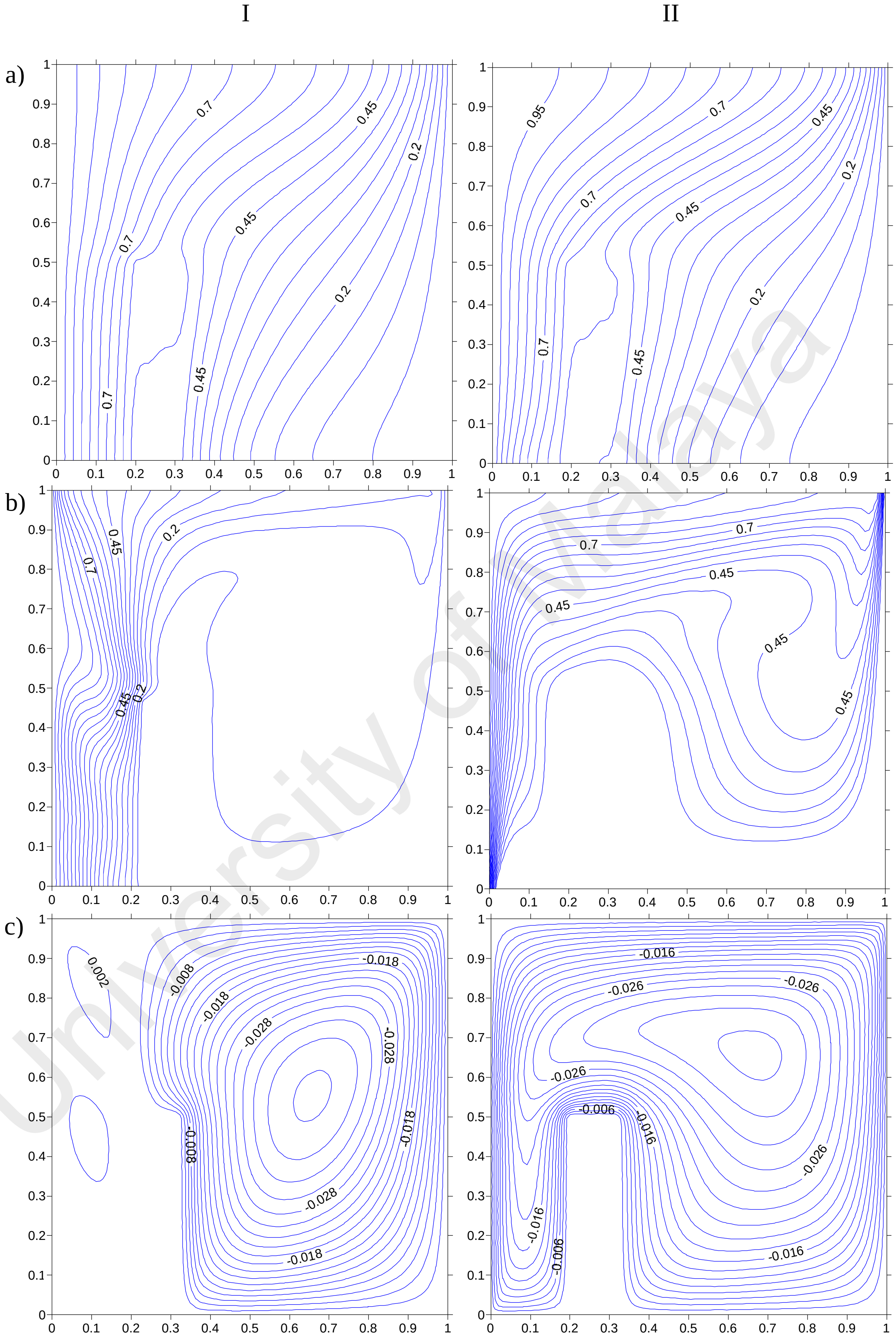


**Figure 6.13:** Effect of $N$ and solid ($S_h$=0.5) at $\bar{x} = 0.25$ , I) $N$ = -0.5 II) $N$=0.5
a) Isotherms b) Iso-concentration c) Streamlines

The position of solid block is further moved to center of cavity to investigate the effect of aiding and opposing flow. Figure 6.14 and figure 6.15 show the isotherms, iso-concentration and streamlines when solid is placed at center of cavity for the height $S_h=0.2$ *and* $S_h=0.5$ respectively. It is seen that the thermal gradient increases due to moving of solid from $\bar{x} = 0.25$ to $\bar{x} = 0.5$. Thus the heat transfer rate increases for the case of solid at center of cavity than being on left side of cavity. Similarly, the distribution of concentration is better in case of solid at center of cavity than being at left side (figure 6.12). The fluid flow direction shifts from being horizontal to oblique towards the lower left and upper right corners of cavity. However, the flow direction is substantially differs for opposing and assisting flow when the height of solid is increased to 0.5. The fluid is more concentrated in the right section of cavity for opposing flow, but it shifts towards left section of cavity for assisting flow as shown by the streamlines of figure 6.15.

Similarly the position of solid block is moved to $\bar{x} = 0.75$ for the solid height $S_h=0.2$ (figure 6.16) *and* $S_h=0.5$(figure 6.17). It is deduced that the heat transfer and mass transfer rate is still higher in case of assisting flow when solid is moved to $\bar{x} = 0.75$. The fluid flow becomes oval shape in the diagonal direction as shown by figure 6.16. However, the similarity between the opposing flow and assisting fluid flow improves when solid height is increased to 0.5 as compared to the case of solid at the center of cavity(figure 6.15)

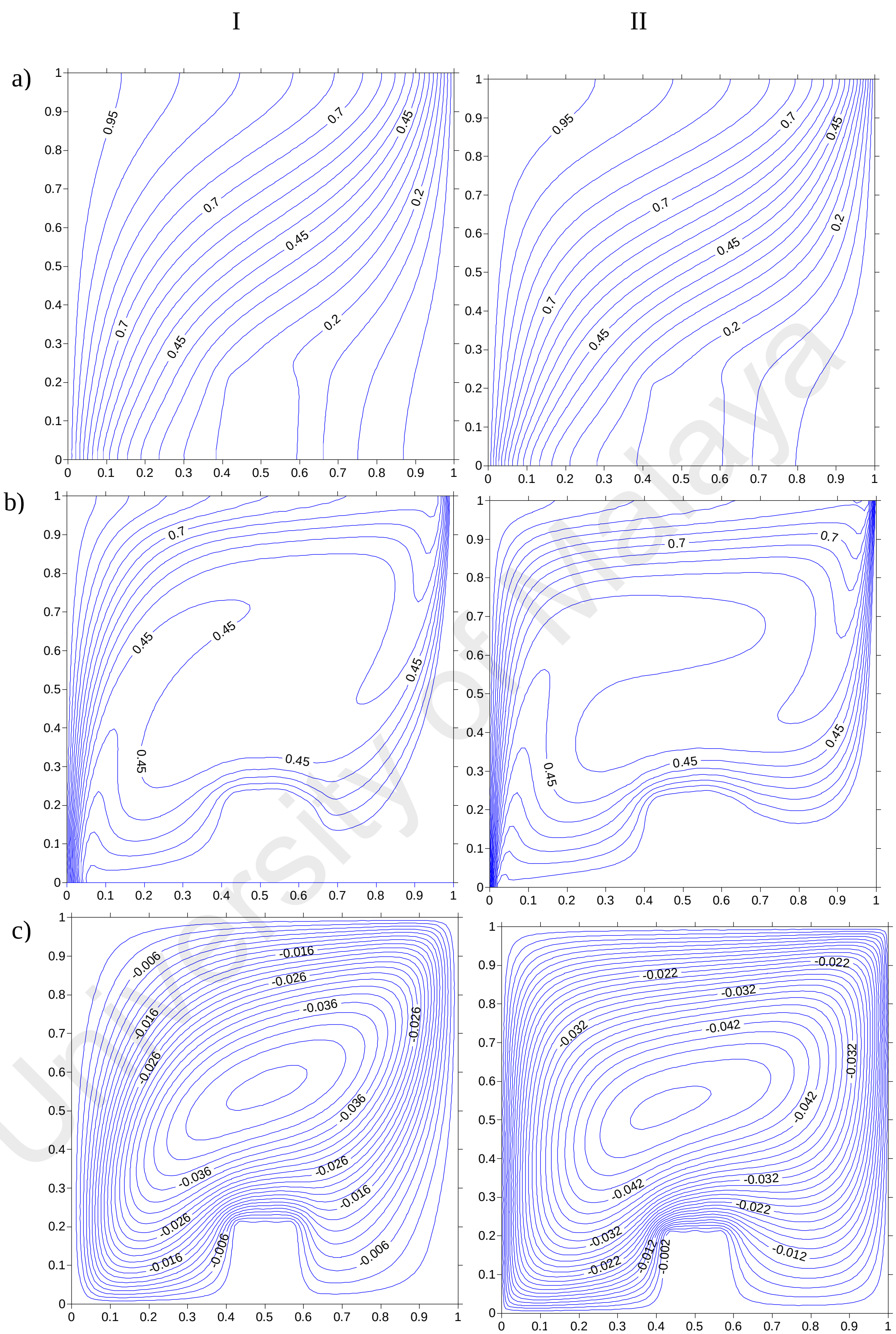


**Figure 6.14:** Effect of $N$ and solid ($S_h=0.2$) at $\bar{x} = 0.5$ , I) $N$ = -0.5 II) $N=0.5$
a) Isotherms b) Iso-concentration c) Streamlines

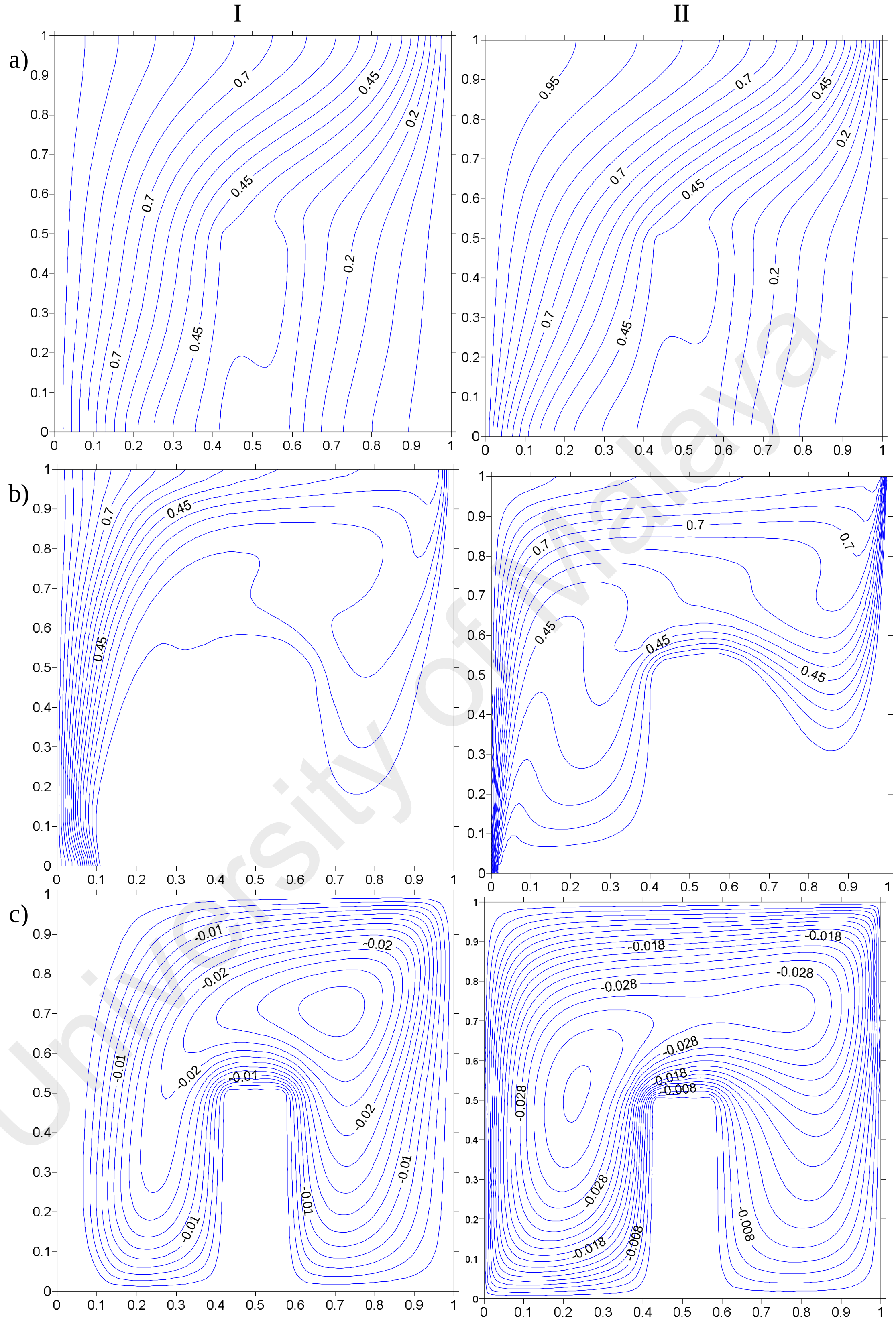


**Figure 6.15:** Effect of $N$ and solid ($S_h=0.5$) at $\bar{x} = 0.5$, I) $N$ = -0.5 II) $N=0.5$
a) Isotherms b) Iso-concentration c) Streamlines

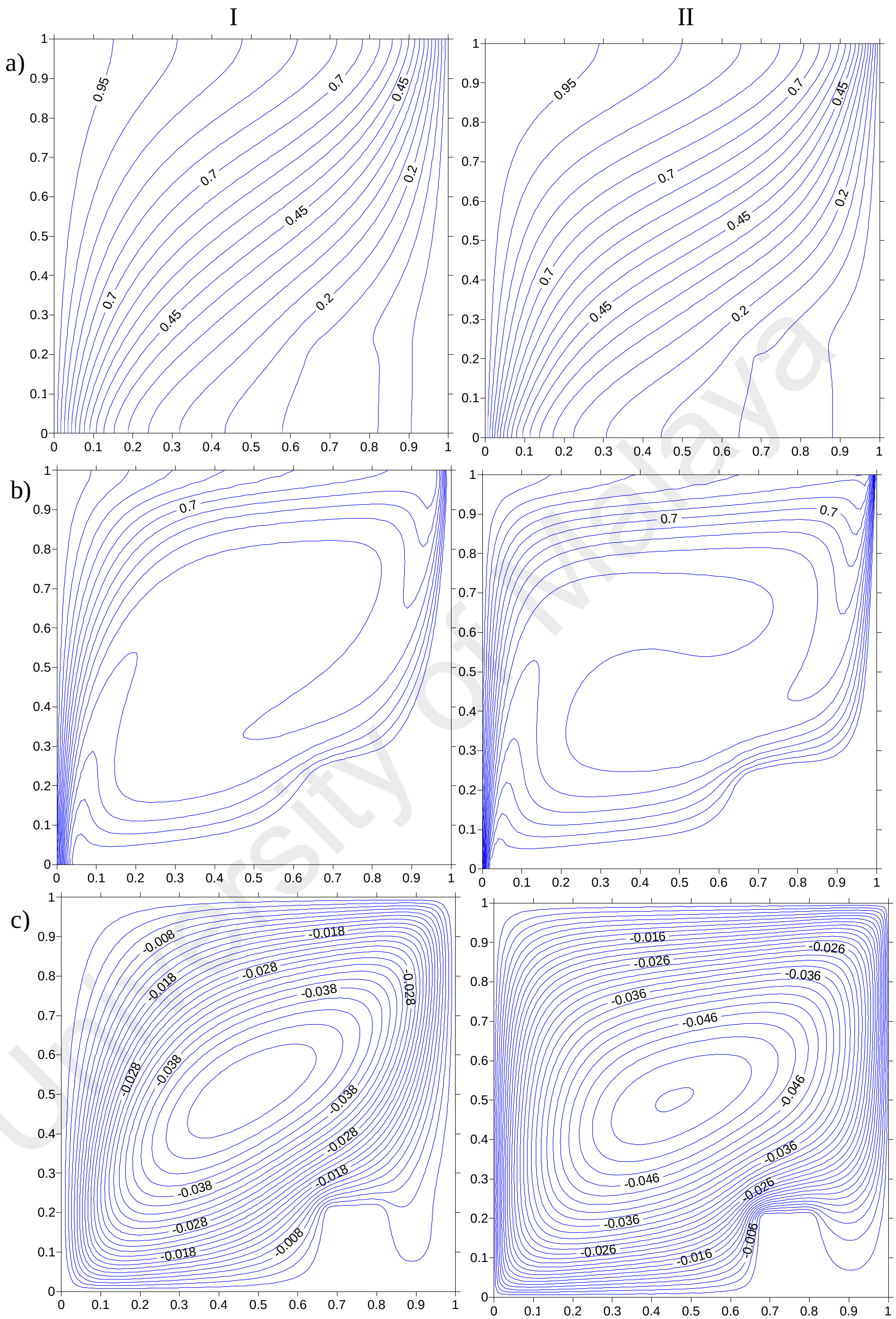


**Figure 6.16:** Effect of $N$ and solid ($S_h$=$0.2$) at $\bar{x} = 0.75$ , I) $N$ = -0.5 II) $N$=$0.5$
a) Isotherms b) Iso-concentration c) Streamlines

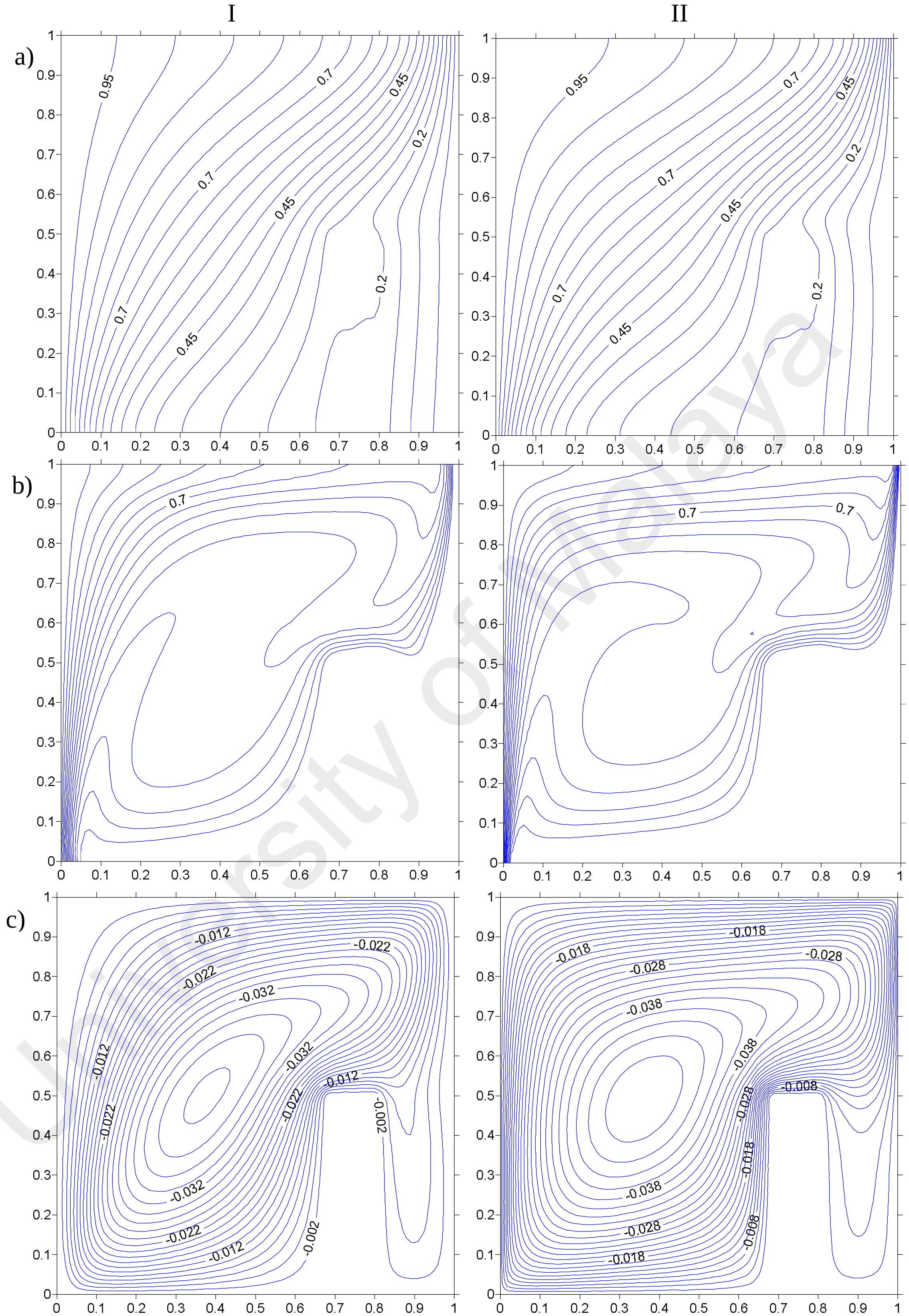


**Figure 6.17:** Effect of *N* and solid ($S_h$=*0.5*) at $\bar{x}$ = 0.75 , I) *N* = -0.5 II) *N=0.5*
a) Isotherms b) Iso-concentration c) Streamlines

The effect of Lewis number on the isothermal lines, iso-concentration lines and streamlines is discussed in the following section. Lewis number is the ratio of thermal diffusivity to the mass diffusivity, thus it indicates the relative diffusion of two quantities. Figure 6.18 to figure 6.23 are obtained for $Ra = 100, Rd = 0.5, N = 0.2\ and\ Kr = 10$ . Figure 6.18 shows the effect of Lewis number when solid block is placed at $\bar{x} = 0.25$ and two values of Lewis number i.e $Le = 5\ and\ Le = 25$. It is seen that the isotherms are not much affected due to change in Lewis number, however the iso-concentration lines get crowded at hot surface due to increase in $Le$. This indicates that the concentration gradient increases with increase in $Le$ which in turn should increase the Sherwood number. It should be noted that the sherwood number indicates the total mass transfer rate with respect to the diffusion rate. Thus, it can be deduced that the decrease in molecular diffusivity is reflected in terms of increase in Lewis number that in turn increases the Sherwood number.

The increase in the height of the solid blocks the concentration distribution to some extent in the right side of cavity as shown by isoconectration lines of figure 6.19. However, the increased Lewis number improves the concentration distribution in the porous medium along with increasing the concentration gradient at the hot surface. Close observation of isothrms reveals that the thermal gradient decreases marginally with increase in Lewis number.

The shifting of solid block to center of cavity reduces the mass concentration towards the lower right section of cavity as shown in figure 6.20. This is because of the reason that the presence of solid wall at center blocks lower right area of cavity. The increase in solid height at center of cavity to $S_h=0.5$ further weakens the presence of mass concentration in the lower right area of cavity (figure 6.21).

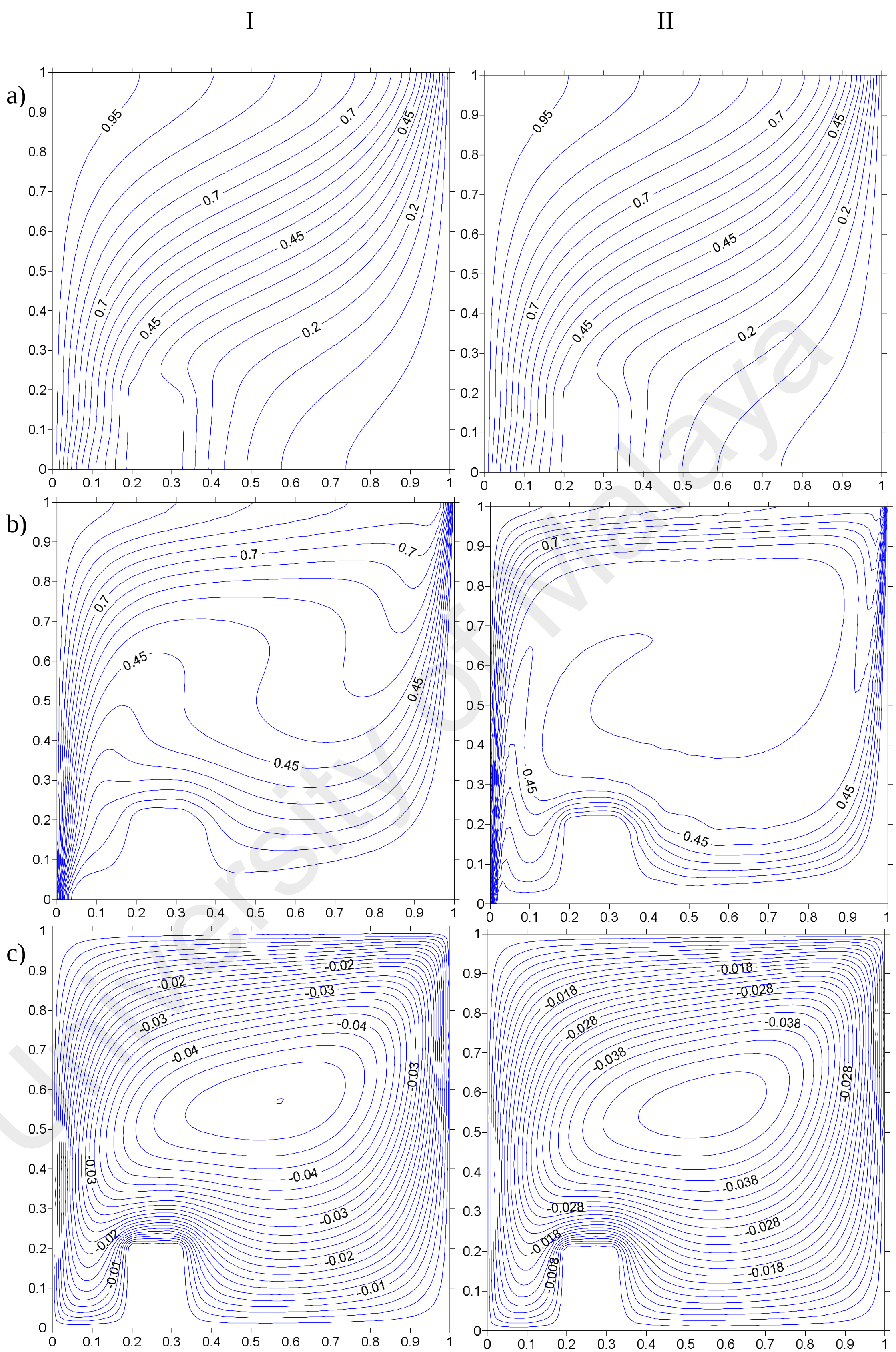


**Figure 6.18:** Effect of $N$ and solid ($S_h=0.2$) at $\bar{x}=0.25$ , I) $Le=5$ II) $Le=25$
a) Isotherms b) Iso-concentration c) Streamlines

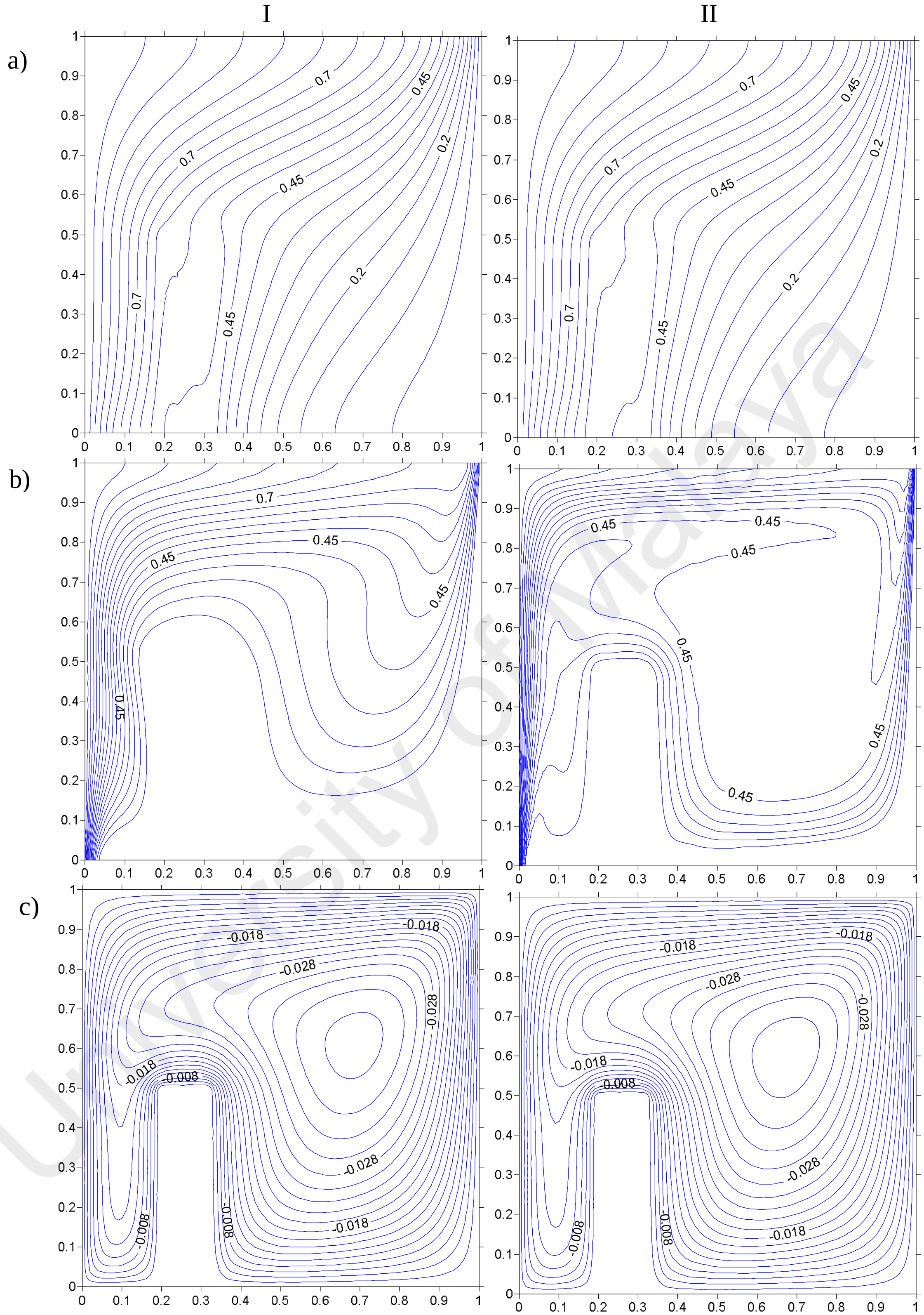


**Figure 6.19:** Effect of $N$ and solid ($S_h=0.5$) at $\bar{x} = 0.25$, I) $Le=5$ II) $Le=25$
a) Isotherms b) Iso-concentration c) Streamlines

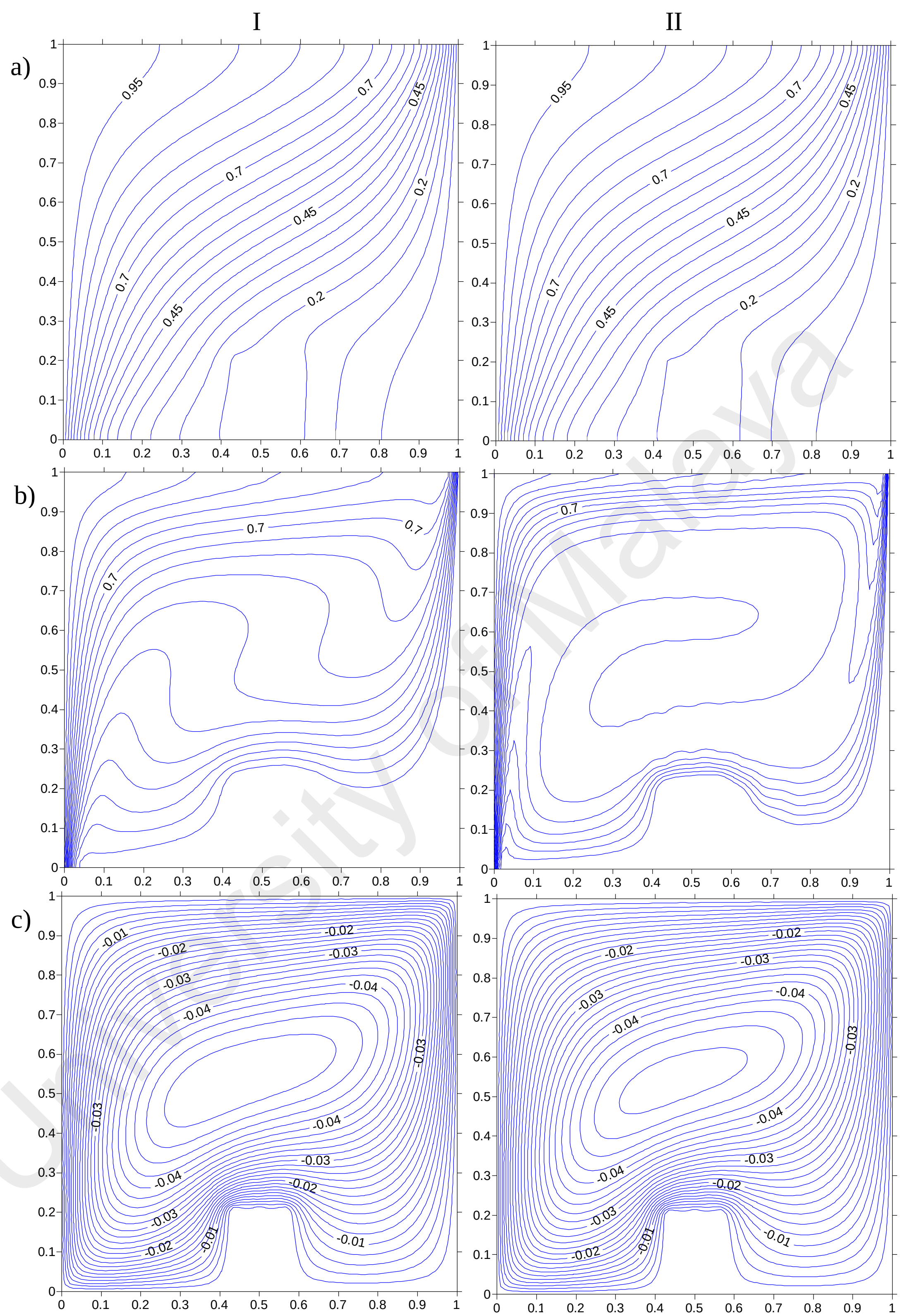


**Figure 6.20:** Effect of $N$ and solid ($S_h$=*0.20*) at $\bar{x} = 0.5$ , I) $Le$=*5* II) $Le$=*25*
a) Isotherms b) Iso-concentration c) Streamlines

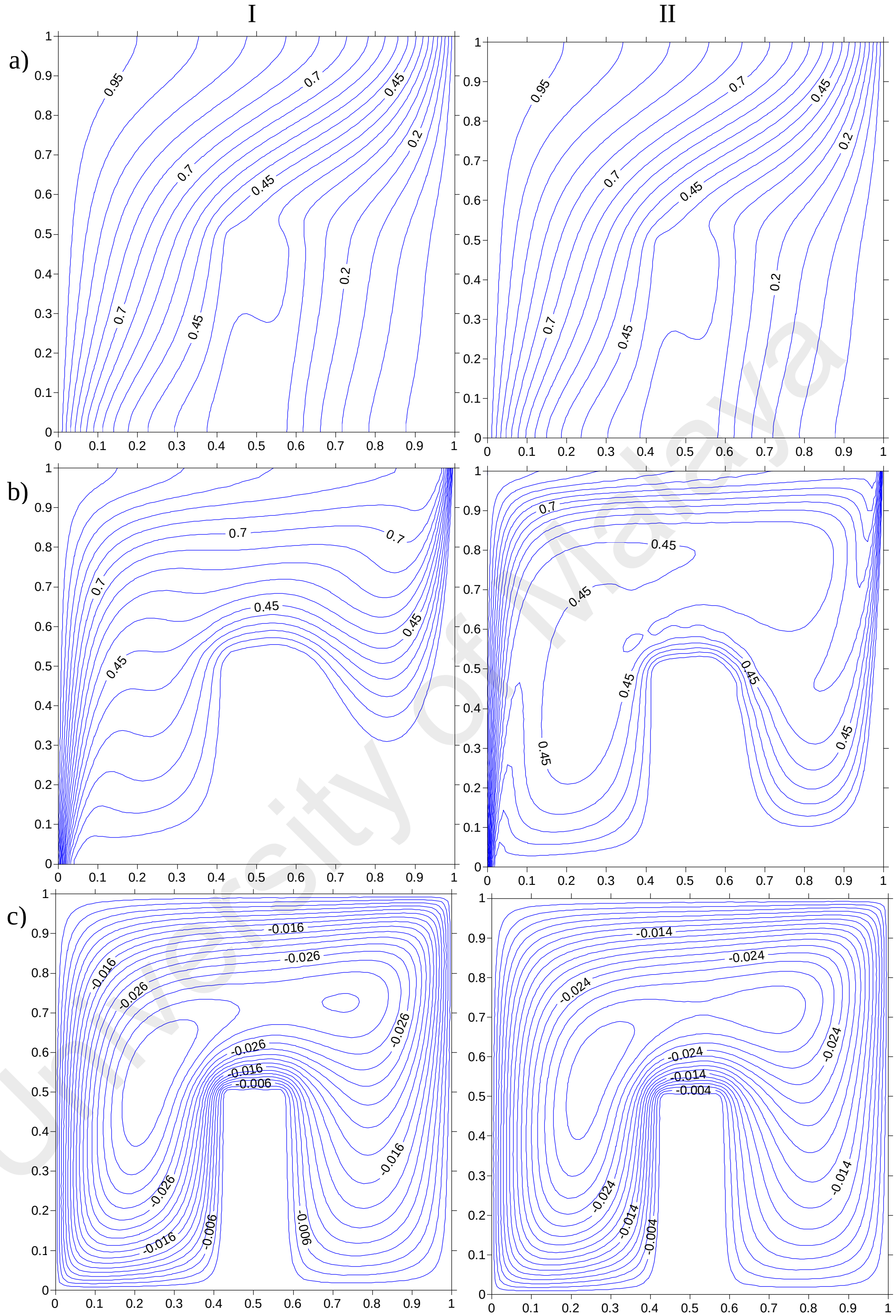


**Figure 6.21:** Effect of $N$ and solid ($S_h=0.5$) at $\bar{x}=0.5$ , I) $Le=5$ II) $Le=25$
a) Isotherms b) Iso-concentration c) Streamlines

Figure 6.22 and figure 6.23 shows the variation in temperature, concentration and streamlines when solid is placed at $\bar{x} = 0.75$ for height of solid $S_h=0.2$ *and* $S_h=0.5$ respectively. It is seen that the isothermal lines tend to move towards the hot surface when solid wall is moved away towards the right side of cavity indicating that the heat transfer rate increases. The clustered isotherms near the hot surface increases the thermal gradient at hot wall that in turn increases the heat transfer rate from hot surface to porous medium. More area towards the bottom right corner of cavity is deprived of mass concentration due to position of solid block at $\bar{x} = 0.75$. This is further aggrieved when height of solid is increased to $S_h=0.5$. As in previous cases, the increase in Lewis number improves the concentration profile to some extent for both the heights of the solid.

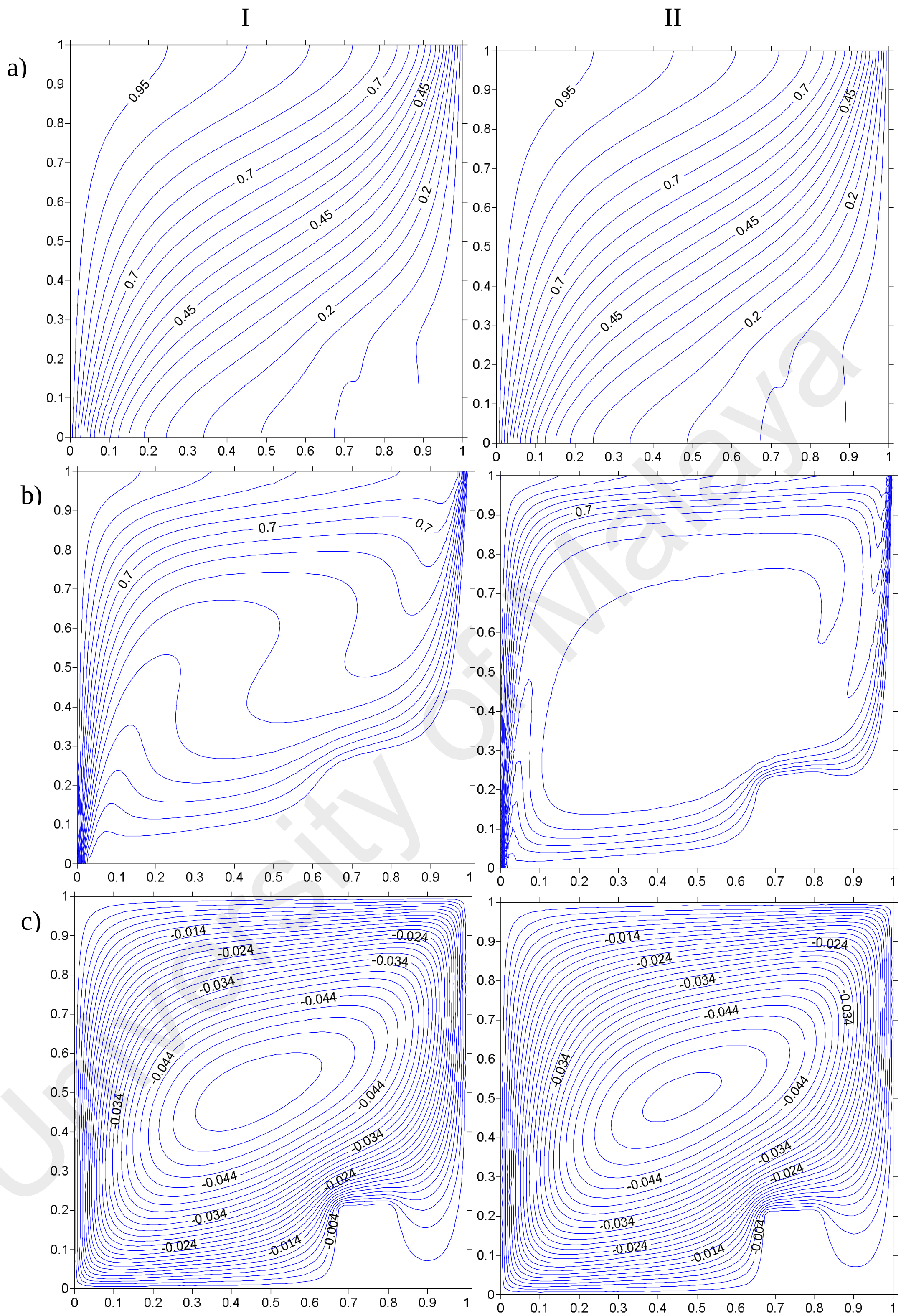




**Figure 6.22:** Effect of *N* and solid ($S_h$=*0.20*) at $\bar{x} = 0.75$ , I) *Le=5* II) *Le=25*
a) Isotherms b) Iso-concentration c) Streamlines

I II

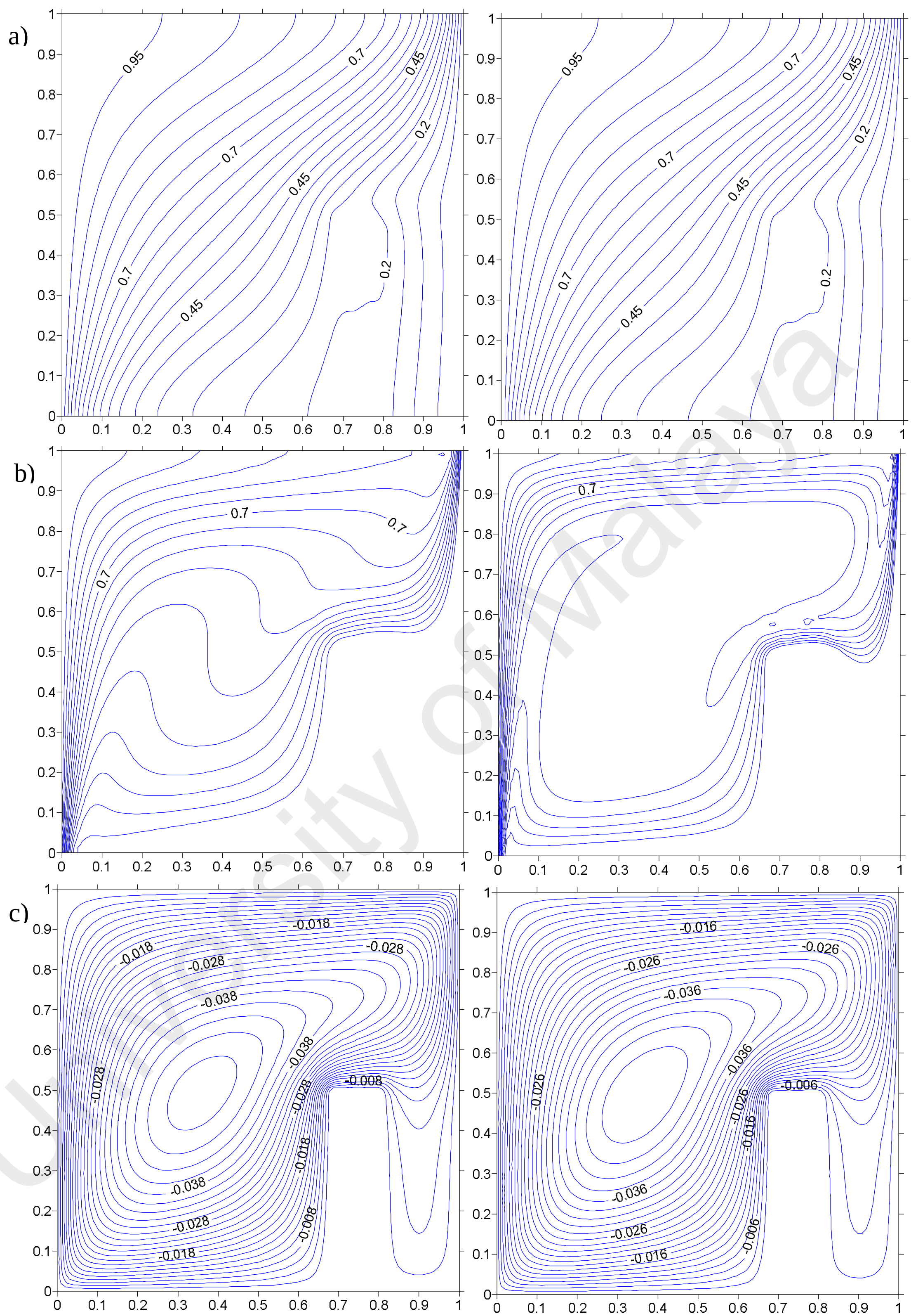




**Figure 6.23:** Effect of *N* and solid ($S_h$=*0.5*) at $\bar{x} = 0.75$ , I) *Le=5* II) *Le=25*
a) Isotherms b) Iso-concentration c) Streamlines

## 6.5 Heat and Mass Transfer

The following section presents the details of heat and mass transfer in terms of Nusselt and Sherwood number at hot surface of the cavity. The variation of Nusselt and Sherwood number along the hot wall as well as with height and location of solid are illustrated in figures 6.24-6.33. The other parameters for these figures are kept as $Ra = 100, Rd = 0.5$. It should be noted that the Nusselt and Sherwood number are represented by temperature and concentration gradients at hot surface as given by equations 6.15 and 6.16 respectively. Figure 6.24 and 6.25 shows the Nusslet and Sherwood number respectively when the solid is placed at $\bar{x} = 0$. For the case of solid wall placed at $\bar{x} = 0$, it should be noted that the values are calculated excluding the portion of hot surface occupied by solid wall. Thus figures 6.24 and 6.25 have varying values of starting point i.e. $\bar{y}$. It is found that the Nusselt number for the smaller value of conductivity ratio (*Kr=0.1*) decreases in a non-linear pattern along the height of cavity. This is very much compatible with the previous studies being carried out for the case of heat transfer in porous cavity. However, for *Kr*=5, the Nusselt number initially increases for a short height of cavity and then decreases at further height of hot surface. On the basis of evidence currently seen in figure 6.24, it can be said that the higher thermal conductivity ratio creates low thermal gradient just above the solid due higher thermal diffusion assisted by increased thermal conductivity of solid. This is further vindicated by a curved isotherm near the hot wall when *Kr* is higher as compared to almost straight isotherm when *Kr* =0.1 of figures 6.2-6.3. Similar trend of Nusselt number is seen when height of solid is increased from 20% to 50%. The Sherwood number also decreases with increase in height of cavity as depicted in figure 6.25. For a given height of cavity, the Sherwood number is higher for the case of longer solid ($S_h$=*0.5*) as compared to shorter solid ($S_h$=*0.5*).

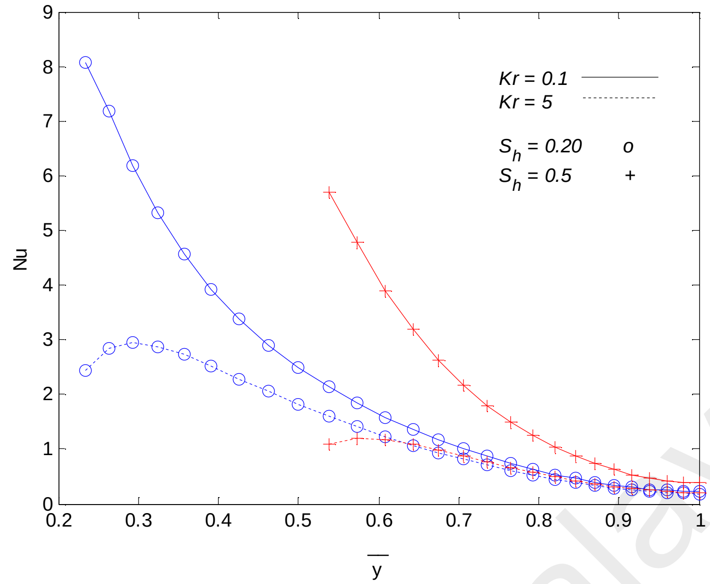


**Figure 6.24:** Nusselt number for solid at left surface $\bar{x} = 0$

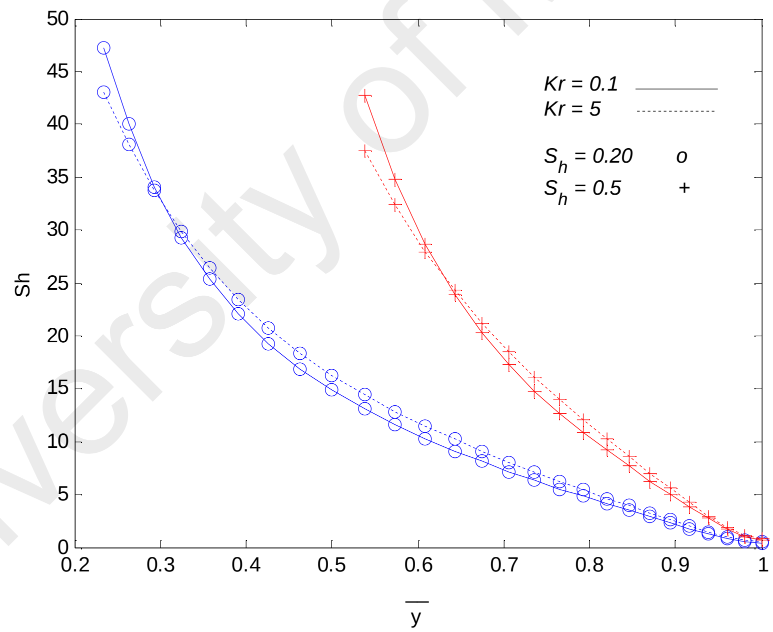


**Figure 6.25:** Sherwood number for solid at left surface $\bar{x} = 0$

Figure 6.26 and 6.27 illustrates the effect of solid being placed at $\bar{x} = 0.25$ on Nusselt and Sherwood number. The solid placed at $\bar{x} = 0.25$ is a position of solid that is close to left edge of cavity than the right edge. It is interesting to note that the behavior of heat transfer as reflected by Nusselt number of figure 6.26 is completely different from that of solid placed at left surface. The Nusselt number decreases slightly at bottom of cavity and the increases until a point thereafter it starts declining again when porous conductivity is much higher than that of solid wall conductivity ($Kr=0.1$). This could be best argued in a way that the presence of a low thermal conductivity solid increases the thermal resistance for heat to flow into porous medium through solid wall thus forcing the heat to find an alternate path of flow. This alternate path exists above the solid wall thus the heat transfer rate increases until the solid height and thereafter it declines due to fluid movement towards the cold surface. However, this behavior of increasing Nusselt number until solid height is suppressed when the conductivity of solid increases ($Kr=5$). In this case, the thermal energy is easily transferred across the solid wall thus not forcing it to find an alternate path. The Nusselt number decreases continuously along the height of cavity though in a bilinear pattern. The mass transfer decreases continuously except for the case of $Kr=0.1$and $S_h=0.5$, where it increases slightly at middle of the hot surface. This could be attributed to increased fluid activity just around the top corner of solid wall which helps in higher mass diffusion as depicted by streamlines of figure 6.5.

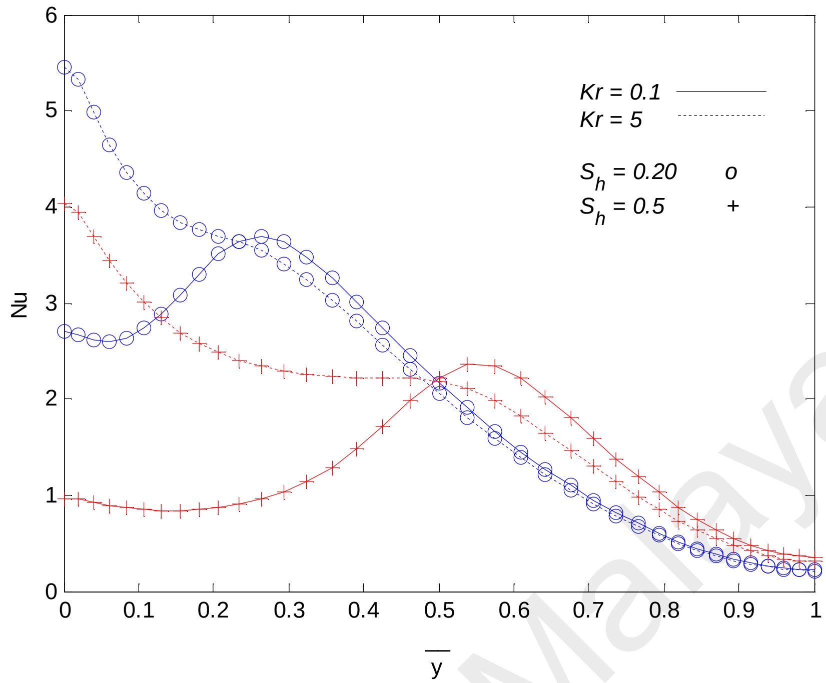


**Figure 6.26:** Nusselt number for solid $\bar{x}$ = 0.25

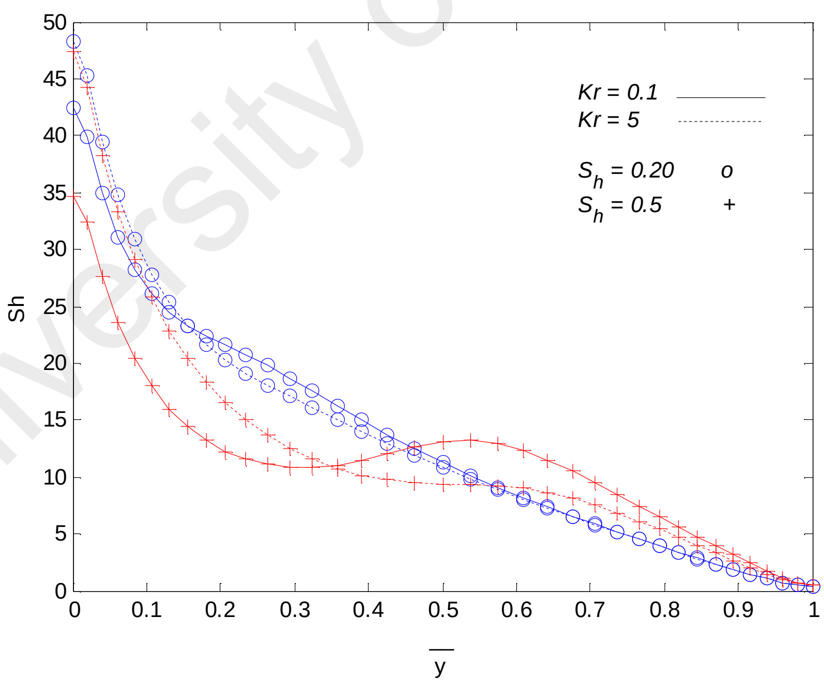


**Figure 6.27:** Sherwood number for solid at $\bar{x}$ = 0.25

It is found that the further away placement of solid from hot surface (figure 6.28-6.29) reduces the uneven variation of Nusselt and Sherwood number caused by nearby placement of solid as seen in previous case (figure 6.26-6.27). The heat and mass transfer rate decreases continuously along the hot surface. This shows that the effect of presence of solid decreases as it moves away from the hot wall. The Nusselt number is higher for shorter solid as compared to that of longer solid. Nusselt number follows bilinear pattern along hot wall for 50% solid height ($S_h=0.5$). However, there is no such bilinear variation for Sherwood number as illustrated by figure 29. Thus the evidence of figures 6.24-6.29 reveals that the presence of solid has predominant effect on heat transfer rate as compared to that of mass transfer, though mass transfer is also affected.

Figures 6.30-6.33 show the Nusselt and Sherwood numbers when the solid is moved to $\bar{x} = 0.75$ and $\bar{x} = 1$. It is found that the farthest the solid placement from hot surface, highest is the Nusselt number at bottom region of hot surface. The influence of thermal conductivity ratio is stronger for higher solid height. It is also noted that the effect of increasing *Kr* diminishes when solid is placed towards the right surface of cavity for $S_h=0.2$. However, the effect of *Kr* is clearly visible even for solid placed at $\bar{x} = 1$ for $S_h=0.5$. The mass transfer rate slightly increases when the solid is moved towards the cold surface but more importantly the influence of thermal conductivity ratio and the solid height decreases as seen by almost overlapping lines in figure 6.33.

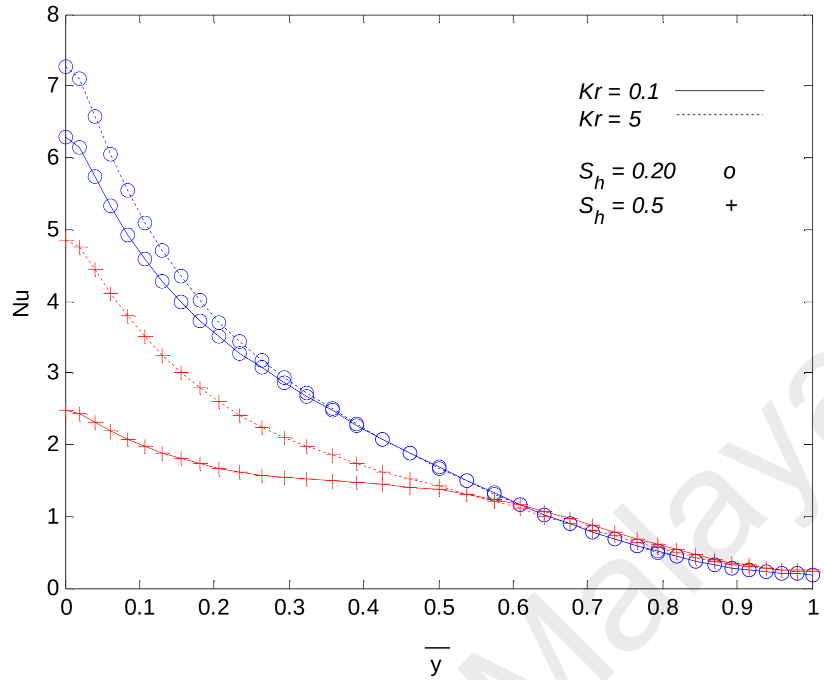


**Figure 6.28:** Nusselt number for solid at $\bar{x} = 0.5$

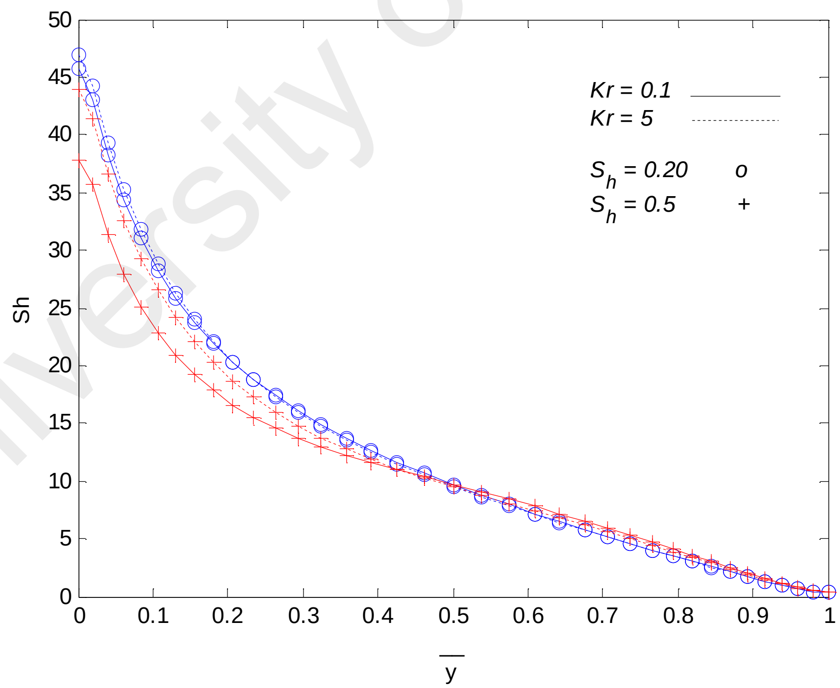


**Figure 6.29:** Sherwood number for solid at $\bar{x} = 0.5$

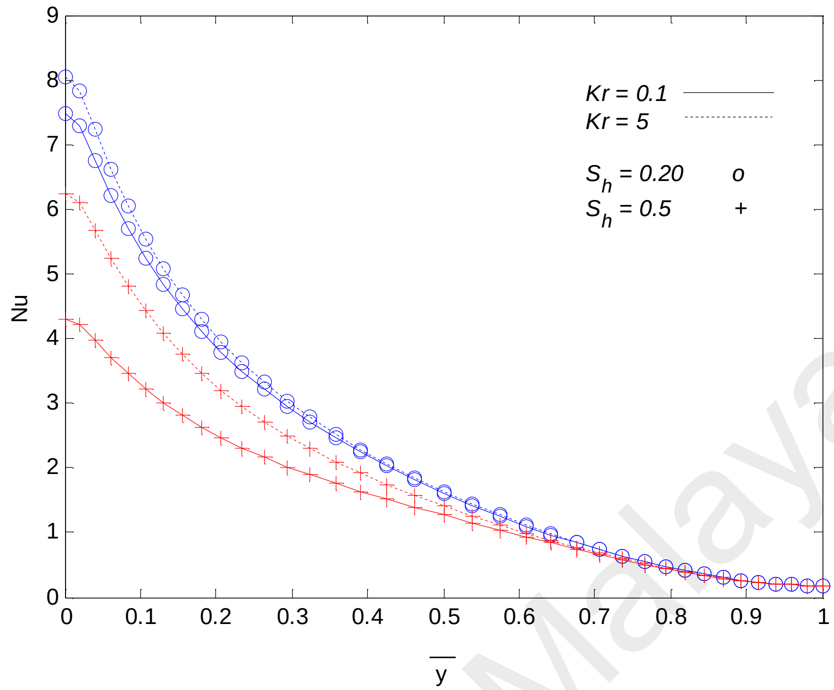


**Figure 6.30:** Nusselt number for solid at $\bar{x} = 0.75$

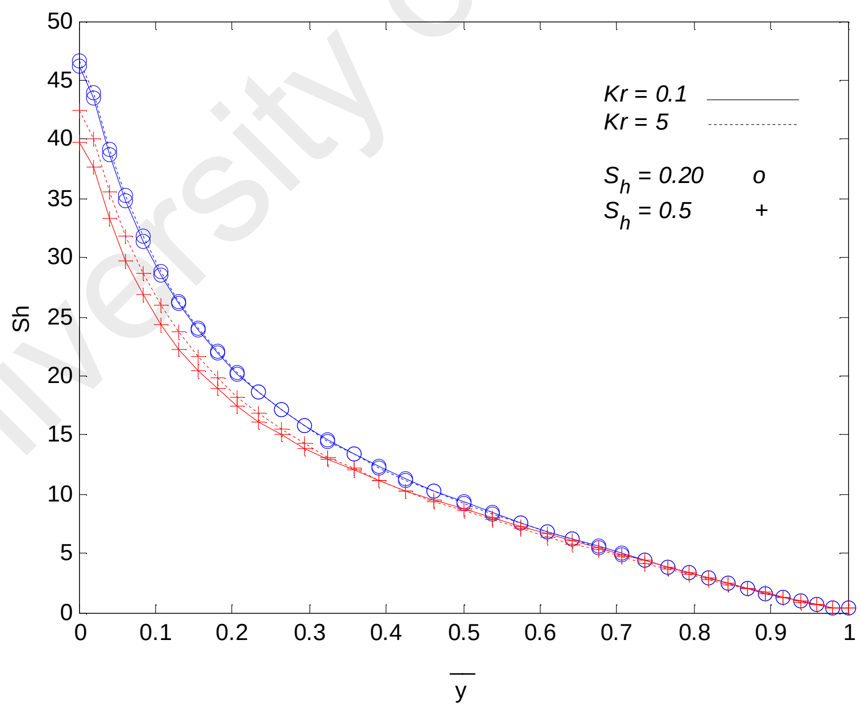


**Figure 6.31:** Sherwood number for solid at $\bar{x} = 0.75$

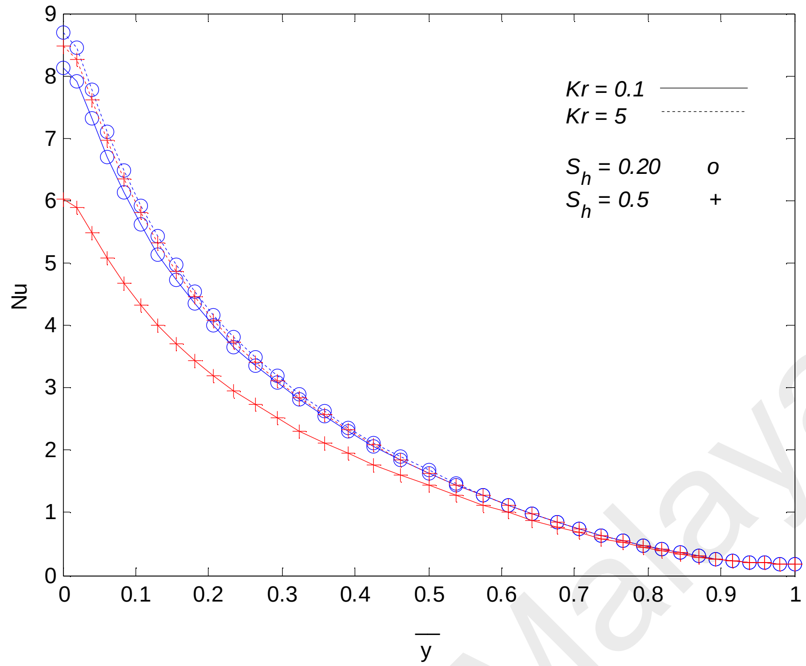


**Figure 6.32:** Nusselt number for solid at $\bar{x} = 1$

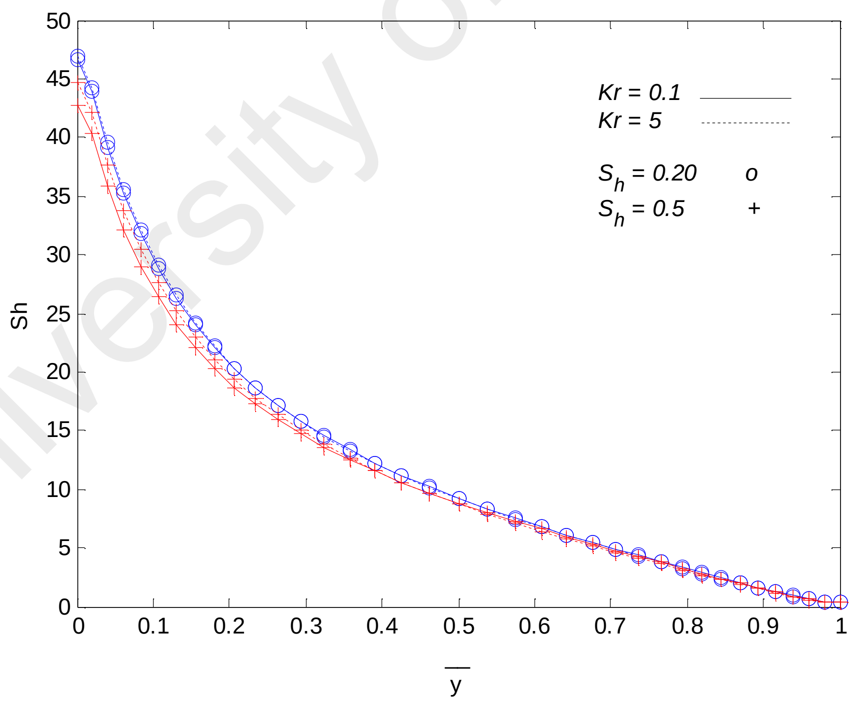


**Figure 6.33:** Sherwood number for solid at $\bar{x} = 1$

# CHAPTER 7 : CONCLUSION

The present study deals with the research pertaining to optimization and investigation of conjugate heat and mass transfer in porous cavity. The various important aspects of conjugate heat transfer, conjugate heat and mass transfer analysis were mathematically modelled and simulated using Matlab. The result obtained from the simulations have been enumerated in the subsequent sections.

## 7.1 Optimized Solution of Conjugate Heat and Mass Transfer in Porous Medium

An optimized and simple algorithm/method for the solution of conjugate heat and mass transfer or just conjugate heat transfer in porous medium is developed. The two algorithms/methods are tested for their viability to solve the physical problem. It can be concluded from this study that the

- Developed algorithm/method has many advantages over conventional computational methods for solving the problem under investigation in terms of efficiency, computational time and computer resource utilization.
- The performance parameters $R_d=0.5$, $N=0.2$, $Ra=100$, $Le=2$, $Kr=5$ for both the algorithm/methods were simulated and tested for a range of solid size in the porous medium. The results obtained from the simulations showed that the developed algorithm/method can tackle any solid size to solve the physical problem whereas the conventional method failed to either converge at smaller solid size or provide less realistic solution for heat transfer. It is found that the developed algorithm could converge in just 268 iterations taking 1366.1 seconds of time for a set of 144 solid elements in the porous region; however the solution could not be converged for conventional method even after 2127 seconds.

- The developed algorithm/method was able to capture realistically the change of gradient across porous solid interface.
- In general, the developed method took less number of iterations for smaller solid size whereas conventional method is able to solve in slightly lesser iterations for higher solid size.
- The solution of developed algorithm/method is much more realistic than the conventional algorithm/method for all the solid sizes considered under current mesh scheme of 36x36.
- The developed algorithm/method is highly suitable for any size and location of solid in porous domain.
- The developed algorithm/method is much easier to implement in computer coding due to its characteristics of single mesh domain as compared to 2 mesh domains of conventional method.

## 7.2 Effect of Size and Location of Solid on Conjugate Heat Transfer in Porous Cavity

The above objective investigated the conjugate heat transfer inside a square porous cavity. Emphasis has been given to understand the heat and fluid flow behavior when the conductivity ratio and location of solid wall is varied. The following conclusion can be drawn from this work based on the simulations conducted.

- The increased conductivity ratio increases the heat transfer rate in the cavity
- The fluid flow direction shifts towards the lower left and upper right corner due to an increase in thermal conductivity ratio
- Two circulation regions are found when the solid wall height is 0.5L and it is placed at the center of cavity

- Fluid flow strength decreases with increase in the solid wall height but increase with increased conductivity ratio.
- Solid wall placed at the center of cavity induces better symmetry in flow pattern as compared to other location being studied.
- Temperature variations inside the solid wall keep decreasing as its position is moved towards the cold surface of cavity.
- Average Nusselt number increase with increase in thermal conductivity ratio
- Generally, the variation in Nusselt number is substantial at smaller values of *Kr*

### 7.3 Conjugate Heat and Mass Transfer in Square Porous Cavity

The aim of the above objective was to investigate the effect of thermal conductivity ratio and placement of a solid in the square porous cavity. An experimental simulation was carried out with respect to heat and mass transfer. Finite element method was used to solve the governing equations. The result obtained from the conducted simulation revealed that the placement of solid has significant effect on the heat and mass transfer behavior in the cavity.

- It is found that the larger area of cavity is occupied by high concentration lines at low value of thermal concavity ratio.
- It is further noted that the temperature variation inside the solid wall decreases owing shifting of solid wall towards the right surface.
- The increased solid height moves the concentration distribution towards upward section of cavity.
- The stream function value is maximum for the case of solid wall placed at right surface of cavity.

- The Nusselt number is much affected due to solid location as compared to Sherwood number.
- The variation in Nusselt and Sherwood number follows multilinear pattern when solid is placed near the hot surface but this effect diminished when the placement of solid is moved towards the cold surface.
- The influence of thermal conductivity is stronger for longer solid as compared to its shorter version. It found that the Sherwood number increased by almost 85% when thermal conductivity ratio is increased from 0.1 to 10 for the case of solid width and height as 25% and 50% respectively

### 7.4 Recommendations for future work

Current study can be extended to:

- Some other geometry such as non-square cavity etc. can be considered to investigate the impact of aspect ratio.
- Magneto hydrodynamic effect is an important phenomenon that can be studied with respect to the size and location of solid in porous medium
- Nano fluid is one of the emerging areas of study in porous medium. The effect of having nano particles in the porous medium can be studied with respect to the size and location of the solid in porous region.
- Viscous Dissipation can be considered along with other effects such as radiation, MHD etc. to investigate the heat and mass transfer behavior.

# REFERENCES


Abd Kadir, N. F., Rees, D. A. S., & Pop, I. (2008). Conjugate forced convection flow past a circular cylinder with internal heat generation in a porous medium. *International Journal of Numerical Methods for Heat & Fluid Flow, 18*(6), 730-744. doi:10.1108/09615530810885542

Ahmed, N. J. S., Badruddin, I. A., Zainal, Z. A., Khaleed, H. M. T., & Kanesan, J. (2009). Heat transfer in a conical cylinder with porous medium. *International Journal of Heat and Mass Transfer, 52*(13-14), 3070-3078. doi:10.1016/j.ijheatmasstransfer.2008.12.030

Ahmed, N. S., Badruddin, I. A., Kanesan, J., Zainal, Z., & Ahamed, K. N. (2011). Study of mixed convection in an annular vertical cylinder filled with saturated porous medium, using thermal non-equilibrium model. *International Journal of Heat and Mass Transfer*, *54*(17), 3822-3825.

Ahmed, N. S., Badruddin, I. A., Zainal, Z., Khaleed, H., & Kanesan, J. (2009). Heat transfer in a conical cylinder with porous medium. *International Journal of Heat and Mass Transfer, 52*(13), 3070-3078.

Al-Amiri, A., Khanafer, K., & Pop, I. (2008). Steady-state conjugate natural convection in a fluid-saturated porous cavity. *International Journal of Heat and Mass Transfer, 51*(17-18), 4260-4275. doi:10.1016/j.ijheatmasstransfer.2007.12.026

Al-Farhany, K., & Turan, A. (2011a). Non-Darcy effects on conjugate double-diffusive natural convection in a variable porous layer sandwiched by finite thickness walls. *International Journal of Heat and Mass Transfer, 54*(13-14), 2868-2879. doi:10.1016/j.ijheatmasstransfer.2011.03.012

Al-Farhany, K., & Turan, A. (2011b). Unsteady Conjugate Natural Convective Heat Transfer in a Saturated Porous Square Domain Generalized Model. *Numerical Heat Transfer, Part A: Applications, 60*(9), 746-765. doi:10.1080/10407782.2011.627793

Aleshkova, I. A., & Sheremet, M. A. (2010). Unsteady conjugate natural convection in a square enclosure filled with a porous medium. *International Journal of Heat and Mass Transfer, 53*(23-24), 5308-5320. doi:10.1016/j.ijheatmasstransfer.2010.07.025

Alhashash, A., Saleh, H., & Hashim, I. (2013). Conjugate Natural Convection in a Porous Enclosure Sandwiched by Finite Walls Under the Influence of Non-uniform Heat Generation and Radiation. *Transport in Porous Media, 99*(3), 453-465. doi:10.1007/s11242-013-0195-1

Ali, F., Khan, I., Samiulhaq, & Shafie, S. (2013). Conjugate effects of heat and mass transfer on MHD free convection flow over an inclined plate embedded in a porous medium. *PLoS One, 8*(6), e65223. doi:10.1371/journal.pone.0065223

Angirasa, D., Peterson, G., & Pop, I. (1997). Combined heat and mass transfer by natural convection with opposing buoyancy effects in a fluid saturated porous medium. *International Journal of Heat and Mass Transfer, 40*(12), 2755-2773.

Babaei, M. (2013). A general approach to approximate solutions of nonlinear differential equations using particle swarm optimization. *Applied Soft Computing, 13*(7), 3354-3365. doi:10.1016/j.asoc.2013.02.005

Badruddin, I. A., Ahmed, N. J. S., Al-Rashed, A. A. A. A., Kanesan, J., Kamangar, S., & Khaleed, H. M. T. (2012). Analysis of heat and mass transfer in a vertical annular porous cylinder using FEM. *Transport in Porous Media, 91*(2), 697-715.

Badruddin, I. A., Ahmed, N. J. S., Al-Rashed, A. A. A. A., Nik-Ghazali, N., Jameel, M., Kamangar, S., . . . Khan, T. M. Y. (2015). Conjugate Heat Transfer in an Annulus with Porous Medium Fixed Between Solids. *Transport in Porous Media, 109*(3), 589-608. doi:10.1007/s11242-015-0537-2

Badruddin, I. A., Al-Rashed, A. A. A. A., Ahmed, N. J. S., & Kamangar, S. (2012). Investigation of heat transfer in square porous-annulus. *International Journal of Heat and Mass Transfer, 55*(7), 2184-2192.

Badruddin, I. A., Al-Rashed, A. A. A. A., Ahmed, N. J. S., Kamangar, S., & Jeevan, K. (2012). Natural convection in a square porous annulus. *International Journal of Heat and Mass Transfer, 55*(23), 7175-7187.

Badruddin, I. A., Al-Rashed, A. A. A. A., Salman Ahmed, N. J., & Kamangar, S. (2012). Investigation of heat transfer in square porous-annulus. *International Journal of Heat and Mass Transfer, 55*(7-8), 2184-2192. doi:10.1016/j.ijheatmasstransfer.2011.12.023

Badruddin, I. A., Zainal, Z., Narayana, A., Seetharamu, K., & Siew, L. W. (2006). Free convection and radiation characteristics for a vertical plate embedded in a porous medium. *International journal for numerical methods in engineering, 65*(13), 2265-2278.

Badruddin, I. A., Zainal, Z. A., Aswatha Narayana, P. A., & Seetharamu, K. N. (2006). Heat transfer in porous cavity under the influence of radiation and viscous dissipation. *International Communications in Heat and Mass Transfer, 33*(4), 491-499. doi:10.1016/j.icheatmasstransfer.2006.01.015

Badruddin, I. A., Zainal, Z. A., Aswatha Narayana, P. A., Seetharamu, K. N., & Siew, L. W. (2006). Free convection and radiation for a vertical wall with varying temperature embedded in a porous medium. *International Journal of Thermal Sciences, 45*(5), 487-493. doi:10.1016/j.ijthermalsci.2005.05.008

Badruddin, I. A., Zainal, Z. A., Khan, Z. A., & Mallick, Z. (2007). Effect of viscous dissipation and radiation on natural convection in a porous medium embedded within vertical annulus. *International Journal of Thermal Sciences, 46*(3), 221-227.

Badruddin, I. A., Zainal, Z. A., Narayana, A. P. A., & Seetharamu, K. N. (2006a). Heat transfer by radiation and natural convection through a vertical annulus embedded in porous medium. *International journal of Heat and Mass Transfer, 33*(2006), 500-507.

Badruddin, I. A., Zainal, Z. A., Narayana, A. P. A., & Seetharamu, K. N. (2006b). Heat transfer in porous cavity under the influence of radiation and viscous dissipation. *International Communications in Heat and Mass Transfer, 33*(2006), 491-499.

Badruddin, I. A., Zainal, Z. A., Narayana, A. P. A., & Seetharamu, K. N. (2006c). Thermal non-equilibrium modeling of heat transfer through vertical annulus embedded with porous medium. *International Journal of Heat and Mass Transfer, 49*(2006), 4955-4965.

Badruddin, I. A., Zainal, Z. A., Narayana, A. P. A., & Seetharamu, K. N. (2007). Numerical analysis of convection conduction and radiation using a non-equilibrium model in a square porous cavity. *International Journal of Thermal Sciences, 46*(46), 20-29.

Badruddin, I. A., Zainal, Z. A., Narayana, A. P. A., Seetharamu, K. N., & Siew, L. W. (2006). Free convection and radiation for a vertical wall with varying temperature embedded in a porous medium*International Journal of Thermal Sciences, 45*(2006), 487-493.

Baytas, A., & Pop, I. (1999). Free convection in oblique enclosures filled with a porous medium. *International Journal of Heat and Mass Transfer, 42*(6), 1047-1057.

Baytas, A. C., Liaqat, A., Grosan, T., & Pop, I. (2001). Conjugate natural convection in a square porous cavity. *Heat and Mass Transfer, 37,* 467-473.

Beckermann, C., Viskanta, R., & Ramadhyani, S. (1986). A numerical study of non-Darcian natural convection in a vertical enclosure filled with a porous medium. *Numerical Heat Transfer, 10*(6), 557-570.

Bejan, A. (1979). On the boundary layer regime in a vertical enclosure filled with a porous medium. *Letters in Heat and Mass Transfer, 6*(2), 93-102.

Bejan, A., & Kraus, A. D. (2003). *Heat transfer handbook* (Vol. 1): John Wiley & Sons.

Belleghem, M. V., Backer, L. D., Janssens, A., & Paepe, M. D. (2012). Conjugate modelling of convective drying phenomena in porous building materials. *Journal of Physics: Conference Series, 395*, 012142. doi:10.1088/1742-6596/395/1/012142

Berletta, A., & Storesletten. (2011). Onset of convective rolls in a circular porous duct with external heat transfer to a thermally stratified environment. *International Journal of Thermal Sciences, 50*(8), 1374-1384.

Betchen, L., Straatman, A., & Thompson, B. (2006). A Nonequilibrium Finite-Volume Model for Conjugate Fluid/Porous/Solid Domains. *Numerical Heat Transfer: Part A: Applications, 49*(6), 543-565. doi:10.1080/10407780500430967

Bullo, F., & Lewis, A. D. (2004). *Geometric control of mechanical systems: modeling, analysis, and design for simple mechanical control systems* (Vol. 49): Springer Science & Business Media.

Cha, O., Chen, K., & Chen, C.-H. (1990). Nonuniform porosity and non-Darcian effects on conjugate mixed convection heat transfer from a plate fin in porous media. *International Journal of Heat and Fluid Flow, 11*(1), 65-71.

Chamkha, A. J., & Ismael, M. A. (2013a). Conjugate heat transfer in a porous cavity filled with nanofluids and heated by a triangular thick wall. *International Journal of Thermal Sciences, 67,* 135-151. doi:10.1016/j.ijthermalsci.2012.12.002

Chamkha, A. J., & Ismael, M. A. (2013b). Conjugate Heat Transfer in a Porous Cavity Heated by a Triangular Thick Wall. *Numerical Heat Transfer, Part A: Applications, 63*(2), 144-158. doi:10.1080/10407782.2012.724327

Chaquet, J. M., & Carmona, E. J. (2012). Solving differential equations with Fourier series and Evolution Strategies. *Applied Soft Computing, 12*(9), 3051-3062. doi:10.1016/j.asoc.2012.05.014

Char, M.-I., & Lin, J.-D. (2001). Conjugate film condensation and natural convection between two porous media seperated by a vertical plate. *ACTA MECHANICA, 148,* 1-15.

Char, M.-I., Lin, J.-D., & Chen, H.-T. (2001). Conjugate mixed convection laminar non-Darcy film condensation along a vertical plate in a porous medium. *International Journal of Engineering Science, 39*(2001), 897-912.

Chen, X., & Sutton, W. H. (2005). Enhancement of heat transfer: Combined convection and radiation in the entrance region of circular ducts with porous inserts. *International Journal of Heat and Mass Transfer, 43*(13), 2421-2429.

Cimolin, F., & Discacciati, M. (2013). Navier–Stokes/Forchheimer models for filtration through porous media. *Applied Numerical Mathematics, 72*, 205-224. doi:10.1016/j.apnum.2013.07.001

Clough, R. W. (1960). The finite element method in plane stress analysis.

Das, R., & Prasad, D. K. (2015). Prediction of porosity and thermal diffusivity in a porous fin using differential evolution algorithm. *Swarm and Evolutionary Computation, 23*, 27-39. doi:10.1016/j.swevo.2015.03.001

De Bonis, M. V., & Ruocco, G. (2008). A generalized conjugate model for forced convection drying based on an evaporative kinetics. *Journal of Food Engineering, 89*(2), 232-240.

de Rocquigny, E., Devictor, N., & Tarantola, S. (2008). *Uncertainty in industrial practice: a guide to quantitative uncertainty management*: John Wiley & Sons.

Defraeye, T., Blocken, B., & Carmeliet, J. (2011). Analysis of convective heat and mass transfer coefficients for convective drying of a porous flat plate by conjugate modelling. *International Journal of Heat and Mass Transfer*. doi:10.1016/j.ijheatmasstransfer.2011.08.047

DeGroot, C. T., & Straatman, A. G. (2011). A Finite-Volume Model for Fluid Flow and Nonequilibrium Heat Transfer in Conjugate Fluid-Porous Domains Using General Unstructured Grids. *Numerical Heat Transfer, Part B: Fundamentals, 60*(4), 252-277. doi:10.1080/10407790.2011.601180

Deng, J., Zhao, L., & Wu, Y. (2015). Efficient algorithms for solving the fractional ordinary differential equations. *Applied Mathematics and Computation, 269*, 196-216. doi:10.1016/j.amc.2015.07.048

Di Pietro, D. A., Flauraud, E., Vohralík, M., & Yousef, S. (2014). A posteriori error estimates, stopping criteria, and adaptivity for multiphase compositional Darcy flows in porous media. *Journal of Computational Physics, 276*, 163-187. doi:10.1016/j.jcp.2014.06.061

El-Shaarawi, M. A. I., Al-Nimr, M. A., & Al Yah, M. M. K. (1999). Transient conjugate heat transfer in a porous medium in concentric annuli. *International Journal of Numerical Methods for Heat & Fluid Flow, 9*(4), 444-462. doi:10.1108/09615539910266602

ElShayeb, M., & Beng, Y. K. (2000). *Applications of finite difference and finite element methods for thermal problems*: Universiti Malaysia Sabah.

Elsheikh, A. (2015). An equation-based algorithmic differentiation technique for differential algebraic equations. *Journal of Computational and Applied Mathematics, 281*, 135-151. doi:10.1016/j.cam.2014.12.026

Feng, S., Iscoe, I. , Seppalainen, T. (1997). A microscopic mechanism for the porous medium equation. *Stochastic Processes and their Applications, 66*( 1997), 147-182.

Gross, R., Bear, M., & Hickox, C. (1986). *The application of flux-corrected transport (FCT) to high Rayleigh number natural convection in a porous medium.* Paper presented at the Proc. 8th Int. Heat Transfer Conf., San Francisco, CA.

Gunzburger, M. D., Peterson, J. S., & Kwon, H. (1999). An Optimization Based Domain Decomposition Method for Partial Differential Equations. *Computers and Mathematics with Applications, 37*(1999), 77-93. doi:10.1016/j.cam.2014.12.032

Henderson, N., Brêttas, J. C., & Sacco, W. F. (2015). Applicability of the three-parameter Kozeny–Carman generalized equation to the description of viscous fingering in simulations of waterflood in heterogeneous porous media. *Advances in Engineering Software, 85*, 73-80. doi:10.1016/j.advengsoft.2015.03.002

Higuera, F. J., & Pop, I. (1997). Conjugate natural convection heat transfer between two porous media separated by a vertical wall. *International Journal of Heat and Mass Transfer, 40*(1), 123-129.

Horgue, P., Soulaine, C., Franc, J., Guibert, R., & Debenest, G. (2015). An open-source toolbox for multiphase flow in porous media. *Computer Physics Communications, 187*, 217-226. doi:10.1016/j.cpc.2014.10.005

Hossain, M. A., & Alim, M. A. (1997). Natural convection-radiation interaction on boundary layer flow along a thin vertical cylinder. *Heat and Mass Transfer, 32*(6), 515-520.

Ingham, D. B., & Pop, I. (1998). *Transport Phenomena in Porous Media*: Elsevier.

Iqbal, Z., Syed, K., & Ishaq, M. (2015). Fin design for conjugate heat transfer optimization in double pipe. *International Journal of Thermal Sciences, 94*, 242-258.

Joshi, Y., & Nakayama , W. (2003). Forced convection: external flows. *Heat Transfer Handbook, ed. Bejan A., Kraus AD: John Wiley & Sons, Inc*.

Juncu, G. (2014). The influence of the porous media permeability on the unsteady conjugate forced convection heat transfer from a porous sphere embedded in a porous medium. *International Journal of Heat and Mass Transfer, 77*, 1124-1132. doi:10.1016/j.ijheatmasstransfer.2014.06.039

Kamali, M. Z. M., Kumaresan, N., & Ratnavelu, K. (2015). Solving differential equations with ant colony programming. *Applied Mathematical Modelling, 39*(10-11), 3150-3163. doi:10.1016/j.apm.2014.11.003

Katsikadelis, J. T. (2011). The BEM for numerical solution of partial fractional differential equations. *Computers & Mathematics with Applications, 62*(3), 891-901. doi:10.1016/j.camwa.2011.04.001

Kaya, A. (2011). Effects of buoyancy and conjugate heat transfer on non-Darcy mixed convection about a vertical slender hollow cylinder embedded in a porous medium with high porosity. *International Journal of Heat and Mass Transfer, 54*(4), 818-825. doi:10.1016/j.ijheatmasstransfer.2010.10.021

Kaya, A. (2012). Effects of Conjugate Heat Transfer on Steady MHD Mixed Convective Heat Transfer Flow over a Thin Vertical Plate Embedded in a Porous Medium with High Porosity. *Mathematical Problems in Engineering, 2012*, 1-19. doi:10.1155/2012/261871

Kaya, A., Aydın, O., & Dincer, I. (2006). Numerical modeling of heat and mass transfer during forced convection drying of rectangular moist objects. *International Journal of Heat and Mass Transfer, 49*(17), 3094-3103.

Khader, M. M., Sweilam, N. H., & Mahdy, A. M. S. (2015). Two computational algorithms for the numerical solution for system of fractional differential equations. *Arab Journal of Mathematical Sciences, 21*(1), 39-52. doi:10.1016/j.ajmsc.2013.12.001

Khan, F. A., Fischer, C., & Straatman, A. G. (2015). Numerical model for non-equilibrium heat and mass exchange in conjugate fluid/solid/porous domains with application to evaporative cooling and drying. *International Journal of Heat and Mass Transfer, 80*, 513-528. doi:10.1016/j.ijheatmasstransfer.2014.09.051

Kimura, S., & Pop, I. (1994). Conjugate convection from a sphere in a porous medium. *International Journal of Heat and Mass Transfer, 37*(14), 2187-2192.

Kumaran, V., & Pop, I. (2006). Steady free convection boundary layer over a vertical flat plate embedded in a porous medium filled with water at 4 C. *International Journal of Heat and Mass Transfer, 49*(17), 3240-3252.

Kuznetsov, A. V., & Nield, D. A. (2001). Effects of Heterogeneity in Forced Convection in a Porous Medium: Triple Layer or Conjugate Problem. *Numerical Heat Transfer, Part A: Applications, 40*(4), 363-385. doi:10.1080/104077801753238158

Lamnatou, C., Papanicolaou, E., Belessiotis, V., & Kyriakis, N. (2009). Conjugate heat and mass transfer from a drying rectangular cylinder in confined air flow. *Numerical Heat Transfer, Part A: Applications, 56*(5), 379-405.

Lamnatou, C., Papanicolaou, E., Belessiotis, V., & Kyriakis, N. (2010). Finite-volume modelling of heat and mass transfer during convective drying of porous bodies – Non-conjugate and conjugate formulations involving the aerodynamic effects. *Renewable Energy, 35*(7), 1391-1402. doi:10.1016/j.renene.2009.11.008

Lee, C. S., Haghighat, F., & Ghaly, W. (2006). Conjugate Mass Transfer Modeling for VOC Source and Sink Behavior of Porous Building Materials: When to Apply It? *Journal of Building Physics, 30*(2), 91-111. doi:10.1177/1744259106067683

Lee, D., Dinov, I., Dong, B., Gutman, B., Yanovsky, I., & Toga, A. W. (2012). CUDA optimization strategies for compute- and memory-bound neuroimaging algorithms. *Comput Methods Programs Biomed, 106*(3), 175-187. doi:10.1016/j.cmpb.2010.10.013

Liu, J.-Y., Minkowycz, W., & Cheng, P. (1986). Conjugated, mixed convection-conduction heat transfer along a cylindrical fin in a porous medium. *International Journal of Heat and Mass Transfer, 29*(5), 769-775.

Lopez Penha, D. J., Stolz, S., Kuerten, J. G. M., Nordlund, M., Kuczaj, A. K., & Geurts, B. J. (2012). Fully-developed conjugate heat transfer in porous media with uniform heating. *International Journal of Heat and Fluid Flow, 38*, 94-106. doi:10.1016/j.ijheatfluidflow.2012.08.007

Mahmud, S., & Fraser, R. A. (2005). Conjugate heat transfer inside a porous channel. *Heat and Mass Transfer, 41*(6), 568-575. doi:10.1007/s00231-004-0563-z

Manole, D., & Lage, J. (1993). Numerical benchmark results for natural convection in a porous medium cavity. *ASME-PUBLICATIONS-HTD, 216*, 55-55.

McCall, J. (2005). Genetic algorithms for modelling and optimisation. *Journal of Computational and Applied Mathematics, 184*(1), 205-222.

Mendez, F., Trevino, C., Pop, I., & Linan, A. (2002). Conjugate free convection along a thin vertical plate with internal nonuniform heat generation in a porous medium. *Heat and Mass Transfer, 38*(2002), 631-638.

Minkowycz, W. J., & Ping, C. (1976). Free convection about a vertical cylinder embedded in a porous medium. *International Journal of Heat and Mass Transfer, 19*(7), 805-813.

Misirlioglu, A., Baytas, A. C., & Pop, I. (2005). Free convection in a wavy cavity filled with a porous medium. *International Journal of Heat and Mass Transfer, 48*(9), 1840-1850.

Modest, M. F. (1993). Radiation heat transfer. *MacGraw-Hill, New York.*

Mohan, V. C., & Talukdar, P. (2010). Three dimensional numerical modeling of simultaneous heat and moisture transfer in a moist object subjected to convective drying. *International Journal of Heat and Mass Transfer, 53*(21), 4638-4650.

Mori, S., Sakakibara, M., & Tanimoto, A. (1974). Steady heat transfer to laminar flow in a circular tube with conduction in the tube wall. *Heat Transfer-Jpn. Res, 3*(2), 37-46.

Moya, S. L., Ramos, E., & Sen, M. (1987). Numerical study of natural convection in a tilted rectangular porous material. *International Journal of Heat and Mass Transfer, 30*(4), 741-756.

Nield, D. A., & Bejan, A. (2006). *Convection in porous media*: Springer Science & Business Media.

Nield, D. A., & Kuznetsov, A. V. (1999). Local thermal nonequilibrium effects in forced convection in a porous medium channel: a conjugate problem. *International Journal of Heat and Mass Transfer, 42,* 3245-3252.

Nield, D. A., & Kuznetsov, A. V. (2004). Forced convection in a bi-disperse porous medium channel: a conjugate problem. *International Journal of Heat and Mass Transfer, 47*(24), 5375-5380. doi:10.1016/j.ijheatmasstransfer.2004.07.018

Nik-Ghazali, N., Badruddin, I. A., Badarudin, A., & Tabatabaeikia, S. (2014). Dufour and Soret Effects on Square Porous Annulus. *Advances in Mechanical Engineering, 6*, 209753.

Ogulu, A., & Amos, E. (2005). Asymptotic approximations for the flow field in a free convective flow of a non-Newtonian fluid past a vertical porous plate. *International Communications in Heat and Mass Transfer, 32*(7), 974-982.

Oliveira, L. S., & Haghighi, K. (1998). Conjugate Heat and Mass Transfer in Convective Drying of Porous Media. *Numerical Heat Transfer, 34*(PartA), 105-117. doi:10.1080/10407789808913980

Paik, S., Nguyen, H. D., & Pop, I. (1998). Transient Conjugate mixed convection from a sphere in a porous medium saturated with cold pure or saline water. *Heat and Mass Transfer, 34*, 237-245.

Pathak, M. G., Mulcahey, T. I., & Ghiaasiaan, S. M. (2013). Conjugate heat transfer during oscillatory laminar flow in porous media. *International Journal of Heat and Mass Transfer, 66*, 23-30. doi:10.1016/j.ijheatmasstransfer.2013.06.060

Pop, I., & Ingham, D. B. (2001). *Convective heat transfer: mathematical and computational modelling of viscous fluids and porous media*: Elsevier.

Pop, I., & Merkin, J. H. (1995). Conjugate free convection on a vertical surface in a saturated porous medium. *Fluid dynamics research, 16*(2-3), 71.

Pop, I., & Na, T.-Y. (2000). Conjugate free convection over a vertical slender hollow cylinder embedded in a porous medium. *Heat and Mass Transfer, 36*(2000), 375-379.

Pop, I., Sunada, J., Cheng, P., & Minkowycz, W. (1985). Conjugate free convection from long vertical plate fins embedded in a porous medium at high Rayleigh numbers. *International Journal of Heat and Mass Transfer, 28*(9), 1629-1636.

Prasad, V., & Kulacki, F. A. (1984). Natural convection in a vertical porous annulus. *International Journal of Heat and Mass Transfer, 27*(2), 207-219.

Rajamani, R., Srinivas, C., Nithiarasu, P., & Seetharamu, K. N. (1995). Convective heat transfer in axisymmetric porous bodies. *International Journal of Numerical Methods for Heat & Fluid Flow, 5*(9), 829 - 837.

Raptis, A. (1998). Radiation and free convection flow through a porous medium. *International Communications in Heat and Mass Transfer, 25*(2), 289-295.

Rashad, A. M., & EL-Hakiem, M. A. (2007). Effect of Radiation on Non-Darcy Free Convection from a Vertical Cylinder Embedded in a Fluid-Saturated Porous Medium with a Temperature-Dependent Viscosity. *Journal of Porous Media, 10*(2), 209-218.

Reda, D. C. (1986). Natural convection experiments with a finite-length, vertical, cylindrical heat source in a water-saturated porous medium. *Nuclear and Chemical Waste Management, 6*(1), 3-14.

Riesinger, C., Neckel, T., Rupp, F., Hinojosa, A. P., & Bungartz, H.-J. (2014). GPU Optimization of Pseudo Random Number Generators for Random Ordinary Differential Equations. *Procedia Computer Science, 29*, 172-183. doi:10.1016/j.procs.2014.05.016

Rohan, E., & Lukeš, V. (2015). Modeling nonlinear phenomena in deforming fluid-saturated porous media using homogenization and sensitivity analysis concepts. *Applied Mathematics and Computation, 267*, 583-595. doi:10.1016/j.amc.2015.01.054

Sadegh Zadeh, K., & Montas, H. J. (2014). Parametrization of flow processes in porous media by multiobjective inverse modeling. *Journal of Computational Physics, 259*, 390-401. doi:10.1016/j.jcp.2013.12.001

Saeid, N. H. (2007). Conjugate natural convection in a porous enclosure: effect of conduction in one of the vertical walls. *International Journal of Thermal Sciences, 46*(6), 531-539.

Saeid, N. H. (2007). Conjugate natural convection in a vertical porous layer sandwiched by finite thickness walls. *International Communications in Heat and Mass Transfer, 34*(2), 210-216. doi:10.1016/j.icheatmasstransfer.2006.11.003

Sakakibara, M., Mori, S., & Tanimoto, A. (1987). Conjugate heat transfer with laminar flow in an annulus. *The Canadian journal of chemical engineering, 65*(4), 541-549.

Saleh, H., & Hashim, I. (2012). Conjugate Natural Convection in a Porous Enclosure with Non-Uniform Heat Generation. *Transport in Porous Media, 94*(3), 759-774. doi:10.1007/s11242-012-0023-z

Salman Ahmed, N. J., Badruddin, I. A., Kanesan, J., Zainal, Z. A., & Nazim Ahamed, K. S. (2011). Study of mixed convection in an annular vertical cylinder filled with saturated porous medium, using thermal non-equilibrium model. *International Journal of Heat and Mass Transfer, 54*(17-18), 3822-3825. doi:10.1016/j.ijheatmasstransfer.2011.05.001

Salman Ahmed, N. J., Badruddin, I. A., Zainal, Z. A., Khaleed, H. M. T., & Kanesan, J. (2009). Heat Transfer in a conical cylinder with porous medium. *International Journal of Heat and Mass Transfer, 52*(2009), 3070-3078.

Salman, A. N. J., Sarfaraz, K., Badruddin, I. A., Al-Rasheed, A. A. A. A., Quadir, G. A., Khaleed, H. M. T., & Khan, T. M. Y. (2014). Conjugate Heat Transfer in Porous Annulus. *Journal of Porous Media, 17*(12), 1109-1119.

Save, Y. D., Narayanan, H., & Patkar, S. B. (2011). Solution of Partial Differential Equations by electrical analogy. *Journal of Computational Science, 2*(1), 18-30. doi:10.1016/j.jocs.2010.12.006

Schittkowski, K. (2004). Data fitting in partial differential algebraic equations: some academic and industrial applications. *Journal of Computational and Applied Mathematics, 163*(1), 29-57. doi:10.1016/j.cam.2003.08.052

Segerlind, L. (1982). Solving the nonlinear airflow equation. *Am. Soc. agric. Engrs, Paper*(82-3017).

Sheremet, M. A., & Pop, I. (2014). Conjugate natural convection in a square porous cavity filled by a nanofluid using Buongiorno's mathematical model.

*International Journal of Heat and Mass Transfer, 79*, 137-145. doi:10.1016/j.ijheatmasstransfer.2014.07.092

Sheremet, M. A., & Trifonova, T. A. (2013a). Unsteady Conjugate Natural Convection in a Vertical Cylinder Containing a Horizontal Porous Layer: Darcy Model and Brinkman-Extended Darcy Model. *Transport in Porous Media, 101*(3), 437-463. doi:10.1007/s11242-013-0253-8

Sheremet, M. A., & Trifonova, T. A. (2013b). Unsteady Conjugate Natural Convection in a Vertical Cylinder Partially Filled with a Porous Medium. *Numerical Heat Transfer, Part A: Applications, 64*(12), 994-1015. doi:10.1080/10407782.2013.811973

Shivakumara, I. S., Prasanna, B. M. R., Rudraiah, N., & Venkatachalappa, M. (2002). Numerical study of natural convection in a vertical cylindrical annulus using a non-Darcy equation. *Journal of Porous Media, 5*(2), 87-102.

Shu, J. J., & Pop, I. (1998). Transient Conjugate Free Convection From a Vertical Flat Plate in a Porous Medium Subjected to a Sudden Change in Surface Heat Flux. *International Journal of Engineering Sciences, 36*(2), 207-214.

Suresh, H., Narayana, P. A., & Seetharamu, K. (2001). Conjugate mixed convection heat and mass transfer in brick drying. *Heat and Mass Transfer, 37*(2-3), 205-213.

Tao, W.-Q. (1987). Conjugated laminar forced convective heat transfer from internally finned tubes. *Journal of heat transfer, 109*(3), 791-795.

Tao, Z., Wu, H., Chen, G., & Deng, H. (2005). Numerical simulation of conjugate heat and mass transfer process within cylindrical porous media with cylindrical dielectric cores in microwave freeze-drying. *International Journal of Heat and Mass Transfer, 48*(3-4), 561-572. doi:10.1016/j.ijheatmasstransfer.2004.09.008

Vafai, K. (2000). Handbook of Porous Media: Marcel Dekker, New York.

Varol, Y., Oztop, H. F., & Pop, I. (2009). Conjugate heat transfer in porous triangular enclosures with thick bottom wall. *International Journal of Numerical Methods for Heat & Fluid Flow, 19*(5), 650-664. doi:10.1108/09615530910963571

Vaszi, A. Z., Elliott, L., Ingham, D. B., & Pop, I. (2002). Conjugate free convection above a heated finite horizontal flat plate embedded in a porous medium. *International Journal of Heat and Mass Transfer, 45*(2002), 2777-2795.

Vaszi, A. Z., Elliott, L., Ingham, D. B., & Pop, I. (2003). Conjugate Free Convection from Vertical Fins Embedded in a Porous Medium. *Numerical Heat Transfer, Part A: Applications, 44*(7), 743-770. doi:10.1080/716100521

Vaszi, A. Z., Elliott, L., Ingham, D. B., & Pop, I. (2004). Conjugate free convection from a vertical plate fin with a rounded tip embedded in a porous medium. *International Journal of Heat and Mass Transfer, 47*(12-13), 2785-2794. doi:10.1016/j.ijheatmasstransfer.2004.01.001

Walker, K. L., & Homsy, G. M. (1978). Convection in a porous cavity. *J. Fluid Mech, 87*(03), 449-474.

Wong, K.-C., & Saeid, N. H. (2009). Jet Impingement Cooling of a Finite Thickness Solid Layer Conjugated with Porous Medium. *Numerical Heat Transfer, Part A: Applications, 55*(7), 706-720. doi:10.1080/10407780902821508

Wu, H., Tao, Z., Chen, G., Deng, H., Xu, G., & Ding, S. (2004). Conjugate heat and mass transfer process within porous media with dielectric cores in microwave freeze drying. *Chemical Engineering Science, 59*(14), 2921-2928. doi:10.1016/j.ces.2004.04.015

Zelinka, I. (2015). A survey on evolutionary algorithms dynamics and its complexity – Mutual relations, past, present and future. *Swarm and Evolutionary Computation*. doi:10.1016/j.swevo.2015.06.002

Zhang, H. J., Zou, Z. P., Li, Y., & Ye, J. (2011). Preconditioned Density-Based Algorithm for Conjugate Porous/Fluid/Solid Domains. *Numerical Heat Transfer, Part A: Applications, 60*(2), 129-153. doi:10.1080/10407782.2011.588567

Zienkiewicz, O., & Cheung, Y. (1965). Finite element method of analysis for arch dam shells and comparison with finite difference procedures. *Theory of Arch Dams*, 123-140.

# LIST OF PUBLICATIONS

## Journal papers Published/Accepted

1. Azeem,,Irfan Anjum Badruddin, Mohd Yamani Idna Idris, N Nik-Ghazali, Salman Ahmed N J & Abdullah A A A Al-Rashed, ConjugateHeatand Mass Transfer in Square Porous Cavity, Indian Journal of Pure and Applied Physics. Vol. 54, December 2016, pp.777-786 (ISI indexed)
2. Irfan Anjum Badruddin, Azeem, Mohd Yamani Idna Idris, N Nik-Ghazali, Salman Ahmed N J & Abdullah A A A Al-Rashed, Simplified Finite Element Algorithm to Solve Conjugate Heat and Mass Transfer in Porous Medium, International Journal of Numerical Methods in Engineering. (ACCEPTED) (ISI Indexed)

## Conference Paper

Azeem, Yunus Khan T.M, Irfan Anjum Badruddin, N Nik-Ghazali, MohdYamani Idna Idris. Influence of Radiation on Double Conjugate Diffusion in a Porous Cavity,International Conference on Condensed Matter & Applied Physics (ICC 2015), October 30-31, 2015 (published in AIP proceedings 2016)